Design and Stability Analysis of an Integrated Controller for Highly Flexible Advanced Aircraft Utilizing the Novel Nonlinear Dynamic Inversion.

Thesis by
Irene M. Gregory
In Partial Fulfillment of the Requirements
for the Degree of
Doctor of Philosophy

California Institute of Technology
Pasadena, California
2005
(submitted July 2004)

To my family
I wouldn't be where I am without you.

Grandpa,
I'm going to get them…

Acknowledgements

This is one section that in a course of writing the dissertation is typically relegated to be the last written and least thought out. I'm sure given some passage of time and reacquired perspective, I will find regrettable omissions both of the people and subjects, and for that I beg forgiveness and understanding.

First and foremost, I would like to thank my advisor, John Doyle, for affording me an opportunity to learn in an exciting and challenging environment and for taking a chance and letting me do a Ph.D. while working full time across the country. John taught me many lessons and exposed me to new experiences and ideas, and for that I will forever be grateful. I want to thank Richard Murray for his guidance through the long years, frankly many more than I thought likely. I love challenge and find life boring in its absence. Starting with my class work and continuing throughout my research, both John and Richard ensured that I was never bored. Thank you for proving once again the old maxim — "what doesn't kill you, will make you stronger."

Thank you Jerry Marsden for taking the time to offer a number of very helpful suggestions in later part of my research. I want to thank John Davidson who was coerced into joining my committee at a very late date, but whose suggestions made this thesis much better. Thank you Charmaine Boyd for looking out for me across the vast distance of our great country; and Lori Brown for keeping an eye out closer to home.

I want to express my special thanks to Antonis Papachristodoulou who has worked hard with me long distance to make sure that a new tool for establishing nonlinear system stability was tried on a new application – an aircraft. I truly believe your help has made this a better piece of research. And thank you Dimitriy Kogan who had to run this tool for a class project and ended up with more than he probably bargained for in the begining.

I want to thank Jorge Tierno for being my tutor when I needed help and being my friend when I most needed one. And I would be most remiss if I did not mention Sonja Glavaski in the same breath as I've mentioned friendship. Thank you for your friendship, your presence has immeasurably enriched my life.

I want to thank my friends and colleagues at NASA Langley for their support, even when that was a needed kick in the pants. I am grateful to Jim Batterson for trying to shield me from project demands to allow me time to complete my research. I particularly want to thank Tom Bundick, who has set an example of professionalism I aspire to imitate in my career and whose sense of humor has made me smile in the darkest of hours. I will miss our discussions when you retire. I want to thank Bart Bacon for being both a sounding board for my technical ideas and a great dance partner. Not many people can discuss nonlinear dynamic inversion implementation and tango's death drop in the same sentence.

I want to thank my friends who have put up with me for years and are still my friends. Thank you for trying to keep me on an even keel and make my life fun. Anna, there's way too much to thank you for in this limited space, but the world should know your MS Word guru status.

And now I come to the last and most important group of people to thank — my family. The full acknowledgement of their contributions would take too long and in some ways are too personal to include here. Words would be completely inadequate to give this justice but I will make an attempt. I can only say with complete certainty that I wouldn't be the person that I am without your influence, guidance, and unconditional love. I have and will always strive to live up to the values you've instilled in me and hope my actions will be worthy of your pride and respect.

It has been a long but rewarding road and now I've come to another fork that I hope will be as challenging. And, once again, I have "… miles to go before I sleep."

Abstract

High performance aircraft of the future will be designed to be lighter, more maneuverable, and operate over an ever expanding flight envelope. This set of conditions will necessarily mean highly flexible vehicles operating in nonlinear regimes. A methodology proposed to better optimize their responses to both pilot input and external disturbances, as well as to decrease the cost of vehicle design is the novel dynamic inversion. The attractiveness of this methodology lies in the fact that the inherent nonlinearities of the problem and the coupled nature of flexible dynamics are explicitly considered.

The contribution of this work to the state of the art is predicated on the development and application of the novel dynamic inversion methodology to handle highly flexible aircraft in an integrated flight/structural mode control manner. The unprecedented small separation between rigid body and flexible dynamics as well as the reciprocal interaction between them due to flight control action are the key elements of the aircraft model. The novel approach to the nonlinear dynamic inversion allows the methodology to more intelligently handle flexible dynamics in the context of the dual objectives of integrated flight/SMC control by altering flexible mode damping without cancellation; thus, improving disturbance response and avoiding the potentially destabilizing effect of pole cancellation close to the jω-axis in case of modeling uncertainty. The necessary level of model complexity for design has been established with particular attention given to understanding physics. The effect of uncertainty in the structural mode dynamics has been addressed.

Further contribution of this work addresses the issue of stability of the dynamic systems driven by nonlinear controllers. One result shows how assessing stability of an n-dimensional system can be reduced to checking stability of a two-dimensional one using algebraic expressions that are based on the vehicle characteristics such as aerodynamic coefficients. This reduces a complicated dynamical problem to something purely algebraic and manageably complex. Another approach is based on algorithmically finding a local Lyapunov function using sum of squares. The presented results are the

first to address the question of stability for the nonlinear dynamic inversion in the presence of flexible dynamics.

Table of Contents

List of Abbreviations

6 DOF six degrees of freedom

AFRL Air Force Research Laboratories

ASE aeroservoelastic

c.g. center of gravity

CD drag coefficient

$C_{D,\delta}$ change in drag due to elevator deflection

CL lift coefficient

$C_{L,\delta}$ change in lift due to elevator deflection

CM aerodynamic moment coefficient about y-axis

CV control variables

Cx aerodynamic force coefficient in x (longitudinal) axis

Cz aerodynamic force coefficient in z (vertical) axis

DASE dynamic aeroelastic

Δ uncertainty

δ elevator angle

E mean aerodynamic cord

$E_{(\bullet,\bullet)}$ flexible dynamics coefficient

EOM equations of motion

GW^* mass distribution

HARV High Angle-of-Attack Research Vehicle

HSCT High Speed Civil Transport

I_y product of inertia about y axis

$L_f h(x)$ derivative of h(x) along f(x)

LQR linear quadratic regulator

m vehicle mass

ma mean axis

MIMO multiple input multiple output

m_μ generalized mass associated with fliexible dynamics

nz normal acceleration

ω	flexible mode frequency
ϕ'	modal slope
PI	proportional plus integral
ps	pilot station
q	pitch rate
$\bar{q}$	dynamic pressure
$\dot{q}$	rate of change of pitch rate
QSAE	quasi-static aeroelastic
RCV	ride control vane
ρ	density
S	planform area
SAS	stability augmentation system
SISO	single input single output
SMC	structural mode control
T	thrust
τ	aerodynamic lag terms
θ	pitch attitude
U	velocity in longitudinal (x) axis
UAV	Uninhabited Aerial Vehicle
V	velocity (speed)
w	velocity in vertical (z) axis
W(x)	dynamic matrix
x	longitudinal
x_f	filter state in W
η	flexible mode displacement
$\dot{\eta}$	rate of change of flexible mode displacement
$\dot{\gamma}/V$	rate of change of flight path angle / velocity
z	vertical
ξ	flexible mode damping

List of Figures

Chapter 1 – Introduction

1.1 Motivation

High performance aircraft of the future will be designed to be lighter, more maneuverable, and operate over an ever expanding flight envelope[1]. This set of conditions will necessarily mean highly flexible vehicles operating in nonlinear regimes. In order to control these vehicles, new methods are being sought to better optimize their responses to both pilot input and external disturbances, as well as to decrease the cost of vehicle design. Over the last decade, dynamic inversion methodology has gained considerable popularity in application to highly maneuverable fighter aircraft[2-5] , as underlying methodology to new generation of highly maneuverable vehicles under development[6-9], and might be of benefit to highly flexible aircraft.

The attractiveness of this methodology lies in the fact that the inherent nonlinearities of the problem are explicitly considered. In other words, a nonlinear control law is designed that globally reduces the aircraft dynamics of interest into a set of integrators and, thus, allows one linear controller to provide desired response throughout the flight envelope. This eliminates the need for extensive linearization of the aircraft model for different flight conditions, design of individual controllers for each of these conditions, and finally performing gain scheduling, which is typically an ad hoc and time consuming procedure to link the individual controllers over the flight envelope. Despite these apparent advantages, dynamic inversion is not a panacea of high performance flight control. A number of issues dealing with global system stability and robustness have not been fully addressed. However, the fighter aircraft examples to which dynamic inversion had been applied have shown that this methodology works for current advanced aircraft[2, 3].

One of the largest differences from the flight control perspective between current and future advanced aircraft is elasticity. All of the aircraft to which dynamic inversion had been applied to date are considered rigid vehicles. In the context of flight control, this means that the frequency separation between the fastest aerodynamic modes and the slowest body deforming mode is typically on the order of 60 rad/sec (10 Hz)[10]. The aircraft of the future will not have this luxury.

One type of aircraft that has gained prominence in recent years is an Uninhabited Aerial Vehicle (UAV). These vehicles span a great variety of missions and hence have a number of very different configurations. One such vehicle is a Helios Prototype designed for very long duration flight, non-stop at least 24 hours at 100,000 ft[11]. As can be seen from Figure 1.1, the aircraft is an ultra-lightweight flying wing, which is inherently very flexible. The wingspan is 247 ft, longer than the wingspans of U.S. Air Force C-5 military transport (222 ft) or Boeing 747 commercial jetliner (215 ft). The aircraft recently crashed and an investigation to determine the causes of the control problems that led to the loss of the craft are still in progress.

Figure 1.1: Helios Prototype long duration solar powered flight (courtesy NASA Dryden Flight Test Center).

Furthermore, conceptual combat UAV designs may incorporate highly flexible delta-type wing shapes. The University of Bath and AFRL undertook an experimental/computational research effort investigating flexible delta wings' nonlinear aeroelastic response due to unsteady vortex flow[12]. And in a recent announcement, QinetiQ, the UK's defense research agency, has designed a flying wing tail-less UAV with no external control surfaces, which uses wing twist and deformation for pitch and roll control. The UAV, called AEUAV-F, applies aeroelasticity to enhance the control power of these controls[13]. Consequently, in light of all these developments, the question of integrated flight/aeroelastic control assumes great prominence.

The aircraft that typifies this new set of complex dynamics is the next generation High Speed Civil Transport (HSCT). This aircraft was chosen as a representative of the

dynamics of interest because very extensive development in modeling and simulation has been performed over a number of years and the available models are of very high fidelity. This vehicle class is 300 ft in length with gross weight of 700,000 lbs. The sheer size of this vehicle is put in perspective by a drawing found in Figure 1.2 that places the aircraft on a football field inside a stadium. While this aircraft is not a traditional high performance aircraft, it does operate over an extensive flight envelope and exhibits elastic characteristics expected of future advanced vehicles. The weight savings produced by lighter materials also result in low frequencies for elastic modes. Generally, these first modes occur around 1.5 Hz (9 - 10 rad/sec) with the first five under 4 Hz, while for a typical subsonic transport this value is 3.2 Hz (20 rad/sec). The implication for this class of vehicles is that the frequency separation between the fastest rigid body dynamics and the slowest elastic mode is less than 10 rad/sec. The lack of separation between rigid and elastic dynamics has significant consequences for flight control and is discussed in detail in later chapters.

If dynamic inversion is to be seriously considered as a methodology for control design of future advanced flexible aircraft, it must be able to deal with the small frequency separation between rigid and elastic modes. Before applying dynamic inversion to a high performance flexible fighter, which includes both elasticity and high performance over an extreme flight envelope, the issue of elasticity must first be resolved. The HSCT class of vehicles mentioned above offers an opportunity to address elasticity through dynamic inversion while operating under a wide range of aerodynamic conditions but without adding the extra complexity of highly nonlinear post-stall aerodynamic regimes and very rapid aircraft response requirements. Hence, a model of such a vehicle is selected here to address the ability of dynamic inversion to handle highly elastic vehicles that require a new approach to flight control due to complexity of their dynamics.

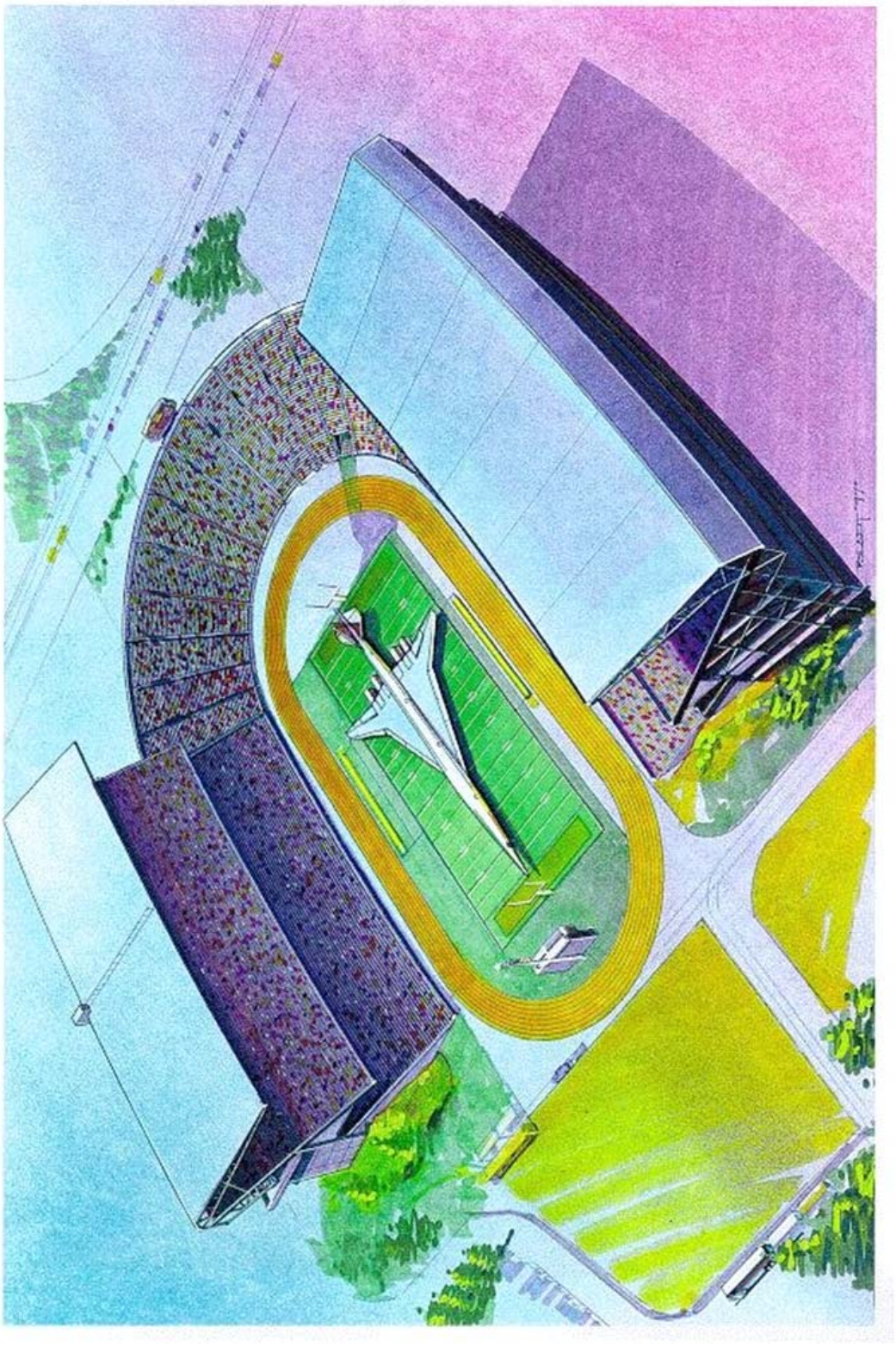

Figure 1.2: HSCT aircraft parked on the football field.

1.2 Integrated Flight/Structural Mode Control and Dynamic Inversion Literature

The state of the art that has bearing on the research presented in this work falls into two separate fields: those of integrated flight/structural mode control and those of dynamic inversion application to aircraft control. The state of the art in dynamic inversion aircraft control is presented first.

1.2.1 Dynamic Inversion Aircraft Control

The application of direct dynamic inversion to aircraft control has reached its peak in open literature with the High Angle-of-Attack Research Vehicle (HARV) project[2-5]. Subsequent to that project, control involving dynamic inversion changed directions and the methodology became an underlying partner for direct adaptive control with neural networks[6, 7]. Dynamic inversion has also been used as the underlying methodology for indirect adaptive control to enhance survivability of the next generation of fighter aircraft and implemented online in real-time[8, 9]. The innovation in both of these methods dealt with adaptively regulating the error in the plant inversion of the rigid vehicles. This new turn did not advance the state of the art of dynamic inversion itself or improve the theoretical underpinning for the methodology beyond that developed in the HARV project, though it has provided some very interesting and useful results in aircraft adaptive control. Consequently describing the state of the art for dynamic inversion itself is going to focus on the results produced for HARV, summarizing some work on robustness issues[5], and discussing the latest result in global stability for nonlinear rigid aircraft pitch-axis models[14].

1.2.1.1 Dynamic Inversion for Aircraft

The nonlinear equations of motion for an aircraft can be written in the control input affine form:

$$\begin{aligned} \dot{x} &= F(u, x) \\ &\approx f(x) + g(x)u \end{aligned} \tag{1.1}$$

where x is the vector of state variables and u is the vector of control effectors. It is often desirable to rewrite the above equation in a normal form, which is very useful in expressing generalized results of feedback linearization[15]. The formal process for transforming the system in (1.1) into normal form does not always work for arbitrary

nonlinear systems; but fortunately, for rigid body aircraft dynamics, it can always be completed. Note that any aircraft outputs are a function of the state variables and can be used as the control variables (CV) for (1.1):

$$CV = CV(x)$$

where CV is the vector of control variables. Rewriting the equations in normal form for aircraft is always possible because (1.1) has CVs for the three axes (pitch, roll, yaw), each including a body rate, and control effectors primarily producing torque in the same three axes. However, in review of aircraft application, the original coordinates prove sufficient in considering the problem. Continuing with the idea that CVs are functions of state variables:

$$C\dot{V} = \frac{\partial CV}{\partial x}\dot{x} = \frac{\partial CV}{\partial x} f(x) + \frac{\partial CV}{\partial x} g(x)u \tag{1.2}$$

Let $y \triangleq CV(x) = h(x)$ then (1.2) can be rewritten as

$$\dot{y} = \frac{\partial h(x)}{\partial x}\dot{x} = h_x(x) f(x) + h_x(x) g(x)u \tag{1.3}$$

So the dynamic inversion part of the control law appears:

$$u^{cmd} = \left[h_x(x)g(x)\right]^{-1}\left[\dot{y}^{des} - h_x(x) f(x)\right] \tag{1.4}$$

with $h_x(x)g(x)$ invertible for all values of x. For an aircraft with multiple control effectors for a single axis, $\left(h_x(x)g(x)\right)^{-1}$ in (1.4) should be interpreted as a (non-unique) right inverse.

The important generalization to notice is that the number of control effectors must equal the number of control variables. Since three control variables (one for each axis) have a strong angular rate content and conventional aircraft typically have three moment-producing controls (differential ailerons, symmetric horizontal tail, and rudder), this control handles conventional aircraft easily. For an aircraft that has multiple control effectors for a single axis, a method to allocate control requirements to the different effectors is required.

1.2.1.2 Dynamic Inversion Fighter Applications

The HARV program was NASA's high angle-of-attack flight test program to explore, among other issues, flight control for low speed, high angle-of-attack, rapid maneuvering.

Honeywell was one of the participants and their dynamic inversion based control law was one of several utilized for this program. The HARV flight control is the most detailed, flight-ready set of control laws designed based on dynamic inversion[2] that is available in open literature.

The Honeywell design methodology consisted of dynamic inversion for flight control laws. μ-synthesis was employed to determine optimal robust performance for special point cases against which the dynamic inversion based performance was compared. The control laws were analyzed using singular value and μ-analysis techniques. They were also extensively exercised with batch and piloted simulation.

1.2.1.3 Control Law – Basics

The conceptual development of the HARV control laws are presented here because these have become a standard initial starting point for other designs including the one pursued here for flexible aircraft. Some of the reasons for this formulation are elaborated upon in this subsection; some are further discussed in the next subsection.

In general, the control variables are modeled with the differential equations

$$\dot{y} = f(u, x) \tag{1.5}$$

which depend on aircraft state variables x and the control effectors u. The differential equations are just the rigid body equations of motion. The state variables – roll, pitch, yaw rates, bank angle, angle-of-attack, sideslip, velocity, and flight path angle – are assumed measured (x^{meas}). The control effectors are aerodynamic surfaces (u_a) and thrust vectoring (u_t).

A desired rate of change of the control variable is selected to achieve satisfactory handling qualities in response to pilot commands. This is modeled with a first-order differential equation

$$\dot{y}^{desired} = \frac{1}{\tau}(y^{cmd} - y^{meas}) \tag{1.6}$$

with a specified time constant, τ, for each control variable based on the MIL-SPECS[16]. The two differential equations for rate of change are then equated which leaves an expression

$$f(u^{cmd}, x^{meas}) = \frac{1}{\tau}(y^{cmd} - y^{meas}) \tag{1.7}$$

to be solved for the control effector commands. Desirable pilot handling qualities are achieved by precompensation of stick and pedal commands, and trim inputs. The pilot inputs are scaled with flight condition dependent gains and a first-order shaping filter to achieve time constants other than those resulting from feedback objectives.

To decrease the sensitivity of the closed loop response to modeling errors and low frequency atmospheric disturbances, integral feedback was incorporated into the desired dynamics without altering the handling qualities as seen by the pilot. With integral feedback, the desired dynamics for the control variables are

$$\dot{y} = \frac{\omega_c}{2}\left[y^{cmd} - 2y^{meas} + \int (y^{cmd} - y^{meas}) \frac{\omega_c\, dt}{2} \right] \tag{1.8}$$

The integral term implies that the control variable will have zero steady state error in response to step commands in the presence of model errors and constant disturbances. Assuming perfect sensors ($y = y^{meas}$), the transfer function between y^{cmd} and y is first order with a time constant given by $2/\omega_c$. Thus, the handling qualities are unaltered from the first order characteristics of the proportional only feedback.

The value of the proportional feedback of the control variable sets the crossover frequency (ω_c) or bandwidth. The bandwidth has an upper limit related to airframe elasticity such that control action does not excite elastic modes.

Stability of the closed loop system is related to the selection of control variables. In the linear case, closed loop poles are equal to open loop zeros in the transfer function between control effectors and control variables[5, 14].

Robust stability consists of basic loop properties that are degraded by high frequency lags; delays; details of the inversion, which depend on control variables and their complements; and state estimation, if state variables are not measured directly. Satisfactory basic loop properties are a prerequisite to achieving satisfactory robustness with respect to more detailed assumptions. The basic loop properties are a Bode gain plot that crosses over at ω_c with a phase margin of 87 deg. This allows for 42 deg. of phase margin degradation associated with details of implementation[2].

The multiple control effectors were allocated according to a special model,

$$\dot{y}^{desired} = B_a u_a + B_t u_t \tag{1.9}$$

where B_a and B_t are control moment effectiveness divided by inertia; hence, they are dependent on the current state measurements. Control commands are given by

$$u_a^{cmd} = \lim\left\{\tilde{B}_a^{-1}\dot{y}^{desired}\right\}$$
$$u_t^{cmd} = \lim\left\{B_t^{-1}\dot{y}^{desired} - B_t^{-1}B_a u_a^{cmd}\right\} \tag{1.10}$$

where $\tilde{B}_a = B_a$ unless division by B_a is unacceptable in which case $\tilde{B}_a$ is set to a specified invertible matrix. Reversion to $\tilde{B}_a$ typically takes place when either dynamic pressure is small or angle-of-attack exceeds stall. The control law is intended to operate only when thrust vectoring is available, so B_t is always an inevitable matrix. Note when aerodynamic surfaces are not limited, $u_t^{cmd} = 0$; otherwise, u_t is only required for what cannot be provided by aerodynamic control surfaces. This is essentially known as a daisy-chain method of control allocation. It is necessary to stop the integration of tracking error under limiting conditions to prevent integrator windup.

1.2.1.4 Control Law – Other Aspects

The special HARV linear model used for design assumes the time rate of change of the control variable is a nonlinear function of the measured state plus linear terms in the control effectors. The model subroutine is part of the implementation and computes the function of the state using aircraft equations of motion evaluated at the measured state.

A reduced aerodynamic data base was obtained with a least squares fit for HARV data with assumptions that aerodynamic coefficients are linear in everything except the angle-of-attack and have angle-of-attack dependent multipliers. The accuracy of the fit was deemed acceptable based on the performance and robustness tests of the computed control laws. This aircraft model database, in a sense, replaces the set of gain schedules regarding inner loop feedback gains that is present in existing flight control systems.

It quickly becomes evident from a variety of sources[2, 5, 17] that CVs play a central role in the dynamic inversion concept. They determine how handling quality specifications are satisfied, how disturbance responses are attenuated, how good zero dynamics are obtained, and how favorable performance/robustness trade-offs for overall closed loop system are achieved. The CVs chosen for each of the aircraft axis initially came from one of the designers with long experience in conventional classical control and then were

modified based on the physics of the high angle-of-attack problem[17]. Essentially, a "judicious" selection of CVs produced a control law that provided good behavior in all the categories mentioned in the above paragraph for HARV. Of course, the "judicious" selection was based on the physics not only of the aircraft generic relations but also on the specifics of the flight regime of interest.

Another example of dynamic inversion based control laws evaluated in a piloted simulation can be found in Reference 3. The control laws for the F-16 piloted evaluation example were designed based on the HARV report. The control laws produced for the HARV program were used with a change in the aerodynamic database to reflect a different vehicle. It is important to reiterate that, in both cases, the vehicles were described by rigid body equations that were an accurate representation of the physical system in the frequency range of interest, *i.e.*, anything that can be affected by a pilot in combination with external inputs.

The question of robustness and stability were addressed, for both of the design examples, during the control law evaluation using μ-analysis, batch, and piloted simulations. The robustness issues associated with dynamic inversion were addressed more generically in Reference 5. These results are summarized in the next section.

1.2.1.5 Robustness Issues

Good nominal response and well-behaved zero dynamics are not enough for a good control law design. These qualities must also be robust with respect to various modeling errors inherent in aircraft systems. The inversion part of the control law produces the desired dynamics exactly only when *f(x)* and *g(x)* are known precisely.

For the rest of this section consider a perturbed model of the aircraft given by

$$\dot{y} = C\dot{V} = \dot{x} = (f + \delta f)(x) + (g + \delta g)u \tag{1.11}$$

and assume for algebraic simplicity that $y=h(x)=x$. A common cause for such model perturbations is the aerodynamic data uncertainty. Another source of perturbation is added to the robustness analysis. In (1.12), the ideal control effector position is replaced with a perturbed value obtained by passing the ideal position through actuator dynamics, flexible structural elements, and other high-frequency uncertainties

$$u = (I + \Delta)g(x)^{-1}(-f(x) + \dot{y}^{des}) \tag{1.12}$$

where $\Delta(s)$ is an arbitrary stable dynamic perturbation, small for low frequency signals, but increasing in size to unity and beyond as frequency increases. A short derivation shows that the resulting dynamic model for $\dot{y} = C\dot{V}$ is then given by

$$\dot{y} = C\dot{V} = (\delta f - \mathbf{D}f) + (I + \mathbf{D})\dot{y}^{des} \tag{1.13}$$

with

$$\mathbf{D} = g\Delta g^{-1} + \delta g g^{-1} + \delta g \Delta g^{-1} \tag{1.14}$$

These equations replace the integrators as a new dynamic model for the CVs. Note that there are two major uncertainty terms. The first term, $(\delta f - \mathbf{D}f)$, is a direct disturbance input to the integrators, while the second term, $(I + \mathbf{D})\dot{y}^{des}$, is a multiplicative perturbation on the control inputs of the integrators. Both terms are correlated through their common perturbation operator **D**, and all functions in this operator, *f, g, δf,* and *δg*, remain dependent on the state vector *x*.

Note that the new model is still almost linear. Only the perturbation terms are not linear. If this fact is ignored for the moment, well-established design methods are available to construct robust controllers. Perhaps the simplest of these are loop-shaping methods, which satisfy norm-based robustness constraints on the CV-feedback loops [18]. If the multiplicative and direct disturbance terms are re-written in terms of $\mathbf{D}_a$ and $\mathbf{D}_m$, which are dependent on y and $\dot{y}^{des}$ terms, respectively (see Ref. 5 for details), then there are two basic constraints:

(1) sufficient conditions for robust stability with respect to the multiplicative term alone

$$\sigma_{\max}\left[(I + K(s)P(s))^{-1}K(s)P(s)\right] < \frac{1}{\sigma_{\max}\left[D_m(s)\right]} \text{ for all } s = j\omega \tag{1.15}$$

(2) sufficient condition for robust stability with respect to the direct disturbance term alone

$$\sigma_{\min}\left[(I + K(s)P(s))\right] > \sigma_{\max}\left[D_a(s)P(s)\right] \text{ for all } s = j\omega \tag{1.16}$$

In these expressions, *P(s)=I/s* is the nominal plant and *K(s)* is the feedback compensator for the CV-loop.

High-frequency constraints are imposed by the multiplicative term, which requires that the loop be rolled off before the magnitude of $\mathbf{D}_m(s)$ exceeds unity. Low-frequency constraints are imposed by the direct disturbance term, which calls for sufficient low-frequency gain to overpower any destabilizing effects of $\mathbf{D}_a(s)$. Combining these two extremes gives the familiar loop-shaping requirements. Whenever the above loop-shaping constraints are widely separated, simple CV compensators suffice like the one employed for HARV aircraft[2].

In more challenging situations, when the frequency-domain constraints are tight, the fact that the direct disturbance and multiplicative perturbations occur together and in a correlated way can no longer be ignored. Any of the sophisticated modern multivariable design tools could then be brought to bear to execute the design. Arguably, the most powerful of these is the μ-synthesis method [19, 20].

If the critical assumption of linearity is removed, the formal design options are much less powerful. This occurs because formal norm-based robustness conditions for general nonlinear perturbations are blunt instruments. Consider the following generalization of (1.15) and (1.16), derived from the small gain theorem (see Ref. 5 for more details).

(1) sufficient condition for robust stability with respect to the nonlinear multiplicative form alone

$$\left\| (I + KP)^{-1} KP \right\| < \frac{1}{\left\| D_m \right\|} \tag{1.17}$$

(2) sufficient condition for robust stability with respect to the nonlinear direct disturbance alone

$$\left\| (I + KP)^{-1} P \right\| < \frac{1}{\left\| D_a \right\|} \tag{1.18}$$

Here the symbol $\| (\cdot) \|$ denotes an induced operator norm. This norm corresponds to the largest input/output gain of the operator taken over all signals. If the operator is linear, the norm is equal to the largest magnitude of its frequency response taken over all frequencies. Thus, the left-hand side of (1.17) is nothing more than the M-peak, the maximum value of the magnitude curve, of the CV-loop's closed loop transfer function.

On the other hand, the right-hand side of (1.17) is more complicated. To examine this term, consider an "optimistic" version of $\mathbf{D}_m$ given by

$$\mathbf{D}_m = g(x)\Delta g(x)^{-1} \tag{1.19}$$

The norm above is equal to the M-peak of the linear actuator/flex perturbation in the control channels of the aircraft and is typically much greater than unity.

Thus, (1.17) can be satisfied only if the M-peak of the CV-loop is much smaller than unity. This requires very small loop gains, *i.e.*, $|K(s)P(s)|<<1$ for all $s=j\omega$. Unfortunately, such gains cannot satisfy (1.18) because it requires large loop gains to make the M-peak of $(1+KP)^{-1}P$ small enough. Thus, the formal robustness guarantees of the nonlinear theory currently do not help in design.

1.2.1.6 Global Stability Results

One aspect of dynamic inversion concept is the presence of hidden zero dynamics. The zero dynamics[15] is a set of system responses that is not observed in the output but is influenced by the control action. They may also present a problem to system performance if not properly handled.

These dynamics are implicitly defined by the selected CVs and must be examined separately to ensure that they are stable and well behaved. While it is far from trivial to establish properties of zero dynamics globally, local properties obtained from linearizations are often enough to identify potential problems[5].

A recent global stability result for dynamic inversion applied to nonlinear rigid aircraft pitch-axis dynamics appeared in Reference 14 and is summarized in this section. Even though both the airplane model and the control law are somewhat simplified, the result is an important building block for future analysis. The following discussion is to establish under what circumstances can necessary and sufficient conditions for global stability of closed loop system with a dynamic inversion controller hold.

The aircraft longitudinal axis model is based on body-axis coordinates with four states (U, velocity in longitudinal (x) axis; W, velocity in vertical (z) axis; q, pitch rate; and θ, pitch attitude) and two control inputs (T, thrust; and δ, elevator angle). To define the equilibrium set, assume T and θ fixed. At equilibrium, $q=0$ and the only unspecified terms are aerodynamic forces and moments. The aerodynamic forces in the U, W degrees of freedom must exactly balance out gravity and thrust forces, thus being completely determined for any point in (U,W) space.

In practice, aircraft stability cannot be expected under all possible flight conditions. For the purpose of analysis, two different sub problems of stability are considered:

1. assume unlimited control authority and work globally, or
2. restrict attention to a subset of the states on which control authority is adequate.

In what follows, only the first sub problem, *i.e.*, the discussion of global results, is considered.

The control problem can be stated as follows:

Given an equilibrium state $\bar{x}$, determine a controller u=K(x, $\bar{x}$) so that $\bar{x}$ is a global attractor for the system

$$\dot{x} = f(x, K(x, \bar{x})) \tag{1.20}$$

Any global attractor must be an equilibrium state. This problem is addressed using dynamic inversion for vehicle models having a unique equilibrium point for appropriately chosen engine thrust, T.

The approach is to invert the rotational degrees of freedom to a set of stable, second order dynamics. The steps include constructing controller K, showing stability of the attitude dynamics, and addressing the stability of zero dynamics. A desired stable set of second-order linear dynamics for θ is

$$\dot{q}_{cmd} = -2\xi\omega q - \omega^2(\theta - \theta_{cmd}) \tag{1.21}$$

With this controller, the closed loop dynamics decouple into velocity dynamics (U,W) given by

$$\begin{bmatrix} \dot{U} \\ \dot{W} \end{bmatrix} = \begin{bmatrix} -Wq \\ Uq \end{bmatrix} + \begin{bmatrix} -g\sin(\theta) \\ g\cos(\theta) \end{bmatrix} + \frac{1}{2m}\rho V^2 S \begin{bmatrix} \bar{C}_x \\ \bar{C}_z \end{bmatrix} + \frac{I_y \dot{q}_{cmd}}{\bar{c}mC_{M,\delta}(\alpha)} \begin{bmatrix} C_{x,\delta} \\ C_{z,\delta} \end{bmatrix} + \begin{bmatrix} T/m \\ 0 \end{bmatrix} \tag{1.22}$$

and attitude dynamics (q,θ) given by

$$\begin{bmatrix} \dot{q} \\ \dot{\theta} \end{bmatrix} = \begin{bmatrix} -2\xi\omega \\ 1 \end{bmatrix} q + \begin{bmatrix} -\omega^2(\theta - \theta_{cmd}) \\ 0 \end{bmatrix} \tag{1.23}$$

The dynamics of the attitude loop, (q,θ), have been reduced to linear by dynamic inversion and converge to $(0,\theta_{cmd})$.

For longitudinal axis models, computer simulations show that the pitch-attitude control strategy presented in (1.21) has excellent stability properties over extreme ranges

of initial and transient state conditions. The global stability result that follows provides an explanation for the above observations.

Theorem[14]**:** Assume that

1. the total drag coefficient

$$\bar{C}_D(\alpha) = C_D(\alpha) - C_{D,\delta}(\alpha)\frac{C_M(\alpha)}{C_{M,\delta}(\alpha)} > 0 \tag{1.24}$$

2. the aerodynamic function satisfy the dissipative condition

$$3\bar{C}_D(\alpha) + \frac{d\bar{C}_L}{d\alpha}(\alpha) > 0 \tag{1.25}$$

3. for a given T and cmd, the following equation of

$$\left(\frac{T}{mg} - \sin(\theta_{cmd})\right)\bar{C}_z(\alpha) - \cos(\theta_{cmd})\bar{C}_x(\alpha) = 0 \tag{1.26}$$

has only one solution $\alpha = \alpha^*$.

Then, for a given T and θ_{cmd}, the closed loop system (1.22)-(1.23) has a unique equilibrium $(\theta^*, q^*, U^*, W^*)$ given by

$$\theta^* = \theta_{cmd},\ q^* = 0$$

and

$$U^* = \sqrt{\frac{-2mg\cos(\theta_{cmd})}{\rho S\bar{C}_z(\alpha^*)}}\cos(\alpha^*), \quad W^* = \sqrt{\frac{-2mg\cos(\theta_{cmd})}{\rho S\bar{C}_z(\alpha^*)}}\sin(\alpha^*) \tag{1.27}$$

where α^* is the unique solution of (1.26).

Moreover any solution $(\theta(t), q(t), U(t), W(t))$ of the closed loop system (1.22)-(1.23) satisfies

$$\theta(t) \to \theta_{cmd},\quad q(t) \to 0,\quad U(t) \to U^*,\quad W(t) \to W^*$$

as $t \to \infty$. That is to say $(\theta_{cmd}, 0, U^*, W^*)$ is a global attractor of the closed loop system (1.22)-(1.23).

In practice, Assumptions 1 and 2 are valid. Hence, whether the system is globally stable or not depends on whether (1.26) has a unique solution, which in turn depends on the engine thrust, T, and the selected pitch attitude command, θ_{cmd}.

Now return to the question of stability of zero dynamics of the closed system (1.22). In the linear case, the issue of stability is related to right half plane zeros in the elevator to pitch angle transfer function. This transfer function has two such zeros[21] and under typical flight conditions for rigid body aircraft, these are both minimum phase. It has been mentioned in Reference 5, as well as in Reference 14, that the zeros of open loop plant become poles of the closed loop system when dynamic inversion is employed. This result has been both observed in practice[2, 5], including present work, and shown mathematically[14].

The stability robustness of the above result to uncertainty in the aerodynamic coefficients must be analyzed. If no uncertainty on the pitch moment exists, then the dynamics of the pitch attitude and the pitch rate are still decoupled from those of the velocities. The stability results for the nominal aerodynamic functions work immediately for the perturbed C_L, C_D, $C_{L,\delta}$ and $C_{D,\delta}$. This generalization is significant because it is the first result obtained for robustness of nonlinear dynamic inversion control laws for rigid fighter aircraft.

1.2.2 Integrated Flight/Structural Mode Control

The state-of-the-art for the second major issue for the research problem is discussed in this section. Since initial development and deployment of the B-1 bomber, which served as the most recent aircraft where structural modes had to be actively controlled, integrated flight/structural mode control (SMC) received limited coverage in open literature. The primary reason for this is unavailability of reasonable fidelity models that are not proprietary. In fact, the high fidelity HSCT model used as a proving ground for the research presented is restricted, though the results obtained with it are now publishable. Hence, the work in this area, until very recently, has concentrated in those agencies and companies that deal with the next generation of supersonic transports and had access to good models (Aerospatiale, Boeing, NASA). Very recently, an interest in this area has reemerged with the advent of different types of UAVs under consideration and will be addressed later in this section.

Conventional aircraft rely on flight control roll-off and notch filtering where controller roll-off is insufficient to attenuate flexible mode excitation. The B-1 bomber most closely approaches the problem of small separation between rigid body and flexible

mode dynamics. The first fuselage bending mode for the B-1 is at 18 rad/sec (2.8 Hz)[22], which makes the rigid body flexible dynamics separation considerably larger than that for an HSCT-type vehicle. The structural mode control system developed for the B-1 was the first of its kind in that it actively managed the flexible dynamics. One of the requirements for this system was that it was to be installed on top of an already existing flight control system and would not interfere with it in any way. Since the system was installed to provide a specific level of ride quality to the crew, the requirement of noninterference with flight control and the design of the two systems separately were consistent with the objective and the dynamics of the aircraft. This approach, while not optimal, was adequate for aircraft displaying the dynamic separation between rigid and flexible dynamics of the B-1. However, as discussed in later chapters and as been confirmed by other researchers[23, 24], the unprecedented small separation between rigid body and flexible modes of the HSCT type vehicle would make this approach completely inadequate. Briefly the reasons for this are that the desired flight controller bandwidth, to satisfy the flying qualities criteria, has less than a decade frequency separation with the first elastic mode. Furthermore, compromising and reducing the controller bandwidth would still result in insufficient roll off to attenuate flexible mode excitation. The elastic modes themselves are too closely spaced to make notch filters, a popular device for vehicles with large dynamic separation and only one or two modes in need of attenuation, an attractive option. The HSCT vehicle is roughly 2.5 times the size of the B-1 (see Fig. 1.3), which partially accounts for the differences in flexible dynamics, but the similarity in shape also foreshadows the similar control problems.

A step towards integrated flight/SMC was taken in Reference 25 where quantitative feedback theory was used for design of a longitudinal pitch-axis flight control system for a highly flexible B-1 type vehicle. The aircraft model utilized in this work was an integrated longitudinal/single flexible mode linear model that was artificially perturbed in the A, B, and C matrices to simulate uncertainty. This work showed that command-following, disturbance rejection, and desired handling qualities could be achieved with a single control surface without employing an active SMC but at the cost of much faster actuator dynamics than those available for the B-1. The dynamics were modeled as first order with 75 rad/sec break frequency vs. 10 rad/sec representative of the B-1.

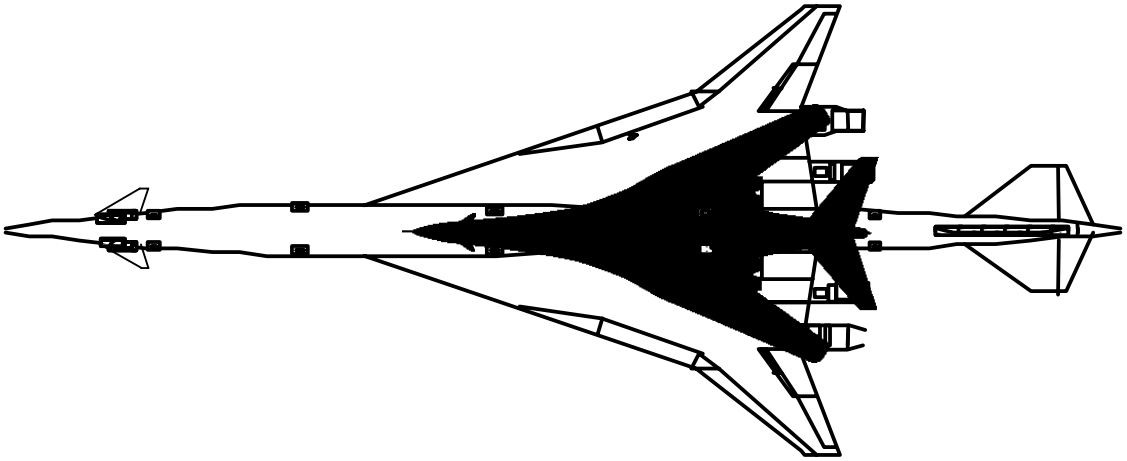

Figure 1.3: HSCT size comparison with B-1.

Work on an integrated flight/SMC control for a highly flexible aircraft with significant cross coupling between flight mechanics and flexible modes appeared in Reference 26. Based on the published open loop poles, the vehicle under consideration was indeed an HSCT class vehicle. The model used for control design and analysis was linear and consisted of the longitudinal rigid body model linearized about a steady-state condition and the aeroelastic model that includes aerodynamic lag terms, τ, (a general discussion of aeroelastic models follows in Chapter 3). These two models are coupled by connecting their respective measured outputs at the same structural points on the aircraft. The combined model is given by

$$\begin{aligned}
&\begin{pmatrix} \dot{x}_r \\ \dot{x}_e \end{pmatrix} = \begin{bmatrix} A_r & 0 \\ 0 & A_e \end{bmatrix} \begin{pmatrix} x_r \\ x_e \end{pmatrix} + \begin{bmatrix} B_r \\ B_e \end{bmatrix} \delta_q \\
&y = \begin{bmatrix} C_r & C_e \end{bmatrix} \begin{pmatrix} x_r \\ x_e \end{pmatrix} + \begin{bmatrix} D_r + D_e \end{bmatrix} \delta_q \\
&\text{where } x_r = \begin{bmatrix} V & \alpha & q & \theta & \int nz \end{bmatrix}^T, \; x_e = \begin{bmatrix} \eta_1 & \dot{\eta}_1 & \tau_1 & \dots & \eta_{10} & \dot{\eta}_{10} & \tau_{10} \end{bmatrix}^T \\
&y = \begin{bmatrix} nz & q & \int nz \end{bmatrix}
\end{aligned} \tag{1.28}$$

with the third order actuator dynamics completing the system. Note that this model does not reflect the interaction between the rigid body and the flexible mode states. The only cross coupling occurs at the output. To control this vehicle model a method that combines full state LQR for rigid body performance with guaranteed flexible mode

stability and output feedback that tries to recover this performance. The full state feedback LQR is used on the combined rigid/elastic model and the performance index weighting matrices are manipulated to place rigid body poles into an eigenspace that would provide the desired performance. The resulting controller would then provide rigid body performance compatible with flexible mode stability. The next step is to obtain an output feedback controller whose resultant closed loop dynamics are as close as possible to the ones produced by the LQR. The approach chosen to produce this output controller is the constrained minimization of the difference between the actual and desired eigenstructure produced by LQR

$$J = \sum_{i=1}^{P} p_i \left\| \lambda_i - \lambda_i^{des} \right\|_F \qquad K_{\min} < K < K_{\max} \tag{1.29}$$

where p_i are scalar weights, and constraints on K are defined for practical consideration of gain scheduling. The results for the model in (1.28) do provide stable pitch rate and normal acceleration response free of significant flexible mode dynamics to 0.1 g command. However, the model does not reflect the inherent complexity of dynamics for the aircraft with cross coupling between rigid body flight dynamics and structural dynamics so the proposed control technique cannot be adequately evaluated.

Other work related to an HSCT class vehicle focused on the attainment of multiple control objectives with minimal architecture[27]. This work approached the problem from classical sequential loop closing perspective. Two channel, two directional crossfeed control law architecture is proposed. One channel is dedicated to the pitch rate, or some blend thereof, and the second channel is the flexible mode dynamics channel. The perceived benefit of this technique is the clear and concise relationship between the design parameters and resulting closed loop features. Knowledge underlying the role of a particular feedback loop, or the effect from a specific dynamic compensation feature, upon the closed loop properties is advantageous. The difficulty arises from the fact that when the loops are closed sequentially, the designer must anticipate effects from the current loop closure upon channels yet to be closed. The control law architecture is provided in Figure 1.4. The elevator belongs to the rigid body channel and the ride control vane (RCV), (see Fig. 1.3), is associated with the flexible dynamics. $P_2(s)$ is a

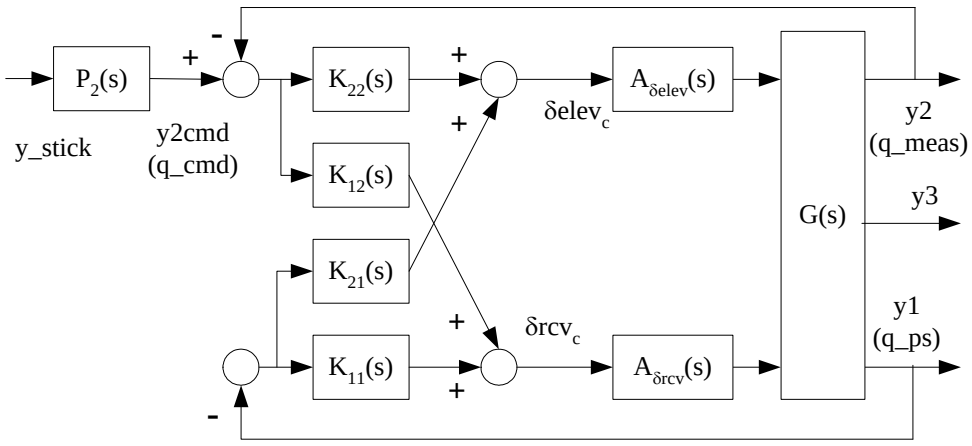

Figure 1.4: Multi-loop control law architecture.

command shaping filter, $A_\delta(s)$ are actuator dynamics, G(s) is the plant, and $K_{ij}(s)$ are individual dynamic filters. In the final result the $K_{ij}(s)$ filters are 3rd, 3rd, 3rd, and 4th order respectively with a 4th order command prefilter $P_2(s)$.

The model used for design and analysis of this controller was similar to the one discussed in this work and is based on the integrated rigid/structural mode dynamics, though necessarily linearized for application of this methodology. The controller simulation results are very favorable in response to small input commands and provide good robustness to gain and phase perturbations in individual loops. Here the difficulty in designing all of the dynamic filters and command prefilter is balanced by a classical controller architecture. This methodology presents a potential linear alternative to the novel dynamic inversion methodology explored in this work.

There is another potentially emerging area of research that employs integrated flight/SMC control. With a myriad of new development efforts for UAVs with a variety of missions, there is a renewed interest in the integrated flight/SMC. In addition to the problem formulated here, another issue arises that is not driven by close proximity of structural dynamics to those of rigid body, but instead by a possibility of designing such control without a good knowledge of the structural model. An adaptive control approach has been proposed to potentially replace structural mode filtering, which occurs in more typical flight vehicles such as missiles where the structural modes are relatively far away from rigid body dynamics compared to an HSCT class aircraft[28]. The control law is

based on the measured output, the regulated output, and the model inversion error. As in other adaptive control methods that utilize model inversion error and then use an adaptive neural network law to drive that error to zero[6, 29], this attempts to do the same but it lacks the inversion error since the structural model is unknown. This inversion model error is provided by an adaptive observer described in detail in Reference 30. At this stage, this approach is a candidate approach to either reducing the dependence of existing design on structural model filtering or eliminating the need for structural filtering in the future design altogether.

1.3 Contribution of This Work

The contribution of this work to the state of the art is predicated on the development and application of dynamic inversion methodology to handle highly flexible aircraft in an integrated flight/structural mode control manner. The development and evaluation are performed on a sophisticated, high fidelity, nonlinear dynamic model across the frequency spectrum. The dynamic nature of structural modes and the flight control reciprocal interaction with flexible modes because of unprecedented small separation between rigid body and flexible modes are the key elements of the aircraft model. An innovation to the standard methodology of dynamic inversion has been introduced in the manner described in this work to accommodate the nature of the vehicle and fulfill the dual objectives of integrated flight/SMC control. These objectives constituted command following, disturbance rejection in the rigid body, improved structural dynamic damping to minimize excitation from turbulence, and rendering the aircraft rigid from the pilot station perspective.

The novel approach to the nonlinear dynamic inversion allows the methodology to more intelligently handle flexible dynamics (or any dynamics with pole-zero pairs very close to the jω-axis). In the standard dynamic inversion, the controlled variable's dynamics are cancelled by the controller, which may or may not be an appropriate approach. This new approach to standard dynamic inversion still maintains control of CVs while the innovation allows a change to the dynamics of the controlled variable without cancellation of its dynamics. This is accomplished by introducing dynamics into the inversion loop itself. What this novel approach enables is altering flexible mode damping without cancellation, thus improving disturbance response and avoiding the

potentially destabilizing effect of pole cancellation close to the jω-axis in case of modeling uncertainty.

The structural nature of the modification to the standard dynamic inversion methodology and its effect on the necessary level model complexity for design has been established with particular attention given to establishing physical understanding of the control design process. Furthermore, the effect of uncertainty in the structural mode dynamics has been addressed as well.

Further contribution is addressing the issue of dynamic inversion and stability of highly flexible aircraft studied in this work from the mathematical perspective. The approach is rather straight forward. The vehicle driven by a controller must reach some equilibrium whose stability must be evaluated. The results show how assessing stability of an n-dimensional system can be reduced to checking stability of a two-dimensional one using algebraic expressions that are based on the vehicle characteristics such as aerodynamic coefficients. This reduces a complicated dynamical problem to something purely algebraic and manageably complex. The results presented are the first to include flexible dynamics in stability analysis of the dynamic inversion methodology. These form an initial basis to more complicated control problem formulation that includes the novel dynamic inversion methodology employed to design an integrated flight/SMC controller for a high fidelity model discussed earlier. The changes in dynamics attributed to the innovation in the inversion methodology are explored for both linear and nonlinear systems. This work has added to both analytical and physical insight regarding the nature of novel dynamic inversion applied to an integrated flight/structural mode control for a high flexible aircraft.

Furthermore, a new tool is introduced in an attempt to systematically find Lyapunov functions that would guarantee local stability for the nonlinear system with the novel dynamic inversion controller alluded to above. The tool, called SOSTOOLS, is based on the Sum of Squares decomposition for finding a Lyapunov function algorithmically.

Portions of this work have been published in publicly available forums and are included in the reference section[31–33].

1.4 Organization of the Thesis

This dissertation is divided into eight chapters each addressing a major component of the work. There are also five appendices each containing important information and results pertinent to the main results but not central to them. The chapters are divided as follows. Chapter 2 provides a brief overview to the dynamic inversion, discussing necessary background for a reader who might not be familiar with the technique. Chapter 3 concentrates on the development of the sophisticated, high fidelity, nonlinear dynamic model of the highly flexible aircraft across the frequency spectrum. The development touches on the general unsteady aerodynamic influences on the structural modes and how his was incorporated in to the standard aircraft equations of motion that retained the reciprocal dynamic rigid body and flexible dynamics. The open loop nature of the vehicle class model such way is also presented.

Chapter 4 introduces the novel dynamic inversion methodology in detail and explores the influence it has on the closed loop system dynamics. The design and evaluation of the control law based on this methodology in the high fidelity, full nonlinear simulation in the presence of turbulence and flexible mode uncertainty is discussed in Chapter 5. Chapter 6 continues the analysis with theoretical stability result concerning dynamic inversion and highly flexible aircraft. Chapter 7 touches on newly evolving methodology of proving stability by finding Lyapunov function based on sum of squares and applying this methodology to the problem at hand. Finally, Chapter 8 contains the conclusions and suggestions for further research.

Appendix A elaborates on the high fidelity simulation model by providing the buildup equations for the aerodynamic coefficients. Appendix B gives visual presentation to the flexible dynamics by showing the shape of the aircraft for the first few modes and then general shape and relative size of the first ten longitudinal modes. Appendix C includes two sub studies. The first involves parametric look at the ability to control both flight and structural deformations with only one surface. The second highlights results of the novel dynamic inversion controller applied to an alternative set of control effectors. Appendix D provides details on calculating *div(G)* that is necessary for proof of stability result in Chapter 6. And finally, Appendix E provides supporting work for stability analysis of the novel dynamic inversion presented in Chapter 7.

Chapter 2 – Introduction and Background to Dynamic Inversion

2.1 Introduction

Dynamic inversion, also known as feedback linearization, fundamentally is an algebraic transformation of a nonlinear system dynamics into a fully or partially linear and controllable one, so that linear control techniques can be applied. It deals with techniques for transforming original system models into equivalent models of a simpler form. The central premise of dynamic inversion control methodology is based on the idea that control effector commands are a sum of signals from essentially two different controllers that together comprise what is commonly known as a dynamic inversion controller. One part of the controller is based on the nonlinear model of the system and generates commands that would cancel the nonlinearities and make the actual system behave in the manner of first order linear dynamics, typically an integrator. The other part of the controller is linear in nature and issues commands that make the linear dynamics behave in a desired way. This linear controller is ideally the same throughout the region of interest, but in practice may be divided into two or three parts each representing a distinct dynamic regime for better system performance. It is designed as any linear controller to provide robustness for dynamics mismatch between the nonlinear system model and the actual system dynamics. The robust performance analysis on the entire dynamic inversion controller can be conducted at different flight conditions using a very powerful linear technique of μ-analysis. However, since the controller is nonlinear in nature and spans the entire flight envelope, one would like to perform analysis that would guarantee stability in the entire operating regime. Part of the current work proposes such a stability test.

A number of references give details on the underlying theory and methodology of dynamic inversion[15, 34]. The brief overview in this chapter provides important highlights that should facilitate the motivation behind the research presented.

2.2 Dynamic Inversion Brief Overview

2.2.1 Input-Output Linearization: SISO Case

Consider a nonlinear system that is affine in control variable *u* described by

$$\begin{aligned} \dot{x} &= F(x,u) \approx f(x) + g(x)u \qquad && x \in \mathbb{R}^n, u \in \mathbb{R} \\ y &= h(x) && y \in \mathbb{R} \end{aligned} \tag{2.1}$$

In order to produce an input-output controller, an explicit relationship between input *u* and output *y* must exist. At this point the notion of relative degree must be introduced. Informally, relative degree r is defined as exactly equal to the number of times one has to differentiate the output *y(t)* at $t=t_o$ in order to have the value of $u(t_o)$ of the input explicitly appearing. In a linear system this is equivalent to the difference between the number of poles and zeros. A system with a relative degree defined in some neighborhood of x^o allows us to transform the nonlinear system into *the normal form.* Prior to giving a formal definition of relative degree some mathematical tools need to be defined.

Definition: Let $h : \mathbb{R}^n \to \mathbb{R}$ be a smooth scalar function, and $f : \mathbb{R}^n \to \mathbb{R}^n$ be a smooth vector field on $\mathbb{R}^n$, then the *Lie derivative of* h *with respect to* f is a vector field defined by

$$L_f h(x) = \frac{\partial h}{\partial x} f(x)$$

Thus, the Lie derivative $L_f h$ is simply a directional derivative of h along the trajectories of the system $\dot{x} = f(x)$. The new notation is convenient for repeated calculation of the derivative with respect to the same or a different vector field. For example, repeated Lie derivatives can be defined recursively

$$L_f^0 h(x) = h(x)$$

$$L_f^k h(x) = L_f L_f^{k-1} h(x) = \frac{\partial (L_f^{k-1} h)}{\partial x} f(x)$$

Similarly, if g is another vector field, then the scalar function $L_g L_f h(x)$ is

$$L_g L_f h(x) = \frac{\partial (L_f h(x))}{\partial x} g(x)$$

The relevance of the Lie derivative to dynamic systems is easily apparent by considering the following SISO system

$$\dot{x} = f(x) + g(x)u$$
$$y = h(x)$$

then the derivatives of the output are

$$\dot{y} = \frac{\partial h}{\partial x}\dot{x} = L_f h(x) + L_g h(x)$$
$$\ddot{y} = \frac{\partial (L_f h + L_g h)}{\partial x}\dot{x} = L_f^2 h(x) + L_g L_f h(x) + L_f L_g h(x) + L_g^2 h(x)$$

and so on. Now the formal definition of relative degree can be given.

Definition: The single-input single-output nonlinear system (2.1) is said to have *relative degree r* at x^o if

$L_g L_f^k h(x) = 0$ for all x in a neighborhood of x^o and all $k<r-1$

$L_g L_f^{r-1} h(x^o) \neq 0$

Note that relative degree cannot be defined when $L_g h(x)$ that is not identically zero (in a neighborhood of x^o) has a zero exactly at the point $x = x^o$. An important property of relative degree is its invariance under coordinate transformation and feedback.

Using the notion of relative degree we introduce state space description of a dynamical system in *normal form*, which makes what transpires in input-output linearization clearer. Suppose the system has relative degree $r<n$ at x^o, then the first r equations are

$$\begin{aligned} \dot{z}_1 &= z_2 \\ \dot{z}_2 &= z_3 \\ &\ldots \\ \dot{z}_{r-1} &= z_r \\ \dot{z}_r &= b(z) + a(z)u \end{aligned} \tag{2.2}$$

There is no special structure for the last $n-r$ equations, which therefore will appear in a form below with input u explicitly present. In addition, the output of the system must be related to these new variables. Hence the rest of the equations are given by

$$\begin{aligned} \dot{z}_{r+1} &= q_{r+1}(z) + p_{r+1}(z)u \\ &\dots \\ \dot{z}_n &= q_n(z) + p_n(z)u \\ y &= z_1 \end{aligned} \tag{2.3}$$

The structure of these equations is nicely illustrated in Figure 2.1.

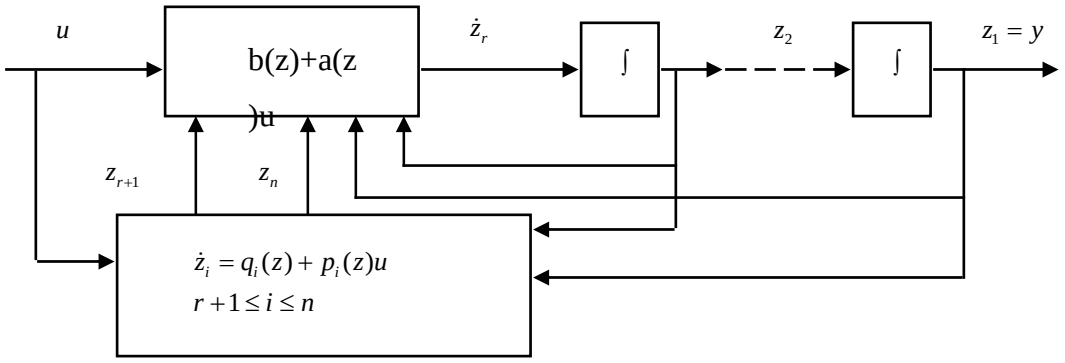

Figure 2.1: Nonlinear system equations in normal form.

Consider a nonlinear system with relative degree $r=n$ and suppose the following control law is chosen

$$u = \frac{1}{a(z)}(-b(z) + v) \qquad \text{where } v \text{ is an external reference input} \tag{2.4}$$

Then the resulting closed-loop system is governed by

$$\begin{aligned} \dot{z}_1 &= z_2 \\ \dot{z}_2 &= z_3 \\ &\dots \\ \dot{z}_{n-1} &= z_n \\ \dot{z}_n &= v \end{aligned} \tag{2.5}$$

that is linear and controllable. In other words, exact linearization via feedback is achieved and input v is connected to output y by a chain of r integrators illustrated below (Figure 2.2).

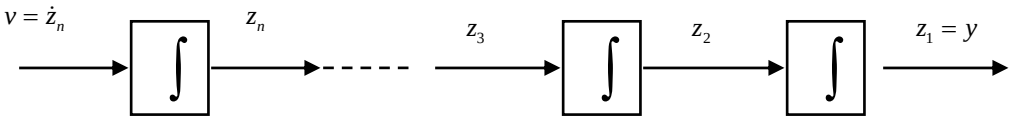

Figure 2.2: Exact feedback linearization.

If a system has *relative degree* $r<n$ for some given output h(x), then partial feedback linearization occurs. This system decomposes into *a linear subsystem*, of dimension r, which is the only one responsible for the input-output behavior, and a possibly nonlinear subsystem, of dimension n-r, whose behavior however does not affect the output. This case is depicted below (Fig. 2.3).

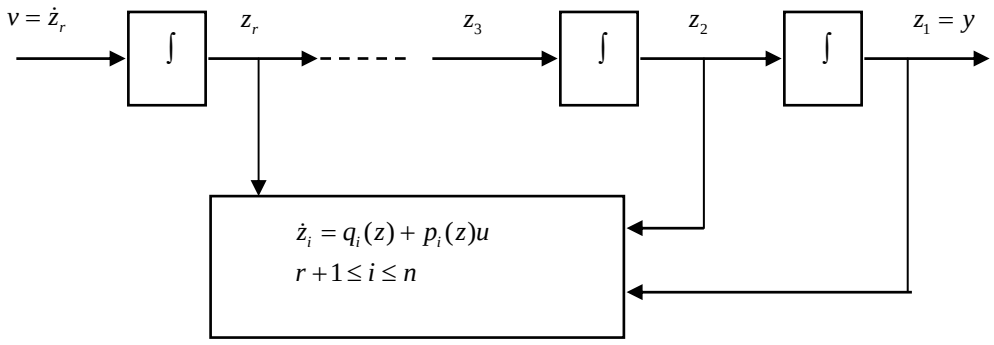

Figure 2.3: Partial feedback linearization.

As can be seen from Figure 2.3, the control u results in partial feedback linearization that makes n-r states unobservable at the output yet still influenced by the control action. These unobservable, *i.e.*, internal dynamics, are also referred to as zero dynamics because they correspond to the dynamics describing the "internal" behavior of the system when input and initial conditions have been chosen in such a way as to constrain the output to remain identically zero. In other words, the dynamics described by

$$\left.\begin{array}{l}\dot{z}_i = q_i(z) + p_i(z)u \\ r+1 \le i \le n\end{array}\right\} \Rightarrow \dot{\varphi} = q(0,\varphi) + p(0,\varphi)u \quad \text{where } z = T(x) = \begin{bmatrix} z_1 \\ \vdots \\ z_r \\ z_{r+1} \\ \vdots \\ z_n \end{bmatrix} \triangleq \begin{bmatrix} \xi \\ \varphi \end{bmatrix} \tag{2.6}$$

with *T(x)*, a diffeomorphism, controlling the behavior of the closed loop system, and thus its stability. These internal dynamics consist of open loop zeros, open loop uncontrollable modes, and open loop modes that are not the primary control objectives.

2.2.1.1 Zero-Dynamics

What happens to the remaining variables, *z*, in the new state vector when *y* is controlled but not *z*? This question deals with so-called zero-dynamics[15] of (2.1) and must be addressed by ensuring that these dynamics are stable and well behaved.

Conceptually, zero dynamics are nothing more than the remaining motions permitted by (2.1) when CVs in the output are constrained to be constant or prescribed. That is, they are the solutions of

$$\frac{dx}{dt} = \mathbf{F}(x,u) \text{ with constraints } \mathbf{H}(x) = c \tag{2.7}$$

If **F**(.,.) and **H**(.,.) were linear functions, *i.e.*, **F**(*x*,*u*)=**F***x*+**G***u* and **H**(*x*)=**H***x*, then these constrained solutions would be determined by the zeros of system (2.1). Specifically, with ν=0, they would satisfy

$$x(t) = \sum_i a_i x_i \exp(z_i t) \tag{2.8}$$

where a_i, i=1,2,..., p, are arbitrary constants and (z_i x), i=1,2,..., p, are zero/zero-direction pairs, defined by a generalized eigenvalue problem[35].

$$0 = \begin{bmatrix} z_i I - F & G \\ H & 0 \end{bmatrix} \begin{bmatrix} x_i \\ u_i \end{bmatrix} \tag{2.9}$$

Note that these constrained solutions are not observable in the outputs, *i.e.*, **H***x*=0, and they are stable and well behaved whenever all zeros of the CVs are located in the left half-plane and have reasonable damping ratios.

Zero dynamics are nonlinear generalizations of these same ideas, and CVs must likewise be chosen to make them stable and well behaved. One can use a linear interpretation to verify this behavior.

Although, all of these concepts have been illustrated on the system transformed into normal form, they could have been similarly derived in the original coordinates. It is instructive to look at internal dynamics in original coordinates since they control the stability of the closed loop system, which is a major part of this research. Let the control law in original coordinates be given by $u = \alpha(x) + \beta(x)\upsilon$. Notice that

$$y \equiv 0 \rightarrow \xi(t) \equiv 0 \rightarrow u \equiv \alpha(x(t)) \tag{2.10}$$

Thus, keeping the output identically zero implies

$y^{(i-1)}(t) = 0 \rightarrow L_f^{i-1}h(x(t)) = 0, \ \forall \ 1 \le i \le r$ and the system dynamics evolve on the subset

$$\mathbf{Z}^* = \left\{ x \in \mathbb{R}^n : h(x) = L_f h(x) = \cdots = L_f^{r-1}h(x) = 0 \right\} \tag{2.11}$$

that, locally around x^o, is exactly the same set of points whose new coordinates $z_1, \ldots, z_r$ are 0 (see Fig 2.4). And the input must be

$$u = u^*(x) \triangleq \alpha(x)\big|_{x \in Z^*} \tag{2.12}$$

which is constrained by

$$0 = y^{(r)}(t) = L_f^r h(x(t)) + L_g L_f^{r-1} h(x(t))u(t) \tag{2.13}$$

The restricted motion of the closed loop system on $\mathbf{Z}^*$, the smooth manifold of dimension n-r, is described by

$$\dot{x} = f^*(x) \triangleq \left[f(x) + g(x)\alpha(x) \right]_{x \in Z^*} \tag{2.14}$$

The vector field $f^*(x)$ is tangent to $\mathbf{Z}^*$ for all $x \in Z^*$, consequently any trajectory of the closed loop system staring at a point of $\mathbf{Z}^*$ remains in $\mathbf{Z}^*$ (for small values of t).

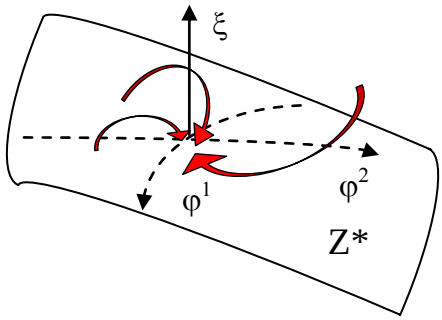

Figure 2.4: Closed loop internal dynamics behavior.

2.2.2 Input-Output Linearization: MIMO Case

Generalizing the SISO results to the multi-input multi-output case, we restrict the analysis to the consideration of systems with equal number of inputs and outputs, *i.e.*, $u, y \in \mathbb{R}^m$,

$$\begin{aligned} \dot{x} &= f(x) + \sum_{i=1}^{m} g_i(x) u_i \\ y_1 &= h_1(x) \\ &\cdots \\ y_m &= h_m(x) \end{aligned} \tag{2.15}$$

with $f(x), g_1(x), \ldots, g_m(x)$ are smooth vector fields, and $h_1(x), \ldots, h_m(x)$ are smooth functions defined on an open set of $\mathbb{R}^n$. One immediate difference is an appropriate definition of the multivariate relative degree.

Definition: A multivariate nonlinear system (15) is said to have *(vector) relative degree* $\{r_1, \ldots, r_m\}$ at x^o if

(1) $L_{gj} L_f^k h_i(x) = 0$ for all x in a neighborhood of x^o and for all

$1 \le j \le m,\ k < r_i - 1,\ 1 \le i \le m$

(2) the *mxm* matrix

$$A(x)=\begin{pmatrix} L_{g_1}L_f^{r_1\text{-}1}h_1(x) & \cdots & L_{g_m}L_f^{r_1\text{-}1}h_m(x) \\ L_{g_1}L_f^{r_2\text{-}1}h_2(x) & \cdots & L_{g_m}L_f^{r_2\text{-}1}h_2(x) \\ \cdots & \cdots & \cdots \\ L_{g_1}L_f^{r_m\text{-}1}h_m(x) & \cdots & L_{g_m}L_f^{r_m\text{-}1}h_m(x) \end{pmatrix}$$

is nonsingular at $x = x^o$.

Assumption 2 is restrictive but it allows a straightforward extension of most of the results developed for SISO case. Nonsingularity of $A(x^o)$ may be interpreted as a multivariable equivalent to the assumption that coefficient

$$\alpha(x^o) = L_g L_f^{r\text{-}1} h(x^o) \tag{2.16}$$

is nonzero in a single-input single-output case, which is fundamental for inversion.

The notion of zero dynamics that parallels the single-input single-output case can now be developed. In order to yield $y(t) \equiv 0$ for all times, the system must evolve on the subset

$$\mathbf{Z}^* = \left\{ x \in \mathbb{R}^n : L_f^k h_i(x) = 0,\ 0 \le k \le r_i - 1,\ 1 \le i \le m \right\} \tag{2.17}$$

under the effect of control $u(t)$ constrained by

$$0 = \begin{pmatrix} L_f^{r_2} h_1(x(t)) \\ L_f^{r_2} h_2(x(t)) \\ \vdots \\ L_f^{r_m} h_m(x(t)) \end{pmatrix} + A(x(t))u(t) = b(x(t)) + A(x(t))u(t) \tag{2.18}$$

The solution to this equation

$$u^* = -A^{-1}(x)b(x) \tag{2.19}$$

is such that the closed loop vector field $f^*(x) \triangleq \left[f(x) + g(x)u^*(x) \right]_{x \in Z^*}$ is tangent to $\mathbf{Z}^*$, and any trajectory of the closed loop system staring at a point of $\mathbf{Z}^*$ remains in $\mathbf{Z}^*$ (for small values of t).

The most important results from the general discussion of dynamic inversion performed on special type of nonlinear systems described in (2.1) and (2.15) are summarized as follows. The feedback linearization problem (exact or partial) is solvable

if and only if the system under consideration has some (vector) relative degree. Furthermore, in case relative degree of the specified input-output is less than the dimension of the state vector, the stability of the closed loop system is governed by the behavior of zero or internal dynamics. At this point it becomes instructive to transition from general nonlinear systems to specificity of aircraft nonlinear system.

2.3 Dynamic Inversion for Aircraft

The fundamentals of dynamic inversion control methodology are based on the idea that control effector commands are a sum of signals from essentially two different controllers that together comprise what is commonly known as a dynamic inversion controller. One part of the controller is based on the nonlinear model of the aircraft and generates commands that would make the actual aircraft behave in the manner of first order linear dynamics, typically an integrator, throughout the flight envelope. The other part of the controller is linear in nature and issues commands that make the linear aircraft dynamics behave in a desired way. This linear controller is ideally the same throughout the flight envelope, but in practice may be divided into two parts such as one for subsonic and one for supersonic flight regimes. It is designed as any linear controller to provide robustness for dynamics mismatch between the onboard aircraft model and the actual vehicle. The robust performance analysis on the entire dynamic inversion controller can be performed at different flight conditions using a very powerful linear technique of μ-analysis. However, since the controller is nonlinear in nature and spans the entire flight envelope one would like to perform analysis that would guarantee robustness in the entire operating regime. Unfortunately, the current state of the art in theory does not provide a meaningful test.

The general format for the dynamic inversion controller explored in this paper can be summarized as follows. Nonlinear aircraft dynamics naturally lend themselves to be expressed in control affine form, which in fact permits the use of dynamic inversion. Consider an input/output nonlinear aircraft dynamics to be given in the form of

$$\dot{x} = F(u, x) \approx f(x) + g(x)u \tag{2.20}$$

where x is the vector of state variables, and u is the vector of control effectors. Note that any aircraft outputs are a function of the state variables and can be used as the CVs for (2.20):

$$y = h(x). \tag{2.21}$$

Continuing with the idea that CVs, *y*, are functions of state variables, we see from (2.22) that the time rate of change of the output is also in the form similar to (2.20) and allows us to solve for the required control inputs:

$$\dot{y} = \frac{\partial h(x)}{\partial x}\dot{x} = h_x(x) f(x) + h_x(x) g(x) u \,. \tag{2.22}$$

So the dynamic inversion part of the control law appears:

$$u^{cmd} = \left[h_x(x) g(x)\right]^{-1} \left[\dot{y}^{des} - h_x(x) f(x)\right] \tag{2.23}$$

with $h_x(x)g(x)$ invertible for all values of *x*. For an aircraft with multiple control effectors for a single axis or more effectors than control objectives, $(h_x(x)g(x))^{-1}$ in (2.23) should be interpreted as a (non-unique) right inverse. A method to allocate control requirements to the different effectors is required in the case of non-unique right inverse[36, 37].

The linear controller defines the desired aircraft dynamics. For the initial application of the dynamic inversion methodology, we applied a simple PI-like controller structure, shown in (2.24), in order to gain better understanding of the results. The integral part of the feedback was incorporated in order to decrease the sensitivity of the closed loop response to modeling errors and low frequency atmospheric disturbances. With integral feedback, the desired dynamics for the control variables are

$$\dot{y}^{des} = K\left[K_{cmd} y^{cmd} - y^{meas} + K_i \int \left(y^{cmd} - y^{meas}\right) dt\right] \tag{2.24}$$

where *K*, K_{cmd}, and K_i are adjustable gains and perfect sensors $(y = y^{meas})$ are assumed in the design. The integral term implies that the control variable will have zero steady state error in response to step commands in the presence of model errors and constant disturbances.

Though not explicitly considered here, desirable pilot handling qualities are achieved by precompensation of stick and pedal commands, and trim inputs. The pilot inputs are scaled with flight condition dependent gains and a first order shaping filter to achieve time constants other than those resulting from feedback objectives.

An illustration of this general concept is depicted in Figure 2.5.

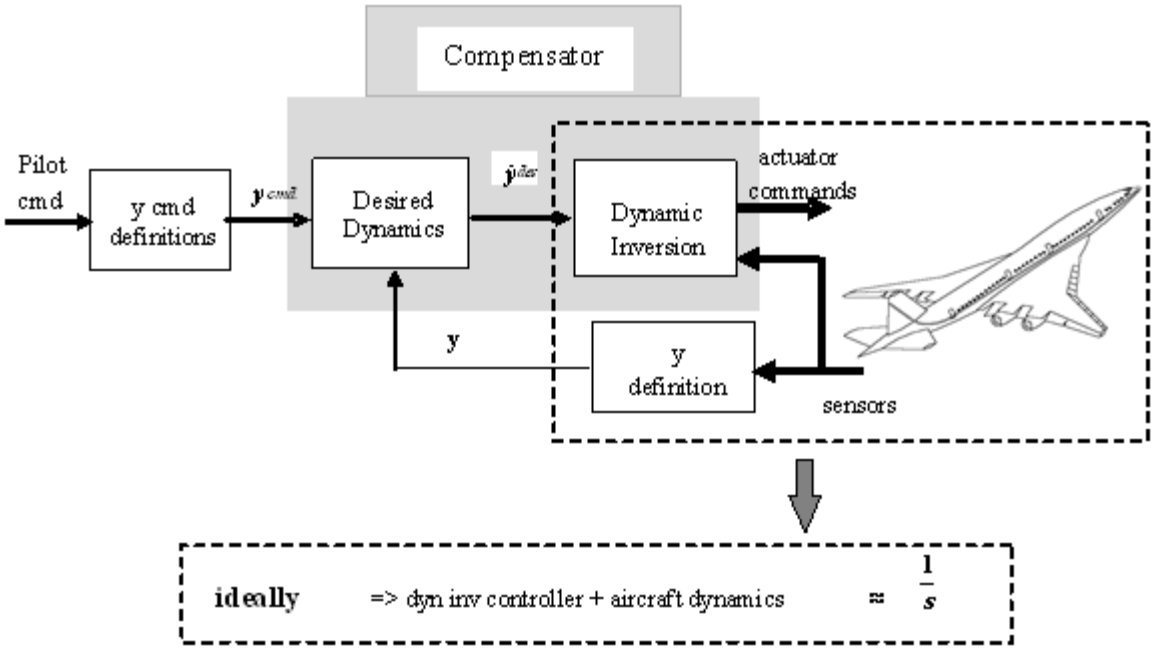

Figure 2.5: General scheme for dynamic inversion control for aircraft.

With this brief overview of dynamic inversion and its general application to aircraft dynamics, there is enough background material to facilitate the discussion of the specific problem of controlling large, highly flexible aircraft that has been the subject of this research.

Chapter 3 – Model Development

3.1 General Equations of Unsteady Motion

The basis for analysis, computation, or simulation of the unsteady motions of a flight vehicle is the mathematical model of the vehicle and its subsystems. An airplane in flight is a very complicated dynamic system. It consists of an aggregate of elastic bodies so connected that both rigid and elastic relative motions can occur. For example, the jet-engine rotor rotates, the control surfaces move about their hinges, and bending and twisting of the various aerodynamic surfaces occur. The external forces that act on the airplane are also complicated functions of its shape and its motion. The model developed to describe these interactions cannot be simple, but yet must be simple enough to be tractable. Traditionally, the vehicle is treated as a single rigid body with six degrees of freedom (6 DOF). This body is free to move in the atmosphere under the actions of gravity and aerodynamic forces – it is primarily the nature and complexity of the aerodynamic forces that distinguish airplanes from other dynamic systems.

The standard dynamic and kinematic equations of motion can be found in any number of references[21, 38], and thus are not given here. These equations consist of 15 coupled nonlinear ordinary differential equations in the independent variable *t* (12 of these are independent) and 3 algebraic equations. It is universally assumed in flight dynamics that the six forces and moments are functions of the six linear and angular velocities (u, v, w, p, q, r) and of a control vector. The latter clearly depends on the particular airplane, but with adequate generality, is written as $c = \begin{bmatrix} \delta_L & \delta_M & \delta_N & \delta_T \end{bmatrix}^T$ that is the roll, pitch, and yaw moments as well as the thrust control. From the standpoint of the mathematical system, the control variables are arbitrary functions of time. One other note: the Earth is treated as flat and stationary in inertial space. These assumptions simplify the model enormously and are acceptable for dealing with most problem of airplane flight.

It has been a long-standing practice to employ non-dimensional derivatives when analyzing the equations of motion or building a simulation of the airplane's behavior. This practice arose from using scaled wind tunnel models to provide data about the full-scale aircraft behavior.

It has been established over a number of years of research that the stability and control characteristics of flight vehicles may be profoundly influenced by the elastic distortions of the structure under dynamic load (like aileron reversal when the surface reverses the sign of the produced force or moment due to the severe elastic distortion)[39-41]. Many of the important distortions can be accounted for simply by altering the aerodynamic derivatives. The assumption is made that the changes in aerodynamic loading take place so slowly that the structure is at all times in static equilibrium. This is equivalent to assuming that the natural frequencies of vibration of the structure are much higher than the frequencies of the rigid-body motions. This is the standard assumption made in analysis for the vast majority of airplanes. When the separation in frequency between the elastic degrees of freedom and the rigid-body motions is not large, then significant inertial coupling can occur between the two. In that case, a dynamic analysis that takes into consideration the time dependence of the elastic motions is required.

Creating a viable aeroservoelastic (ASE) model for a class of large aircraft (B-747 weight class, 300 ft in length) with low frequency elastic modes (1+Hz) is a difficult problem. Traditionally, aeroservoelastic models either are created strictly for flutter analysis, which has much higher frequencies than flight control, or are simply appended to the rigid body models without accurate rigid-body/elastic cross-coupling. Neither case is useful for an HSCT-type aircraft because they both misrepresent dynamics involved in flight control. In fact, rigid-body/ASE interactions have been shown to be a major issue for control system design[23]. This work does not intend to address general modeling issues since these are beyond what is necessary for flight control; however, the significant progress that has been made under the auspices of the High Speed Research program in addressing these issues can be found in Reference 42 and other documents referenced therein[43-45]. The specific modeling issues pertaining to flight control, such as inertial coupling and unsteady aerodynamics, are briefly covered in this chapter.

3.2 Coupled Quasi-Steady/Dynamic Aeroelastic Equation Development

The problem is to augment the nonlinear quasi-static aeroelastic (QSAE) simulation with linear dynamic aeroelastic (DASE) effects while preserving the nonlinear QSAE

characteristics. This problem was motivated by the fact that conventional rigid body 6 DOF nonlinear simulation equations typically have quasi-static correction factors applied to the aerodynamics. Rigid body equations with QSAE corrections make use of two assumptions: (1) the airplane's deformation state is always in equilibrium with the air loads, (2) the air loads are well approximated by their steady flow solution. When the dynamic aeroelastic degrees of freedom are added to a 6 DOF simulation, the added elastic modes bring their own QSAE effect, and unless these are removed, the QSAE effects are double book kept in the simulation. The QSAE effects supplied with conventional "rigid" model are derived from high-fidelity finite element structural models and with higher-fidelity (for steady effects) aero codes than used to form dynamic aeroelastic models. Therefore, it is desired to retain the original QSAE effects.

In either case, the DASE integration with nonlinear simulation occurs as follows. The core of the simulation is a mathematical model represented by the equation

$$\dot{x}_{NL} = F(x_{NL}, u_{NL}) \tag{3.1}$$

where x_{NL} denotes an array of state variables that specify the aircraft motion. The function $F(x_{NL}, u_{NL})$ represents the solution to the nonlinear 6 DOF equations, which are based on information derived from an aerodynamic database as well as from models of the atmosphere, aircraft mass distribution, engine performance, and actuator characteristics. The initial conditions are computed using a constrained nonlinear optimization process that determines the equilibrium point where selected "trim-to" x_{NL} response values are generated from a set of "trim-with" u_{NL} variables. The equilibrium point is referred to as the trim point even though nonzero accelerations may be specified in the x_{NL} vector. Each selected output represents one degree of freedom or one constrained equation of motion. The trim procedure may contain a maximum of 11 equations defining three linear accelerations, three angular accelerations, aircraft velocity, rate of climb, sideslip, roll rate, and pitch rate. The u_{NL} set may include three linear velocities, three angular velocities, pitch angle, bank angle, control surface deflections, and engine thrust.

Aircraft structural dynamics are modeled by adding the unsteady aerodynamic part of the linear equations to the nonlinear simulation in the following manner

$$\dot{x} = F(x_{NL}, u_{NL}) + \Delta F_A x + \Delta F_B u \tag{3.2}$$

where *x* denotes a state vector that combines x_{NL} with the structural degrees of freedom. Similarly, *u* represents a vector of input variables. Defining the linear structural response equations in a manner that allows for efficient computation while maintaining model fidelity in "rigid" and flexible dynamic frequency range has been a major issue.

Of the two methods proposed in Reference 42, the method based on rational function approximation of unsteady aerodynamics was chosen to provide the DASE vehicle model. To accurately represent the underlying physics, the model for a class of highly flexible vehicles is derived from a more fundamental set of equations. The generalized force equation (3.3), is used to represent the equations of motion. The terms on the left hand side are rigid and elastic displacement states respectively and the terms on the right represent the generalized aerodynamic forces and moments acting on the airplane

$$\left(Ms^2 + Ds + K\right) \mathrm{X} = F^a = \bar{q}\,\hat{Q}\,\xi \tag{3.3}$$

where *M* is the generalized mass matrix, *D* is the generalized damping, and *K* is the generalized stiffness. The state vector X is a vector of rigid displacements, elastic displacements, and control deflections. The generalized coordinate ξ is in terms of rigid rates, elastic displacements, and gust velocities. The generalized mass matrix consists of vehicle mass and appropriate moments of inertia all modified by aerodynamic force and moment derivatives with respect to unsteady aerodynamic accelerations such as $(\dot{u}, \dot{v}, \dot{w}, \dot{p}, \dot{q}, \dot{r})$.

For a typical rigid body vehicle, the aerodynamic forces and moments are considered in steady state and the only unsteady aerodynamic terms are those associated with gust velocities. However, in an elastic aircraft all aerodynamic forces must be considered as unsteady. The generalized force, *Q*, premultiplied by dynamic pressure, is a complex matrix representing unsteady aerodynamic forces, which are Mach number and frequency dependent, arising from motion of the generalized coordinates, ξ. In order to express (3.3) in a state space representation, the generalized aerodynamic force matrix is

approximated with rational functions in s. This rational function approximation, described in detail in Reference 44, explicitly introduces state dependence on control surface rates and acceleration not typically present in standard equations of motion. The acceleration terms are from inertial mass coupling of actuators to the fuselage and directly influence aircraft states.

In order to focus on the question of rigid body and structural deformations, the equations of motion were separated into longitudinal and lateral-directional parts. As is generally the case with rigid aircraft, with the exception of rapid maneuvering at very high angles of attack, the longitudinal and lateral-directional separation holds for structural deformations of the vehicle. Thus, two different axes of motion can be studied separately without loss of important dynamics. This entire work focuses on the longitudinal axes of motion, and any future reference to the equations of motion pertains strictly to the longitudinal axes.

3.3 Aircraft Equations of Motion

The aircraft longitudinal equations of motion based on the properly integrated quasi-steady/dynamic aeroelastics consist of four aircraft states (u, w, θ, q), i flexible mode representations $(\eta_i, \dot{\eta}_i)$, and third order actuator dynamics $(\delta_j, \dot{\delta}_j, \ddot{\delta}_j)$ for j surfaces that reflect the presence inertial mass coupling of actuators to the fuselage and directly influence aircraft states.

$$\begin{pmatrix} \dot{u} \\ \dot{w} \\ \dot{q} \\ \dot{\theta} \\ \ddot{\eta}_j \\ \dot{\eta}_j \\ \dot{\delta}_p \\ \ddot{\delta}_p \\ \dddot{\delta}_p \end{pmatrix} = \begin{pmatrix} -qw - g\sin\theta + \dfrac{T}{m} \\ qu + g\cos\theta \\ 0 \\ q \\ 0 \\ \dot{\eta}_j \\ 0 \\ 0 \\ 0 \end{pmatrix} + \overline{a} \begin{pmatrix} \dfrac{C_x(\alpha,M) + C_{xq}(\alpha,M) + C_{x\dot{q}}(\alpha,M) + C_{x\dot{\alpha}}(\alpha,M)}{m} \\ \dfrac{C_z(\alpha,M) + C_{zq}(\alpha,M) + C_{z\dot{q}}(\alpha,M) + C_{z\dot{\alpha}}(\alpha,M)}{m} \\ \overline{c}\dfrac{C_M(\alpha,M) + C_{Mq}(\alpha,M) + C_{M\dot{q}}(\alpha,M) + C_{M\dot{\alpha}}(\alpha,M)}{I_y} \\ 0 \\ 0 \\ 0 \\ 0 \\ 0 \\ 0 \end{pmatrix}$$

$$+ \overline{a} \begin{pmatrix} \dfrac{C_{x,\eta_i}(\alpha,M,GW^*)}{m} \\ \dfrac{C_{z,\eta_i}(\alpha,M,GW^*)}{m} \\ \dfrac{\overline{c}C_{M,\eta_i}(\alpha,M,GW^*)}{I_y} \\ 0 \\ \dfrac{\overline{q}C_{\eta_j\eta_i}(M,GW^*)}{m_\eta} \\ 0 \\ 0 \\ 0 \\ 0 \end{pmatrix} \eta_i + \overline{a} \begin{pmatrix} \dfrac{C_{x,\dot{\eta}_i}(\alpha,M,GW^*)}{m} \\ \dfrac{C_{z,\dot{\eta}_i}(\alpha,M,GW^*)}{m} \\ \dfrac{\overline{c}C_{M,\dot{\eta}_i}(\alpha,M,GW^*)}{I_y} \\ 0 \\ \dfrac{\overline{q}C_{\eta_j\dot{\eta}_i}(M,GW^*)}{m_\eta} \\ 0 \\ 0 \\ 0 \\ 0 \end{pmatrix} \dot{\eta}_i + \frac{\overline{aq}}{m_\eta} \begin{pmatrix} 0 \\ 0 \\ 0 \\ 0 \\ C_{\eta_j\ddot{\eta}_i}(M,GW^*) \\ 0 \\ 0 \\ 0 \\ 0 \end{pmatrix} \ddot{\eta}_i$$

$$+ \frac{\overline{a}}{m_\eta} \begin{bmatrix} 0 & 0 & 0 \\ 0 & 0 & 0 \\ 0 & 0 & 0 \\ 0 & 0 & 0 \\ C_{\eta_i u}(M,GW^*) & C_{\eta_i w}(M,GW^*) & C_{\eta_i q}(M,GW^*) \\ 0 & 0 & 0 \\ 0 & 0 & 0 \\ 0 & 0 & 0 \\ 0 & 0 & 0 \end{bmatrix} \begin{pmatrix} u \\ w \\ q \end{pmatrix}$$

$$+\frac{\bar{a}}{m_\eta}\begin{bmatrix} 0 & 0 & 0 \\ 0 & 0 & 0 \\ 0 & 0 & 0 \\ 0 & 0 & 0 \\ C_{\eta_i \dot{u}}(M, GW^*) & C_{\eta_i \dot{w}}(M, GW^*) & C_{\eta_i \dot{q}}(M, GW^*) \\ 0 & 0 & 0 \\ 0 & 0 & 0 \\ 0 & 0 & 0 \\ 0 & 0 & 0 \end{bmatrix} \begin{pmatrix} \dot{u} \\ \dot{w} \\ \dot{q} \end{pmatrix} + \begin{pmatrix} 0 \\ 0 \\ 0 \\ 0 \\ 0 \\ 0 \\ 0 \\ 0 \\ \dfrac{C^{cmd}_{\delta_p, \delta_p}(\alpha, M, GW^*)}{m} \end{pmatrix} \delta_p^c$$

$$+\bar{a}\begin{bmatrix} \dfrac{C_{x,\delta_p}(\alpha, M, GW^*)}{m} & \dfrac{C_{x,\dot{\delta}_p}(\alpha, M, GW^*)}{m} & \dfrac{C_{x,\ddot{\delta}_p}(\alpha, M, GW^*)}{m} \\ \dfrac{C_{z,\delta_p}(\alpha, M, GW^*)}{m} & \dfrac{C_{z,\dot{\delta}_p}(\alpha, M, GW^*)}{m} & \dfrac{C_{z,\ddot{\delta}_p}(\alpha, M, GW^*)}{m} \\ \dfrac{\bar{c} C_{M,\delta_p}(\alpha, M, GW^*)}{I_y} & \dfrac{\bar{c} C_{M,\dot{\delta}_p}(\alpha, M, GW^*)}{I_y} & \dfrac{\bar{c} C_{M,\ddot{\delta}_p}(\alpha, M, GW^*)}{I_y} \\ 0 & 0 & 0 \\ \dfrac{C_{\eta_j,\delta_p}(M, GW^*)}{m_\eta} & \dfrac{C_{\eta_j,\dot{\delta}_p}(M, GW^*)}{m_\eta} & \dfrac{C_{\eta_j,\ddot{\delta}_p}(M, GW^*)}{m_\eta} \\ 0 & 0 & 0 \\ 0 & 1 & 0 \\ 0 & 0 & 1 \\ \dfrac{C_{\delta_p,\delta_p}(\alpha, M, GW^*)}{m} & \dfrac{C_{\delta_p,\dot{\delta}_p}(\alpha, M, GW^*)}{m} & \dfrac{C_{\delta_p,\ddot{\delta}_p}(\alpha, M, GW^*)}{m} \end{bmatrix} \begin{pmatrix} \delta_p \\ \dot{\delta}_p \\ \ddot{\delta}_p \end{pmatrix}$$

(3.4)

where m = vehicle mass,

m_η = generalized mass associated with an elastic mode

$\bar{a} = \frac{1}{2}\rho S V^2$ and $\bar{q} = \frac{1}{2}\rho V^2$, ρ = density, S = planform area, V = speed

and for $1 \le i, j \le N < \infty$, $N \in \mathbb{N}$, $1 \le p \le P \in \mathbb{N}$

The modal characterization of the aircraft is typically provided in terms of an orthogonal set of *in vacuo* modes. Each mode has an associated apparent mass which is simply vehicle mass modified by appropriate unsteady aerodynamic accelerations and properly scaled. The total structural displacement of the vehicle is a superposition of an infinite number of *in vacuo* modes, $z(x,y,t) = \sum_{i=1}^{\infty} \phi_i(x,y)\eta_i(t)$ where $\phi_i(x,y)$ is ith mode shape. In practice, the number of retained structural modes, *N*, is chosen by engineering judgment when the vehicle's elastic behavior is deemed "close enough." Thus, the above equations represent full nonlinear DASE longitudinal system with N elastic modes and P control actuators. It is interesting to note how such a vehicle would respond to a surface deflection at its tail generating a pitching moment. Such a response is illustrated in Figure 3.1 where both rigid aircraft and dominant first fuselage bending more are displayed. The initial response to nose down moment for the elastic vehicle is non-minimum phase, *i.e.*, response is in direction opposite of that commanded. This type of response has implications for flight control design and will be further discussed in the following chapters.

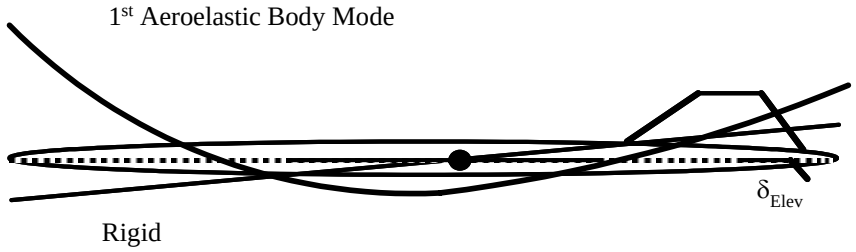

Figure 3.1: Vehicle response to elevator deflection:
(+) deflection (down) produces nose down moment.

The aircraft simulation used to numerically evaluate the results of this work uses the general model of equations of motion displayed in (3.4) with 20 flexible modes in the longitudinal and lateral-directional axis and third order actuator dynamics for each of the control surfaces on the airplane that include leading edge flaps, trailing edge flaps, rudder, ailerons, stabilator, elevator, and ride control vanes (see Fig. 3.2). The details as

to what is exactly included in each of these aerodynamic coefficients and how the force and moments coefficients are built-up are given in Appendix A. The equations in (3.4) result in a very large dimensionality of the model making it completely unsuitable for

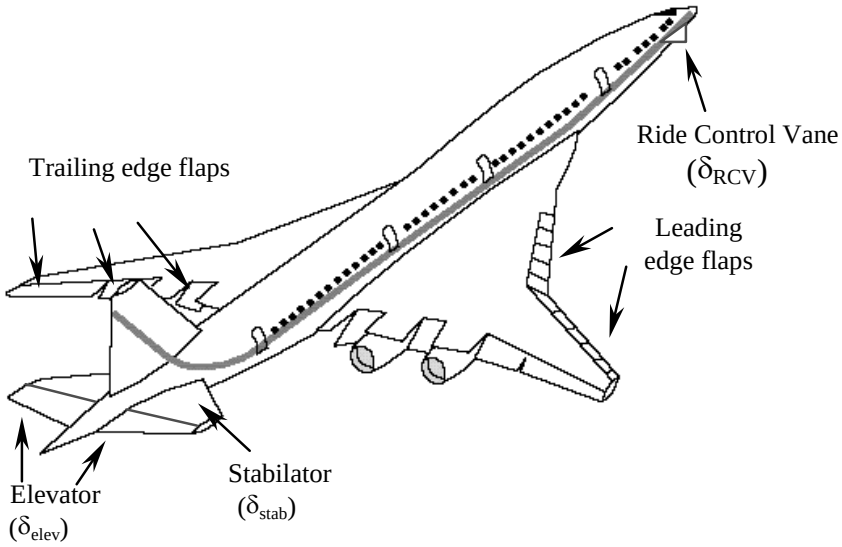

Figure 3.2: HSCT configuration.

both controller design and any analytical analysis. In fact, it would be difficult, if not impossible, to understand the fundamental dynamics of the rigid body and elastic mode interaction for a vehicle where there is minimal separation between these sets of dynamics and the close clustering among the elastic modes themselves. This understanding lies at the core of exploring dynamic inversion applicability to just such problems. Hence, simplifying assumptions that retain the important dynamics are imperative. The simplifying assumptions about the relative influence of some force and moment coefficients are made.

Assume that the following coefficients are negligible

$$\begin{aligned} &C_{(\bullet),\dot{q}} = C_{(\bullet),\dot{\alpha}} \approx 0 \qquad C_{(\bullet),q} \approx 0 \qquad C_{u,\eta,\dot{\eta}} \approx 0 \qquad C_{x,\eta} = C_{x,\dot{\eta}} \approx 0 \\ &C_{\eta,\dot{u},\dot{w},\dot{q}} \approx 0 \qquad C_{\eta,u} \approx 0 \qquad C_{\eta,\ddot{\eta}} \approx 0 \end{aligned} \tag{3.5}$$

and for control law design assume that the unsteady aerodynamic effects are small, $\dot{\delta} = \ddot{\delta} \approx 0$. Since designing a controller commanding actuator rates and accelerations is impractical, then the longitudinal DASE equations of motion simplify to

$$\begin{pmatrix} \dot{u} \\ \dot{w} \\ \dot{q} \\ \dot{\theta} \\ \ddot{\eta}_j \\ \dot{\eta}_j \end{pmatrix} = \begin{pmatrix} -qw - g\sin\theta + T/\mathrm{M} \\ qu + g\cos\theta \\ 0 \\ q \\ 0 \\ \dot{\eta}_j \end{pmatrix} + \bar{a} \begin{pmatrix} C_x(\alpha, M)/\mathrm{M} \\ C_z(\alpha, M)/\mathrm{M} \\ \bar{c}C_M(\alpha, M)/I_y \\ 0 \\ 0 \\ 0 \end{pmatrix} + \bar{a} \begin{pmatrix} C_{x,\eta_i}(\alpha, M, GW^*)/\mathrm{M} \\ C_{z,\eta_i}(\alpha, M, GW^*)/\mathrm{M} \\ \bar{c}C_{M,\eta_i}(\alpha, M, GW^*)/I_y \\ 0 \\ \frac{\bar{q}}{m} C_{\eta_j\eta_i}(M, GW^*) \\ 0 \end{pmatrix} \eta_i$$

$$+ \frac{\bar{a}}{m} \begin{bmatrix} 0 & 0 & 0 \\ 0 & 0 & 0 \\ 0 & 0 & 0 \\ 0 & 0 & 0 \\ C_{\eta_i u}(M, GW^*) & C_{\eta_i w}(M, GW^*) & C_{\eta_i q}(M, GW^*) \\ 0 & 0 & 0 \end{bmatrix} \begin{pmatrix} u \\ w \\ q \end{pmatrix}$$

$$+ \bar{a} \begin{pmatrix} C_{x,\dot{\eta}_i}(\alpha, M, GW^*)/\mathrm{M} \\ C_{z,\dot{\eta}_i}(\alpha, M, GW^*)/\mathrm{M} \\ \bar{c}C_{M,\dot{\eta}_i}(\alpha, M, GW^*)/I_y \\ 0 \\ \frac{\bar{q}}{m} C_{\eta_j\dot{\eta}_i}(M, GW^*) \\ 0 \end{pmatrix} \dot{\eta}_i + \bar{a} \begin{pmatrix} C_{x,\delta_p}(\alpha, M, GW^*)/\mathrm{M} \\ C_{z,\delta_p}(\alpha, M, GW^*)/\mathrm{M} \\ \bar{c}C_{M,\delta_p}(\alpha, M, GW^*)/I_y \\ 0 \\ C_{\eta_j,\delta_p}(M, GW^*)/m \\ 0 \end{pmatrix} \delta_p$$

with $1 \le i, j \le 20$ and $1 \le p \le 5$

(3.6)

A short remark on the composition of the coefficients $C_{\eta_j\dot{\eta}_i}$ and $C_{\eta_j\eta_i}$. In general, the frequency ω_j and damping ζ_j of the j[th] mode are contained in the $C_{\eta_j\dot{\eta}_j}$ and $C_{\eta_j\eta_j}$ respectively. This convention is followed with one exception. When uncertainty is introduced into the flexible modes, it is convenient to extract (ω_j, ζ_j) from the coefficients and treat them separately.

The next question to be asked is how many elastic modes must be included in the controller design. Can the model be reduced further and by how much and still retain the essential dynamics? Exploring this question is the focus of the rest of this chapter.

3.4 HSCT Dynamic Behavior

Typically, in trying to understand new complicated dynamics, we look for the simplest system to begin. In this case, the choice of a linear system at a flight condition where flexible modes are most prominent appears to be a logical place to start. The original aircraft system is described by a combined nonlinear/linear model with dynamics of interest, close proximity flexible modes, comprising the linear part of the model. Hence, choosing low altitude, low speed, light aircraft and linearizing the DASE model at this condition provides a good starting point in open loop system dynamic interactions.

The linear representation of the EOM, with third order actuator dynamics, 20 elastic modes and 5 control surfaces, assumes the form given in (3.7).

$$\begin{bmatrix} \dot{u} \\ \dot{w} \\ \dot{\theta} \\ \dot{q} \\ .... \\ \dot{\eta}_j \\ \ddot{\eta}_j \\ \dot{\delta}_p \\ \ddot{\delta}_p \\ \dddot{\delta}_p \end{bmatrix} = \begin{bmatrix} \bar{X}_u & \bar{X}_w & \bar{X}_\theta & \bar{X}_q & \bar{X}_{\eta_i} & \bar{X}_{\dot{\eta}_i} & \bar{X}_{\delta_p} & \bar{X}_{\dot{\delta}_p} & \bar{X}_{\ddot{\delta}_p} \\ \bar{Z}_u & \bar{Z}_w & \bar{Z}_\theta & \bar{Z}_q & \bar{Z}_{\eta_i} & \bar{Z}_{\dot{\eta}_i} & \bar{Z}_{\delta_p} & \bar{X}_{\dot{\delta}_p} & \bar{X}_{\ddot{\delta}_p} \\ \overline{TH}_u & \overline{TH}_w & 0 & 1 & 0 & 0 & 0 & 0 & 0 \\ \bar{M}_u & \bar{M}_w & 0 & \bar{M}_q & \bar{M}_{\eta_i} & \bar{M}_{\dot{\eta}_i} & \bar{M}_{\delta_p} & \bar{M}_{\dot{\delta}_p} & \bar{M}_{\ddot{\delta}_p} \\ 0 & 0 & 0 & 0 & 0 & 1 & 0 & 0 & 0 \\ \bar{E}_u & \bar{E}_w & \bar{E}_\theta & \bar{E}_q & \bar{E}_{\eta_i} & \bar{E}_{\dot{\eta}_i} & \bar{E}_{\delta_p} & \bar{E}_{\dot{\delta}_p} & \bar{E}_{\ddot{\delta}_p} \\ 0 & 0 & 0 & 0 & 0 & 0 & 0 & 1 & 0 \\ 0 & 0 & 0 & 0 & 0 & 0 & 0 & 0 & 1 \\ 0 & 0 & 0 & 0 & 0 & 0 & \bar{C}_{\delta_p} & \bar{C}_{\dot{\delta}_p} & \bar{C}_{\ddot{\delta}_p} \end{bmatrix} \begin{bmatrix} u \\ w \\ \theta \\ q \\ \\ \eta_i \\ \dot{\eta}_i \\ \delta_p \\ \dot{\delta}_p \\ \ddot{\delta}_p \end{bmatrix} + \begin{bmatrix} 0 \\ 0 \\ 0 \\ 0 \\ .... \\ 0 \\ 0 \\ 0 \\ 0 \\ \bar{C}_{\delta cm_p} \end{bmatrix} \delta_{cmd_p}$$

$$for\ i, j = \{1, 2, ..., 20\}\ and\ p = \{1, ..., 5\}$$

(3.7)

The control surfaces that might be used for longitudinal control on this vehicle are two trailing edge surfaces per wing, stabilator, elevon, and ride control vanes (see Fig. 3.2). The 20 symmetric elastic modes subdivide into primary fuselage modes and wing modes. The details of these modes are given in Appendix B.

It is of interest to look at the linear dynamics in terms of frequency response and pole location with actuator dynamics present before any further simplifications are made. Since the model contains closely spaced flexible modes in proximity to rigid body dynamics, the actuator dynamics would invariably play a significant role in their response. Before proceeding further it is important to mention the sensors measuring the

response of the vehicle. These are rate gyros and accelerometers located on the fuselage centerline, starting at the nose and going backwards all the way to the tail. Among these, two locations are of particular interest, the first is the pilot station (ps) and the second one is referred to as mean axis (ma). Since the mean axis refers to an imaginary line that approximates the middle of a rigid vehicle and does not physically exist, it is approximated by a sensor measurement that shows the least flexible mode contamination in measuring pitch rate; in this case is located behind the c.g. The physical locations of these sensors are at 359 inches and 2459 inches from the nose, respectively.

The effectiveness of control surfaces in producing pitch rate at different sensor locations on the aircraft fuselage is illustrated in Figures 3.3 and 3.4. As expected the elevon alone and in combination with the stabilator, creating an all-movable tail, has a far more powerful effect on the pitch rate across the frequency range than the RCV because of its much larger size. However, another important characteristic that is present for all responses is the excitation of the higher frequency dynamics and, in some cases (*e.g.*, q_ps), more excitation than at the lower frequencies. These responses underline the flexible nature of the vehicle under study and strongly suggest that some sort of counter damping to the movable tail excitation will be required for a satisfactory vehicle control. The significantly larger effect of the all-movable tail (stab+2*elev) compared to just the elevon suggests a powerful control effector for flight control but also reinforces the previous statement on counteracting high frequency dynamic excitation.

The observations made regarding open loop pitch rate dynamics also hold for normal acceleration. Consider nz response at the pilot station (nz_ps) and mean axis approximation (nz_ma) to different control surfaces depicted in Figures 3.5 and 3.6. Note a very large high frequency excitation at the pilot station from both only elevon and especially all-movable tail deflection (see Fig. 3.6). One positive fact emerges from both pitch rate response and normal acceleration response observations is that at the pilot station, the RCV has a significant impact on high frequency dynamics while its impact on the mean axis dynamics is significantly less. This would imply that the RCV can be used to counteract the high frequency dynamic excitation at the pilot station produced by the elevon or all-movable tail while having a limited impact on resisting the whole vehicle rotation as measured by the mean axis response.

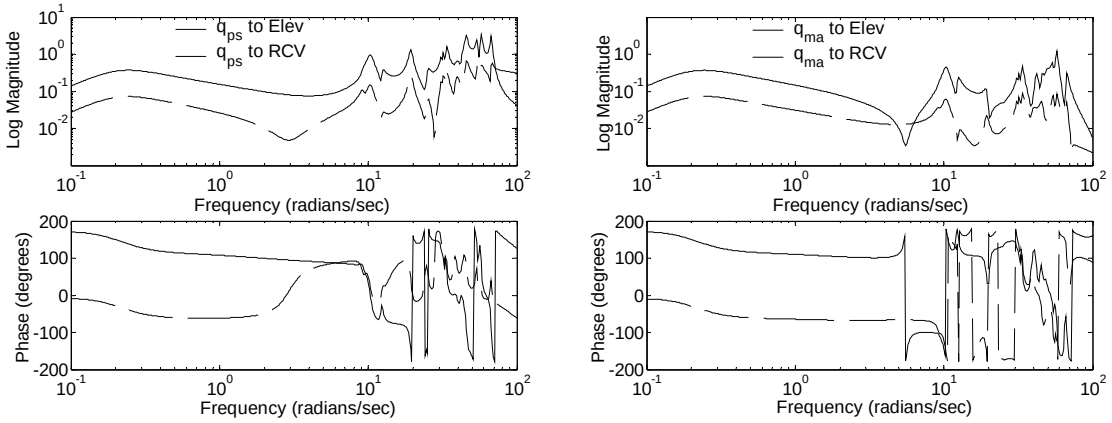

Figure 3.3: Open loop frequency response of pitch rate at the pilot station (q_{ps}) and mean axis approximation (q_{ma}) responses to control excitation at the back, elevon (solid), and the front, ride control vane (dashed), of the aircraft.

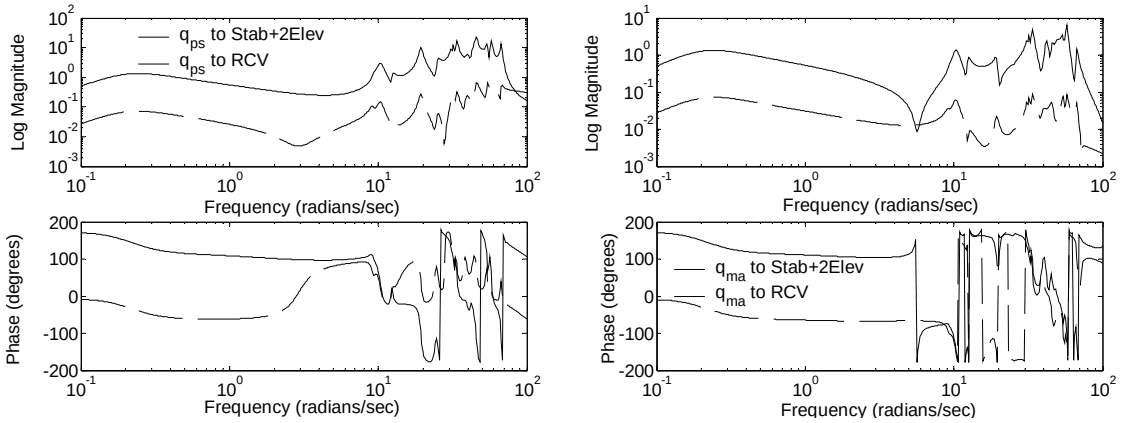

Figure 3.4: Open loop frequency response of pitch rate at the pilot station (q_{ps}) and mean axis approximation (q_{ma}) responses to control excitation at the back, all-movable tail (solid), and the front, ride control vane (dashed), of the aircraft.

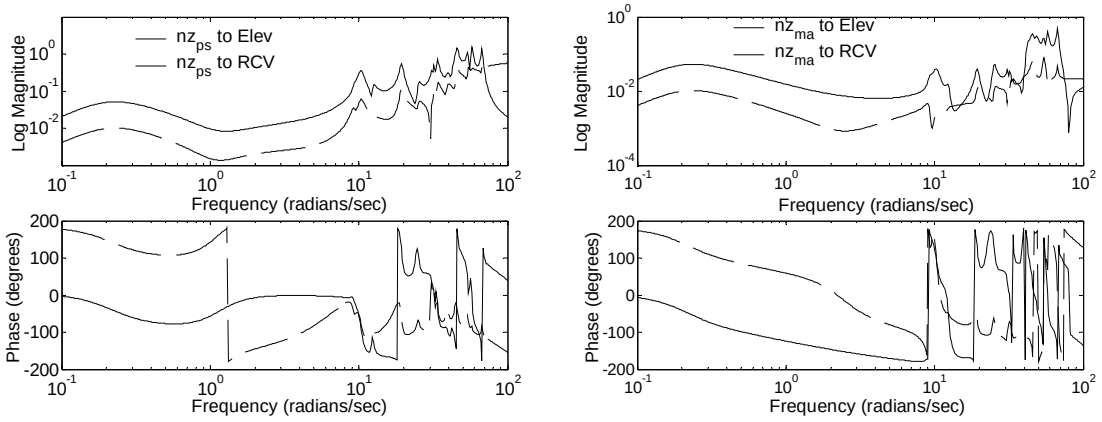

Figure 3.5: Open loop frequency response of normal acceleration at the pilot station (nz_{ps}) and mean axis approximation (nz_{ma}) responses to control excitation at the back, elevon (solid), and the front, ride control vane (dashed), of the aircraft (original response in g's).

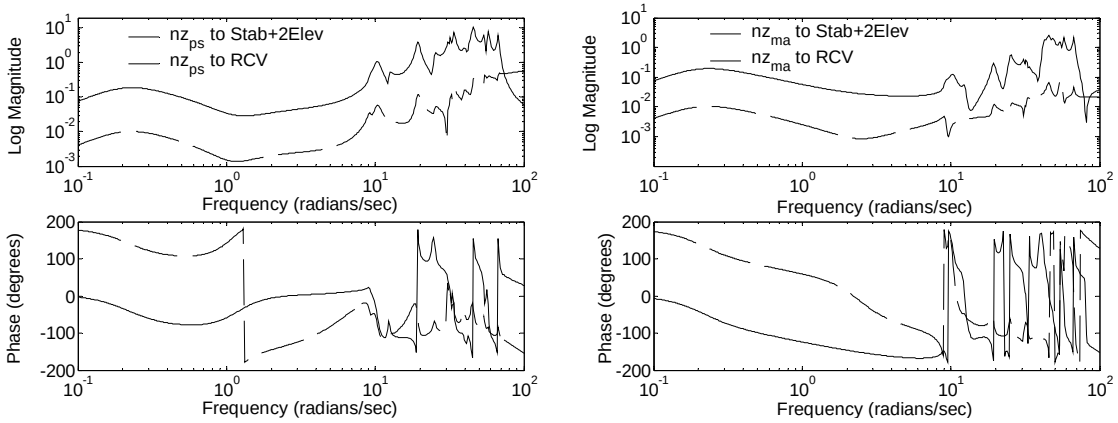

Figure 3.6: Open loop frequency response of normal acceleration at the pilot station (nz_{ps}) and mean axis approximation (nz_{ma}) responses to control excitation at the back, all-movable tail (solid), and the front, ride control vane (dashed), of the aircraft (original response in g's).

Having explored the control effectiveness of various surfaces, the next logical question in model analysis is the impact of the actuator dynamics themselves. Figures 3.7 and 3.8 illustrated the open loop response of pitch rate and normal acceleration respectively for a system with and without actuator dynamics present. The most striking

impact is on the high frequency dynamics. The presence of actuator dynamics continues excitation of high frequency modes while their absence allows for the dynamic roll off and modal attenuation. This observation is very important for control design purposes since typically actuator dynamics are not considered during the design process. The implication here is that the controller must roll off significantly before the excitation of flexible modes due to actuator dynamics comes into play.

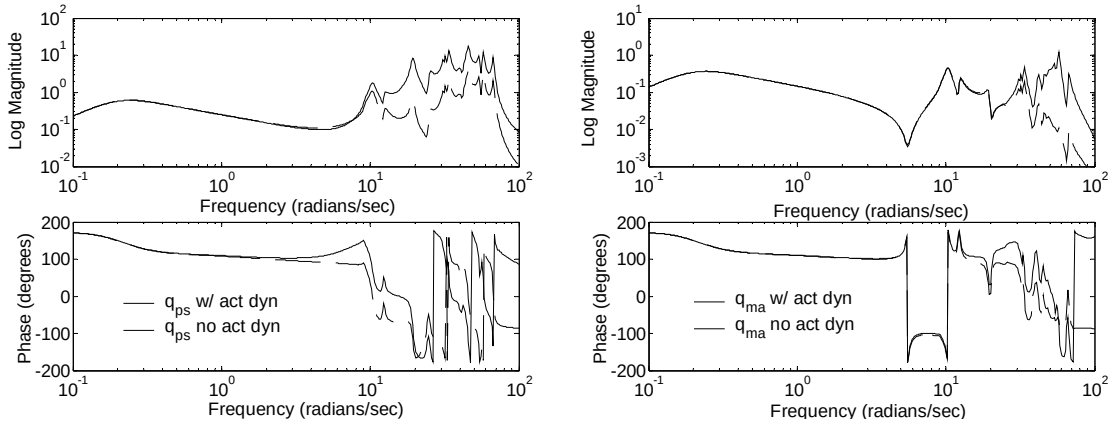

Figure 3.7: Pitch rate dynamics comparison of system with (solid) and without (dashed) actuator dynamics.

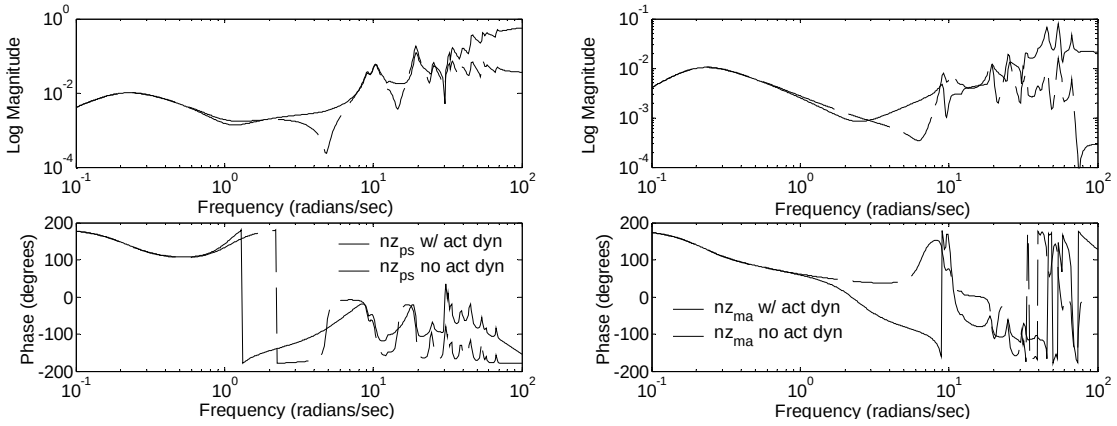

Figure 3.8: Normal acceleration dynamic response to elevator excitation comparison of system with (solid) and without (dashed) actuator dynamics (original response in g's).

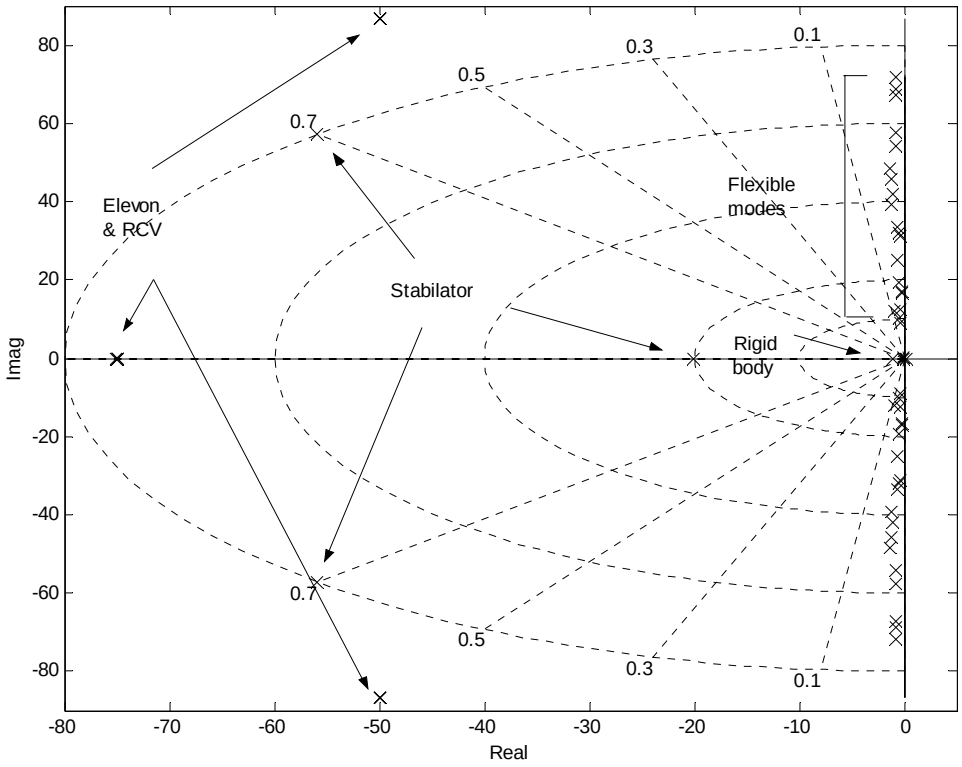

Figure 3.9: Open loop pole locations of a linear system at Mach =0.24 and 1,000 ft, Mass Cruise Final.

At this point it might be interesting to look at the actual pole locations for the system represented by (3.7). Figures 3.9 and 3.10 give the pole location of the system in (3.7) with 20 elastic modes and actuator dynamics for stabilator, elevon, and RCV. Figure 3.9 provides a large-scale overview of the entire system. Note the very fast actuator dynamics of the elevon and the RCV as well as the somewhat slower but still fast stabilator dynamics. Also note the 20 flexible modes along the imaginary axis and how closely a number of them are clustered together. Figure 3.10 gives an enlargement of a section of Figure 3.9 to better illustrate the dynamics that become very important in controller design that is described in the subsequent chapter. The vehicle has what is commonly referred to as a degenerate short period, where the eigenvalues are real and one is very low frequency. This leads to a potential coupling between the short period

and the phugoid in the closed loop response. Note that the first eight modes are at lower frequency, or right at it for mode eight, than the first break frequency for the slowest control surface, the stabilator. This means that all of these modes get the full energy transmission without attenuation every time the stabilator moves. Therefore, the first 8 elastic modes in the model are used in the controller design.

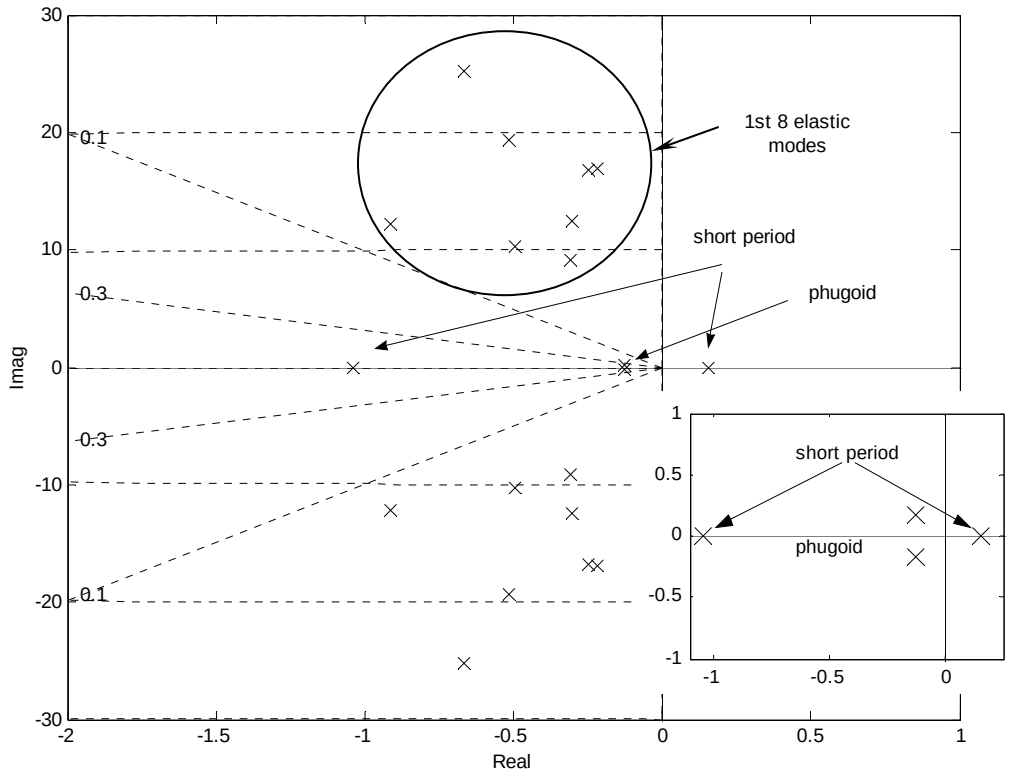

Figure 3.10: Enlarged area of the linear system above.

Furthermore, the first frequency breakpoint for the elevator and other surfaces is at 75 rad/sec, which is higher than all of the 20 flexible modes modeled. Thus, unlike more traditional vehicles where the flexible modes are typically at frequencies where control activity energy is already attenuated so their excitation is not that severe and certainly not at frequencies that interfere with flight control.

Another question worth considering is the effect inertial actuator mass coupling, which manifests itself as the actuator dynamics acceleration term, has on excitation of

higher frequencies. The largest high frequency excitation of concern is at the pilot station and that is where this segment of analysis concentrates. Figures 3.11 and 3.12 below illustrate the difference a factor of 10 in actuator acceleration term has on the open loop dynamics. The pitch rate response shows some difference in magnitude of high frequency dynamics with a change in the inertial mass coupling acceleration terms (see Fig. 3.11).

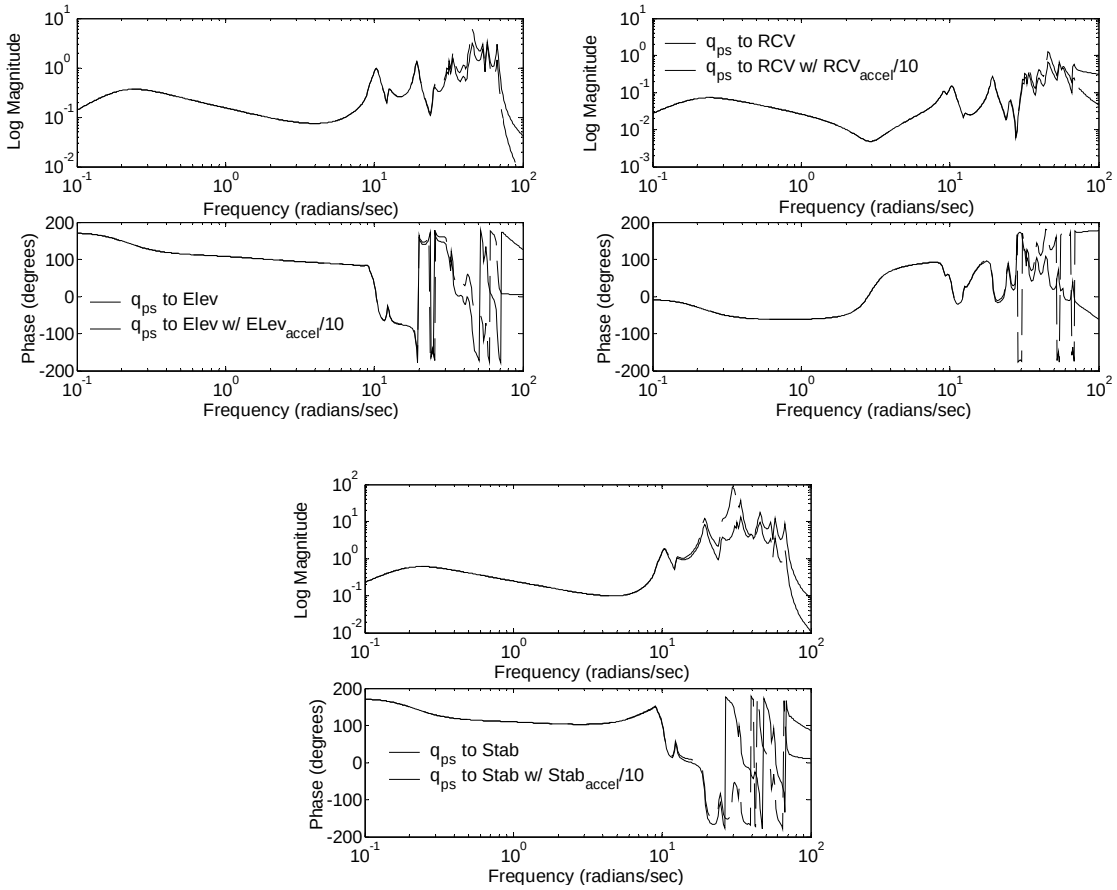

Figure 3.11: Effect on pitch rate at pilot station of inertial coupling terms of stabilator, elevon, and RCV.

All three control surfaces show higher excitation by the reduced magnitude acceleration term. In addition, this difference is even more pronounced for normal

acceleration as illustrated in Figure 3.12. These phenomena may seem intuitively contradictory and requires further discussion.

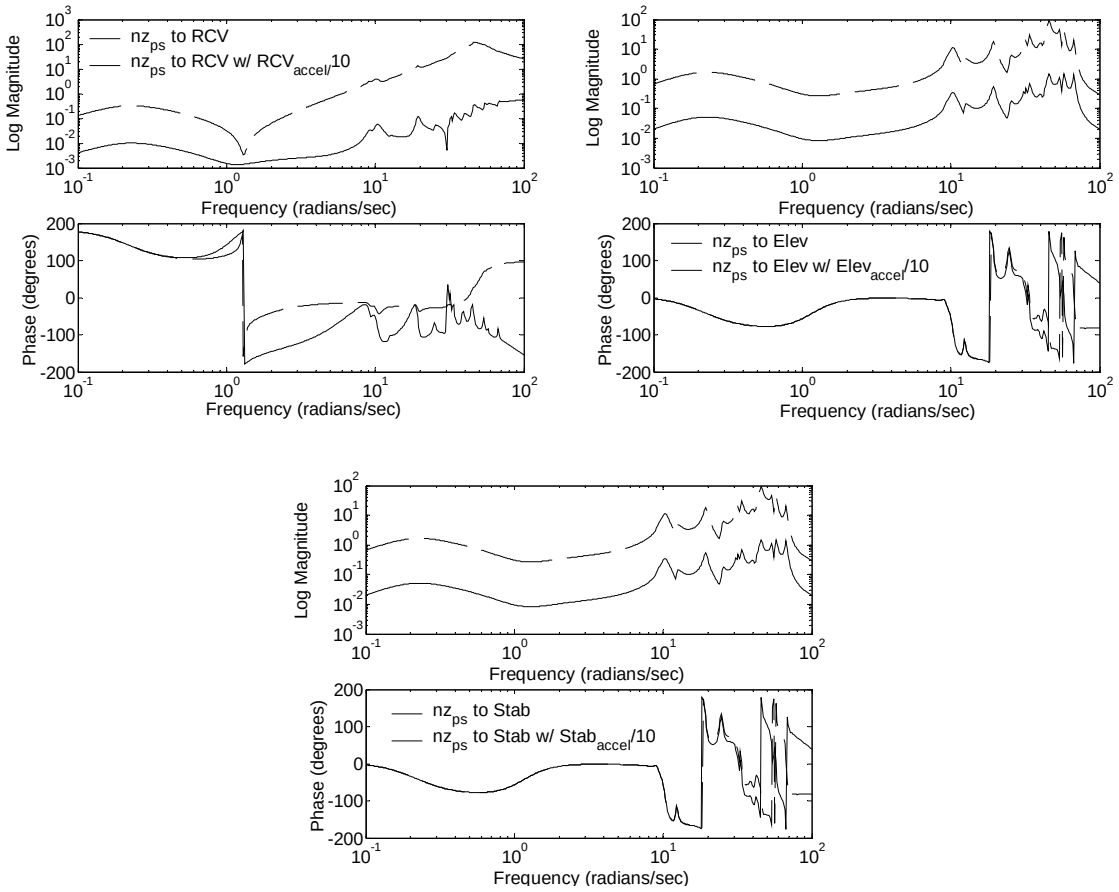

Figure 3.12: Effect on normal acceleration at pilot station of inertial coupling terms of stabilator, elevon, and RCV.

Consider 3rd order actuator dynamics that are modeled as a transfer function

$$\frac{\delta}{\delta_{cmd}} = \frac{\omega^2}{s^2 + 2\zeta\omega s + \omega^2}\frac{a}{s+a}$$

The acceleration term $\ddot{\delta}/10$ is propagated through the dynamics as follows

$$\frac{\delta}{\delta_{cmd}} = \frac{\omega^2 a}{s^3 + \frac{(2\zeta\omega + a)}{10}s^2 + (2\zeta\omega a + \omega^2)s + \omega^2 a}$$

This decreases damping as shown in Figure 3.13 for both slower stabilator and faster elevon and RCV; and the flexible modes in q_{ps} are excited more by stabilator than by the faster actuators for decreased inertial damping in corresponding frequency range. In addition, as seen from Figure 3.12, the nz_{ps} response, as a whole, is shifted higher implying that the change in inertial coupling changes the response over low and high frequencies. For explanation consider the equation for nz_{ps}

$$nz_{ps} = nz_{cg} + \frac{l_{ps}}{g}\dot{q} + \sum_{i=1}^{20}\frac{\phi_i^{ps}}{g}\ddot{\eta}_i \quad \text{where} \quad nz_{cg} = \frac{\dot{w} - u\dot{q}}{g}.$$

Thus, in $\dot{w}, \dot{q}, \ddot{\eta}$ equations of (3.4), the term $\ddot{\delta}$ is 10 times smaller and since this is viewed as inertial coupling, the appearance is of a lighter airplane. If the airplane is lighter, it is easier to maneuver given a specific surface size. Based on these observations the attenuation of flexible modes can be considerably improved if the actuators are mass balanced as much as possible.

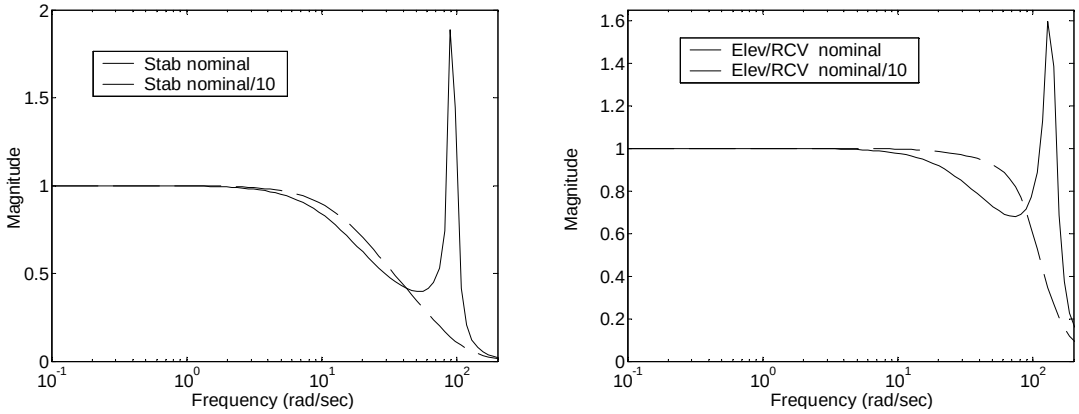

Figure 3.13. Third-order actuator model response for original $\ddot{\delta}$ and $\ddot{\delta}/10$.

3.5 Summary

This chapter presents a brief overview of the general equations of unsteady motion for an aircraft. It then proceeded to development of coupled quasi-steady/dynamic aeroservoelastic equations that are required for an aircraft whose flexible modes are low enough frequency to start impacting rigid body flight dynamics and hence are no longer

validly represented as quasi-static states. Continuing this development the dynamics associated with the specific vehicle under study are presented and discussed in detail at a flight condition that makes the flexible mode interaction with the rigid flight dynamics most pronounced. The specific dynamics description prepares the background and highlights some issues that arise in controller design for the HSCT vehicle under study that is presented in Chapter 5.

Chapter 4 – Introduction to Novel Dynamic Inversion

4.1 Introduction

An innovation has been added to the standard methodology of dynamic inversion in the manner described in this work to accommodate the highly flexible nature of the advanced aircraft and fulfill the dual objectives of integrated flight/SMC control. The novel approach to the nonlinear dynamic inversion allows the methodology to more intelligently handle flexible dynamics (or any dynamics with pole-zero pairs very close to the jω-axis). In the standard dynamic inversion, the controlled variable's dynamics are cancelled by the controller, which may or may not be an appropriate approach. This new approach to standard dynamic inversion still maintains control of CVs while the innovation allows a change to the dynamics of the controlled variable without cancellation of its dynamics. This is accomplished by introducing dynamics into the inversion loop itself. What this novel approach enables is altering flexible mode damping without cancellation, thus improving disturbance response and avoiding the potentially destabilizing effect of pole cancellation close to the jω-axis in case of modeling uncertainty.

This chapter introduces the novel dynamic inversion and explores the effects on the closed loop dynamics the innovation has both analytically and numerically. In order to make the problem mathematically tractable and to gain better understanding of dynamic interactions in a closed loop system under novel dynamic inversion, the aircraft model has been simplified from the very complicated one described in Chapter 3 while retaining the essential characteristics. These essential characteristics are the interaction of flexible modes on rigid body dynamics and vice versa. What is not retained is the interaction of flexible modes among themselves, but based on experience it is not a critical element of the dynamic behavior. The simplification involved considers longitudinal dynamics with a single elastic mode and a control law based on novel dynamic inversion only. In addition, throughout this chapter the analysis considers the inner loop of the dynamic inversion only, *i.e.*, the $\dot{y}^{des}$ to y portion. It is important to note that the nature of $\dot{y}^{des}$ impacts the overall closed loop dynamics but will not be discussed here.

The influence that novel dynamic inversion has on the closed loop dynamics is studied analytically for both linear and nonlinear systems as well as different cases of dynamics for the new methodology. In addition, the affects the dynamics of the innovative dynamic inversion have on the closed loop system response is studied through pole movement as a function of the innovation's dynamics. The model involved considers a linearized version of the aircraft dynamics while still retaining essential characteristics such as rigid body/flexible mode coupling. The initial linear system considered is short period longitudinal dynamics with a single elastic mode to which dynamic inversion, both original and novel concept, is applied to show the affects on aircraft dynamics due to the introduced modifications. The complexity of the model is then gradually increased to include more dynamics.

This chapter is organized as follows. Following the introduction, section 2 introduces the novel dynamic inversion followed by a section discussing model selection for use in the symbolic analysis. Section 4 explores the linear system case. Three different variations in the novel dynamic inversion dynamics are explored in this section. Section 5 discusses the same three variations for a nonlinear system. Following this, the second major portion of this chapter considers the influence of novel dynamic inversion on system response. To provide context for the results that follow it, section 6 discusses the standard dynamic inversion results as applied to the short period plus one elastic mode linear equations of motion. The following section then deals with the innovation introduced into the dynamic inversion that is the primary focus of this chapter. The subsequent sections address the increasing complexity of the model by introducing full longitudinal dynamics and additional flexible modes, respectively. The final section explores how uncertainty introduced into elastic mode frequency and damping influences closed loop dynamics that are found in the traditional rigid body frequency range. The conclusions that are drawn from this analysis then follow.

Throughout this chapter, the analysis considers the inner loop of the dynamic inversion only, *i.e.*, the y to $\dot{y}^{des}$ portion. It is important to note that the nature of $\dot{y}^{des}$ impacts the overall closed loop dynamics but will not be discussed here.

4.2 Novel Dynamic Inversion

The presence of flexible modes in the close proximity to rigid body dynamics that are typically controlled raises a new set of challenges for the control engineer in utilizing dynamic inversion. In order to design a successful controller, the method of novel dynamic inversion was developed to influence the damping of elastic modes so that the response to system disturbances and model uncertainties is acceptable. This is accomplished by introducing dynamics into the inversion loop itself. The analytical description of a simplified version of such dynamics and their influence on the closed loop is the main result of the first part of this chapter.

The modification to dynamic inversion is introduced in the forward section of the dynamic inversion feedback loop and is illustrated in Figure 4.1. Since the problem formulation is MIMO, a matrix $W(x)$ is introduced to limit the frequency range of the dynamics that are passed to the inverse of the effective control effectiveness matrix that produces actuator commands.

4.3 Novel Dynamic Inversion General Case

For the general nonlinear system of the form

$$\begin{aligned} \dot{x} &= f(x) + g(x)\delta \\ y &= h(x) \end{aligned} \tag{4.8}$$

and the filter $W(x)$ represented by (4.9) and shown in Figure 4.1

$$\begin{aligned} \dot{x}_f &= A_f x_f + B_f \bar{u} \\ y_f &= C_f x_f + D_f \bar{u} \end{aligned} \tag{4.9}$$

the inversion loop from $\dot{y}^{des}$ to y is

$$\begin{pmatrix} \dot{x} \\ \dot{x}_f \end{pmatrix} = \begin{pmatrix} f(x) - g(x)\big(h(x)g(x)\big)^{-1} D_f h(x) f(x) \\ -B_f h(x) f(x) \end{pmatrix} + \begin{bmatrix} g(x)\big(h(x)g(x)\big)^{-1} C_f \\ A_f \end{bmatrix} x_f + \begin{bmatrix} g(x)\big(h(x)g(x)\big)^{-1} D_f \\ B_f \end{bmatrix} \dot{y}^{des} \tag{4.10}$$

with

$$\begin{aligned} \bar{u} &= \dot{y}^{des} - h(x) f(x) \\ \delta &= \big(h(x)g(x)\big)^{-1} y_f \end{aligned}$$

Three different variations in the novel dynamic inversion dynamics are explored. In this analysis, the filter is limited to a first order system in each loop, the exact nature of which will be made more precise later in the chapter. Specific cases for the $W(x)$ structure are explored on a simplified model introduced in the following section.

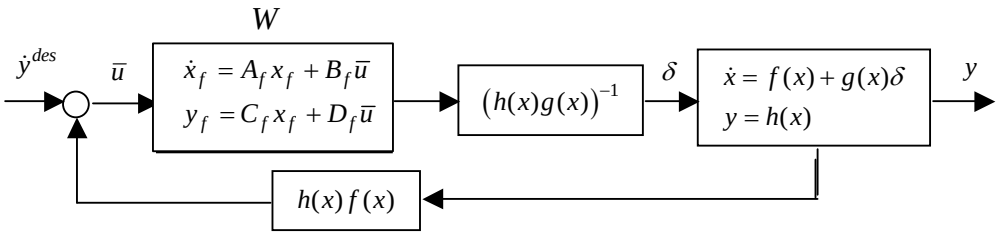

Figure 4.1: Novel dynamic inversion – *the* introduction of a filter into the inversion loop.

4.4 Model Selection

Specifically, the model is limited to the full longitudinal flight dynamics with a single flexible mode that is the dominant fuselage bending mode, *i.e.*, the worse-case dynamic interaction. The aircraft equations of motion are given below.

$$\begin{pmatrix}\dot{u}\\ \dot{w}\\ \dot{q}\\ \dot{\theta}\\ \ddot{\eta}\\ \dot{\eta}\end{pmatrix}=\begin{pmatrix}-qw-g\sin\theta+T/m\\ qu+g\cos\theta\\ 0\\ q\\ 0\\ \dot{\eta}\end{pmatrix}+\frac{1}{2}\rho SV^2\left\{\begin{pmatrix}C_x(\alpha)/m\\ C_z(\alpha)/m\\ \overline{c}C_M(\alpha)/I_y\\ 0\\ 0\\ 0\end{pmatrix}+\begin{pmatrix}C_{x,\eta}(\alpha)/m\\ C_{z,\eta}(\alpha)/m\\ \overline{c}C_{M,\eta}(\alpha)/I_y\\ 0\\ \frac{\overline{q}}{m_\eta}C_{\eta\eta}\\ 0\end{pmatrix}\eta\right.$$

$$\left.+\begin{pmatrix}\frac{C_{x,\dot{\eta}}(\alpha)}{m}\\ \frac{C_{z,\dot{\eta}}(\alpha)}{m}\\ \frac{\overline{c}C_{M,\dot{\eta}}(\alpha)}{I_y}\\ 0\\ \frac{\overline{q}}{m_\eta}C_{\eta\dot{\eta}}\\ 0\end{pmatrix}\dot{\eta}+\begin{bmatrix}0&0&0\\0&0&0\\0&0&0\\0&0&0\\\frac{C_{\eta u}}{m_\eta}&\frac{C_{\eta w}}{m_\eta}&\frac{C_{\eta q}}{m_\eta}\\0&0&0\end{bmatrix}\begin{pmatrix}u\\w\\q\end{pmatrix}+\begin{pmatrix}\frac{C_{x,\delta_1}(\alpha)}{m}&0\\ \frac{C_{z,\delta_1}(\alpha)}{m}&\frac{C_{z,\delta_2}(\alpha)}{m}\\ \frac{\overline{c}C_{M,\delta_1}(\alpha)}{I_y}&\frac{\overline{c}C_{M,\delta_2}(\alpha)}{I_y}\\ 0&0\\ \frac{C_{\eta,\delta_1}}{m_\eta}&\frac{C_{\eta,\delta_2}}{m_\eta}\\ 0&0\end{pmatrix}\begin{pmatrix}\delta_1\\ \delta_2\end{pmatrix}\right\} \tag{4.11}$$

with

$$y_{sensed}=\begin{pmatrix}q_{ma_{sensed}}\\ q_{ps_{sensed}}-q_{ma_{sensed}}\end{pmatrix}=\begin{pmatrix}q+\phi'\ddot{\eta}\\ \Delta\phi'\ddot{\eta}\end{pmatrix}$$

as desired outputs.

The analyses begin with a linear system representation and then proceed to a nonlinear model.

4.5 Linear Case

This section compares the closed loop linear dynamics for three representations of the $W(x)$ filter. The general representation of the inversion loop is illustrated in Figure 4.2.

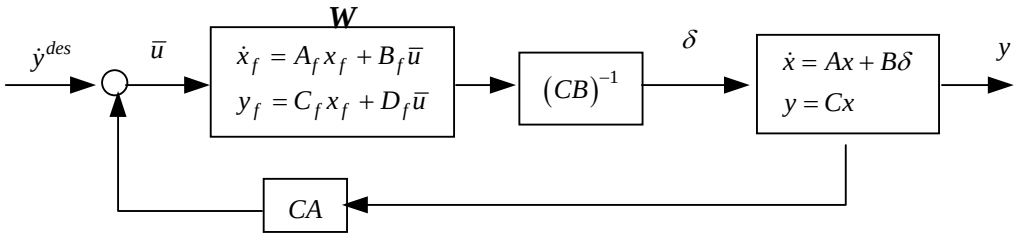

Figure 4.2: Novel dynamic inversion - introduction of a filter into the inversion loop – linear case.

The linear system representation of the longitudinal dynamics with one flexible mode is given by

$$\begin{bmatrix} \dot{u} \\ \dot{w} \\ \dot{q} \\ \dot{\theta} \\ \ddot{\eta} \\ \dot{\eta} \end{bmatrix} = \begin{bmatrix} X_u & X_w & X_q & X_\theta & 0 & 0 \\ Z_u & Z_w & Z_q & Z_\theta & Z_{\dot{\eta}} & Z_\eta \\ M_u & M_w & M_q & M_\theta & M_{\dot{\eta}} & M_\eta \\ 0 & 0 & 1 & 0 & 0 & 0 \\ 0 & E_w & E_q & 0 & -2\varsigma\omega & -\omega^2 \\ 0 & 0 & 0 & 0 & 1 & 0 \end{bmatrix} \begin{bmatrix} u \\ w \\ q \\ \theta \\ \dot{\eta} \\ \eta \end{bmatrix} + \begin{bmatrix} X_{\delta_1} & 0 \\ Z_{\delta_1} & Z_{\delta_2} \\ M_{\delta_1} & M_{\delta_2} \\ 0 & 0 \\ E_{\delta_1} & E_{\delta_2} \\ 0 & 0 \end{bmatrix} \begin{bmatrix} \delta_1 \\ \delta_2 \end{bmatrix}$$

$$\begin{bmatrix} q_{ma} \\ q_{ps} - q_{ma} \end{bmatrix} = \begin{bmatrix} 0 & 0 & 1 & 0 & \phi' & 0 \\ 0 & 0 & 0 & 0 & \Delta\phi' & 0 \end{bmatrix} \begin{bmatrix} u \\ w \\ q \\ \theta \\ \dot{\eta} \\ \eta \end{bmatrix} \tag{4.12}$$

The control effector commands in terms of the inversion loop variables are given by

$$\begin{aligned} \delta &= (CB)^{-1} y_f \\ \bar{u} &= \dot{y}^{des} - CAx \end{aligned} \tag{4.13}$$

and for

$$
\begin{aligned}
W(x) = I_{2x2}: \quad & \delta = (CB)^{-1}\bar{u} \\
& \delta = (CB)^{-1}\left[\dot{y}^{des} - CAx\right] \\
W(x) = \begin{bmatrix} \dot{x}_f = A_f x_f + B_f \bar{u} \\ y_f = C_f x_f + D_f \bar{u} \end{bmatrix}: \quad & \delta = (CB)^{-1}\left(C_f x_f + D_f \bar{u}\right) \\
& \delta = (CB)^{-1}\left(C_f x_f + D_f \dot{y}^{des} - D_f CAx\right)
\end{aligned}
\tag{4.14}
$$

The specifics for each case are explored below.

4.5.1 Case 1: Standard Dynamic Inversion

Applying the standard dynamic inversion to the system in (4.12) results in the closed loop system

$$
\begin{bmatrix} \dot{u} \\ \dot{w} \\ \dot{q} \\ \dot{\theta} \\ \ddot{\eta} \\ \dot{\eta} \end{bmatrix} = \begin{bmatrix} \bar{X}_u & \bar{X}_w & \bar{X}_q & \bar{X}_\theta & \bar{X}_{\dot{\eta}} & \bar{Z}_\eta \\ \bar{Z}_u & \bar{Z}_w & \bar{Z}_q & \bar{Z}_\theta & \bar{Z}_{\dot{\eta}} & \bar{Z}_\eta \\ 0 & 0 & 0 & 0 & 0 & 0 \\ 0 & 0 & 1 & 0 & 0 & 0 \\ 0 & 0 & 0 & 0 & 0 & 0 \\ 0 & 0 & 0 & 0 & 1 & 0 \end{bmatrix} \begin{bmatrix} u \\ w \\ q \\ \theta \\ \dot{\eta} \\ \eta \end{bmatrix} + \begin{bmatrix} \bar{X}_{\delta 1} & \bar{X}_{\delta 2} \\ \bar{Z}_{\delta 1} & \bar{Z}_{\delta 2} \\ 1 & \bar{M}_{\delta 2} \\ 0 & 0 \\ 0 & \bar{E}_{\delta 2} \\ 0 & 0 \end{bmatrix} \begin{bmatrix} \dot{y}_1 \\ \dot{y}_2 \end{bmatrix}^{des}
$$

$$
\begin{bmatrix} \dot{y}_1 \\ \dot{y}_2 \end{bmatrix} = \begin{bmatrix} \dot{y}_1^{des} \\ \dot{y}_2^{des} \end{bmatrix}
\tag{4.15}
$$

Thus, there is separation between controlled and zero dynamics in the sense that the $(q, \theta, \dot{\eta}, \ddot{\eta})$ equations do not contain (u, w) dynamics. And if the controlled dynamics are stable by design, then the overall system stability depends only on the (u, w) dynamics. This is a linear case of the stability result that will be presented in Chapter 6.

4.5.2 Case 2: Filter in the Flexible Dynamics Loop

Introducing a filter into the dynamic inversion loop complicates the standard relationship. For a filter in one of the two loops the state space representation for W is

$$
W = \begin{bmatrix} 1 & 0 \\ 0 & \dfrac{1}{bs+1} \end{bmatrix} \Rightarrow \begin{aligned} \dot{x}_f &= A_f x_f + \begin{bmatrix} 0 & b_f \end{bmatrix} \begin{bmatrix} \bar{u}_1 \\ \bar{u}_2 \end{bmatrix} \\ y_f &= \begin{bmatrix} 0 \\ 1 \end{bmatrix} x_f + \begin{bmatrix} 1 & 0 \\ 0 & 0 \end{bmatrix} \begin{bmatrix} \bar{u}_1 \\ \bar{u}_2 \end{bmatrix} \end{aligned}
\tag{4.16}
$$

and the general linear closed loop relationships are

$$A_c = \begin{bmatrix} A - B(CB)^{-1} D_f CA & B(CB)^{-1} C_f \\ -B_f CA & A_f \end{bmatrix}$$
$$B_c = \begin{bmatrix} B(CB)^{-1} D_f \\ B_f \end{bmatrix} \qquad C_c = \begin{bmatrix} C & 0 \end{bmatrix} \tag{4.17}$$

Employing the relations for closed loop (A_c, B_c, C_c) results in

$$\begin{bmatrix} \dot{u} \\ \dot{w} \\ \dot{q} \\ \dot{\theta} \\ \ddot{\eta} \\ \dot{\eta} \\ \dot{x}_f \end{bmatrix} = \begin{bmatrix} \bar{X}_u & \bar{X}_w & \bar{X}_q & \bar{X}_\theta & \bar{X}_{\dot{\eta}} & \bar{X}_\eta & \bar{X}_{\delta 2} \\ \bar{Z}_u & \bar{Z}_w & \bar{Z}_q & \bar{Z}_\theta & \bar{Z}_{\dot{\eta}} & \bar{Z}_\eta & \bar{Z}_{\delta 2} \\ 0 & -\phi' E_w & -\phi' E_q & 0 & -\phi' E_{\dot{\eta}} & -\phi' E_\eta & -\phi' \bar{E}_{\delta 2} \\ 0 & 0 & 1 & 0 & 0 & 0 & 0 \\ 0 & E_w & E_q & 0 & E_{\dot{\eta}} & E_\eta & \bar{E}_{\delta 2} \\ 0 & 0 & 0 & 0 & 1 & 0 & 0 \\ 0 & -\frac{\Delta\phi'}{b} E_w & -\frac{\Delta\phi'}{b} E_q & 0 & -\frac{\Delta\phi'}{b} E_{\dot{\eta}} & -\frac{\Delta\phi'}{b} E_\eta & -\frac{1}{b} \end{bmatrix} \begin{bmatrix} u \\ w \\ q \\ \theta \\ \dot{\eta} \\ \eta \\ x_f \end{bmatrix} + \begin{bmatrix} \bar{X}_{\delta 1} & 0 \\ \bar{Z}_{\delta 1} & 0 \\ 1 & 0 \\ 0 & 0 \\ 0 & 0 \\ 0 & 0 \\ 0 & \frac{1}{b} \end{bmatrix} \begin{bmatrix} \dot{y}_1^{des} \\ \dot{y}_2^{des} \end{bmatrix}$$

$$\begin{bmatrix} \dot{y}_1 \\ \dot{y}_2 \end{bmatrix} = \begin{bmatrix} 0 & 0 & 0 & 0 & 0 & 0 & 0 \\ 0 & \Delta\phi' E_w & \Delta\phi' E_q & 0 & \Delta\phi' E_{\dot{\eta}} & \Delta\phi' E_\eta & 1 \end{bmatrix} \begin{bmatrix} u \\ w \\ q \\ \theta \\ \dot{\eta} \\ \eta \\ x_f \end{bmatrix} + \begin{bmatrix} 1 & 0 \\ 0 & 0 \end{bmatrix} \begin{bmatrix} \dot{y}_1^{des} \\ \dot{y}_2^{des} \end{bmatrix} \tag{4.18}$$

where

$$E_{\dot{\eta}} = -2\zeta\omega \quad E_\eta = -\omega^2 \quad \bar{E}_{\delta_2} = 1/\Delta\phi'$$

and

$$\bar{X}_u = X_u - \frac{X_{\delta_1} E_{\delta_2} M_u}{\left(E_{\delta_2} M_{\delta_1} - E_{\delta_1} M_{\delta_2}\right)} \qquad \bar{X}_w = X_w - \frac{X_{\delta_1} E_{\delta_2} \left(M_w + \phi' E_w\right)}{\left(E_{\delta_2} M_{\delta_1} - E_{\delta_1} M_{\delta_2}\right)}$$
$$\bar{X}_q = X_q - \frac{X_{\delta_1} E_{\delta_2} \left(M_q + \phi' E_q\right)}{\left(E_{\delta_2} M_{\delta_1} - E_{\delta_1} M_{\delta_2}\right)} \qquad \bar{X}_\theta = X_\theta - \frac{X_{\delta_1} E_{\delta_2} M_\theta}{\left(E_{\delta_2} M_{\delta_1} - E_{\delta_1} M_{\delta_2}\right)}$$
$$\bar{X}_{\dot{\eta}} = -\frac{X_{\delta_1} E_{\delta_2} \left(M_{\dot{\eta}} + \phi' E_{\dot{\eta}}\right)}{\left(E_{\delta_2} M_{\delta_1} - E_{\delta_1} M_{\delta_2}\right)} \qquad \bar{X}_\eta = -\frac{X_{\delta_1} E_{\delta_2} \left(M_\eta + \phi' E_\eta\right)}{\left(E_{\delta_2} M_{\delta_1} - E_{\delta_1} M_{\delta_2}\right)}$$

$$\bar{X}_{\delta_1} = \frac{X_{\delta_1} E_{\delta_2}}{\left(E_{\delta_2} M_{\delta_1} - E_{\delta_1} M_{\delta_2}\right)} \qquad \bar{X}_{\delta_2} = -\frac{X_{\delta_1}\left(M_{\delta_2} + \phi' E_{\delta_2}\right)}{\Delta\phi'\left(E_{\delta_2} M_{\delta_1} - E_{\delta_1} M_{\delta_2}\right)}$$

$$\bar{Z}_u = Z_u - \frac{\left(Z_{\delta_1} E_{\delta_2} - Z_{\delta_2} E_{\delta_1}\right) M_u}{\left(E_{\delta_2} M_{\delta_1} - E_{\delta_1} M_{\delta_2}\right)} \qquad \bar{Z}_w = Z_w - \frac{\left(Z_{\delta_1} E_{\delta_2} - Z_{\delta_2} E_{\delta_1}\right)\left(M_w + \phi' E_w\right)}{\left(E_{\delta_2} M_{\delta_1} - E_{\delta_1} M_{\delta_2}\right)}$$

$$\bar{Z}_q = Z_q - \frac{\left(Z_{\delta_1} E_{\delta_2} - Z_{\delta_2} E_{\delta_1}\right)\left(M_q + \phi' E_q\right)}{\left(E_{\delta_2} M_{\delta_1} - E_{\delta_1} M_{\delta_2}\right)} \qquad \bar{Z}_\theta = Z_\theta - \frac{\left(Z_{\delta_1} E_{\delta_2} - Z_{\delta_2} E_{\delta_1}\right) M_\theta}{\left(E_{\delta_2} M_{\delta_1} - E_{\delta_1} M_{\delta_2}\right)}$$

$$\bar{Z}_{\dot{\eta}} = Z_{\dot{\eta}} - \frac{\left(Z_{\delta_1} E_{\delta_2} - Z_{\delta_2} E_{\delta_1}\right)\left(M_{\dot{\eta}} + \phi' E_{\dot{\eta}}\right)}{\left(E_{\delta_2} M_{\delta_1} - E_{\delta_1} M_{\delta_2}\right)} \qquad \bar{Z}_\eta = Z_\eta - \frac{\left(Z_{\delta_1} E_{\delta_2} - Z_{\delta_2} E_{\delta_1}\right)\left(M_\eta + \phi' E_\eta\right)}{\left(E_{\delta_2} M_{\delta_1} - E_{\delta_1} M_{\delta_2}\right)}$$

$$\bar{Z}_{\delta_1} = \frac{Z_{\delta_1} E_{\delta_2} - Z_{\delta_2} E_{\delta_1}}{E_{\delta_2} M_{\delta_1} - E_{\delta_1} M_{\delta_2}} \qquad \bar{Z}_{\delta_2} = -\frac{Z_{\delta_1}\left(M_{\delta_2} + \phi' E_{\delta_2}\right) - Z_{\delta_2}\left(M_{\delta_1} + \phi' E_{\delta_1}\right)}{\Delta\phi'\left(E_{\delta_2} M_{\delta_1} - E_{\delta_1} M_{\delta_2}\right)}$$

or in other words

$$\begin{bmatrix} \dot{u} \\ \dot{w} \\ \dot{q} \\ \dot{\theta} \\ \ddot{\eta} \\ \dot{\eta} \\ \dot{x}_f \end{bmatrix} = \begin{bmatrix} \bar{A}_x & \bar{B}_{x\delta_2} \\ \bar{A}_z & \bar{B}_{z\delta_2} \\ -\phi' A_{\dot{\eta}} & -\phi'/\Delta\phi' \\ A_\theta & 0 \\ A_{\dot{\eta}} & 1/\Delta\phi' \\ A_\eta & 0 \\ \Delta\phi' A_f A_{\dot{\eta}} & A_f \end{bmatrix} \begin{bmatrix} x \\ x_f \end{bmatrix} + \begin{bmatrix} \bar{B}_{x\delta_1} & 0 \\ \bar{B}_{z\delta_1} & 0 \\ 1 & 0 \\ 0 & 0 \\ 0 & 0 \\ 0 & 0 \\ 0 & B_f \end{bmatrix} \begin{bmatrix} \dot{y}_1^{des} \\ \dot{y}_2^{des} \end{bmatrix} \tag{4.19}$$

$$\begin{bmatrix} \dot{y}_1 \\ \dot{y}_2 \end{bmatrix} = \begin{bmatrix} 0 & 0 \\ \Delta\phi' A_{\dot{\eta}} & 1 \end{bmatrix} \begin{bmatrix} x \\ x_f \end{bmatrix} + \begin{bmatrix} 1 & 0 \\ 0 & 0 \end{bmatrix} \begin{bmatrix} \dot{y}_1^{des} \\ \dot{y}_2^{des} \end{bmatrix}$$

where $\bar{A}_{(\cdot)}, \bar{B}_{(\cdot)}$ are appropriate elements of the closed loop A_c and B_c matrices, *e.g.*,

$$\bar{A}_x = [\bar{X}_u \quad \bar{X}_w \quad \bar{X}_q \quad \bar{X}_\theta \quad \bar{X}_{\dot{\eta}} \quad \bar{X}_\eta] \text{ and } \bar{B}_{x\delta_2} = [\bar{X}_{\delta_1}]$$

Note that the introduction of a filter into the flexible dynamics loop alters these dynamics. Specifically, in the closed loop **A** matrix $\dot{q} = -\phi'\ddot{\eta}$ or $-\phi' A_{\dot{\eta}} x - \phi'/\Delta\phi' x_f = -\phi'\left(A_{\dot{\eta}} x + 1/\Delta\phi' x_f\right)$. The input/output decoupling of pitch rate response dynamics, characteristic of dynamic inversion, is preserved despite introduction of a filter into the inversion loop. Since the filter introduces a change in flexible dynamics, in order to recover $\dot{q}_{ma} = \dot{q}_{ma}^{des}$ this change in flexible dynamics must be subtracted from the closed loop pitch rate dynamics. Another way to look at the closed

loop pitch rate dynamics is as an error between the original and new filter induced dynamics, which are equal to the flexible modes.

4.5.3 Case 3: Filters in Both Flight and Flexible Dynamics Loops

The state space form for $W(x)$ is

$$W = \begin{bmatrix} \dfrac{1}{as+1} & 0 \\ 0 & \dfrac{1}{bs+1} \end{bmatrix} \Rightarrow \begin{aligned} \dot{x}_f &= \begin{bmatrix} -1/a & 0 \\ 0 & -1/b \end{bmatrix} x_f + \begin{bmatrix} 1/a & 0 \\ 0 & 1/b \end{bmatrix} \begin{bmatrix} \bar{u}_1 \\ \bar{u}_2 \end{bmatrix} \\ y_f &= \begin{bmatrix} 1 & 0 \\ 0 & 1 \end{bmatrix} x_f + \begin{bmatrix} 0 & 0 \\ 0 & 0 \end{bmatrix} \begin{bmatrix} \bar{u}_1 \\ \bar{u}_2 \end{bmatrix} \end{aligned} \tag{4.20}$$

and the resulting closed loop system is

$$\begin{bmatrix} \dot{u} \\ \dot{w} \\ \dot{q} \\ \dot{\theta} \\ \ddot{\eta} \\ \dot{\eta} \\ \dot{x}_{fa} \\ \dot{x}_{fb} \end{bmatrix} = \begin{bmatrix} X_u & X_w & X_q & X_\theta & 0 & 0 & X_{\delta_1} & 0 \\ Z_u & Z_w & Z_q & Z_\theta & Z_{\dot{\eta}} & Z_\eta & Z_{\delta_1} & Z_{\delta_2} \\ M_u & M_w & M_q & M_\theta & M_{\dot{\eta}} & M_\eta & M_{\delta_1} & M_{\delta_2} \\ 0 & 0 & 1 & 0 & 0 & 0 & 0 & 0 \\ 0 & E_w & E_q & 0 & E_{\dot{\eta}} & E_\eta & E_{\delta_1} & E_{\delta_2} \\ 0 & 0 & 0 & 0 & 1 & 0 & 0 & 0 \\ Fa_u & Fa_w & Fa_q & Fa_\theta & Fa_{\dot{\eta}} & Fa_\eta & Fa_a & 0 \\ 0 & Fb_w & Fb_q & 0 & Fb_{\dot{\eta}} & Fb_\eta & 0 & Fb_b \end{bmatrix} \begin{bmatrix} u \\ w \\ q \\ \theta \\ \dot{\eta} \\ \eta \\ x_{fa} \\ x_{fb} \end{bmatrix} + \begin{bmatrix} 0 & 0 \\ 0 & 0 \\ 0 & 0 \\ 0 & 0 \\ 0 & 0 \\ 0 & 0 \\ Fa_{\delta_1} & 0 \\ 0 & Fb_{\delta_2} \end{bmatrix} \begin{pmatrix} \dot{y}_1^{des} \\ \dot{y}_2^{des} \end{pmatrix}$$

$$\begin{bmatrix} \dot{y}_1 \\ \dot{y}_1 \end{bmatrix} = \begin{bmatrix} M_u & M_w + \phi' E_w & M_q + \phi' E_q & M_\theta & M_{\dot{\eta}} + \phi' E_{\dot{\eta}} & M_\eta + \phi' E_\eta & 1 & 0 \\ 0 & \Delta\phi' E_w & \Delta\phi' E_q & 0 & \Delta\phi' E_{\dot{\eta}} & \Delta\phi' E_\eta & 0 & 1 \end{bmatrix} \begin{bmatrix} u \\ w \\ q \\ \theta \\ \dot{\eta} \\ \eta \\ x_{fa} \\ x_{fb} \end{bmatrix}$$

$$+ \begin{bmatrix} 0 & 0 \\ 0 & 0 \end{bmatrix} \begin{pmatrix} \dot{y}_1^{des} \\ \dot{y}_2^{des} \end{pmatrix} \tag{4.21}$$

where

$$E_{\dot{\eta}} = -2\zeta\omega \quad E_{\eta} = -\omega^2 \quad \bar{E}_{\delta_2} = 1/\Delta\phi'$$

$$Fa_u = -\frac{M_u}{a} \quad Fa_w = -\frac{M_w + \phi' E_w}{a} \quad Fa_q = -\frac{M_q + \phi' E_q}{a} \quad Fa_\theta = -\frac{M_\theta}{a}$$

$$Fa_{\dot{\eta}} = -\frac{M_{\dot{\eta}} + \phi' E_{\dot{\eta}}}{a} \quad Fa_\eta = -\frac{M_\eta + \phi' E_\eta}{a} \quad Fa_a = -\frac{1}{a} \quad Fa_{\delta_1} = \frac{1}{a}$$

$$Fb_w = -\frac{\Delta\phi' E_w}{b} \quad Fb_q = -\frac{\Delta\phi' E_q}{b} \quad Fb_{\dot{\eta}} = -\frac{\Delta\phi' E_{\dot{\eta}}}{b} \quad Fb_\eta = -\frac{\Delta\phi' E_\eta}{b}$$

$$Fb_b = -\frac{1}{b} \quad Fb_{\delta_2} = \frac{1}{b}$$

or

$$\begin{bmatrix} \dot{x} \\ \dot{x}_{fa} \\ \dot{x}_{fb} \end{bmatrix} \triangleq \begin{bmatrix} \dot{u} \\ \dot{w} \\ \dot{q} \\ \dot{\theta} \\ \dot{\eta} \\ \ddot{\eta} \\ \dot{x}_{fa} \\ \dot{x}_{fb} \end{bmatrix} = \begin{bmatrix} A_x & B_{x\delta_1} & B_{x\delta_2} \\ A_w & B_{z\delta_1} & B_{z\delta_2} \\ A_q & B_{q\delta_1} & B_{q\delta_2} \\ A_\theta & 0 & 0 \\ A_{\dot{\eta}} & B_{\dot{\eta}\delta_1} & B_{\dot{\eta}\delta_2} \\ A_\eta & 0 & 0 \\ A_{fa}A_q & A_{fa} & 0 \\ A_{fb}A_{\dot{\eta}} & 0 & A_{fb} \end{bmatrix} \begin{bmatrix} x \\ x_{fa} \\ x_{fb} \end{bmatrix} + \begin{bmatrix} 0 & 0 \\ 0 & 0 \\ 0 & 0 \\ 0 & 0 \\ 0 & 0 \\ 0 & 0 \\ B_{fa1} & 0 \\ 0 & B_{fb2} \end{bmatrix} \begin{bmatrix} \dot{y}_1^{des} \\ \dot{y}_2^{des} \end{bmatrix} \tag{4.22}$$

$$\begin{bmatrix} \dot{y}_1 \\ \dot{y}_2 \end{bmatrix} = \begin{bmatrix} A_q + \phi' A_{\dot{\eta}} & 1 & 0 \\ \Delta\phi' A_{\dot{\eta}} & 0 & 1 \end{bmatrix} \begin{bmatrix} x \\ x_{fa} \\ x_{fb} \end{bmatrix} + \begin{bmatrix} 0 & 0 \\ 0 & 0 \end{bmatrix} \begin{bmatrix} \dot{y}_1^{des} \\ \dot{y}_2^{des} \end{bmatrix}$$

or

$$\begin{bmatrix} \dot{x} \\ \dot{x}_f \end{bmatrix} = \begin{bmatrix} A_x & B_x \\ A_{x_f,x} & A_{x_f} \end{bmatrix} \begin{bmatrix} x \\ x_f \end{bmatrix} + \begin{bmatrix} 0 \\ B_{x_f} \end{bmatrix} \dot{y}^{des}$$

Note that the open loop A and B matrices constitute part of A_c directly related to the nonfilter states. The change of dynamics for the entire closed loop comes from the interaction with the additional filter states. The $\dot{y}$ response is that of the open loop system augmented with filter states. It is through these states, x_f, that $\dot{y}^{des}$ enters $\dot{y}$. In a sense, this can be interpreted as an increase in relative degree of a system from $\dot{y}^{des}$ to y. The system relative degree changes from 1 to 2 when a first order filter is introduced into both loops of the inversion loop; the higher the degree of the filter the higher is the

relative degree. When a filter is introduced into one of the two loops the relative degree in that direction changes in a similar fashion.

4.6 Nonlinear Case

A parallel development is undertaken for a nonlinear system model and the results are similar. For convenience, define the general system in section 4.4 as

$$\begin{pmatrix} \dot{u} \\ \dot{w} \\ \dot{q} \\ \dot{\theta} \\ \ddot{\eta} \\ \dot{\eta} \end{pmatrix} = \begin{pmatrix} f_{\dot{u}}(x) \\ f_{\dot{w}}(x) \\ f_{\dot{q}}(x) \\ f_{\dot{\theta}}(x) \\ f_{\ddot{\eta}}(x) \\ f_{\dot{\eta}}(x) \end{pmatrix} + \begin{pmatrix} g_{\dot{u}1}(x) & 0 \\ g_{\dot{w}1}(x) & g_{\dot{w}2}(x) \\ g_{\dot{q}1}(x) & g_{\dot{q}2}(x) \\ 0 & 0 \\ g_{\ddot{\eta}1}(x) & g_{\ddot{\eta}2}(x) \\ 0 & 0 \end{pmatrix} \begin{pmatrix} \delta_1 \\ \delta_2 \end{pmatrix} \tag{4.23}$$

$$y_{sensed} = \begin{pmatrix} q_{ma_{sens}} \\ q_{ps_{sens}} - q_{ma_{sens}} \end{pmatrix} = \begin{pmatrix} q + \phi' \dot{\eta} \\ \Delta\phi' \dot{\eta} \end{pmatrix}$$

4.6.1 Case 1: Standard Dynamic Inversion

In the standard case, for this 2-input, 2-output system the following expressions give the inversion variables in specific terms

$$h(x) f(x) = \begin{pmatrix} f_{\dot{q}}(x) + \phi' f_{\ddot{\eta}}(x) \\ \Delta\phi' f_{\ddot{\eta}}(x) \end{pmatrix} \triangleq \begin{pmatrix} \bar{f}_q \\ \bar{f}_{\dot{\eta}} \end{pmatrix}$$

$$\left(h(x)g(x)\right)^{-1} = \begin{pmatrix} g_{\dot{q}}(x) + \phi' g_{\ddot{\eta}}(x) \\ \Delta\phi' g_{\ddot{\eta}}(x) \end{pmatrix}^{-1}$$

$$\left(h(x)g(x)\right)^{-1} = \begin{pmatrix} g_{\dot{q}1}(x) + \phi' g_{\ddot{\eta}1}(x) & g_{\dot{q}2}(x) + \phi' g_{\ddot{\eta}2}(x) \\ \Delta\phi' g_{\ddot{\eta}1}(x) & \Delta\phi' g_{\ddot{\eta}2}(x) \end{pmatrix}^{-1}$$

$$= \left[g_{\dot{q}1}(x)\Delta\phi' g_{\ddot{\eta}2}(x) - \Delta\phi' g_{\ddot{\eta}1}(x) g_{\dot{q}2}(x) \right]^{-1} \begin{pmatrix} \Delta\phi' g_{\ddot{\eta}2}(x) & -g_{\dot{q}2}(x) - \phi' g_{\ddot{\eta}2}(x) \\ -\Delta\phi' g_{\ddot{\eta}1}(x) & g_{\dot{q}1}(x) + \phi' g_{\ddot{\eta}1}(x) \end{pmatrix}$$

$$\triangleq \mathbf{\Delta} \begin{pmatrix} \Delta\phi' g_{\ddot{\eta}2}(x) & -g_{\dot{q}2}(x) - \phi' g_{\ddot{\eta}2}(x) \\ -\Delta\phi' g_{\ddot{\eta}1}(x) & g_{\dot{q}1}(x) + \phi' g_{\ddot{\eta}1}(x) \end{pmatrix}$$

as well as the control input coming into the system

$$\begin{aligned}\delta &= \left(h(x)g(x)\right)^{-1}\left[\dot{y}_{des} - h(x)f(x)\right] \\ &= \begin{pmatrix} g_{\dot{q}}(x) + \phi' g_{\ddot{\eta}}(x) \\ \Delta\phi' g_{\ddot{\eta}}(x) \end{pmatrix}^{-1}\left[\begin{pmatrix} \dot{y}_1^{des} \\ \dot{y}_2^{des} \end{pmatrix} - \begin{pmatrix} f_{\dot{q}}(x) + \phi' f_{\ddot{\eta}}(x) \\ \Delta\phi' f_{\ddot{\eta}}(x) \end{pmatrix}\right]\end{aligned} \tag{4.24}$$

Combining these different parts into the closed loop system results in

$$\begin{pmatrix} \dot{u} \\ \dot{w} \\ \dot{q} \\ \dot{\theta} \\ \ddot{\eta} \\ \dot{\eta} \end{pmatrix} = \begin{pmatrix} f_{\dot{u}}(x) \\ f_{\dot{w}}(x) \\ f_{\dot{q}}(x) \\ f_{\dot{\theta}}(x) \\ f_{\ddot{\eta}}(x) \\ f_{\dot{\eta}}(x) \end{pmatrix} + \begin{pmatrix} g_{\dot{u}1}(x) & 0 \\ g_{\dot{w}1}(x) & g_{\dot{w}2}(x) \\ g_{\dot{q}1}(x) & g_{\dot{q}2}(x) \\ 0 & 0 \\ g_{\ddot{\eta}1}(x) & g_{\ddot{\eta}2}(x) \\ 0 & 0 \end{pmatrix} \begin{pmatrix} g_{\dot{q}}(x) + \phi' g_{\ddot{\eta}}(x) \\ \Delta\phi' g_{\ddot{\eta}}(x) \end{pmatrix}^{-1}\left[\begin{pmatrix} \dot{y}_1^{des} \\ \dot{y}_2^{des} \end{pmatrix} - \begin{pmatrix} f_{\dot{q}}(x) + \phi' f_{\ddot{\eta}}(x) \\ \Delta\phi' f_{\ddot{\eta}}(x) \end{pmatrix}\right] \tag{4.25}$$

$$y_{sensed} = \begin{pmatrix} q_{ma_{sens}} \\ q_{ps_{sens}} - q_{ma_{sens}} \end{pmatrix} = \begin{pmatrix} q + \phi'\dot{\eta} \\ \Delta\phi'\dot{\eta} \end{pmatrix}$$

with the expanded version

$$\begin{pmatrix} \dot{u} \\ \dot{w} \\ \dot{q} \\ \dot{\theta} \\ \ddot{\eta} \\ \dot{\eta} \end{pmatrix} = \begin{pmatrix} f_{\dot{u}}(x) - g_{u1}(x)\dfrac{g_{\ddot{\eta}2}(x)f_{\dot{q}}(x) + g_{\dot{q}2}(x)f_{\ddot{\eta}}(x)}{\left(g_{\dot{q}1}(x)g_{\ddot{\eta}2}(x) - g_{\ddot{\eta}1}(x)g_{\dot{q}2}(x)\right)} \\ f_{\dot{w}}(x) - \dfrac{g_{w1}(x)g_{\ddot{\eta}2}(x) - g_{w2}(x)g_{\ddot{\eta}1}(x)}{\left(g_{\dot{q}1}(x)g_{\ddot{\eta}2}(x) - g_{\ddot{\eta}1}(x)g_{\dot{q}2}(x)\right)} f_{\dot{q}}(x) - \dfrac{g_{w2}(x)g_{\dot{q}1}(x) - g_{w1}(x)g_{\dot{q}2}(x)}{g_{\dot{q}1}(x)g_{\ddot{\eta}2}(x) - g_{\ddot{\eta}1}(x)g_{\dot{q}2}(x)} f_{\ddot{\eta}}(x) \\ 0 \\ f_{\dot{\theta}}(x) \\ 0 \\ f_{\dot{\eta}}(x) \end{pmatrix} + \begin{pmatrix} \dfrac{g_{u1}(\cdot)g_{\ddot{\eta}2}(\cdot)}{\left(g_{\dot{q}1}(\cdot)g_{\ddot{\eta}2}(\cdot) - g_{\ddot{\eta}1}(\cdot)g_{\dot{q}2}(\cdot)\right)} & \dfrac{-g_{u1}(\cdot)\left(g_{\dot{q}2}(\cdot) + \phi' g_{\ddot{\eta}2}(\cdot)\right)}{\Delta\phi'\left(g_{\dot{q}1}(\cdot)g_{\ddot{\eta}2}(\cdot) - g_{\ddot{\eta}1}(\cdot)g_{\dot{q}2}(\cdot)\right)} \\ \dfrac{g_{w1}(x)g_{\ddot{\eta}2}(x) - g_{w2}(x)g_{\ddot{\eta}1}(x)}{\left(g_{\dot{q}1}(\cdot)g_{\ddot{\eta}2}(\cdot) - g_{\ddot{\eta}1}(\cdot)g_{\dot{q}2}(\cdot)\right)} & \dfrac{-g_{w1}(\cdot)\left(g_{\dot{q}2}(\cdot) + \phi' g_{\ddot{\eta}2}(\cdot)\right) + g_{w2}(\cdot)\left(g_{\dot{q}1}(\cdot) + \phi' g_{\ddot{\eta}1}(\cdot)\right)}{\Delta\phi'\left(g_{\dot{q}1}(\cdot)g_{\ddot{\eta}2}(\cdot) - g_{\ddot{\eta}1}(\cdot)g_{\dot{q}2}(\cdot)\right)} \\ 1 & -\dfrac{\phi'}{\Delta\phi'} \\ 0 & 0 \\ 0 & \dfrac{1}{\Delta\phi'} \\ 0 & 0 \end{pmatrix} \begin{pmatrix} \dot{y}_1^{des} \\ \dot{y}_2^{des} \end{pmatrix}$$

$$
\begin{aligned}
y_{sensed} &= \begin{pmatrix} q_{ma_{sens}} \\ q_{ps_{sens}} - q_{ma_{sens}} \end{pmatrix} = \begin{pmatrix} q + \phi'\dot{\eta} \\ \Delta\phi'\dot{\eta} \end{pmatrix} \\
\dot{y}_{sensed} &= \begin{pmatrix} \dot{q}_{ma_{sens}} \\ \dot{q}_{ps_{sens}} - \dot{q}_{ma_{sens}} \end{pmatrix} = \begin{pmatrix} \dot{q} + \phi'\ddot{\eta} \\ \Delta\phi'\ddot{\eta} \end{pmatrix} \\
&= \begin{pmatrix} \dot{y}_1^{des} - \dfrac{\phi'}{\Delta\phi'}\dot{y}_2^{des} + \phi'\left(\dfrac{1}{\Delta\phi'}\dot{y}_2^{des}\right) \\ \Delta\phi'\left(\dfrac{1}{\Delta\phi'}\dot{y}_2^{des}\right) \end{pmatrix} \quad \Rightarrow \quad \dot{y}_{sensed} = \begin{pmatrix} \dot{y}_1^{des} \\ \dot{y}_2^{des} \end{pmatrix}
\end{aligned}
\tag{4.26}
$$

As expected for standard dynamic inversion, $\dot{y} = \dot{y}^{des}$ is recovered and the controlled variables equations have no influence from the (u, w) dynamics. Furthermore, for convenience rewrite the closed loop system as

$$
\begin{pmatrix} \dot{u} \\ \dot{w} \\ \dot{q} \\ \dot{\theta} \\ \ddot{\eta} \\ \dot{\eta} \end{pmatrix} = \begin{pmatrix} \hat{f}_{\dot{u}}(x) \\ \hat{f}_{\dot{w}}(x) \\ 0 \\ f_{\dot{\theta}}(x) \\ 0 \\ f_{\dot{\eta}}(x) \end{pmatrix} + \begin{pmatrix} \hat{g}_{\dot{u}1}(x) & \hat{g}_{\dot{u}2}(x) \\ \hat{g}_{\dot{w}1}(x) & \hat{g}_{\dot{w}2}(x) \\ 1 & \hat{g}_{\dot{q}2}(x) \\ 0 & 0 \\ 0 & \hat{g}_{\ddot{\eta}2}(x) \\ 0 & 0 \end{pmatrix} \begin{pmatrix} \dot{y}_1^{des} \\ \dot{y}_2^{des} \end{pmatrix}
\tag{4.27}
$$

$$
\dot{x}_c = \hat{f}(x) + \hat{g}_1(x)\dot{y}_1^{des} + \hat{g}_2(x)\dot{y}_2^{des}
$$

This result is equivalent to the one presented in Chapter 6 for a system with a single flexible mode. The next step is to add a single level of complexity in the inversion loop and trace its resulting influence on the closed loop dynamics.

4.6.2 Case 2: Filter in the Flexible Dynamics Loop

In this specific case, the filter equation (4.9) becomes

$$
W = \begin{bmatrix} 1 & 0 \\ 0 & \dfrac{1}{bs+1} \end{bmatrix} \quad \Rightarrow \quad \begin{aligned} \dot{x}_f &= A_f x_f + \begin{bmatrix} 0 & b_f \end{bmatrix} \begin{bmatrix} \bar{u}_1 \\ \bar{u}_2 \end{bmatrix} \\ y_f &= \begin{bmatrix} 0 \\ 1 \end{bmatrix} x_f + \begin{bmatrix} 1 & 0 \\ 0 & 0 \end{bmatrix} \begin{bmatrix} \bar{u}_1 \\ \bar{u}_2 \end{bmatrix} \end{aligned}
\tag{4.28}
$$

The control input coming into the system in this case is

$$
\begin{aligned}
\delta &= \begin{pmatrix} g_{\dot{q}}(x) + \phi' g_{\ddot{\eta}}(x) \\ \Delta\phi' g_{\ddot{\eta}}(x) \end{pmatrix}^{-1} y_f \\
&= \mathbf{\Delta} \begin{pmatrix} \Delta\phi' g_{\ddot{\eta}2}(x) & -g_{\dot{q}2}(x) - \phi' g_{\ddot{\eta}2}(x) \\ -\Delta\phi' g_{\ddot{\eta}1}(x) & g_{\dot{q}1}(x) + \phi' g_{\ddot{\eta}1}(x) \end{pmatrix} \left\{ \begin{bmatrix} 0 \\ 1 \end{bmatrix} x_f + \begin{bmatrix} 1 & 0 \\ 0 & 0 \end{bmatrix} \begin{bmatrix} \bar{u}_1 \\ \bar{u}_2 \end{bmatrix} \right\} \\
&= \mathbf{\Delta} \begin{pmatrix} -g_{\dot{q}2}(x) - \phi' g_{\ddot{\eta}2}(x) \\ g_{\dot{q}1}(x) + \phi' g_{\ddot{\eta}1}(x) \end{pmatrix} x_f + \mathbf{\Delta} \begin{pmatrix} \Delta\phi' g_{\ddot{\eta}2}(x) & 0 \\ -\Delta\phi' g_{\ddot{\eta}1}(x) & 0 \end{pmatrix} \begin{bmatrix} \bar{u}_1 \\ \bar{u}_2 \end{bmatrix} \\
&= \mathbf{\Delta} \begin{pmatrix} -g_{\dot{q}2}(x) - \phi' g_{\ddot{\eta}2}(x) \\ g_{\dot{q}1}(x) + \phi' g_{\ddot{\eta}1}(x) \end{pmatrix} x_f + \mathbf{\Delta} \begin{pmatrix} \Delta\phi' g_{\ddot{\eta}2}(x) & 0 \\ -\Delta\phi' g_{\ddot{\eta}1}(x) & 0 \end{pmatrix} \left(\begin{bmatrix} \dot{y}_1^{des} \\ \dot{y}_2^{des} \end{bmatrix} - \begin{pmatrix} \bar{f}_q(x) \\ \bar{f}_{\dot{\eta}}(x) \end{pmatrix} \right)
\end{aligned}
\tag{4.29}
$$

Calculating sub-elements of the closed loop system:

$$\begin{pmatrix} g_{\dot{u}1}(x) & 0 \\ g_{\dot{w}1}(x) & g_{\dot{w}2}(x) \\ g_{\dot{q}1}(x) & g_{\dot{q}2}(x) \\ 0 & 0 \\ g_{\ddot{\eta}1}(x) & g_{\ddot{\eta}2}(x) \\ 0 & 0 \end{pmatrix} \mathbf{\Delta} \left\{ \begin{pmatrix} -g_{\dot{q}2}(x) - \phi' g_{\ddot{\eta}2}(x) \\ g_{\dot{q}1}(x) + \phi' g_{\ddot{\eta}1}(x) \end{pmatrix} x_f + \begin{pmatrix} \Delta\phi' g_{\ddot{\eta}2}(x) & 0 \\ -\Delta\phi' g_{\ddot{\eta}1}(x) & 0 \end{pmatrix} \left(\begin{bmatrix} \dot{y}_1^{des} \\ \dot{y}_2^{des} \end{bmatrix} - \begin{pmatrix} \overline{f}_q(x) \\ \overline{f}_{\dot{\eta}}(x) \end{pmatrix} \right) \right\}$$

$$= \begin{pmatrix} \dfrac{g_{\dot{u}1}(x)\left(-g_{\dot{q}2}(x) - \phi' g_{\ddot{\eta}2}(x)\right)}{\Delta\phi'\left(g_{\dot{q}1}(x) g_{\ddot{\eta}2}(x) - g_{\ddot{\eta}1}(x) g_{\dot{q}2}(x)\right)} \\ \dfrac{g_{\dot{w}1}(x)\left(-g_{\dot{q}2}(x) - \phi' g_{\ddot{\eta}2}(x)\right) + g_{\dot{w}2}(x)\left(g_{\dot{q}1}(x) + \phi' g_{\ddot{\eta}1}(x)\right)}{\Delta\phi'\left(g_{\dot{q}1}(x) g_{\ddot{\eta}2}(x) - g_{\ddot{\eta}1}(x) g_{\dot{q}2}(x)\right)} \\ \dfrac{-\phi'}{\Delta\phi'} \\ 0 \\ \dfrac{1}{\Delta\phi'} \\ 0 \end{pmatrix} x_f$$

$$+ \begin{pmatrix} \dfrac{g_{\dot{u}1}(x) g_{\ddot{\eta}2}(x)}{\left(g_{\dot{q}1}(x) g_{\ddot{\eta}2}(x) - g_{\ddot{\eta}1}(x) g_{\dot{q}2}(x)\right)} & 0 \\ \dfrac{g_{\dot{w}1}(x) g_{\ddot{\eta}2}(x) - g_{\dot{w}2}(x) g_{\ddot{\eta}1}(x)}{\left(g_{\dot{q}1}(x) g_{\ddot{\eta}2}(x) - g_{\ddot{\eta}1}(x) g_{\dot{q}2}(x)\right)} & 0 \\ 1 & 0 \\ 0 & 0 \\ 0 & 0 \\ 0 & 0 \end{pmatrix} \left(\begin{bmatrix} \dot{y}_1^{des} \\ \dot{y}_2^{des} \end{bmatrix} - \begin{pmatrix} \overline{f}_q(x) \\ \overline{f}_{\dot{\eta}}(x) \end{pmatrix} \right)$$

and applying to the closed loop system results in

$$\begin{pmatrix} \dot{u} \\ \dot{w} \\ \dot{q} \\ \dot{\theta} \\ \ddot{\eta} \\ \dot{\eta} \end{pmatrix} = \begin{pmatrix} f_{\dot{u}}(x) \\ f_{\dot{w}}(x) \\ f_{\dot{q}}(x) \\ f_{\dot{\theta}}(x) \\ f_{\ddot{\eta}}(x) \\ f_{\dot{\eta}}(x) \end{pmatrix} + \frac{1}{\Delta\phi'} \begin{pmatrix} \dfrac{g_{\dot{u}1}(x)\left(-g_{\dot{q}2}(x) - \phi' g_{\ddot{\eta}2}(x)\right)}{\left(g_{\dot{q}1}(x)g_{\ddot{\eta}2}(x) - g_{\ddot{\eta}1}(x)g_{\dot{q}2}(x)\right)} \\ \dfrac{g_{\dot{w}1}(x)\left(-g_{\dot{q}2}(x) - \phi' g_{\ddot{\eta}2}(x)\right) + g_{\dot{w}2}(x)\left(g_{\dot{q}1}(x) + \phi' g_{\ddot{\eta}1}(x)\right)}{\left(g_{\dot{q}1}(x)g_{\ddot{\eta}2}(x) - g_{\ddot{\eta}1}(x)g_{\dot{q}2}(x)\right)} \\ -\phi' \\ 0 \\ 1 \\ 0 \end{pmatrix} x_f$$

$$+ \begin{pmatrix} \dfrac{g_{\dot{u}1}(x)g_{\ddot{\eta}2}(x)}{\left(g_{\dot{q}1}(x)g_{\ddot{\eta}2}(x) - g_{\ddot{\eta}1}(x)g_{\dot{q}2}(x)\right)} & 0 \\ \dfrac{g_{\dot{w}1}(x)g_{\ddot{\eta}2}(x) - g_{\dot{w}2}(x)g_{\ddot{\eta}1}(x)}{\left(g_{\dot{q}1}(x)g_{\ddot{\eta}2}(x) - g_{\ddot{\eta}1}(x)g_{\dot{q}2}(x)\right)} & 0 \\ 1 & 0 \\ 0 & 0 \\ 0 & 0 \\ 0 & 0 \end{pmatrix} \left(\begin{bmatrix} \dot{y}_1^{des} \\ \dot{y}_2^{des} \end{bmatrix} - \begin{pmatrix} \overline{f}_q(x) \\ \overline{f}_{\dot{\eta}}(x) \end{pmatrix} \right) x_f$$

$$\dot{x}_f = A_f x_f + \begin{bmatrix} 0 & b_f \end{bmatrix} \left(\begin{bmatrix} \dot{y}_1^{des} \\ \dot{y}_2^{des} \end{bmatrix} - \begin{pmatrix} \overline{f}_q(x) \\ \overline{f}_{\dot{\eta}}(x) \end{pmatrix} \right) \tag{4.30}$$

The combined expanded version is

$$\begin{pmatrix} \dot{u} \\ \dot{w} \\ \dot{q} \\ \dot{\theta} \\ \ddot{\eta} \\ \dot{\eta} \\ \dot{x}_f \end{pmatrix} = \begin{pmatrix} f_{\dot{u}}(x) - \dfrac{g_{\dot{u}1}(x)g_{\ddot{\eta}2}(x)}{\left(g_{\dot{q}1}(x)g_{\ddot{\eta}2}(x) - g_{\ddot{\eta}1}(x)g_{\dot{q}2}(x)\right)}\left(f_{\dot{q}}(x) + \phi' f_{\ddot{\eta}}(x)\right) \\ f_{\dot{w}}(x) - \dfrac{g_{\dot{w}1}(x)g_{\ddot{\eta}2}(x) - g_{\dot{w}2}(x)g_{\ddot{\eta}1}(x)}{\left(g_{\dot{q}1}(x)g_{\ddot{\eta}2}(x) - g_{\ddot{\eta}1}(x)g_{\dot{q}2}(x)\right)}\left(f_{\dot{q}}(x) + \phi' f_{\ddot{\eta}}(x)\right) \\ f_{\dot{q}}(x) - \left(f_{\dot{q}}(x) + \phi' f_{\ddot{\eta}}(x)\right) \\ f_{\dot{\theta}}(x) \\ f_{\ddot{\eta}}(x) \\ f_{\dot{\eta}}(x) \\ b_f \Delta\phi' f_{\ddot{\eta}}(x) \end{pmatrix} + \begin{pmatrix} \dfrac{g_{\dot{u}1}(x)g_{\ddot{\eta}2}(x)}{\left(g_{\dot{q}1}(x)g_{\ddot{\eta}2}(x) - g_{\ddot{\eta}1}(x)g_{\dot{q}2}(x)\right)}\dot{y}_1^{des} \\ \dfrac{g_{\dot{w}1}(x)g_{\ddot{\eta}2}(x) - g_{\dot{w}2}(x)g_{\ddot{\eta}1}(x)}{\left(g_{\dot{q}1}(x)g_{\ddot{\eta}2}(x) - g_{\ddot{\eta}1}(x)g_{\dot{q}2}(x)\right)}\dot{y}_1^{des} \\ \dot{y}_1^{des} \\ 0 \\ 0 \\ 0 \\ b_f \dot{y}_2^{des} \end{pmatrix}$$

$$+ \begin{pmatrix} \dfrac{1}{\Delta\phi'}\dfrac{g_{\dot{u}1}(x)\left(-g_{\dot{q}2}(x) - \phi' g_{\ddot{\eta}2}(x)\right)}{\left(g_{\dot{q}1}(x)g_{\ddot{\eta}2}(x) - g_{\ddot{\eta}1}(x)g_{\dot{q}2}(x)\right)} \\ \dfrac{1}{\Delta\phi'}\dfrac{g_{\dot{w}1}(x)\left(-g_{\dot{q}2}(x) - \phi' g_{\ddot{\eta}2}(x)\right) + g_{\dot{w}2}(x)\left(g_{\dot{q}1}(x) + \phi' g_{\ddot{\eta}1}(x)\right)}{\left(g_{\dot{q}1}(x)g_{\ddot{\eta}2}(x) - g_{\ddot{\eta}1}(x)g_{\dot{q}2}(x)\right)} \\ \dfrac{-\phi'}{\Delta\phi'} \\ 0 \\ \dfrac{1}{\Delta\phi'} \\ 0 \\ A_f \end{pmatrix} x_f \tag{4.31}$$

The closed loop system can be rewritten as

$$\begin{pmatrix} \dot{u} \\ \dot{w} \\ \dot{q} \\ \dot{\theta} \\ \ddot{\eta} \\ \dot{\eta} \\ \dot{x}_f \end{pmatrix} = \begin{pmatrix} \hat{f}_{\dot{u}}(x) \\ \hat{f}_{\dot{w}}(x) \\ -\phi' f_{\ddot{\eta}}(x) \\ q \\ f_{\ddot{\eta}}(x) \\ \dot{\eta} \\ b_f \Delta\phi' f_{\ddot{\eta}}(x) \end{pmatrix} + \begin{pmatrix} \hat{A}_u / \Delta\phi' \\ \hat{A}_w / \Delta\phi' \\ -\phi' / \Delta\phi' \\ 0 \\ \dfrac{1}{\Delta\phi'} \\ 0 \\ A_f \end{pmatrix} x_f + \begin{pmatrix} \hat{g}_{\dot{u}1}(x)\dot{y}_1^{des} \\ \hat{g}_{\dot{w}1}\dot{y}_1^{des} \\ \dot{y}_1^{des} \\ 0 \\ 0 \\ 0 \\ b_f \dot{y}_2^{des} \end{pmatrix}$$

$$\dot{y}_{sensed} = \begin{pmatrix} \dot{q}_{ma_{sens}} \\ \dot{q}_{ps_{sens}} - \dot{q}_{ma_{sens}} \end{pmatrix} = \begin{pmatrix} \dot{q} + \phi' \ddot{\eta} \\ \Delta\phi' \ddot{\eta} \end{pmatrix} \tag{4.32}$$

$$= \begin{pmatrix} \dot{y}_1^{des} \\ \Delta\phi' f_{\ddot{\eta}}(x) + x_f \end{pmatrix} \quad \text{with } x_f = f\left(\dot{y}_2^{des}\right)$$

or

$$\begin{pmatrix} \dot{u} \\ \dot{w} \\ \dot{q} \\ \dot{\theta} \\ \ddot{\eta} \\ \dot{\eta} \\ \cdots \\ \dot{x}_f \end{pmatrix} = \begin{pmatrix} \hat{f}_{\dot{u}}(x) + \Delta\hat{f}_{\dot{u}}(f_{\ddot{\eta}}(x)) \\ \hat{f}_{\dot{w}}(x) + \Delta\hat{f}_{\dot{w}}(f_{\ddot{\eta}}(x)) \\ 0 + \Delta\hat{f}_{\dot{q}}(f_{\ddot{\eta}}(x)) \\ f_{\dot{\theta}}(x) \\ 0 + \Delta\hat{f}_{\ddot{\eta}}(f_{\ddot{\eta}}(x)) \\ f_{\dot{\eta}}(x) \\ \cdots \\ B_f\left(h(x)f(x)\right) \end{pmatrix} + \begin{pmatrix} \hat{g}_{\dot{u}2}(x) \\ \hat{g}_{\dot{w}2}(x) \\ \hat{g}_{\dot{q}2}(x) \\ 0 \\ \hat{g}_{\ddot{\eta}2}(x) \\ 0 \\ \cdots \\ A_f \end{pmatrix} x_f + \begin{pmatrix} \hat{g}_{\dot{u}1}(x) & 0 \\ \hat{g}_{\dot{w}1}(x) & 0 \\ 1 & 0 \\ 0 & 0 \\ 0 & 0 \\ 0 & 0 \\ \cdots & \cdots \\ 0 & B_f \end{pmatrix} \begin{pmatrix} \dot{y}_1^{des} \\ \dot{y}_2^{des} \end{pmatrix} \tag{4.33}$$

$$\begin{pmatrix} \dot{x}_c \\ \dot{x}_f \end{pmatrix} = \begin{bmatrix} \hat{f}(x) + \Delta\hat{f}(f_{\ddot{\eta}}(x)) \\ B_f\left(h(x)f(x)\right) \end{bmatrix} + \begin{bmatrix} \hat{g}_2(x) \\ A_f \end{bmatrix} x_f + \begin{bmatrix} \hat{g}_1(x) & 0 \\ 0 & B_f \end{bmatrix} \begin{pmatrix} \dot{y}_1^{des} \\ \dot{y}_2^{des} \end{pmatrix}$$

Note the similarities with the linear case. This is to be expected since the nonlinear system is assumed to be affine in controls and the filter is a linear system. This view provides another indication that the change in the flexible dynamics due to filter introduction in the inversion loop appears as a delta on the closed loop dynamics of the standard dynamic inversion.

The connection between Cases 1and 2 comes from letting the filter $W = \begin{bmatrix} 1 & 0 \\ 0 & 1/bs+1 \end{bmatrix} \to \begin{bmatrix} 1 & 0 \\ 0 & 1 \end{bmatrix}$. This implies that

$$\begin{aligned} \dot{x}_f &= A_f x_f + B_f \bar{u} \\ y_f &= C_f x_f + D_f \bar{u} \end{aligned} \to \begin{aligned} 0 &= A_f x_f + B_f \bar{u} \\ y_f &= C_f x_f + D_f \bar{u} \end{aligned}$$

$$\begin{aligned} 0 &= \begin{bmatrix} -1/b \end{bmatrix} x_f + \begin{bmatrix} 0 & 1/b \end{bmatrix} \begin{pmatrix} \bar{u}_1 \\ \bar{u}_2 \end{pmatrix} \\ y_f &= \begin{bmatrix} 0 \\ 1 \end{bmatrix} x_f + \begin{bmatrix} 1 & 0 \\ 0 & 0 \end{bmatrix} \begin{pmatrix} \bar{u}_1 \\ \bar{u}_2 \end{pmatrix} \end{aligned} \to \begin{aligned} x_f &= \bar{u}_2 \\ y_f &= \begin{bmatrix} 0 \\ 1 \end{bmatrix} \bar{u}_2 + \begin{bmatrix} 1 & 0 \\ 0 & 0 \end{bmatrix} \begin{pmatrix} \bar{u}_1 \\ \bar{u}_2 \end{pmatrix} \end{aligned}$$

$$\Downarrow$$

$$\begin{pmatrix} \dot{x}_c \\ 0 \end{pmatrix} = \begin{bmatrix} \hat{f}(x) + \Delta\hat{f}(f_{\ddot{\eta}}(x)) \\ B_f\left(h(x)f(x)\right) \end{bmatrix} + \begin{bmatrix} \hat{g}_2(x) \\ -1/b \end{bmatrix} \bar{u}_2 + \begin{bmatrix} \hat{g}_1(x) & 0 \\ 0 & 1/b \end{bmatrix} \begin{pmatrix} \dot{y}_1^{des} \\ \dot{y}_2^{des} \end{pmatrix}$$

$$\Downarrow$$

$$\begin{pmatrix} \dot{x}_c \\ 0 \end{pmatrix} = \begin{bmatrix} \hat{f}(x) + \Delta\hat{f}(f_{\ddot{\eta}}(x)) \\ B_f\left(h(x)f(x)\right) \end{bmatrix} + \begin{bmatrix} \hat{g}_2(x) \\ -1/b \end{bmatrix}\left(\dot{y}_2^{des} - \overline{f}_{\ddot{\eta}}(x)\right) + \begin{bmatrix} \hat{g}_1(x) & 0 \\ 0 & 1/b \end{bmatrix}\begin{pmatrix} \dot{y}_1^{des} \\ \dot{y}_2^{des} \end{pmatrix}$$

$$\Downarrow$$

$$B_f\left(h(x)f(x)\right) = -\overline{f}_{\ddot{\eta}}(x)$$

$$\dot{x}_c = \hat{f}(x) + \Delta\hat{f}(f_{\ddot{\eta}}(x)) + \hat{g}_2(x)\left(\dot{y}_2^{des} - \overline{f}_{\ddot{\eta}}(x)\right) + \hat{g}_1(x)\dot{y}_1^{des}$$

$$\Downarrow$$

$$\dot{x}_c = \hat{f}(x) + \Delta\hat{f}(f_{\ddot{\eta}}(x)) - \hat{g}_2(x)\overline{f}_{\ddot{\eta}}(x) + \hat{g}_1(x)\dot{y}_1^{des} + \hat{g}_2(x)\dot{y}_2^{des}$$

$$\Downarrow$$

$$\Delta\hat{f}(f_{\ddot{\eta}}(x)) = \hat{g}_2(x)\overline{f}_{\ddot{\eta}}(x)$$

$$\dot{x}_c = \hat{f}(x) + \hat{g}_1(x)\dot{y}_1^{des} + \hat{g}_2(x)\dot{y}_2^{des}$$

In abusing the functional notation a bit, $\Delta\hat{f}\left(f_{\ddot{\eta}}(x)\right)$ simply implies that the difference in dynamics between the two cases is a function of the flexible modes as the detailed expansion indicates.

$$\begin{pmatrix} \Delta\hat{f}_{\dot{u}}(f_{\ddot{\eta}}(x)) \\ \Delta\hat{f}_{\dot{w}}(f_{\ddot{\eta}}(x)) \\ \Delta\hat{f}_{\dot{q}}(f_{\ddot{\eta}}(x)) \\ 0 \\ \Delta\hat{f}_{\ddot{\eta}}(f_{\ddot{\eta}}(x)) \\ 0 \end{pmatrix} = \begin{pmatrix} g_{\dot{u}1}(x)\dfrac{g_{\dot{q}2}(x) - g_{\ddot{\eta}2}(x)\phi'}{\left(g_{\dot{q}1}(x)g_{\ddot{\eta}2}(x) - g_{\ddot{\eta}1}(x)g_{\dot{q}2}(x)\right)} f_{\ddot{\eta}}(x) \\ \dfrac{g_{\dot{w}2}(x)\left(g_{\dot{q}1}(x) - g_{\ddot{\eta}1}(x)\phi'\right) - g_{\dot{w}1}(x)\left(g_{\dot{q}2}(x) + g_{\ddot{\eta}2}(x)\phi'\right)}{g_{\dot{q}1}(x)g_{\ddot{\eta}2}(x) - g_{\ddot{\eta}1}(x)g_{\dot{q}2}(x)} f_{\ddot{\eta}}(x) \\ -\phi' f_{\ddot{\eta}}(x) \\ 0 \\ f_{\ddot{\eta}}(x) \\ 0 \end{pmatrix} \quad (4.34)$$

A filter in a single loop provides a good intermediate case to connect the stability results of the standard dynamic inversion in the presence of strong flight/structural mode dynamic interactions and a novel dynamic inversion on a full scale, highly complex, high fidelity aircraft simulation. The choice of the model that dispenses with higher frequency elastic modes and actuator dynamics allows for fulfilling the stated controller objectives by only introducing a modification in the structural dynamics loop. Recall that the original control objectives are to design an integrated flight/SMC controller that would

make the aircraft behave as a rigid body in response to a flight command while improving very lightly damped low frequency structural modes without their outright cancellation. The additional higher order dynamics present in the high fidelity model also introduce more complicated rigid body/flexible mode interactions that necessitate an introduction of the modification filter into both loops to achieve the stated control objectives. Thus, Case 2 appears to be an appropriate bridge between standard dynamic inversion analytical results and high fidelity simulation studies. This will be used in Chapter 7 for assessing the stability of the novel dynamic inversion.

4.7 Standard Dynamic Inversion – Short Period

This section starts the second half the chapter that deals with the relationship between the novel dynamic inversion and the specific response of aircraft dynamics, which start from the simplest and increase in complexity. The aircraft model used to explore the analytical response relationships considered in this section has the standard short period approximation plus an elastic mode[21] and has been modified to show the interaction between rigid and flexible body dynamics. The equations expressed in dimensional derivatives are given below:

$$\begin{bmatrix} \dot{w} \\ \dot{q} \\ \ddot{\eta} \\ \dot{\eta} \end{bmatrix} = \begin{bmatrix} Z_w & Z_q & Z_{\dot{\eta}} & Z_\eta \\ M_w & M_q & M_{\dot{\eta}} & M_\eta \\ E_w & E_q & -2\zeta\omega & -\omega^2 \\ 0 & 0 & 1 & 0 \end{bmatrix} \begin{bmatrix} w \\ q \\ \dot{\eta} \\ \eta \end{bmatrix} + \begin{bmatrix} Z_\delta & Z_{rcv} \\ M_\delta & M_{rcv} \\ E_\delta & E_{rcv} \\ 0 & 0 \end{bmatrix} \begin{bmatrix} \delta \\ RCV \end{bmatrix} \tag{4.35}$$

The controlled variables are consistent with those used for the HSCT aircraft controller in Chapter 5 and are described in the following equation

$$y = \begin{bmatrix} q_{ma} \\ q_{ps} - q_{ma} \end{bmatrix} = \begin{bmatrix} 0 & 1 & \phi'_{ma} & 0 \\ 0 & 0 & \phi'_{ps} - \phi'_{ma} & 0 \end{bmatrix} \begin{bmatrix} w \\ q \\ \dot{\eta} \\ \eta \end{bmatrix}$$
$$= \begin{bmatrix} 0 & 1 & \phi'_{ma} & 0 \\ 0 & 0 & \Delta\phi' & 0 \end{bmatrix} \begin{bmatrix} w \\ q \\ \dot{\eta} \\ \eta \end{bmatrix} \tag{4.36}$$

where ϕ' is the slope of the mode shape.

Applying the standard dynamic inversion to a set of linear equations in general gives the following results.

$$\begin{aligned} \dot{x} &= Ax + Bu = Ax + B\left\{(CB)^{-1}\left(\dot{y}^{des} - CAx\right)\right\} \\ &= \left(A - B(CB)^{-1} CA\right)x + B(CB)^{-1}\dot{y}^{des} \\ &\rightarrow C\dot{x} = \dot{y} = \dot{y}^{des} \end{aligned} \tag{4.37}$$

Thus, applying (4.37) to the dynamics described by (4.35) and (4.36) gives the transfer function matrix for the closed loop

$$\frac{y}{\dot{y}^{des}} = \begin{bmatrix} 1/s & 0 \\ 0 & 1/s \end{bmatrix} \tag{4.38}$$

The closed loop system dynamics from $\dot{y}^{des}$ to $\dot{y}$ are given by (4.39).

$$\begin{bmatrix} \dot{w} \\ \dot{q} \\ \ddot{\eta} \\ \dot{\eta} \end{bmatrix} = \begin{bmatrix} \bar{Z}_w & \bar{Z}_q & \bar{Z}_{\dot{\eta}} & \bar{Z}_{\eta} \\ 0 & 0 & 0 & 0 \\ 0 & 0 & 0 & 0 \\ 0 & 0 & 1 & 0 \end{bmatrix} \begin{bmatrix} w \\ q \\ \dot{\eta} \\ \eta \end{bmatrix} + \begin{bmatrix} \bar{Z}_{\dot{y}1} & \bar{Z}_{\dot{y}2} \\ 1 & \bar{M}_{\dot{y}2} \\ 0 & \bar{E}_{\dot{y}2} \\ 0 & 0 \end{bmatrix} \begin{bmatrix} \dot{y}_1 \\ \dot{y}_2 \end{bmatrix}^{des}$$
$$\begin{bmatrix} \dot{y}_1 \\ \dot{y}_2 \end{bmatrix} = \begin{bmatrix} \dot{y}_1^{des} + \left(\bar{M}_{\dot{y}2} + \phi'\bar{E}_{\dot{y}2}\right)\dot{y}_2^{des} \\ \Delta\phi'\bar{E}_{\dot{y}2}\dot{y}_2^{des} \end{bmatrix} = \begin{bmatrix} \dot{y}_1^{des} \\ \dot{y}_2^{des} \end{bmatrix}$$
$$\text{where} \quad \bar{M}_{\dot{y}2} = -\phi'\bar{E}_{\dot{y}2} \quad \text{and } \Delta\phi'\bar{E}_{\dot{y}2} = 1 \tag{4.39}$$

The set of closed loop poles, shown in expression (4.40), contains two poles at s=0 that correspond to the integrators shown in (4.38) plus those coinciding with the transmission zeros of the open loop system.

$$\left\{ Z_w + Z_\delta \left(\frac{E_w M_{rcv} - E_{rcv} M_w}{E_{rcv} M_\delta - E_\delta M_{rcv}} \right) + Z_{rcv} \left(\frac{E_\delta M_w - E_w M_\delta}{E_{rcv} M_\delta - E_\delta M_{rcv}} \right) ,\ 0,\ 0,\ 0 \right\} \qquad (4.40)$$

These are the internal or zero dynamics; one root corresponding to the vertical velocity *w*, which is not directly controlled in the problem formulation, and the other to s=0. So the results are standard as expected when standard dynamic inversion is applied to an aircraft.

However, this methodology works well if the only interest is in controlling the dynamics from some commanded pitch rate coming from either a pilot stick or an autopilot command, but it has no effect on controlling disturbances or improving robustness to model uncertainties that always exist.

4.8 Novel Dynamic Inversion – Short Period.

In order to illustrate just how the novel dynamic inversion influences the closed loop dynamics, several variations of the simplified open loop system and $W(x)$ are presented. The introduction of the dynamics matrix $W(x)$ into the inversion loop is illustrated in Figure 4.3.

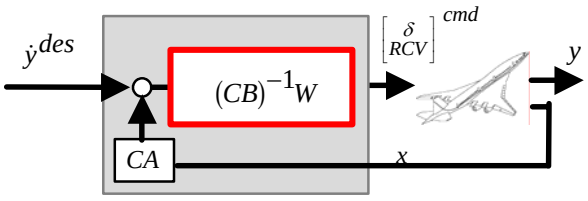

Figure 4.3: Novel dynamic inversion.

The initial step is to start looking at SISO system dynamics and begin with short period dynamics only. Let $W(x)$ equal a first order filter. The closed loop dynamics and transfer function are presented in (4.41).

$$W = \frac{1}{as+1}$$

$$\frac{y}{\dot{y}^{des}} = \frac{q_{ma}}{\dot{q}_{ma}^{des}} = \frac{s^2 + \left(\frac{1}{a} - Z_w + M_w \frac{Z_\delta}{M_\delta}\right)s + \frac{Z_\delta M_w - Z_w M_\delta}{aM_\delta}}{s\left[s^2 + \left(\frac{1}{a} - M_q - Z_w\right)s + \left(Z_w M_q - Z_q M_w + \frac{Z_\delta M_w - Z_w M_\delta}{aM_\delta}\right)\right]} \tag{4.41}$$

Note that the right side of (4.41) is no longer a pure integrator as is the case for standard dynamic inversion (see (4.38)). The filter $W(x)$ in the loop introduces another pole-zero pair that precludes pole-zero cancellation resulting from the standard dynamic inversion. The movement of the poles with the changing value of *a* is illustrated in Figure 4.4. For *a*>1, the non-integrator closed loop dynamics are concentrated around open loop poles, as follows from (4.41). On the other hand, for *a*<1, the short period dynamics become faster as both non-integrator poles move further into the left-half plane. It is interesting to note that as $1/a \to \infty$ the pole-zero cancellation is recovered and $\frac{y}{\dot{y}^{des}} \to \frac{1}{s}$. While this result may not be particularly interesting when dealing with rigid body dynamics, its real value is recognized when the flexible mode dynamics are explored.

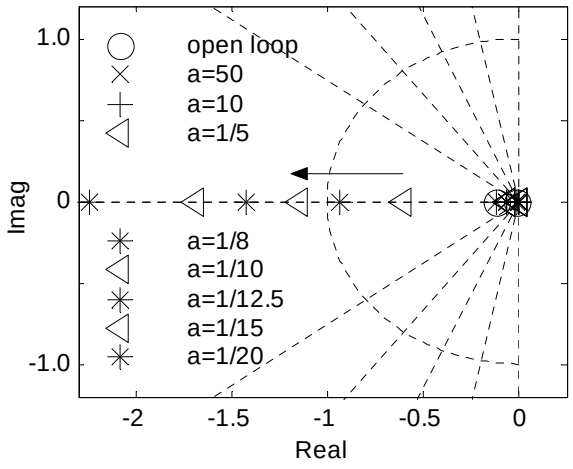

Figure 4.4: Short period closed loop poles as *a* changes.

Consider a similar SISO system setup, but this time dealing with typical second-order flexible mode dynamics

$$\begin{bmatrix} \ddot{\eta} \\ \dot{\eta} \end{bmatrix} = \begin{bmatrix} -2\zeta\omega & -\omega^2 \\ 1 & 0 \end{bmatrix} \begin{bmatrix} \dot{\eta} \\ \eta \end{bmatrix} + \begin{bmatrix} E_\delta \\ 0 \end{bmatrix} \delta$$

$$W = \frac{1}{bs+1}$$

$$\frac{y}{\dot{y}^{des}} = \frac{\dot{\eta}}{\ddot{\eta}^{des}} = \frac{1/b}{s^2 + \left(\frac{1}{b} + 2\zeta\omega\right)s + \omega^2} \tag{4.42}$$

$$\rightarrow \hat{\omega} = \omega, \text{ and } \hat{\zeta} = \zeta + \frac{1}{2\omega b}$$

The resulting closed loop system dynamics are again altered by the introduction of a filter $W(x)$. As (4.42) clearly shows, the damping of the closed loop elastic mode is controlled by the time constant of the filter $W(x)$ that modifies the standard dynamic inversion procedure. The change in the damping and hence the movement of the elastic mode dipole is illustrated in Figure 4.5. For the values of b>1, the elastic mode dipole barely moves from the open loop dynamics. However for b<1, there is a pronounced movement in the poles along the line of constant frequency and increasing damping for diminishing b. In fact, for b=1/17.5, the damping becomes supercritical and the elastic mode dipole becomes a pair of real poles that approach s=0, 1/b in the limit and

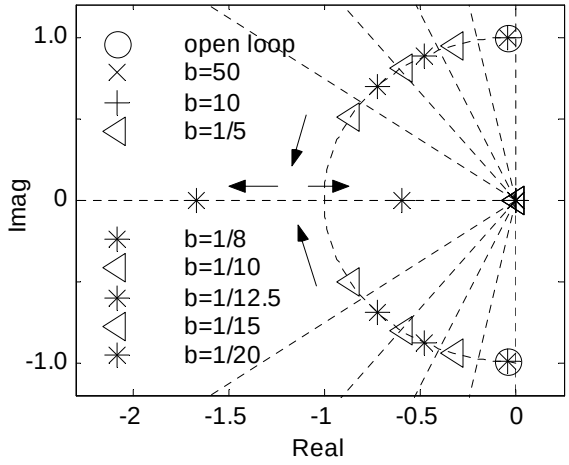

Figure 4.5: Flexible mode closed loop poles as b changes.

recovering the pole-zero cancellation with $\frac{y}{\dot{y}^{des}} \to \frac{1}{s}$. This observation that an addition of a filter into a dynamic inversion loop influences damping in a SISO system is carried through to a MIMO system that combines short period and elastic mode dynamics.

A small observation regarding the SISO examples of systems (4.41) and (4.42) – introducing the filter $W(x)$ is equivalent to placing unmodeled first order actuator dynamics in the dynamic inversion control. One would expect that as the actuator bandwidth increases, the $\frac{y}{\dot{y}^{des}} \to \frac{1}{s}$, which is precisely the case.

The combined short period/one elastic mode MIMO system open loop dynamics are given by (4.35) and (4.36). The addition of the matrix $W(x)$ into the feedforward loop modifies the results of the standard dynamic inversion. Let $W(x)$ be a diagonal matrix of first order filters given by (4.43), which can also be expressed in state space system as shown.

$$
\begin{aligned}
W &= \begin{bmatrix} \frac{1}{as+1} & 0 \\ 0 & \frac{1}{bs+1} \end{bmatrix} \\
\begin{bmatrix} \dot{x}_a \\ \dot{x}_b \end{bmatrix} &= \begin{bmatrix} -\frac{1}{a} & 0 \\ 0 & -\frac{1}{b} \end{bmatrix} \begin{bmatrix} x_a \\ x_b \end{bmatrix} + \begin{bmatrix} \frac{1}{a} & 0 \\ 0 & \frac{1}{b} \end{bmatrix} \bar{u} \\
\dot{\bar{x}} &= \bar{A}\bar{x} + \bar{B}\bar{u} \\
\bar{y} &= \bar{x} \text{ and } \bar{u} = \dot{y}^{des} - CAx
\end{aligned}
\tag{4.43}
$$

The block diagram that illustrates this modification is given in Figure 4.6. Combining the novel dynamic inversion with the aircraft equations results in the following set of dynamics, expressed in matrix notation

$$
\begin{aligned}
\begin{bmatrix} \dot{x} \\ \dot{\bar{x}} \end{bmatrix} &= \begin{bmatrix} A & B(CB)^{-1} \\ -\bar{B}CA & \bar{A} \end{bmatrix} \begin{bmatrix} x \\ \bar{x} \end{bmatrix} + \begin{bmatrix} 0 \\ \bar{B} \end{bmatrix} \dot{y}^{des} \\
y &= \begin{bmatrix} C & 0 \end{bmatrix} \begin{bmatrix} x \\ \bar{x} \end{bmatrix}
\end{aligned}
\tag{4.44}
$$

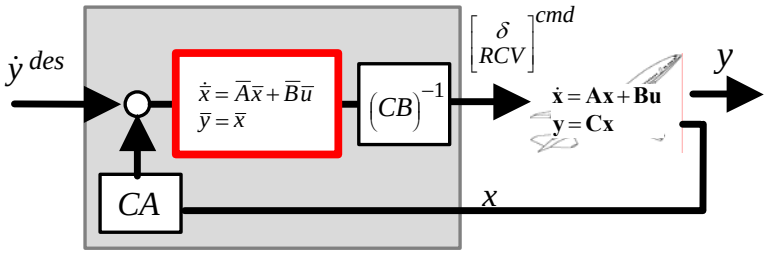

Figure 4.6: Novel dynamic inversion with dynamics in the dynamic matrix $W(x)$.

Clearly (4.44) shows that as expected the dynamics of filter $W(x)$ alter the closed loop dynamics. After some algebraic manipulation, the result is a very large and messy analytical expression for the closed loop poles. In order to understand how the first order filter matrix influences the dynamic inversion inner loop, it is instructive to look at the pole movement while holding one of the time constants fixed and changing the other. Looking at the numeric values of the closed loop poles, it becomes immediately apparent that for $a \neq 0$ and $b \neq 0$ two of the six poles are integrators. Another pole maintains a value in the neighborhood of *1/a*. However, there are no longer poles coincident with open loop transmission zeros, so there is no pole-zero cancellation.

Figures 4.7 and 4.8 illustrate the pole movement as the filter time constants are varied. In Figure 4.7, *b* is fixed and *a* is allowed to vary over the same range as was previously shown in Figure 4.4. Notice that short period poles move in the manner similar to that observed in the SISO short period case, while the flexible mode dipole remains essentially fixed in the neighborhood that is specified by the given value of *b*. In fact the movement of the faster of the two short period poles is clearly visible in the figure. Similar phenomenon is observed in Figure 4.8, where *a* is fixed and *b* is allowed to vary. The short period dynamics remain essentially fixed on the real axis while the elastic mode dipole travels along fixed frequency and increasing damping with decreasing value of *b*. Again this is similar to what has been observed in the SISO elastic mode case and shown in Figure 4.5.

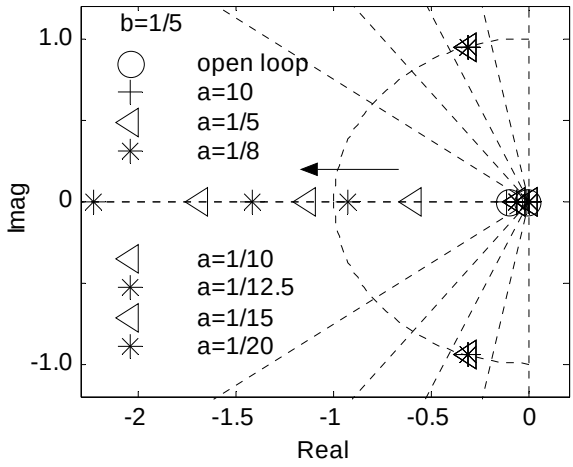

Figure 4.7: Closed loop poles for short period + 1 flexible mode with *a* changing, *b*=1/5.

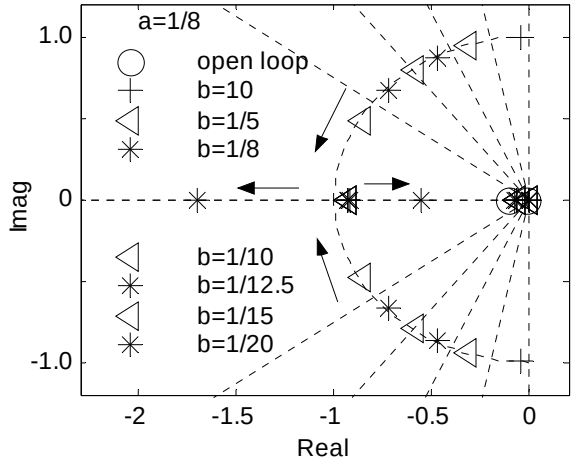

Figure 4.8: Closed loop poles for short period + 1 flexible mode with *b* changing, *a*=1/8.

The fact that while one filter time constant is fixed the other can be varied to manipulate a set of dynamics that are of interest is very useful in design. At first glance, it would not be surprising that the time constants modify the system in the decoupled manner described. There is some frequency separation between the short period and the elastic dynamics. Furthermore, q_{ma} is predominantly rigid body whereas $q_{ps} - q_{ma}$ is predominantly elastic based. However, the frequency separation causing decoupling is a

very deceptive conclusion in this case as examination of full longitudinal plus flexible mode dynamics will show.

4.9 Additional Flexible Modes

Additional complexity in structural dynamics is explored in this section. The longitudinal plus 1 flexible mode equations of motion (4.45) are augmented by 3 additional flexible modes with all the associated interdependencies of rigid and elastic dynamics as well as inter-mode dependencies. Thus, the system dynamics consist of 12 states and retain the same control variables as have been used throughout. In the

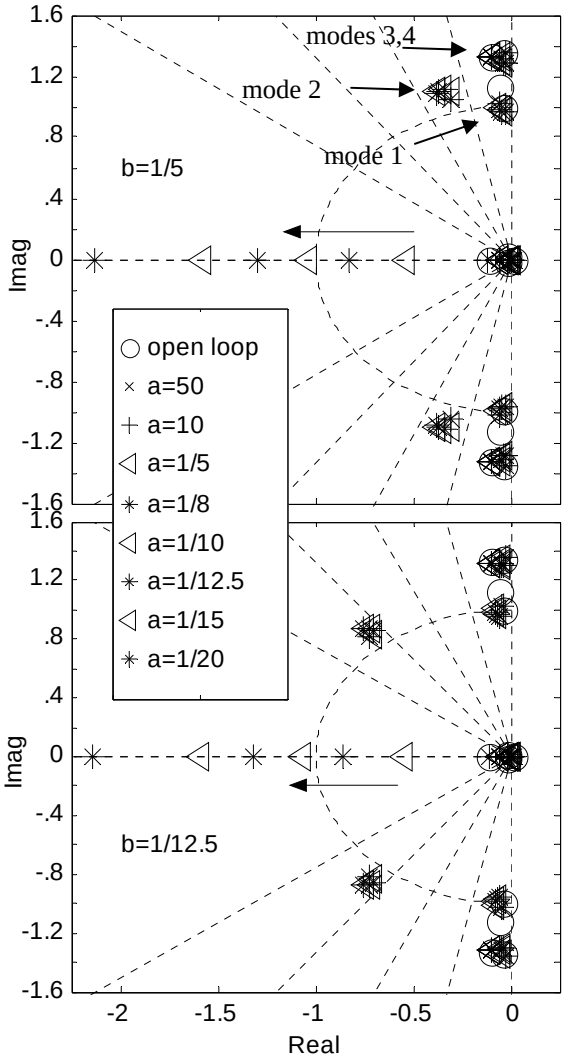

Figure 4.9: Longitudinal + 4 modes with *a* changing.

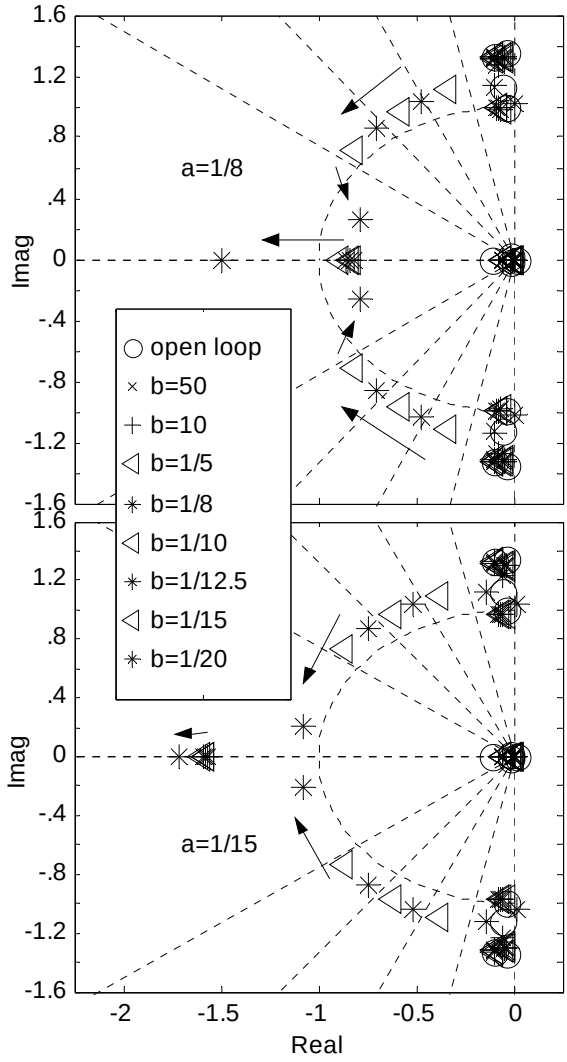

Figure 4.10: Longitudinal + 4 modes with *b* changing.

now familiar process, one of the time constants in $W(x)$ is kept fixed while the other varies. The results are illustrated in Figures 4.9 and 4.10. For a changing *a* with constant *b*, figure 4.9 shows the movements of short period poles while all but one flexible mode remain clustered near their open loop positions. The pole corresponding to the primary fuselage bending mode has migrated away from its open loop position to a higher damping. When *b* is changing while *a* is held constant, the pole movement, illustrated in Figure 4.10, is similar to the one observed in the prior section. The poles of the flexible modes that are not primarily fuselage modes (modes 1, 3 and 4) form tight clusters around their open loop positions. The primary fuselage bending mode poles (mode 2) follow the previously established movement pattern of increased damping with decreasing *b* along what is essentially a constant frequency. There is also movement from the rigid body poles with the amount dependent on the value of constant *a*.

Hence, the introduction of additional modes to the dynamics has not changed the observed general pattern of behavior from either rigid body or flexible dynamics. The additional flexible modes do not significantly alter the dependence of the primary flexible mode on the $W(x)$ time constant *b*, nor do they have a large influence on the interaction between rigid body and flexible mode dynamics. From the physics perspective of this problem, this result is not surprising, since the additional flexible modes are primarily wing modes and are not significantly affected by the fuselage mounted control surfaces considered here. Similar behavior has been observed with a much higher number of elastic modes, some of which were fuselage modes, but beyond effective power of the controller. Thus it appears that a reasonable independence of control still exists for longitudinal plus flexible mode system dynamics under the dynamic inversion modification described in this chapter. Granted this apparent separation exists in a perfect world, and once unmodeled dynamics as well as actuator dynamics are introduced the separation is not as clean, however, enough decoupling still exists to allow for a great deal of controller tuning to be done through $W(x)$.

The analytical expression for the transfer function matrix, not shown here, is no longer a diagonal set of integrators but instead is a fully populated matrix. This follows, as it did in SISO system, from the fact that introducing additional dynamics into the dynamic inversion loop precludes the pole-zero cancellation required to give the diagonal

set of integrators. While not as elegant mathematically, this result allows control of flexible mode damping and thus tailor the disturbance response of the closed loop in addition to the commanded variable response.

4.10 Adding Complexity

Consider the full longitudinal model with a single flexible mode. Retaining the same control variables as used above in (4.36), the system dynamics are given by

$$\begin{bmatrix} \dot{u} \\ \dot{w} \\ \dot{q} \\ \dot{\theta} \\ \ddot{\eta} \\ \dot{\eta} \end{bmatrix} = \begin{bmatrix} X_u & X_w & X_q & X_\theta & 0 & 0 \\ Z_u & Z_w & Z_q & Z_\theta & Z_{\dot{\eta}} & Z_\eta \\ M_u & M_w & M_q & M_\theta & M_{\dot{\eta}} & M_\eta \\ 0 & 0 & 1 & 0 & 0 & 0 \\ 0 & E_w & E_q & 0 & -2\varsigma\omega & -\omega^2 \\ 0 & 0 & 0 & 0 & 1 & 0 \end{bmatrix} \begin{bmatrix} u \\ w \\ q \\ \theta \\ \dot{\eta} \\ \eta \end{bmatrix} + \begin{bmatrix} X_\delta & 0 \\ Z_\delta & Z_{rcv} \\ M_\delta & M_{rcv} \\ 0 & 0 \\ E_\delta & E_{rcv} \\ 0 & 0 \end{bmatrix} \begin{bmatrix} \delta \\ RCV \end{bmatrix} \tag{4.45}$$

Following the same process as before, the direct dynamic inversion produces results seen in (4.38). The closed loop poles are

$$\begin{Bmatrix} \pm \ u - w \text{ dynamics} \\ 0,\ 0,\ 0,\ 0 \end{Bmatrix} \tag{4.46}$$

The closed loop poles are a set comprised of 4 poles of internal dynamics that coincide with open loop transmission zeros of the system in (4.45) and of two poles at s=0 which correspond to the integrators found in (4.38). The closed loop system dynamics from $\dot{y}^{des}$ to $\dot{y}$ are given by (4.47). From this equation, it is apparent that the controlled variables are independent of the u-w dynamics. Furthermore, the steady-state system internal dynamics are described by motion on the u-w-η-manifold.

$$\begin{bmatrix} \dot{u} \\ \dot{w} \\ \dot{q} \\ \dot{\theta} \\ \ddot{\eta} \\ \dot{\eta} \end{bmatrix} = \begin{bmatrix} \bar{X}_u & \bar{X}_w & \bar{X}_q & \bar{X}_\theta & X_{\dot{\eta}} & Z_\eta \\ \bar{Z}_u & \bar{Z}_w & \bar{Z}_q & \bar{Z}_\theta & \bar{Z}_{\dot{\eta}} & \bar{Z}_\eta \\ 0 & 0 & 0 & 0 & 0 & 0 \\ 0 & 0 & 1 & 0 & 0 & 0 \\ 0 & 0 & 0 & 0 & 0 & 0 \\ 0 & 0 & 0 & 0 & 1 & 0 \end{bmatrix} \begin{bmatrix} u \\ w \\ q \\ \theta \\ \dot{\eta} \\ \eta \end{bmatrix}$$

$$+ \begin{bmatrix} \bar{X}_{\dot{y}1} & \bar{X}_{\dot{y}2} \\ \bar{Z}_{\dot{y}1} & \bar{Z}_{\dot{y}2} \\ 1 & \bar{M}_{\dot{y}2} \\ 0 & 0 \\ 0 & \bar{E}_{\dot{y}2} \\ 0 & 0 \end{bmatrix} \begin{bmatrix} \dot{y}_1 \\ \dot{y}_2 \end{bmatrix}^{des}$$

$$\begin{bmatrix} \dot{y}_1 \\ \dot{y}_2 \end{bmatrix} = \begin{bmatrix} \dot{y}_1^{des} + \left(\bar{M}_{\dot{y}2} + \phi' \bar{E}_{\dot{y}2} \right) \dot{y}_2^{des} \\ \Delta\phi' \bar{E}_{\dot{y}2} \dot{y}_2^{des} \end{bmatrix} = \begin{bmatrix} \dot{y}_1^{des} \\ \dot{y}_2^{des} \end{bmatrix} \qquad (4.47)$$

where $\bar{M}_{\dot{y}2} = -\phi' \bar{E}_{\dot{y}2}$ and $\Delta\phi' \bar{E}_{\dot{y}2} = 1$

Introducing modification to the dynamic inversion as shown in the earlier section, the result is no longer a clean separation as has been observed with short period approximation and an elastic mode. The closed loop A matrix structure resembles the more fully populated one of the open loop (4.45) rather than the nice decoupled one of the closed loop (4.47). The pole movement associated with changing time constants of the transfer matrix $W(x)$ is shown in Figures 4.11 and 4.12. The closed loop poles structure of $\{*,\ *,\ *, *,\ *,\ *, 0,\ 0\}$ applies to both of the figures.

For changing *a*, time constant of the measured mean axis pitch rate, there is the expected movement of the longitudinal poles that has been previously seen in Figures 4.4 and 4.7, but there is also some minor movement of the flexible mode as illustrated in Figure 4.11. When the value of *b* is allowed to change, as shown in Figure 4.12, the flexible mode follows the now familiar pattern witnessed in Figures 4.5 and 4.8 of changing damping along a constant frequency. However, there is also movement of longitudinal poles, the extent of which depends on the value of *a*. This begins to constrain some of the decoupling freedom in the control design. Taking another step

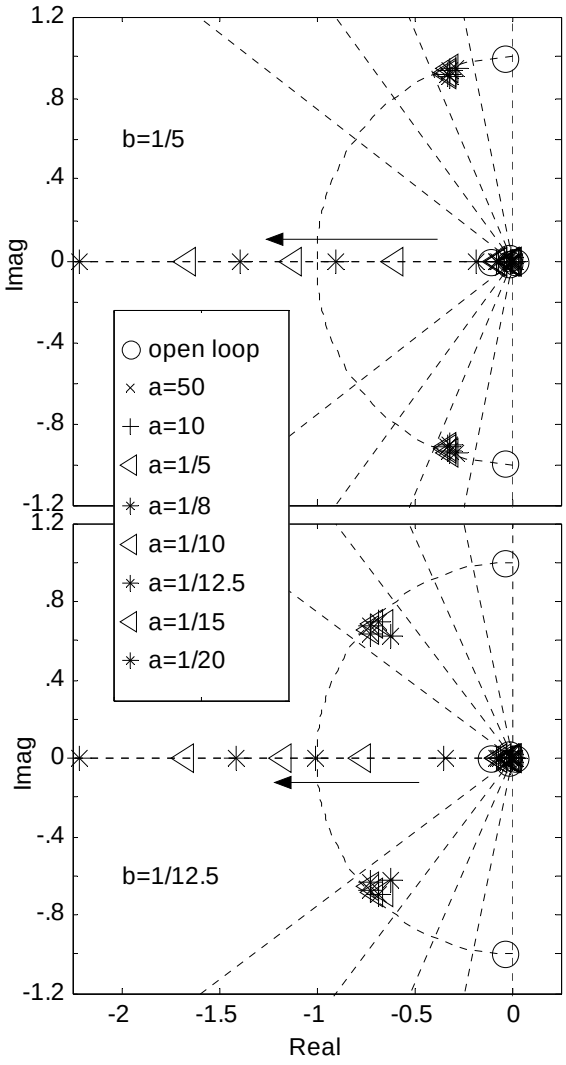

Figure 4.11: Longitudinal + 1 mode with *a* changing.

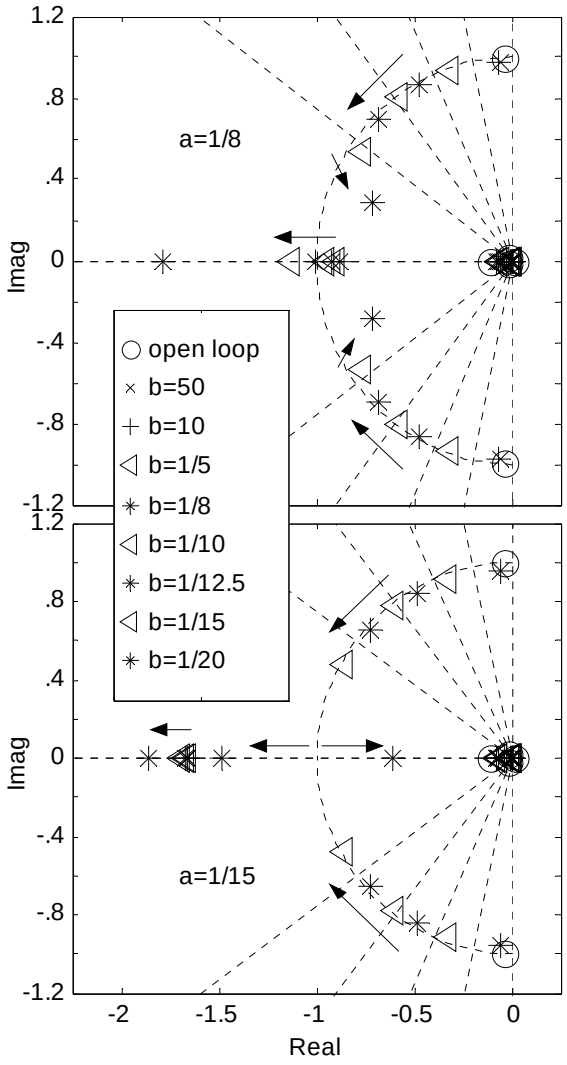

Figure 4.12: Longitudinal + 1 mode with *b* changing.

towards a real flexible aircraft, an additional level of complexity is introduced in the following section.

4.11 Adding Uncertainty in Flexible Mode

As with any control methodology, the issue of robustness must be addressed. The work in the previous chapter considered parametric uncertainty in the frequency and damping of the primary fuselage flexible mode. It was found that the novel dynamic inversion methodology produced a controller with good stability robustness to the

indicated uncertainty. In this section, the dynamics discussed earlier in this chapter are revisited and the effects parametric uncertainty in frequency and damping of a flexible mode have on the closed inner loop behavior of the system is explored.

Consider for clarity, the simplest available set of dynamics, those of short period plus 1 flexible mode described by (4.35) and (4.36), and introduce damping and frequency multiplicative uncertainty

$$\begin{aligned} \omega &\to \omega\left(1+\Delta_\omega\right) \qquad \text{where } \Delta_\omega \in \left\{\delta : |\delta| \le 1, \delta \in \mathbb{R}\right\} \\ \varsigma &\to \varsigma\left(1+\Delta_\varsigma\right) \qquad \text{where } \Delta_\varsigma \in \left\{\delta : |\delta| \le 1, \delta \in \mathbb{R}\right\} \end{aligned} .$$

The closed loop perturbed system dynamics associated with the standard dynamic inversion are given in (4.48). Note that the difference between nominal (4.39) and perturbed closed loop system is in the $\ddot{\eta}$ equation with appearance of $2\bar{\varsigma}\bar{\omega}$ and $\bar{\omega}^2$ terms. Both are dependent on the nominal frequency and damping as well as the introduced uncertainty (4.48).

$$\begin{bmatrix} \dot{w} \\ \dot{q} \\ \ddot{\eta} \\ \dot{\eta} \end{bmatrix} = \begin{bmatrix} \bar{Z}_w & \bar{Z}_q & \bar{Z}_{\dot{\eta}} & \bar{Z}_\eta \\ 0 & 0 & 0 & 0 \\ 0 & 0 & 2\bar{\varsigma}\bar{\omega} & \bar{\omega}^2 \\ 0 & 0 & 1 & 0 \end{bmatrix} \begin{bmatrix} w \\ q \\ \dot{\eta} \\ \eta \end{bmatrix} + \begin{bmatrix} \bar{Z}_{\dot{y}1} & \bar{Z}_{\dot{y}2} \\ 1 & \bar{M}_{\dot{y}2} \\ 0 & \bar{E}_{\dot{y}2} \\ 0 & 0 \end{bmatrix} \begin{bmatrix} \dot{y}_1 \\ \dot{y}_2 \end{bmatrix}^{des} \tag{4.48}$$

$$\text{where } \bar{\omega} = \left(2\omega\Delta_\omega\right)^{1/2} \text{ and } \bar{\varsigma} = \frac{\omega\Delta_\varsigma + \varsigma\Delta_\omega}{\left(2\omega\Delta_\omega\right)^{1/2}}$$

The transfer function of the closed inner loop dynamics, shown in (4.49), is no longer the integrator chain seen in (4.38).

$$\begin{bmatrix} y_1 \\ y_2 \end{bmatrix} = \begin{bmatrix} \frac{1}{s} & \frac{-\phi'\left(2\bar{\varsigma}\bar{\omega}s + \bar{\omega}^2\right)}{\left(s^2 + 2\bar{\varsigma}\bar{\omega}s + \bar{\omega}^2\right)} \\ 0 & \frac{s}{s^2 + 2\bar{\varsigma}\bar{\omega}s + \bar{\omega}^2} \end{bmatrix} \begin{bmatrix} \dot{y}_1^{des} \\ \dot{y}_2^{des} \end{bmatrix} \tag{4.49}$$

And the closed loop poles associated with the perturbed system are

$$\left\{ \bar{Z}_w,\ 0,\ -\bar{\varsigma}\bar{\omega} \pm \left(\bar{\omega}^2 \left(\bar{\varsigma}^2 - 1 \right) \right)^{1/2} \right\} =$$

$$\left\{ \begin{array}{c} Z_w + Z_\delta \left(\dfrac{E_w M_{rcv} - E_{rcv} M_w}{E_\delta M_{rcv} - E_{rcv} M_\delta} \right) + Z_{rcv} \left(\dfrac{E_\delta M_w - E_w M_\delta}{E_\delta M_{rcv} - E_{rcv} M_\delta} \right), \quad 0, \\ -\omega\Delta_\zeta - \zeta\Delta_\omega \pm \left(\omega^2 \Delta_\zeta^2 + 2\omega\zeta\Delta_\zeta\Delta_\omega + \zeta^2\Delta_\omega^2 - 2\omega\Delta_\omega \right)^{1/2} \end{array} \right\} \tag{4.50}$$

Since the nature of the uncertainty did not change the open loop transmission zeros and this is a direct dynamic inversion, the first two poles coincide with the open loop transmission zeros as was seen earlier in (4.40). The two integrators, however, have changed into poles that are a function of $\bar{\varsigma}$ and $\bar{\omega}$, which are given in terms of their components in (4.50). As is evident from (4.48), the w internal dynamics remain independent of attitude dynamics and are only indirectly influenced by the flexible mode uncertainty through state variables $\dot{\eta}$ and η in the $\dot{w}$ equation. This is also confirmed by coincidence of transmission zeros with closed loop poles.

The same observation holds for a full longitudinal system with a flexible mode. The closed loop dynamics of direct dynamic inversion are given in (4.51). Again the difference between the nominal closed loop (4.47) and the perturbed system resides in the $\ddot{\eta}$ equation with reappearance of $2\bar{\varsigma}\bar{\omega}$ and $\bar{\omega}^2$ terms.

$$\begin{bmatrix} \dot{u} \\ \dot{w} \\ \dot{q} \\ \dot{\theta} \\ \ddot{\eta} \\ \dot{\eta} \end{bmatrix} = \begin{bmatrix} \bar{X}_u & \bar{X}_w & \bar{X}_q & \bar{X}_\theta & X_{\dot{\eta}} & Z_\eta \\ \bar{Z}_u & \bar{Z}_w & \bar{Z}_q & \bar{Z}_\theta & \bar{Z}_{\dot{\eta}} & \bar{Z}_\eta \\ 0 & 0 & 0 & 0 & 0 & 0 \\ 0 & 0 & 1 & 0 & 0 & 0 \\ 0 & 0 & 0 & 0 & 2\bar{\varsigma}\bar{\omega} & \bar{\omega}^2 \\ 0 & 0 & 0 & 0 & 1 & 0 \end{bmatrix} \begin{bmatrix} u \\ w \\ q \\ \theta \\ \dot{\eta} \\ \eta \end{bmatrix} + \begin{bmatrix} \bar{X}_{\dot{y}1} & \bar{X}_{\dot{y}2} \\ \bar{Z}_{\dot{y}1} & \bar{Z}_{\dot{y}2} \\ 1 & \bar{M}_{\dot{y}2} \\ 0 & 0 \\ 0 & \bar{E}_{\dot{y}2} \\ 0 & 0 \end{bmatrix} \begin{bmatrix} \dot{y}_1 \\ \dot{y}_2 \end{bmatrix}^{des} \tag{4.51}$$

$$\begin{bmatrix} \dot{y}_1 \\ \dot{y}_2 \end{bmatrix} = \begin{bmatrix} \dot{y}_1^{des} + \phi'\left(2\bar{\varsigma}\bar{\omega}\dot{\eta} + \bar{\omega}^2\eta\right) \\ \dot{y}_2^{des} + \Delta\phi'\left(2\bar{\varsigma}\bar{\omega}\dot{\eta} + \bar{\omega}^2\eta\right) \end{bmatrix}$$

The transfer function of the closed inner loop dynamics, shown in (4.52), is very similar to the one for short period found in (4.49). There is no longer a chain of integrators present. However, in the limit as $\Delta_\varsigma \to 0$ and $\Delta_\omega \to 0$ the chain of integrators, as seen in (4.38) is recovered.

$$\begin{bmatrix} y_1 \\ y_2 \end{bmatrix} = \begin{bmatrix} \frac{1}{s} & \frac{-\phi'\left(2\bar{\varsigma}\bar{\omega}s + \bar{\omega}^2\right)}{\Delta\phi' s\left(s^2 + 2\bar{\varsigma}\bar{\omega}s + \bar{\omega}^2\right)} \\ 0 & \frac{s}{s^2 + 2\bar{\varsigma}\bar{\omega}s + \bar{\omega}^2} \end{bmatrix} \begin{bmatrix} \dot{y}_1^{des} \\ \dot{y}_2^{des} \end{bmatrix} \tag{4.52}$$

The first four closed loop poles, described in (4.53) correspond to open loop transmission zeros which is similar to the observed behavior of the short period system and show no dependence of internal dynamics on the uncertainty. The two remaining poles changed from dynamic inversion produced integrators to functions of uncertainty, again in a manner similar to the short period system.

$$\left\{ \begin{array}{c} \pm \ u - w \text{ dynamics, } 0, 0, \\ -\omega\Delta_\zeta - \zeta\Delta_\omega \pm \left(\omega^2\Delta_\zeta^2 + 2\omega\zeta\Delta_\zeta\Delta_\omega + \zeta^2\Delta_\omega^2 - 2\omega\Delta_\omega\right)^{1/2} \end{array} \right\} \tag{4.53}$$

Thus when uncertainty is added into the direct dynamic inversion, whether the system is a short period approximation or the full longitudinal model, the resulting closed loop dynamics are governed by the open loop transmission zeros and flexible mode uncertainty. This points to a potentially serious issue with stability of direct dynamic inversion. System stability is affected by uncertainty in the dynamics far separated in frequency from the dynamics that actually go unstable. In this case, flexible mode uncertainty could drive one of the dynamic inversion integrator poles unstable for large enough Δ_ς and Δ_ω. The existence of potentially unstable closed loop poles confirms the disadvantage of direct inversion especially with lightly damped dynamics of the flexible modes.

For control design there are two questions that are important to consider. The first is what happens for a given controller designed using the novel dynamic inversion as a range of uncertainty is considered. The second is does enough decoupling between the rigid body and flexible mode dynamics still exist so that time constants of the matrix $W(x)$ might be used to tune the controller.

To answer the first question, consider longitudinal dynamics with one flexible uncertain mode in the context of novel dynamic inversion. The plot in Figure 4.13 illustrates the pole migration for changing frequency uncertainty while maintaining a constant damping uncertainty and a fixed value of *a* and *b* time constants of $W(x)$. The

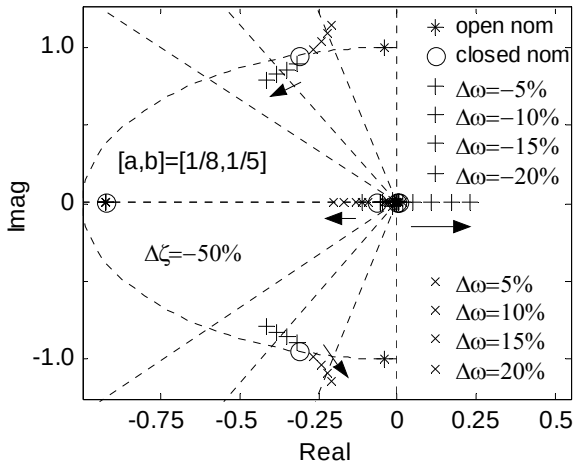

Figure 4.13: Closed loop poles for longitudinal + 1 flexible mode with {a,b,Δζ} constant, Δω,vaying.

frequency uncertainty is used because as will be shown in Chapter 5 it has been found to be the driving factor. Also, as the frequency of the flexible mode decreases, the low frequency instability it causes becomes more pronounced. However, recall that the nature of $\dot{y}^{des}$ dynamics has a pronounced affect on the overall system stability that is not taken into consideration in this analysis. In the implemented controller closed loop system, discussed in Chapter 5, the low frequency dynamics were not as sensitive to uncertainty due to the use of second order filters in the $W(x)$ dynamics matrix. The influence of second order filters is not discussed in this chapter.

To address the second question, consider again the longitudinal plus one flexible mode dynamics (4.45) and apply novel dynamic inversion. In order to explicitly consider system uncertainty during the design phase, a controller is designed on a nominal system and then applied to a system perturbed in flexible mode frequency and damping. Once the uncertainty parameter boundaries are set, the affect of independent manipulation of the *a* and *b* time constants of the matrix $W(x)$ on the behavior of the closed loop system is explored. This behavior is illustrated in Figures 4.14 and 4.15. It is interesting to note that in Figure 4.14 while *a* is varied with *b* fixed the rigid body poles move while the flexible mode remains completely stationary unlike the clustering observed in Figure 4.11 where no uncertainty was present in the system. The unstable low frequency rigid body pole also seems to be insensitive to the variation in *a*. This would imply that the closed loop flexible mode associated poles are dominated by uncertainty and *b*, unlike the nominal case where *a* had some influence.

In Figure 4.15, the time constant *b* is varied while *a* remains fixed. The results show the higher frequency rigid body dynamics remain fixed contrary to what was observed in Figure 4.12 when no uncertainty was present. The flexible mode no longer follows the familiar pattern of changing damping along constant frequency. It now changes both frequency and damping with changing *b*. The low frequency rigid body pole also moves with changing *b*, becoming more unstable with smaller *b*.

This observed behavior suggests that the presence of uncertainty overwhelms the influence of the modification matrix $W(x)$ on the low frequency rigid body dynamics. The effect on the controller design is somewhat limiting in that very low frequency

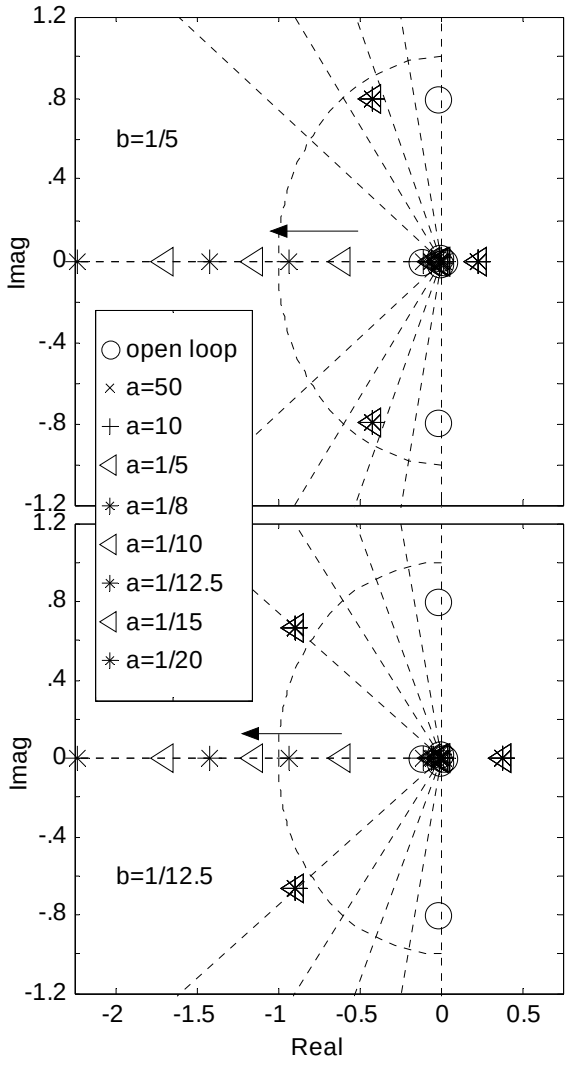

Figure 4.14: Longitudinal + 1 mode with {Δω,Δζ}={-20%, -50%} *a* changing, *b*=(1/5, 1/12.5).

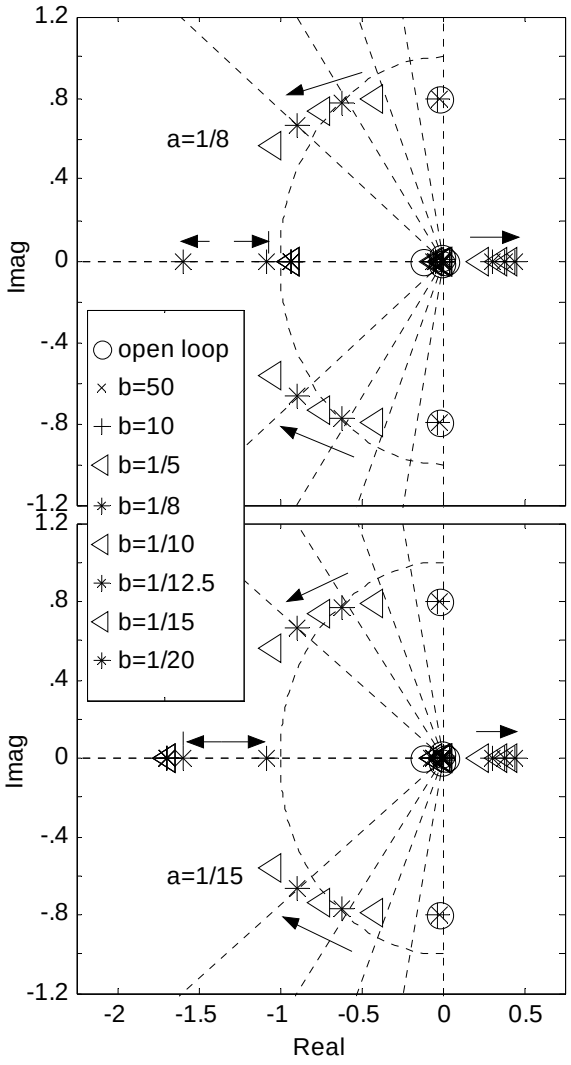

Figure 4.15: Longitudinal + 1 mode with {Δω,Δζ}={-20%, -50%} *b* changing, *a*=(1/8,1/15).

dynamics must now be carefully considered when attempting to specify the desired flexible mode damping via the adjustment of the *b* time constant of the matrix $W(x)$. As previously mentioned, the problem is somewhat mitigated by the use of second order filters on the diagonal of $W(x)$ as well as the effect of the $\dot{y}^{des}$ dynamics on overall closed loop stability.

4.12 Conclusion

This chapter introduced the novel dynamic inversion methodology. The first half of the chapter focused on exploring the effect of the additional dynamics, introduced by the novel dynamic inversion, on the closed loop system in an analytical manner. The aircraft equations of motion were simplified to include the longitudinal axis and one flexible mode. This simplification retained the crucial rigid/flexible mode dynamic interactions while making the problem mathematically tractable. The changes in dynamics attributed to the innovation in the inversion methodology have been traced for both linear and nonlinear systems. The modification alters the internal dynamics of the system and destroys the separation between internal dynamics and controlled dynamics that was present for the standard inversion case. However, when additional dynamics of $W(x)$ are present in one loop, the input-output dynamics reflect the modification in the altered loop and recover the standard integrator in the nominal one. This work has added to both analytical and physical insight regarding the nature of the novel dynamic inversion applied to an integrated flight/SMC control for a highly flexible aircraft.

The second half of the chapter focused on specific effects that the additional dynamics associated with the novel dynamic inversion have on the response of the closed loop aircraft system. The additional dynamics have been analytically explored on longitudinal and symmetric flexible dynamics of varying complexity. While the model used here is much simpler than the full model for which the controller introduced in next chapter was designed, the results are revealing nonetheless. This chapter provides some analytical basis and further insight into the workings of dynamic inversion methodology that has been modified to address the problem associated with these large, flexible aircraft.

There exists a large degree of freedom to control rigid body and flexible dynamics independently of one another in the novel dynamic inversion context. The apparent separation in controlling the short period and elastic mode dynamics through novel dynamic inversion is valuable when control of disturbances is as important as control of commanded variable. Specifically, the ability to alter the damping of elastic modes as well as cancel their response to the commanded vehicle motion is the main objective of an integrated flight/SMC control that is required for advanced, large, flexible aircraft.

The increased complexity of system dynamics that included full longitudinal as well as multiple symmetric flexible mode dynamics showed that a certain degree of separation in controlling rigid body and flexible dynamics still exists. However, the introduction of parametric uncertainty into frequency and damping of the dominant flexible mode also showed the coupling between very low frequency rigid body and flexible dynamics. This coupling must be carefully considered during a controller design process since in the real world application there is always uncertainty present in the system.

Chapter 5 – Novel Dynamic Inversion Controller

5.1 Introduction

To provide an integrated flight/SMC controller for complex dynamics exemplified by the large, flexible transport aircraft whose model is described in detail in Chapter 3, the method of dynamic inversion is considered. Over the last decade, dynamic inversion methodology has gained considerable popularity in application to highly maneuverable fighter aircraft[2, 3, 5] and might be of benefit to highly flexible aircraft. The attractiveness of this methodology lies in the fact that the inherent nonlinearities of the problem are explicitly considered. In other words, a nonlinear control law is designed that globally reduces the aircraft dynamics of interest into a set of integrators and thus, allows one linear controller to provide desired response throughout the flight envelope. This eliminates the need for extensive linearization of the aircraft model for different flight conditions, design of individual controllers for each of these conditions, and finally performing gain scheduling, which is typically an ad hoc and time consuming procedure, to link the individual controllers over the flight envelope.

The work presented in this chapter is a first step in determining whether dynamic inversion is a viable methodology to address the whole flight control problem of advanced flexible aircraft. The methodology is applied over a section of the flight envelope that includes the approach-to-land condition at the end of cruise, which makes for the worse case flight/flexible dynamics interaction. The problem is formulated to provide command following to pilot/autopilot inputs while minimizing elastic deflection at the pilot station. The aircraft has RCVs, all movable tail, and independently moving elevator. The controller is designed on a reduced longitudinal elastic model, which is open loop unstable, with 8 elastic modes considered, and then applied to the full nonlinear longitudinal elastic model of 20 modes. As the first step, a standard dynamic inversion controller design was attempted, but failed to produce a stable closed loop system. This result is discussed in more detail in a later section. The results from the novel dynamic inversion controller, however, show substantially increased damping of the fuselage bending modes, which attenuates any excitation due to turbulence, and coordinated pitching of the entire vehicle thus minimizing the bending at the pilot station.

These results are compared to those of a controller designed for performance on a QSAE vehicle only, in order to provide a reference for low frequency flight performance as well as high frequency dynamic response.

As the vehicle models developed and matured, so has the dynamic inversion controller design. Initially, the vehicle did not have RCVs so the control had to be designed using the available surfaces. With development of RCV, the alternative control strategies did not have to be used; however, they produced some very interesting and useful results that are instructive for this class of vehicles. The results from these designs are described in detail in Appendix C.

5.2 Control Problem Formulation

Several issues specific to the dynamic inversion control methodology had to be addressed first in designing a controller for an elastic airplane. These issues included selection of the control variables in such a way as to ensure the system was minimum phase. And, more importantly, an issue that had not been addressed before in any implementation of the methodology was how to handle state dependence, in addition to the standard actuator position, on actuator rates and accelerations. This means, for example, that the rate of change of pitch rate, $\dot{q}$, depends not only on the elevator deflection but also on the elevator rate and its acceleration. Such dependence is very much a characteristic of elastic aircraft. Traditionally, dynamic inversion has been applied to aircraft that are modeled such that the aircraft states and actuator dynamics (rates, accelerations) form a block diagonal matrix, thus enabling separation and an inversion controller that commands only the actuator position. For the elastic aircraft, the validity of such separation depends on the contribution of unsteady aerodynamics and inertial mass coupling to control effectiveness, which has been touched on in Chapter 3. The effect of actuator dynamics on the controller and the robustness of the closed loop system to these dynamics are explicitly addressed in the simulation analysis presented later in this chapter.

5.3 Philosophy Behind Novel Dynamic Inversion

Consider a very fundamental look at the dynamic inversion controller. Essentially an error between the desired state of controlled variables and an actual state is fed through

the inverse of the control effectiveness matrix in order to obtain actuator commands to drive that error to zero. As with any system, there are dynamics that are not of interest or are not directly controllable. For an aircraft with sufficient control degrees of freedom, it is possible to select a set of controlled variables, such as rotational velocities, and design a controller that in the closed loop would keep rotational degrees of freedom independent of the translational axes. Hence, provided that the translational dynamics follow certain assumptions, *e.g.,* they are stable, we are ensured that the desired dynamics are not corrupted by the translational degrees of freedom and the system is stable by design. In the case of a flexible vehicle, the nature of internal system dynamics changes. The translational and rotational degrees of freedom can still be separated and rotation can be controlled without interference from the former, but now the dynamics in the frequency range beyond the controller bandwidth must be considered. These dynamics become internal dynamics as well as influence the controlled dynamics and the internal dynamics of the translational degrees of freedom. Specifically, assume that there is interest in controlling the pitch rate of the aircraft as well as the behavior of the first few fuselage flexible modes that come close to the pilot operating bandwidth. Two things make this problem very different from a typical one. First, in typical cases the actuator dynamics are fast enough to be negligible within the frequency range of interest. Second, the higher frequency dynamics are sufficiently far enough away from both the controller bandwidth and the actuator dynamic frequency and can be neglected. If these dynamics are close enough to the actuator dynamic frequencies such that their effect cannot be ignored, then they are dealt with on separate basis employing notch filters. However, in the problem under consideration neither case holds. In this problem, there are several actuators for controlling the vehicle with different dynamic capabilities. In addition, the higher frequency dynamics are very close to the dynamics being controlled and hence cannot be discounted or controlled with notch filters. As already mentioned in Chapter 3 during the discussion of the open loop dynamics, the proximity of flexible mode dynamics to the flight dynamics as well as close clustering of a number of flexible modes suggest a need for an integrated flight/SMC law for optimum aircraft performance.

In fact, further modifications are required for successful implementation of an integrated flight/SMC controller using dynamic inversion. The modifications to the

methodology and the motivation behind them are discussed in detail below. A dynamic inversion controller designed in a typical manner, *i.e.*, dynamic cancellation in the frequency range of interest, and then applied to the entire system that includes higher frequency modes and actuator dynamics behaves nothing like the design. Consider only the system dynamics for which the controller has been designed and then add the actuator dynamics. The resulting system immediately reflects the destabilizing effect of this addition on the closed loop system. The dynamics that are destabilized are the flexible modes, which are half as fast as the slowest actuator, *i.e.*, ~12 rad/sec. This is reflected in Figure 5.3 presented in a later part of the chapter. If the actuator dynamics are sped up to about 6 to 7 times the speed of the primary fuselage mode under control then the original controller functions as per design. Hence, somehow the original controller must be modified in order to effectively deal with actuator dynamics as well as higher frequency dynamics that are also destabilized by the presence of actuator dynamics. (Recall from Chapter 3 Figures 3.7 and 3.8 the effect the presence of actuator dynamics had on open loop response.) One way of doing this is to make sure that the controller bandwidth is as small as the performance requirements allow and have the controller roll-off as quickly as possible past that bandwidth frequency.

Consider again the control variables of interest, $[q_{ma}, q_{ps} - q_{ma}]$. The difference between the desired and the actual dynamics can be compared at two different frequency intervals. The first frequency interval upper bound is restricted to the highest frequency of the system model used for controller. In this range, the error between desired and actual is, in fact, something that the controller is designed to drive to zero. The second interval contains the frequencies higher than those of the design model. In this case, the error is in reality just the actual system response in that frequency range. If this were fed back to the controller, then the controller would attempt to react to this error for which it was not designed, move the actuator in response to these higher frequencies and hence start destabilizing the system in both frequency intervals. One solution would be to impose a low-pass filter on the error fed into the control effectiveness matrix in order to minimize the impact of the higher frequency dynamics and thus let the controller deal with the problem for which it was designed. For this purpose, the aforementioned filter

would be placed in the inversion loop of the controller preceding the feed into the control effectiveness matrix.

Further consideration must be given to the question of direct flexible mode control *within the frequency range of the design model*. Applying standard dynamic inversion to this portion of the problem has several drawbacks. First, canceling dynamics close to the jω-axis is not very prudent in case there are model mismatches and exact cancellation does not occur. More importantly, simply canceling flexible mode dynamics only means that they are not observed at the pilot station, it does nothing to improve their response to turbulence or other excitation. So instead of cancellation, the proper objective for flexible modes is to improve their dynamic response by increasing their damping ratio and design the flight control portion of the compensator such that it minimizes the excitation of flexible modes in the first place. These dual objectives, in addition to discussion in the paragraph above, lead to the development of the novel dynamic inversion technique that is the subject of this research.

The linear controller portion can also be viewed as specifying the desired dynamics of the variable being controlled that the inversion part of the controller will match where dynamic inversion is perfect. With this in mind, the linear controller portion started as a PI compensator. The PI controller, also known as a lag compensator, is essentially a low-pass filter. The attenuation characteristic of the PI compensator is useful and permits an increase in loop gain. The lag part of the phase-shift characteristic is detrimental to system performance (destabilizing effect) but must be tolerated. The proportional part increases the gain of the system at low frequencies for better performance response while the integral part rolls off the controller for better response to high frequency dynamics and disturbance attenuation. That is a classical reason and approach to pitch rate control, which is made even more important here by the fact of close proximity of flexible modes to the pilot bandwidth. The case in the other loop, elimination of elastic mode excitation at the pilot station, produces the best response with only a proportional controller. The destabilizing effect of the lag on the phase at high frequency plays a decisive role.

The details of the novel dynamic inversion controller design based on the principals discussed in this section are described below, followed by analysis of the actual controller.

5.4 Controller Design

The first task in the controller design is to choose control variables (CVs) such that the resulting open loop system is minimum phase. The phase minimality is not a necessary requirement but it provides more freedom with linear controller design. Pitch rate as a control variable was chosen due to readily available sensor data at multiple locations and its use in conventional control systems. Since we are interested in controlling the oscillation at the pilot station caused by the vehicle's aeroelastic response in addition to conventional command following, the sensor located at the pilot station and one approximating the mean axis were chosen. The available control surfaces on the vehicle configuration considered are RCV, stabilator and elevator, which together comprise an all-movable tail. Both sensor locations and available control surfaces used are illustrated in Figure 5.1. It has been recognized by the controls community working on the aeroservoelastic control problem that multiple locations for the sensor arrays are a necessary prerequisite to design, irrespective of the methodology. With the chosen sensor and actuator locations, the open loop system is minimum phase, thus allowing us to proceed to the question of required model fidelity for design and the overall performance of the controllers.

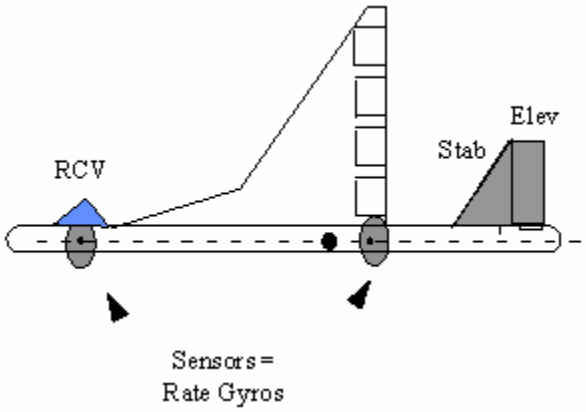

Figure 5.1: Sensors and actuators used in the study.

One of the characteristics of a large flexible transport aircraft (700,000+ lbs category) is the clustering of the flexible modes and the first couple of elastic modes being within the typical pilot bandwidth. The latter fact necessitates an integrated stability

augmentation system/structural mode control (SAS/SMC) design. To fulfill the fundamental functions of stabilizing the vehicle, precisely tracking pilot commands and rejecting turbulence while suppressing flexible modes at the pilot station, a PI compensator structure was chosen for the linear part of the dynamic inversion controller based on the reasons given above. The conceptual representation is shown in Figure 5.2.

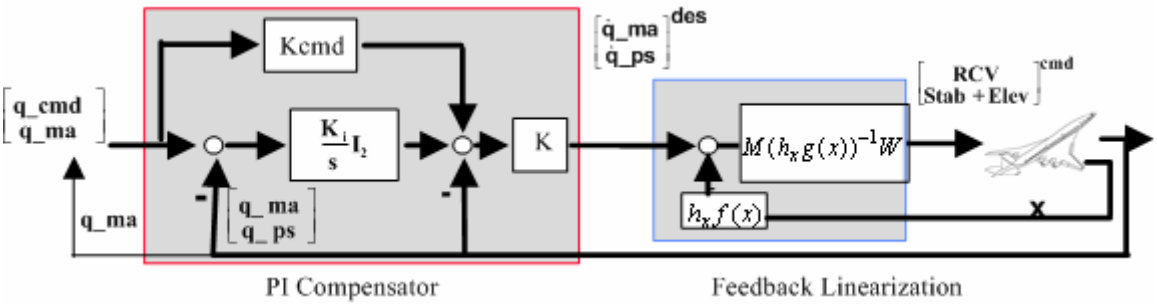

Figure 5.2: Conceptual dynamic inversion control law block diagram.

The controller scheme is a basic regulator and hence poses a question of which variable to regulate in order to control the pilot station pitch rate response. Since the objective is to have the aircraft follow a commanded pitch rate, the pilot station as well as the mean body must track it. That initial thinking proved very erroneous and only underscores the difficulty in dealing with a highly flexible vehicle. Applying the suggested strategy resulted in a controller that would try to bend the aircraft and snap the pilot station to follow the commanded input. Recall from Figure 3.1 in Chapter 3 that the initial response at the pilot station to a pitching command is to bend in the direction opposite to the command. In other words, the control variables $[q_{ma}, q_{ps}]$ exacerbated the flexibility problem, not improved it. Reflecting on these results, it became apparent that the controller really must render the aircraft as close to a rigid body as possible while maintaining desired command following response. Hence, the pilot station response must be compared to that of the mean axis of the aircraft and the difference, which is the flexible dynamics contamination, minimized.

The model used for design included longitudinal rigid body states, $[u, w, q, \theta]$, plus the first 8 flexible modes. Because the frequency of these modes was sufficiently close to

longitudinal modes, it was deemed necessary to attempt to directly control them before rolling off the controller. The pitch rates being fedback, $[q_{ma}, q_{ps}]$, are sensed by rate gyros placed along the centerline of the fuselage. It is anticipated, though not implemented in the first application, that the first several flexible modes can be estimated with very good accuracy and the rigid body states are readily measurable.

Recall from Chapter 2 that the input/output aircraft dynamics represented by (2.20) are affine in control and the desired dynamics have the form of a PI-controller given by (2.24). In terms of the aircraft equations of motion and longitudinal axis in particular the system is given by (2.6). Recall that as discussed in Chapter 3 the dynamic part of the aeroelastic equations are linear so the entire system is a nonlinear/linear hybrid that assumes the form below

$$\begin{pmatrix} \dot{u} \\ \dot{w} \\ \dot{q} \\ \dot{\theta} \\ \ddot{\eta}_j \\ \dot{\eta}_j \end{pmatrix} = \begin{pmatrix} -qw - g\sin\theta + T/\mathrm{M} \\ qu + g\cos\theta \\ 0 \\ q \\ 0 \\ 0 \end{pmatrix} + \bar{a} \begin{pmatrix} C_x(\alpha, M)/\mathrm{M} \\ C_z(\alpha, M)/\mathrm{M} \\ \bar{c}C_M(\alpha, M)/I_y \\ 0 \\ 0 \\ 0 \end{pmatrix} + \bar{a} \begin{pmatrix} C_{x,\eta_i}(\alpha, M, GW^*)/\mathrm{M} \\ C_{z,\eta_i}(\alpha, M, GW^*)/\mathrm{M} \\ \bar{c}C_{M,\eta_i}(\alpha, M, GW^*)/I_y \\ 0 \\ 0 \\ 0 \end{pmatrix} \eta_i +$$

$$\bar{a} \begin{pmatrix} C_{x,\dot{\eta}_i}(\alpha, M, GW^*)/\mathrm{M} \\ C_{z,\dot{\eta}_i}(\alpha, M, GW^*)/\mathrm{M} \\ \bar{c}C_{M,\dot{\eta}_i}(\alpha, M, GW^*)/I_y \\ 0 \\ 0 \\ 0 \end{pmatrix} \dot{\eta}_i + \begin{bmatrix} 0 & 0 & 0 & 0 & 0 \\ 0 & 0 & 0 & 0 & 0 \\ 0 & 0 & 0 & 0 & 0 \\ 0 & 0 & 0 & 0 & 0 \\ E_{\eta_i u} & E_{\eta_i w} & E_{\eta_i q} & \frac{-\omega^2}{m} + E_{\eta_j \eta_i} & \frac{-2\zeta\omega}{m} + E_{\eta_j \dot{\eta}_i} \\ 0 & 0 & 0 & 0 & 1 \end{bmatrix} \begin{pmatrix} u \\ w \\ q \\ \eta_i \\ \dot{\eta}_i \end{pmatrix}$$

$$+\bar{a} \begin{pmatrix} C_{x,\delta_p}(\alpha, M, GW^*)/\mathrm{M} \\ C_{z,\delta_p}(\alpha, M, GW^*)/\mathrm{M} \\ \bar{c}C_{M,\delta_p}(\alpha, M, GW^*)/I_y \\ 0 \\ E_{\eta_j,\delta_p}/\bar{a}m \\ 0 \end{pmatrix} \delta_p \qquad \text{with } 1 \le i, j \le 8 \text{ and } 1 \le p \le 2 \text{ and } \bar{a} = \frac{1}{2}\rho S V^2 \tag{5.1}$$

$$y = \begin{bmatrix} q_{ma} \\ q_{ps} - q_{ma} \end{bmatrix} = \begin{bmatrix} 0 & 0 & 1 & 0 & 0 & \phi'_{ma_i} \\ 0 & 0 & 0 & 0 & 0 & \phi'_{ps_i} - \phi'_{ma_i} \end{bmatrix} \begin{pmatrix} u \\ w \\ q \\ \eta_i \\ \dot{\eta}_i \end{pmatrix} \tag{5.2}$$

or equivalently

$$y = \begin{bmatrix} q + \sum_{i=1}^{8} \phi'_{ma_i} \dot{\eta}_i \\ \sum_{i=1}^{8} \Delta\phi'_i \dot{\eta}_i \end{bmatrix}$$

where ϕ'_i is the slope of the i[th] mode at either pilot station or mean axis location. It is instructive to look at the composition of the measured pitch rate variables used for control. Note from (5.2) that $q_{ps} - q_{ma}$ is just the difference in flexible mode contribution; if the mean axis sensor picks up a minimal amount of flexible dynamics, then this quantity represents only the flexible dynamics at the pilot station which the controller is trying to eliminate. Moreover, the number of flexible modes selected for the design model depended largely on the minimum number of modes necessary to produce a stable closed loop system, particularly for higher frequency dynamics. The cutoff frequency for the inclusion of the modes, in this case resulting in the first eight, correlates to the lowest frequency of the actuator dynamics (stabilator at 20 rad/sec). Also, because the flexible modes are so closely spaced, the highest mode included was in the mid 20s rather than exactly at 20 rad/sec.

The controller design involved selecting gains K_{cmd}, K_i, and K as well as finding the dynamic matrix $W(x)$ such that the steady state error has been minimized and the damping of the first couple of fuselage flexible modes has been increased. The feedback linearization part of the total controller had to take care of increasing the damping of the flexible modes, which allowed the PI compensator to deal with command following part. In order to produce a satisfactory linear system for the PI compensator to control, the dynamic matrix *W(x)* was created from the following parts.

First, to abide by the physical limitations of the aircraft, a constant matrix was used to modify the control effectiveness matrix $h_x g(x)$. The RCV is both relatively small and

has negligible impact on the vehicle pitch rate and should not participate in pitching the entire vehicle, hence the rigid body contribution to calculating the RCV command is zeroed by an appropriate constant matrix M. Because the elevator has significant contribution to the control of the rigid body, in this initial application, it was geared to the stabilator, and what effects the stabilator command effects the elevator command as well. Thus, the feedback linearization part is a 2x2 MIMO problem. Furthermore, in order to stabilize the system, improve the flexible modes damping, and the rigid body response, a diagonal dynamic matrix W was used. Another reason for the elevator/stabilator gearing is that the QSAE control law, used here for comparison, also employed such gearing. The details of the dynamic inversion control law are illustrated in (5.3). Note that best results obtained in this configuration required just proportional controller for $\Delta\phi_i'\dot{\eta}_i$ variable for reasons touched in an earlier discussion.

$$K_{cmd} = \begin{bmatrix} 1.25 & 0 \\ 0 & 0.85 \end{bmatrix} \qquad K = \begin{bmatrix} 1.25 & 0 \\ 0 & 2 \end{bmatrix} \qquad K_i = \begin{bmatrix} 0.75 & 0 \\ 0 & 0 \end{bmatrix}$$

$$M\left(h_x g(x)\right)^{-1} = \begin{bmatrix} \bar{g}_{11} & \bar{g}_{12} \\ \bar{g}_{21} & 0 \end{bmatrix} \qquad W = \begin{bmatrix} \frac{8}{s+8}\frac{10}{s+10} & 0 \\ 0 & \frac{5}{s+5}\frac{20}{s+20} \end{bmatrix} \tag{5.3}$$

In contrast to the $W(x)$ dynamics explored in the previous chapter, which were first order, the dynamics in the actual controller are second order filters. This approach was necessitated by the need to roll off the controller as quickly as possible before the actuator dynamics come into play. Recall that the first breakpoint for the third order stabilator dynamics is at 20 rad/sec, same as one of the time constants for a filter in the flexible dynamics loop. The pitch rate loop also had to be rolled off quickly so as to minimize the flexible mode excitation. The lower frequency filters in both loops served as a mechanism to balance the speed of the pitch rate response and the increased damping of the first few fuselage bending modes as well as the stability of the higher frequency modes. Higher order filters were unnecessary and inadvisable based on desire for 40 db/decade roll off of the loop shape at the crossover frequency.

Though not explicitly mentioned here, desirable pilot handling qualities are achieved by precompensation of stick and pedal commands, and trim inputs that exist as part of the

nonlinear simulation. The pilot inputs are scaled with flight condition dependent gains and a first-order shaping filter to achieve time constants other than those resulting from feedback objectives.

The evaluation of the controller was done on the full nonlinear high fidelity longitudinal model plus 20 symmetric elastic modes with actuator rate and deflection limits and was conducted in the presence of three levels of turbulence (none, moderate, and severe vertical turbulence).

5.5 Controller Results

5.5.1 Standard vs. Novel Dynamic Inversion

As has been mentioned in the earlier sections, a standard dynamics inversion controller design was attempted, if rather unsuccessfully. The inversion could control the first fuselage bending mode with some modest success but the higher frequency modes, especially the fuselage rather than the wing ones, went unstable as Figure 5.3 illustrates. Any adjustment to the desired dynamics to increase damping of the first fuselage mode drove the higher frequency modes more unstable. Figure 5.3 provides a good overview of the dynamics of all 20 flexible modes as well as a close up of the dynamics of the first 8 for open loop, standard dynamic inversion, and novel dynamic inversion. The inability of the standard dynamic inversion to handle flexible dynamics in the integrated flight/SMC context motivated the development of the novel dynamic inversion methodology.

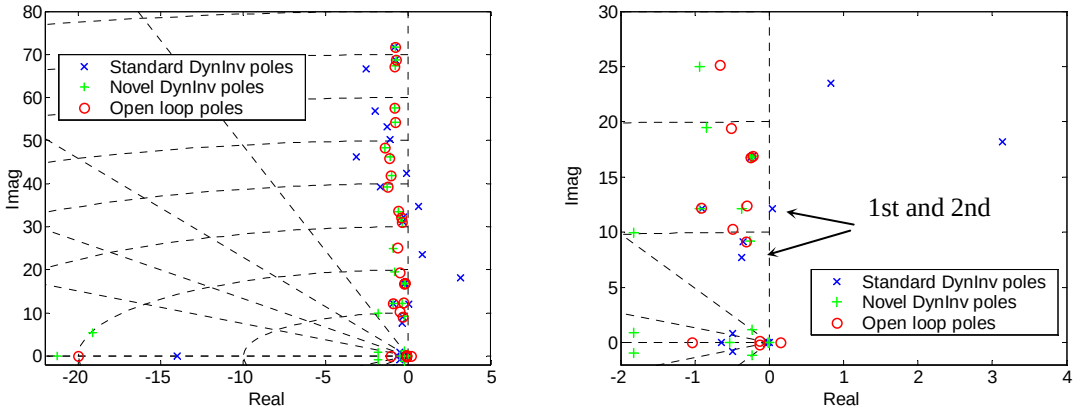

Figure 5.3. Standard vs. Novel dynamic inversion closed loop system.

5.5.2 Novel Dynamic Inversion Controller

The open loop aircraft is characterized by a moderately unstable short period and a typical flexible mode damping of less than 7%. In particular, the damping of the first two fuselage bending modes is 5% and 2.5% respectively. The achieved level of damping on the first couple fuselage bending modes are on the order of 20% for the first and 5% for the second fuselage mode (sequentially mode 8), which is also much higher in frequency and is the last mode being actively controlled by the dynamic inversion controller. The effect on the damping of the other flexible modes, be they wing modes of the design model or modes of frequencies above that of mode 8, is neutral to positive. In other words, no modes were pushed towards the jω-axis as a result of the novel dynamic inversion controller. In fact, this was a balancing act between improving the damping of the fuselage modes within the frequency range of the design model and speeding up the flight controller response and destabilizing higher frequency modes.

The simulation analysis of the controller has been performed on the high fidelity, fully nonlinear model and the results are presented below. The established baseline is 0.5 stick pitch rate command in the presence of no turbulence. The baseline closed loop pitch rate and normal acceleration response to 0.5 stick pitch rate command as well as corresponding actuator behavior is illustrated in Figures 5.4 and 5.5. In this case the controller succeeds in making the flexible airplane behave essentially like a rigid one as evidenced by virtual overlap of pitch rate response at the pilot station and mean axis as well as normal acceleration response devoid of high frequency dynamics. Note that the way the controller achieves its objectives is to blunt an initial sharp actuator deflection to quickly follow the pitch rate command, which abates flexible mode excitation and enables the RCV to counteract the excitation that does occur. The controller then overcompensates by allowing a large overshoot to speed up the response, though a large overshoot is a typical characteristic of pitch rate response type controllers.

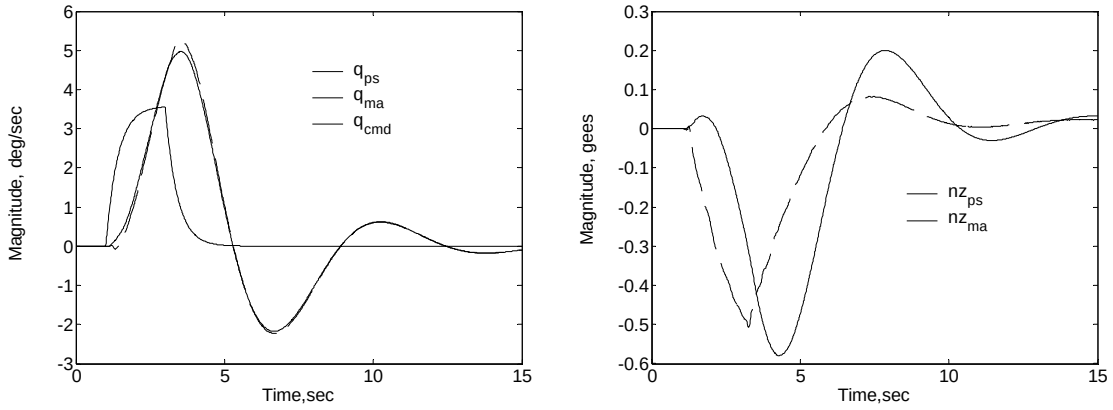

Figure 5.4: Pitch rate and nz response to 0.5 stick pitch rate command with no vertical turbulence at pilot station (dashed) and mean axis (solid).

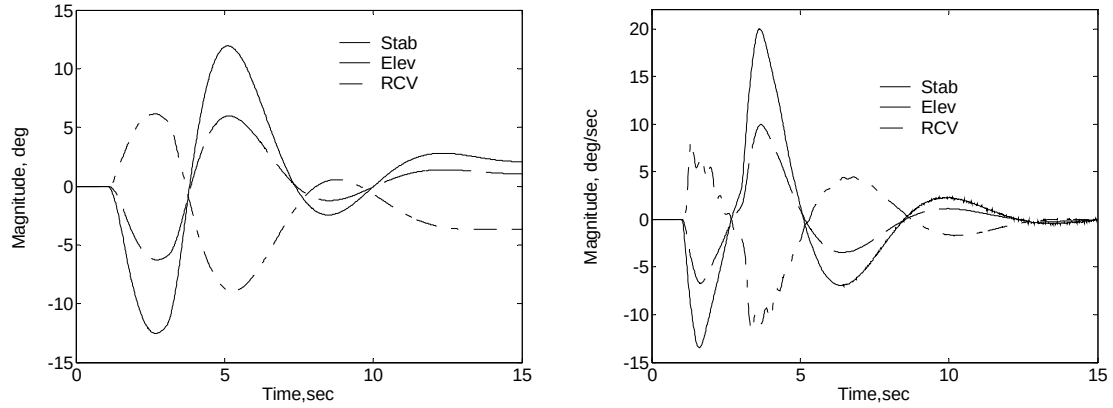

Figure 5.5: Actuator displacement and rate response to 0.5 stick pitch rate command with no vertical turbulence.

5.5.2.1 Turbulence Response

Further analyses include controller performance in severe and moderate turbulence (see Figs. 5.7-5.10) as well as under conditions that cause surface saturations in the presence of the aforementioned turbulence (see Figs. 5.11-5.14). Turbulence was injected into the high fidelity simulation as $[u_{gust}, w_{gust}, \dot{w}_{gust}]$. The level of turbulence is determined based on the values provided in Reference 46 and generated by the standard atmospheric simulation Dryden filter. The actual turbulence profiles used are

documented in Figure 5.6. Since turbulence was generated each time it was used for analysis, there are four profiles given in Figure 5.6. Note that moderate turbulence has roughly one half the magnitude peak-to-peak of the severe turbulence.

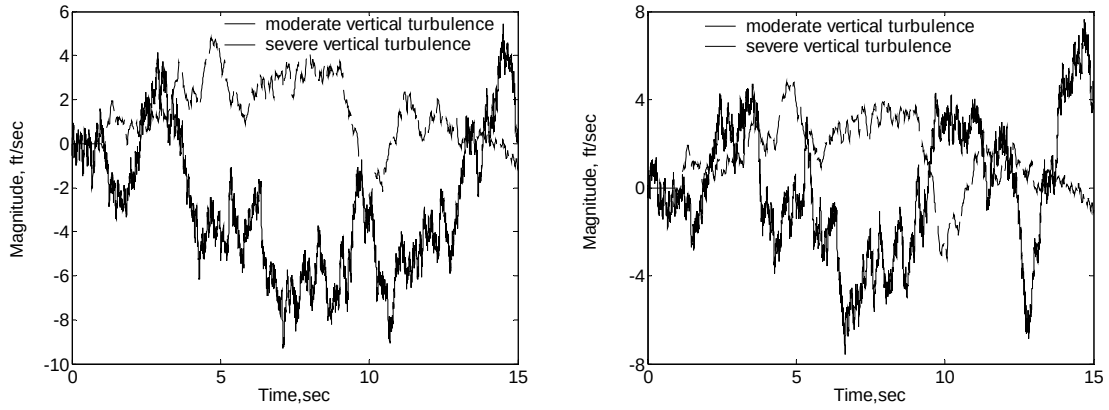

Figure 5.6: Vertical turbulence in the severe and moderate range for saturated actuators and no saturation cases.

The pilot station is more affected by turbulence than the mean axis representing the whole of the vehicle both in pitch rate and in normal acceleration responses (see Fig. 5.7). The severe turbulence excites the flexible modes and this excitation manifests itself as high frequency oscillations superimposed on the response of the vehicle to 0.5 stick pitch rate command. The turbulence most influences the measured normal acceleration, especially at the pilot station. The dynamic inversion controller is attempting to counteract this flexible mode excitation as evident from the highly oscillatory RCV rate response documented in Figure 5.8. However, the RCV does not have sufficient authority and speed of response to completely cancel flexible mode excitation from turbulence, hence the high frequency oscillations. In general, the control surface deflections are on par with those of the baseline case (see Fig. 5.5). All three control surfaces are somewhat effected by the turbulence though their rates are again on par with those of the baseline with the exception the RCV rate which shows significant manifestation of turbulence in its higher peak rate magnitude.

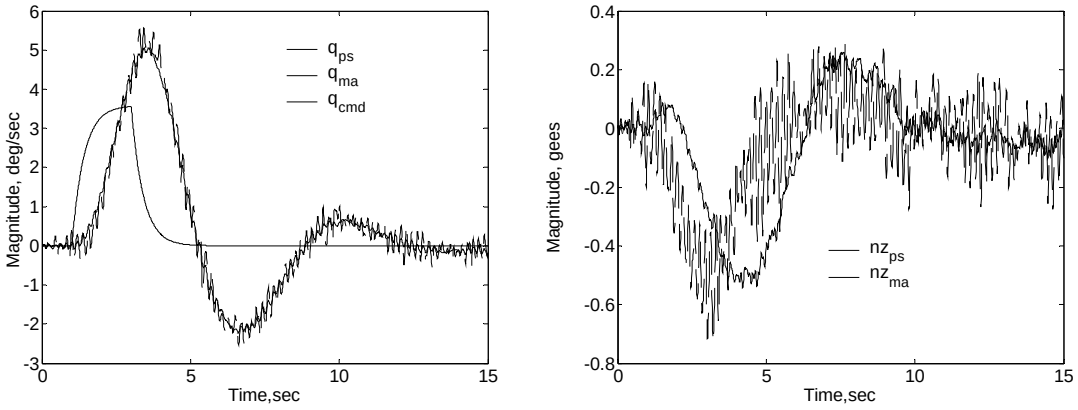

Figure 5.7: Pitch rate and nz response to pitch rate command in severe vertical turbulence to 0.5 stick at pilot station (dashed) and mean axis (solid).

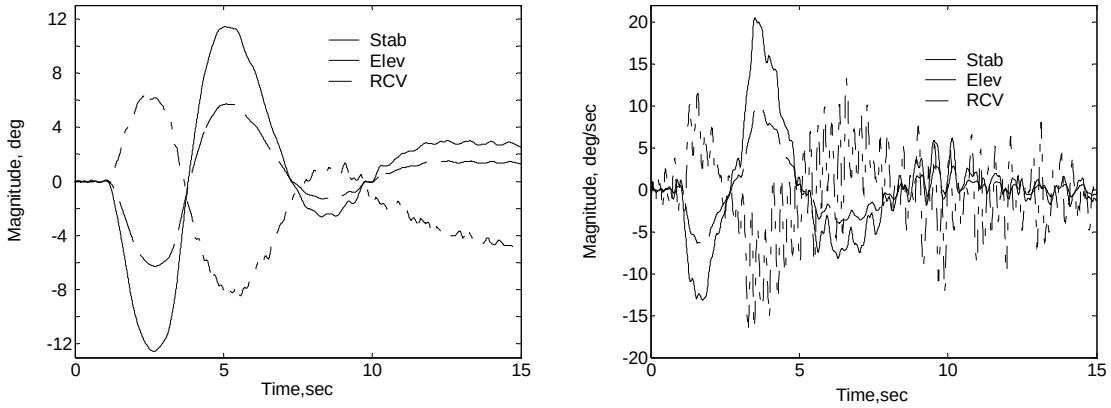

Figure 5.8: Actuator response to pitch rate command in severe vertical turbulence to 0.5 stick.

The response to moderate turbulence follows the analysis with the magnitude of the high frequency oscillatory response significantly less in both pitch rate and normal acceleration responses (see Fig. 5.9) as well as rate response of the RCV in an attempt to control these oscillations. Similarly, the actuator response is similar to the baseline

response (see Fig. 5.5) with RCV peak magnitude rate somewhat higher as a consequence of attempting to counteract turbulence excitation effect on elastic modes (see Fig. 5.10).

Another important aspect of controller analysis is response to commands that saturates control surfaces and to make it more difficult this command occurs under severe and moderate turbulence. In order to achieve saturation at this flight condition, the gain

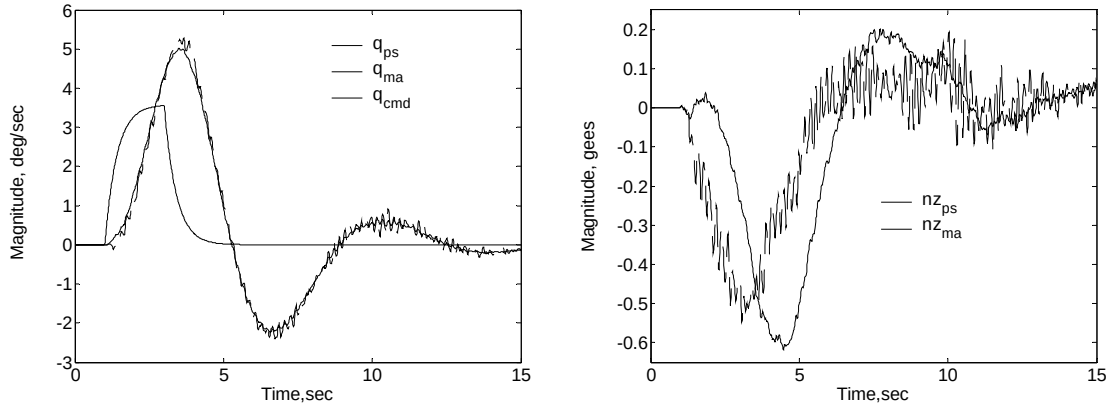

Figure 5.9: Pitch rate and nz response to pitch rate command in moderate vertical turbulence to 0.5 stick at pilot station (dashed) and mean axis (solid).

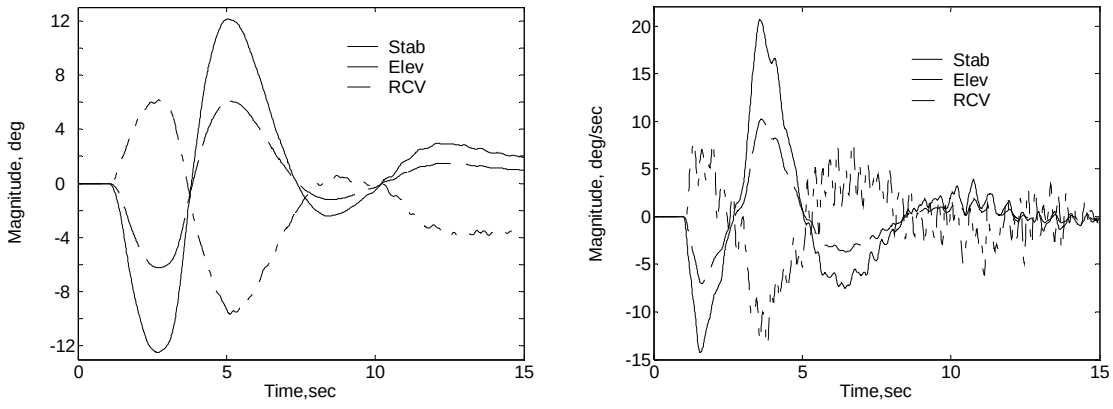

Figure 5.10: Actuator response to pitch rate command in moderate vertical turbulence to 0.5 stick.

between stick and pitch rate command had to be increased by a factor of two. Hence, surface displacement and rate saturation has occurred for both elevon and stabilator for a full stick pitch rate command (see Fig. 5.12). System response to this command in the presence of severe atmospheric turbulence is illustrated in Figure 5.11. Note that the magnitude of the pitch rate command is 15 deg/sec compared to 3.5 deg/sec for baseline case (see Fig. 5.4). Because of the control surface displacement saturation, the pitch rate response does not reach the proportionately large overshoot observed for baseline. The normal acceleration, especially at the pilot station, again exhibits high frequency oscillations superimposed on the command response (see Fig. 5.11). The magnitude of these high frequency oscillations is comparable to those seen in the presence of severe turbulence but without surface saturation. The reason that these magnitudes are comparable is that the RCV is the surface attempting to damp out high frequency oscillations, and it is one surface that does not saturate (see Fig. 5.12). The reason that there are high frequency oscillations present is that the RCV does not have sufficient authority and speed of response to completely cancel flexible mode excitation from turbulence.

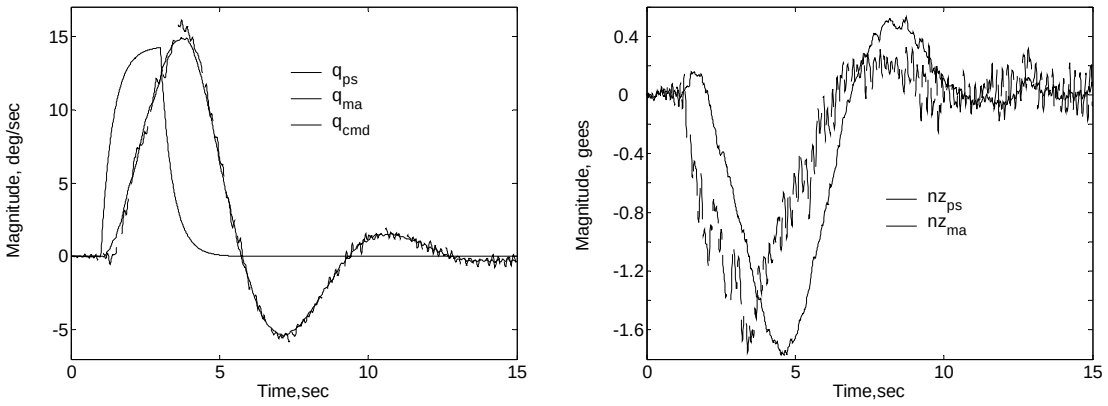

Figure 5.11: Pitch rate and nz response to pitch rate command of full stick that saturates controls in severe vertical turbulence at pilot station (dashed) and mean axis (solid).

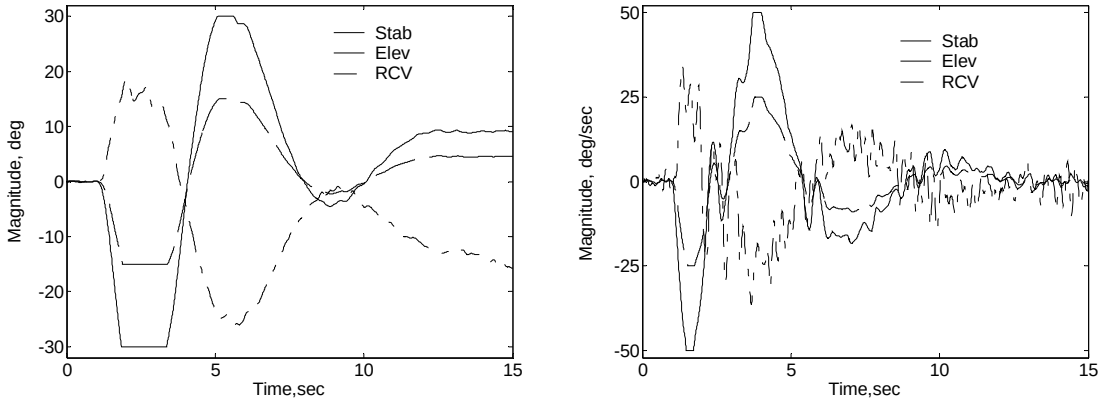

Figure 5.12: Actuator response to pitch rate command of full stick that saturates controls in severe vertical turbulence.

The response to moderate turbulence in the presence of control surface saturation, shown in Figures 5.13 and 5.14, combines the response to saturation discussed above and response to moderate turbulence with no saturation earlier in this section. The pitch rate response and normal acceleration show some high frequency dynamics (see Fig. 5.13). The actuator dynamics show surface displacement saturation for stabilator and elevon (see Fig. 5.14), which limits the magnitude of pitch rate response and by association normal acceleration. The rates for these surfaces are also saturated and it leaves the RCV, which is considerably faster to work to cancel out the elastic mode excitation from turbulence that manifests itself as high frequency oscillations superimposed on the commanded response in both pitch rate and normal acceleration.

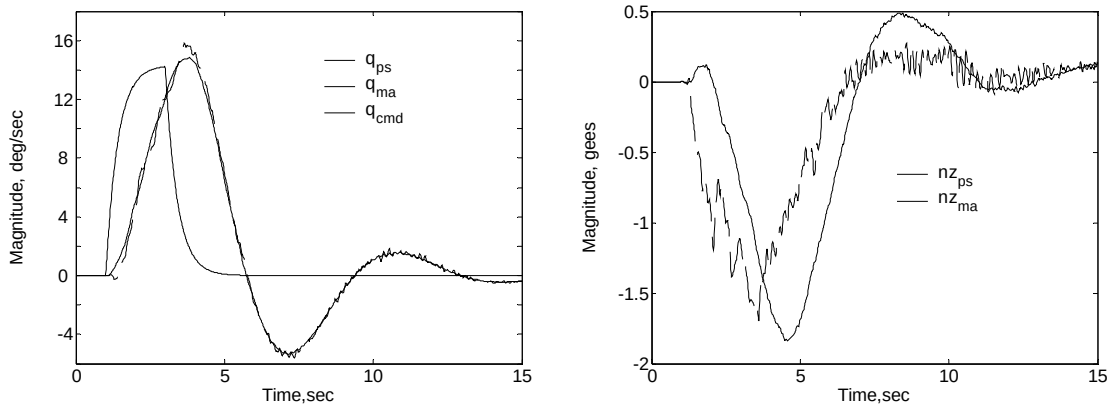

Figure 5.13: Pitch rate and nz response to pitch rate command of full stick that saturates controls in moderate vertical turbulence at pilot station (dashed) and mean axis (solid).

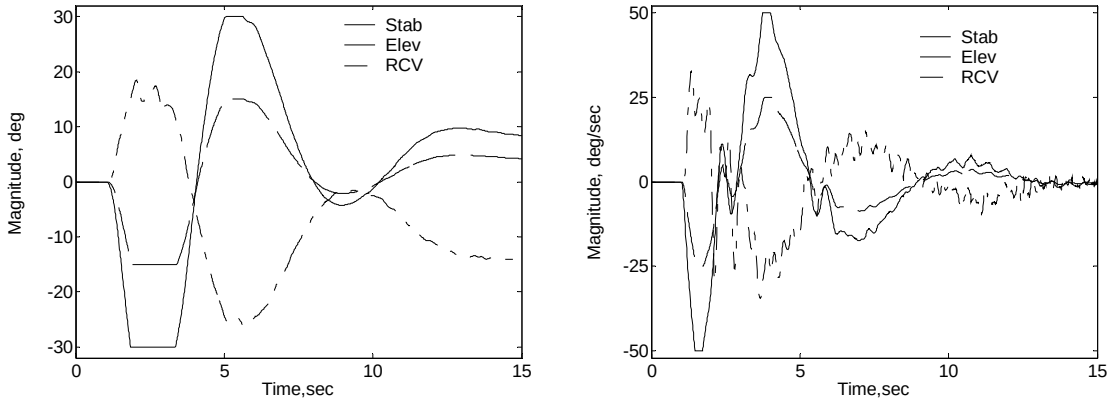

Figure 5.14: Actuator response to pitch rate command of full stick that saturates controls in moderate vertical turbulence.

5.5.2.2 Uncertainty Analysis

The final analysis performed for the novel dynamic inversion controller is assessing its stability with respect to uncertainty in the flexible modes. Specifically robust stability is checked with respect to varying frequency and damping of the first two elastic modes. The variations are modeled as real parameter variations. The μ-analysis indicates that the closed loop system is guaranteed robust stability to 15% variation in frequency and 50%

variation in damping for each mode, which is well within expected envelope of model fidelity. Figure 5.15 illustrates the results of the robustness analysis. The dominant parameter influencing stability is frequency variation. An important point is the fact that uncertainty in flexible modes causes the system to go unstable at very low frequencies and not at where the system is uncertain. This is a result of the coupling of the elastic modes into the zero dynamics of the closed loop airplane. The analytical basis for this coupling was explored in Chapter 4. From the physics perspective, the decrease in flexible mode frequency (destabilizing uncertainty is negative delta) changes the vehicle deformation that in turn alters its lift locally and influences the low frequency phugoid like dynamics. Recall, that this aircraft has a degenerate short period, *i.e.*, two real eigenvalues, and the typical clear separation between the short period dynamics and the phugoid does not really exist. The open loop dynamics are illustrated in Chapter 3, Figure 3.10.

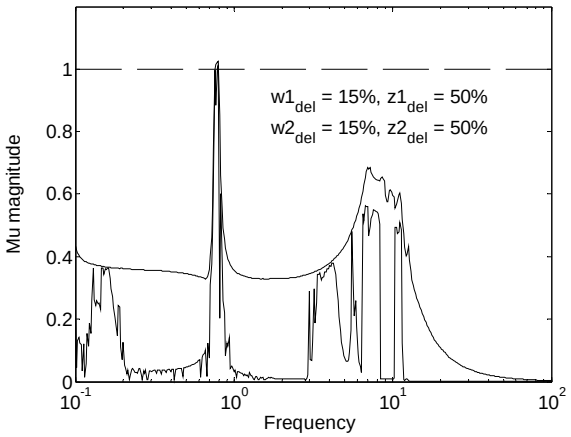

Figure 5.15: Robust stability analysis. (μ lower and upper bounds with μ=1 robust stability boundary)

5.5.3 Importance of Integrated Design

In order to check the speed and character of the response of the novel dynamic inversion controller against the accepted norm, a controller[47] designed and tuned in a

QSAE piloted simulation was used. The analysis performed here are not intended to show how well the novel dynamic inversion controller performs in general against the QSAE one, but to evaluate the character of the response and to emphasize the need to approach the design process from the integrated flight/SMC perspective.

To compare the responses of the novel dynamic inversion controller to that of the QSAE $\dot{\gamma}/V$ response type, the high fidelity, fully nonlinear simulation was again employed. The responses shown are to 0.5 stick throw in the presence of moderate vertical turbulence. The responses of the dynamic inversion controller are co-plotted with the responses of the controller designed for the QSAE aircraft using classical techniques and evaluated for performance in the piloted simulation on a QSAE aircraft. This controller is evaluated on a dynamic aeroelastic model along with the dynamic inversion controller not for the purpose of showing that it performs badly but to show that it actually excites flexible modes and makes it much more difficult for a separate SMC controller to work. This argues for an integrated design approach in contrast to Reference 22. It is also used to show that the novel dynamic inversion controller has similar performance in the pilot's bandwidth range. The dynamic inversion controller response is slightly slower, but it remains to be determined in a piloted evaluation whether there is a perceptible effect on flying qualities.

Figure 5.16 illustrates the response to 0.5 stick throw at the pilot station of pitch rate. Figure 5.17 shows the mean axis response, which is approximated by a sensor placed behind the center of gravity, exhibits the least amount of excitation due to oscillation of the flexible modes. The novel dynamic inversion pitch rate response at the pilot station and at the mean axis essentially overlap, as is evident from Figure 5.18. The QSAE controller on the other hand excites flexible modes, particularly at the pilot station.

The normal acceleration at the pilot station is plotted in Figure 5.19. The sensed mean axis response is plotted in Figure 5.20. Both of the figures indicate that the QSAE controller induces normal acceleration by exciting the flexible modes of the vehicle. It is particularly bad at the pilot station where the absolute g excursion is 400% as the stick is reversed. Even the sensed mean axis where flexible mode influence is minimized by the physics shows a 60% g variation at the same point. The novel dynamic inversion controller on the other hand achieves its stated objective of minimizing pilot station

oscillation with respect to the mean axis. In fact, based on the response in Figures 5.16-5.20, it can be concluded that the novel dynamic inversion controller makes the fuselage behave essentially like a rigid aircraft by keeping the pilot station response very close to that of the sensed mean axis.

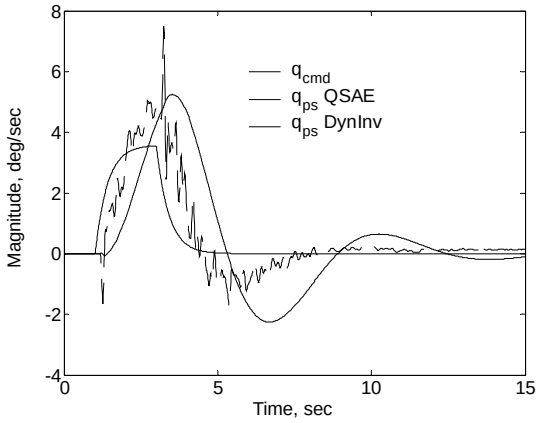

Figure 5.16: Pitch rate response at the pilot station to 0.5 stick throw.

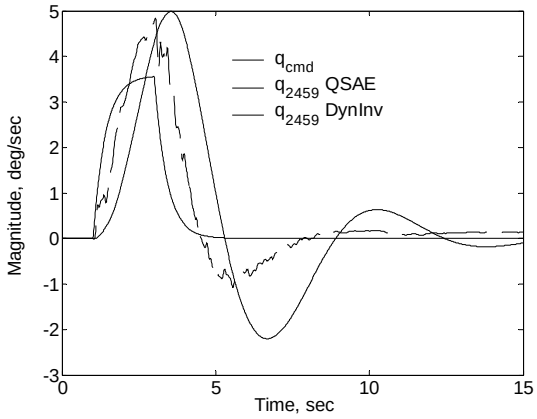

Figure 5.17: Pitch rate response at the mean axis sensor to 0.5 stick throw.

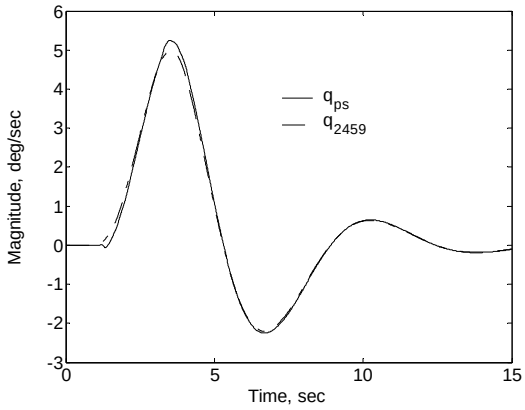

Figure 5.18: Pitch rate response at the pilot station and measured mean axis of the dynamic inversion controller to 0.5 stick throw.

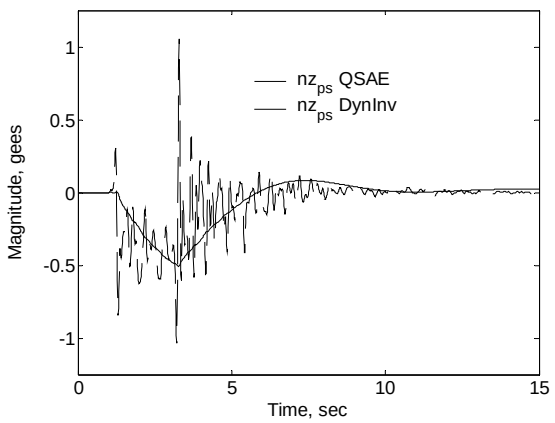

Figure 5.19: Nz response at the pilot station to 0.5 stick throw.

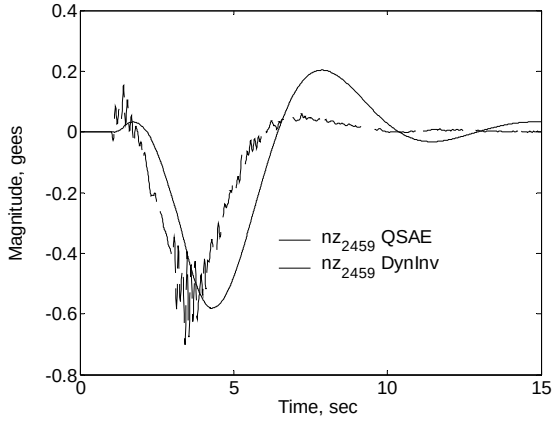

Figure 5.20: Nz response at the sensed mean axis to 0.5 stick throw.

To further illustrate that the novel dynamic inversion controller achieves its objectives with performance comparable to that of the QSAE controller at low frequencies, control activity is considered. In Figure 5.21, the deflections for the control surfaces available to both controllers are shown. The magnitudes are normalized by the maximum available deflection to show just how much of the available control power is used by each controller. It is interesting to note that the novel dynamic inversion controller uses less stabilator and consequently less elevator than does the QSAE controller. Apparently, although the RCV deflection is small, it does contribute enough moment to lessen the required tail deflection or it could be due to a slower response. Also of interest is the fact that for the dynamic inversion control, the RCV and the tail surfaces are deflected simultaneously, as if to say that the controller is anticipating the bending of the aircraft as it tries to pitch and is actively trying to minimize the ensuing bending and then snapping effect at the pilot station.

The actuator rates are also presented in Figure 5.22 for comparison. Similar to the deflections, the surface rates are normalized by their respective limits. The stabilator is considered a slow surface while both the elevator and the RCV are considered fast surfaces. It is interesting to note that the flexible nature of the vehicle drives the stabilator rate of the QSAE controller to its limit, at around 3 seconds. This is another

indication of potential difficulties when SAS and SMC are designed independently for this class of vehicles.

Frequency response is often helpful in identifying which dynamics are contributing to the behavior seen in the time response. In a typical aircraft, turbulence excites the flexible modes, not the pilot inputs. Several frequency response plots are presented here to illustrate the difficulty of the problem under consideration by showing a transfer function that represents a typical operating bandwidth of a pilot on the same plots as the

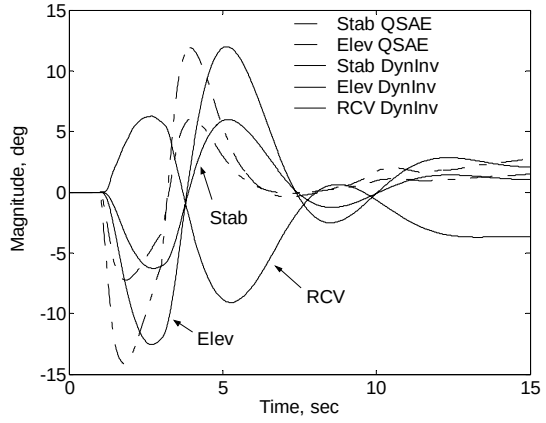

Figure 5.21: Actuator surface deflection.

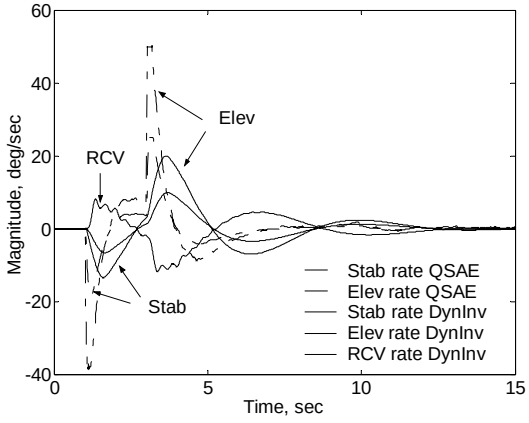

Figure 5.22: Actuator surface rates.

closed loop frequency responses. At the frequency of the first flexible mode, the pilot command is attenuated by less than half. It becomes quickly apparent from the responses in Figures 5.23 and 5.24 that the flexible modes are clustered together and, as previously mentioned several of the elastic modes are well within the pilot's bandwidth. Hence, the typical 1 decade plus separation between rigid body and flexible modes that is characteristic of most piloted vehicles does not exist for this type of aircraft. Also, as has been pointed out, the elastic modes are very lightly damped and, thus, easily excitable.

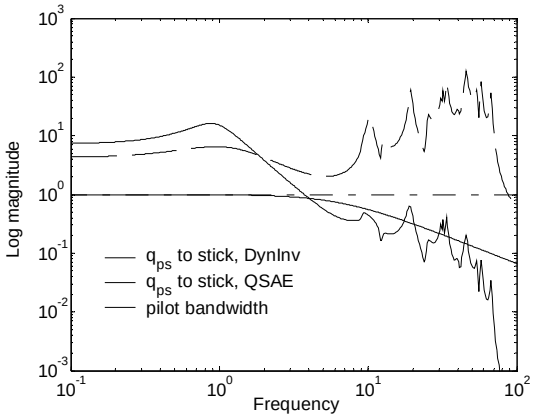

Figure 5.23: Frequency response pitch rate at the pilot station to stick input.

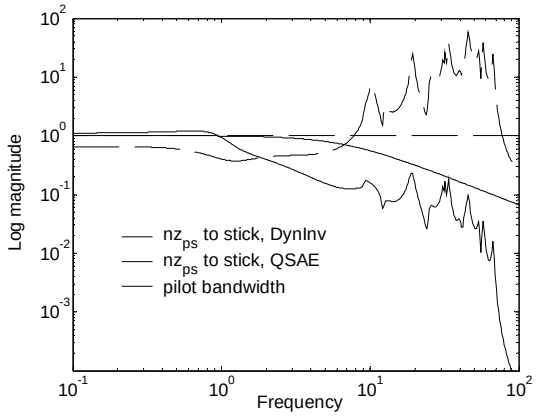

Figure 5.24: Frequency response nz at the pilot station to stick input.

As can be seen from the frequency responses in Figures 5.23 and 5.24, the dynamic inversion control law attenuates flexible modes that are within a decade of the pilot bandwidth while the control law designed on the QSAE aircraft amplifies the flexible modes in the same range. While this fact is not surprising it does make the objectives of a separate SMC design so much more difficult on an all ready difficult problem.

The frequency response to turbulence shown in Figure 5.25 is even more pronounced. The open loop system frequency response is co-plotted with the dynamic inversion and QSAE response to turbulence. It is interesting to note that the QSAE attenuates turbulence better than the dynamic inversion controller at the lower frequencies and does somewhat better than the open loop at the first two flexible modes, but then matches the response of the open loop system. The dynamic inversion controller, while not

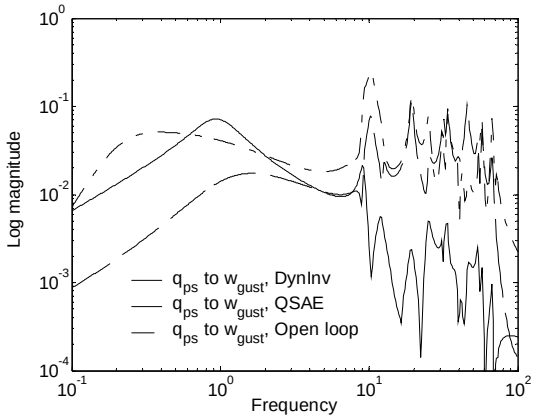

Figure 5.25: Frequency response of the pitch rate at the pilot station to vertical turbulence.

attenuating as much as the QSAE at the lower frequencies, does better than the open loop and has a superior response starting with the flexible modes frequencies.

After looking at the time and frequency response comparisons between the novel dynamic inversion and QSAE controllers, it is interesting to look at the actual pole locations that govern the observed responses. The poles of the open loop, QSAE, and novel dynamic inversion controllers are illustrated in Figure 5.26, with each plot showing a progressively smaller section of the s-plane enlarged for better viewing. Note that actuator dynamics remain primarily unchanged in all cases as seen from the very high frequency pole locations in the upper left quadrant plot. The upper right quadrant gives a nice overview of the flexible modes near the jω-axis and poles associated with different compensator dynamics. The plot in the lower left quadrant provides a very nice illustration of flexible modes within the frequency range controlled by dynamic inversion compensator. Note the positive movement of the elastic modes toward increased damping relative to their open loop locations, especially the first fuselage bending mode around 10 rad/sec. Looking at the locations of the elastic modes and particularly first fuselage bending mode for the QSAE controller, it becomes apparent that any indirectly induced movement is destabilizing. But even without any pole movement, the control surface deflections at the tail excite modes with 4%-5% damping ratio that resonate along

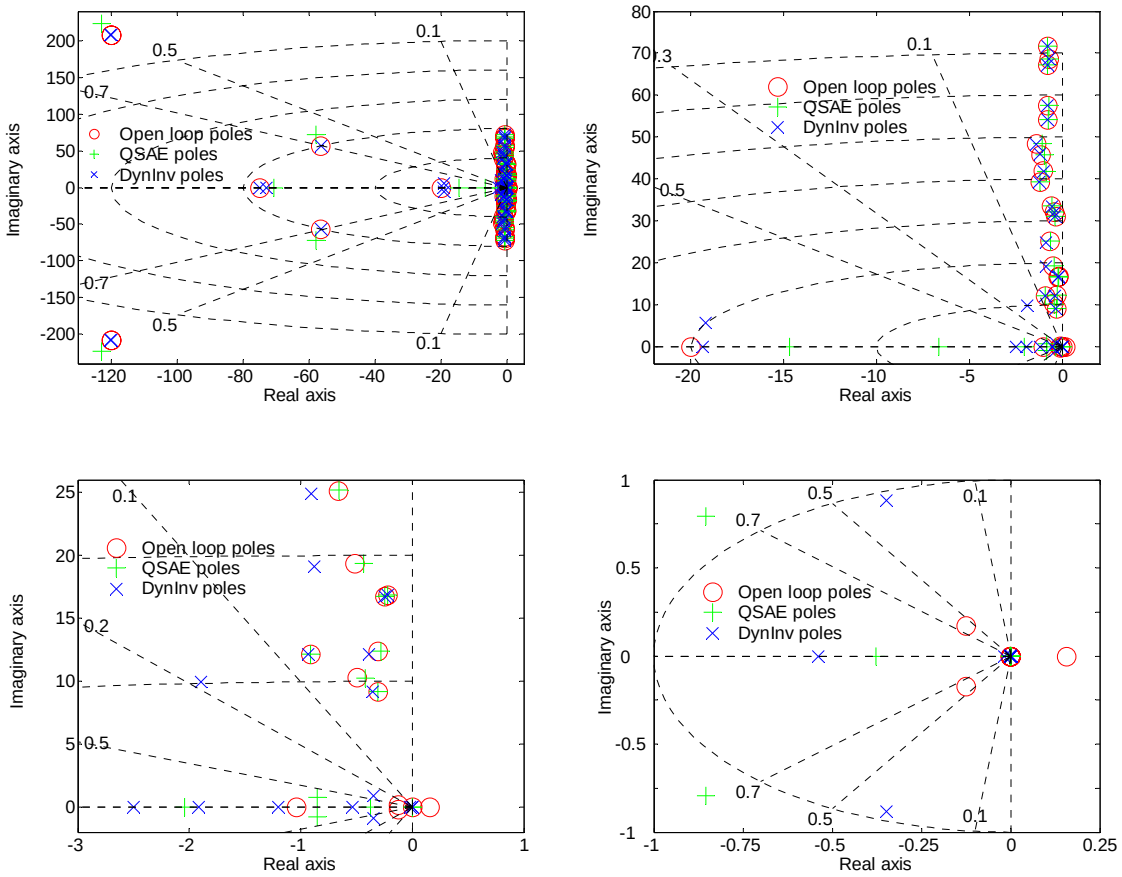

Figure 5.26: Pole map of the entire 20 mode system with third order longitudinal dynamics. Progressively enlarged sections showcasing different dynamic aspects.

the entire fuselage according to their mode shapes. Since there is no attempt to either minimize the initial excitation or to damp it out once it begins, the large high frequency oscillations observed in the pitch rate and normal acceleration response for the QSAE controller is to be expected. One further observation related to the rigid body dynamics as seen in the plot in the lower right quadrant shows comparable dynamics between the two controllers. Some of the differences relate to the different response types, with dynamic inversion based on q response and QSAE based on $\dot{\gamma}/V$ response, the dynamic inversion has faster short period dynamics but less damped phugoid dynamics of comparable frequency than the QSAE compensator.

As the controller comparison demonstrates, an integrated flight/SMC control is a more effective option for achieving optimum vehicle performance. Using separate flight and SMC control would result in the two controllers fighting each other's actions, in addition to the fact that the SMC controller would try to damp out an already excited mode rather than minimizing the excitation in the first place as the integrated controller would.

5.6 Summary

An initial application of the novel dynamic inversion control methodology to a flexible vehicle is presented in this chapter. While the standard dynamic inversion has been applied to aircraft that could be treated as rigid, it never has had to contend with a piloted aircraft whose first few flexible modes resided well within the pilot's bandwidth. The associated problems as well as the proposed modifications to the standard dynamic inversion to deal with them have been presented. The resulting novel dynamic inversion controller was assessed in a high fidelity nonlinear simulation under a variety of conditions including severe turbulence, saturated control surfaces, and uncertainty in the flexible modes.

The results obtained in this initial application are very promising. The novel dynamic inversion controller makes a highly flexible aircraft appear as essentially rigid to pilot in response to his commands. In addition, the damping ratio of the primary fuselage structural mode has been increased from around 5% to close to 20%. The second fuselage flexible mode damping was improved as well, and the higher frequency mode dynamics either remained the same or slightly improved. Furthermore, the aircraft had a favorable response to moderate an severe turbulence. The vehicle was robust to 50% variation in damping and 15% uncertainty in the frequency of the first two flexible modes as well as remained stable for saturated control surfaces.

The obtained results were compared to a controller designed on a QSAE aircraft model and tuned for performance in extensive piloted simulations. While the dynamic inversion controller has not yet been tuned in piloted simulation, the response at lower frequency is similar to that of the QSAE controller. Although it is expected that the QSAE controller would not attenuate the flexible modes since it is not designed on a flexible model, it exacerbates the problem of flexible mode control by a separately

designed SMC. Thus, the results of this work also advocate the integrated design of the SAS/SMC controller to maximize the performance of the aircraft.

Another interesting observation is that a number of flexible modes are primarily wing modes and require wing surfaces to attenuate them. While fuselage mounted control effectors do a good job on the fuselage bending modes they have little to no effect on the wing modes which in turn contribute to the excitation of fuselage modes and to a slight heave of the entire aircraft.

Chapter 6 – Stability

6.1 Introduction

The results in this chapter are an assessment of stability of the dynamic inversion in the presence of high degree of rigid body/dynamic aeroelastic coupling and an integrated flight/SMC control system. The method of reasoning follows the work of Morton, *et al.* that applied to a SISO rigid body fighter control system. This work builds on the results in Reference 14 and adds a new level of complexity that is the flexible aircraft dynamics, which cannot be ignored even in the most basic flight control as well as an integrated MIMO flight/SMC control system.

The whole of this thesis deals with the design of nonlinear controllers for a highly flexible aircraft. Each preceding chapter dealt with a different aspect of that design. The issue that remains to be addressed is that of the stability of the dynamic systems driven by these controllers. The approach is rather straight forward. The vehicle driven by a controller must reach some equilibrium whose stability must be evaluated. The results in this chapter show how assessing stability of an n-dimensional system can be reduced to checking stability of a two-dimensional one using algebraic expressions that are based on the vehicle characteristics such as aerodynamic coefficients. This reduces a complicated dynamical problem to something purely algebraic and manageably complex.

In order to make the problem mathematically tractable, the aircraft dynamics have been simplified for analytical work while retaining the essential characteristics. These essential characteristics are the influence of flexible modes on rigid body dynamics and vice versa. What is not retained is the interaction of flexible modes among themselves, but based on experience, it is not a critical element of the dynamic behavior. The simplification involved considering longitudinal dynamics with a single elastic mode and a control law based on standard dynamic inversion only. In addition, throughout this chapter the analysis considers the inner loop of the dynamic inversion only, *i.e.*, the $\dot{y}^{des}$ to y portion. It is important to note that the nature of $\dot{y}^{des}$ impacts the overall closed loop dynamics but will not be discussed here.

This chapter is organized as follows. Section two discusses system stability from an abstract nonlinear system perspective. Section three introduces aircraft equations of

motion used for analysis followed by a definition of equilibrium set in section four. Section five presents the dynamic inversion decoupling of the closed loop system. Section six addresses global stability for a two-dimensional system, followed by general global stability result in section seven. Concluding remarks follow in section eight.

6.2 System Stability

Consider the issue of stability of a highly coupled rigid body flexible dynamics aircraft. The integrated flight/SMC dynamic inversion controller produces a closed loop system that separates into controlled dynamics and internal dynamics. The controlled dynamics are stable by design and the stability of the closed loop system depends on stability of internal dynamics. If a commanded change in flight condition is executed by the controller, then the closed loop system would be considered nonautonomous through the control action that occurs over a finite interval of time. The question of stability then translates into whether the resulting flight condition is a stable one and was the transition to this new state done in a bounded way.

The stability problem is to be addressed from a more general nonlinear system perspective while providing specific algebraic conditions for aircraft that would establish these stability guarantees. A special case for a control action is assumed. The dynamic inversion controller and the selected output control variables are such that the closed loop system is separated into a string of integrators corresponding to the controlled states and internal dynamics that are a function of open loop and controller states. Furthermore, the internal dynamics belong to a two-dimensional system; thus, there are special tools that can be introduced to show global stability of the closed loop system. The special case of a closed loop nonlinear system that is reduced from an n-dimensional to a two-dimensional system is predicated on the controller having sufficient degree of freedom and the controlled variables selected such that the closed loop dynamic separation mentioned above occurs. An example of such a case would be an integrated flight/SMC controller of longitudinal aircraft dynamics with flexible mode and attitude dynamics as control variables.

After the dynamic inversion controller decomposes the closed loop system into two subsystems, controlled and internal dynamics, the questions that remain to be answered are what are the equilibria and are the internal dynamics stable in the neighborhood. The

determination of the equilibria is a static behavior issue, independent of the control design, and is vehicle specific based essentially on the aerodynamics. As will be shown in a later section, the stability of the equilibria depends on the stability of system zero (or internal) dynamics in the neighborhood, which is reduced to a set of algebraic conditions to be checked. However, prior to developing the algebraic conditions, these questions are addressed in a more abstract manner on a nonlinear system.

The actions of a controller are transient, or implicitly time dependent, as it transfers the closed loop system from one state to another. As the target state is achieved, in the limit the controlled states go to their commanded values and the only nonconstant dynamics left are the internal dynamic states. So as $t \to \infty$, the internal dynamics go from being, implicitly through control action, a nonautonomous system to an autonomous one, all control action has stopped. Mathematically, the autonomous system $\dot{x} = f(x)$ is called a limiting system of $\dot{x} = f(x,t)$ [48]. The idea behind limiting systems is to use asymptotic behavior of the time-dependent function $f(x,t)$ in the investigation of the asymptotic behavior of solutions of $\dot{x} = f(x,t)$. Specifically, the idea is used extensively in the study of asymptotically autonomous case, *i.e.*, $\dot{x} = f(x) + g(x,t)$ where the perturbation $g(x,t) \to 0$ as $t \to \infty$. Intuitively the limiting behavior of the time-dependent law is portrayed by the time-independent equation $\dot{x} = f(x)$. It can be said that the latter is a limiting equation of $\dot{x} = f(x) + g(x,t)$, and in fact it is the limiting equation since a unique equation exists in this case.

To summarize, the steps that will be taken to show closed loop system stability are as follows. The determination of stability of an n-dimensional system is reduced to that of a two-dimensional nonautonomous one via a dynamic inversion controller. The nonautonomous system is then reduced to its autonomous limiting system and the stability of the limiting system is established. The stability of the autonomous system is shown in two steps that produce vehicle specific conditions. The first step establishes the boundedness of the solution using the Lyapunov argument. Then given that the limiting system is two-dimensional with a solution that is bounded and unique, the solution must be either an equilibrium or a limit cycle. A vehicle specific condition is then established to eliminate the possibility of the limit cycle.

The following gives the requirements for showing stability, as outlined above, on a nonlinear system in the abstract. Consider a nonlinear system $\dot{x} = f(x) + g(x)u$ with a closed loop dynamic inversion controller that decomposes a closed loop system into $n-2$ integrators that are made stable by the desired dynamics and internal dynamics that can be written as

$$\dot{x}_i = f(x_i) + \hat{g}(x_c, \hat{x}_c, \dot{x}_{des}, t), \qquad x_i \in Q \subset \mathbf{R}^2, \quad x_c, \hat{x}_c, \dot{x}_{des} \in \mathbf{R}^{n-2} \tag{6.4}$$

where Q is an open set in $\mathbf{R}^2$, (x_i, x_c) are internal and controlled states respectively, and $(\hat{x}_c, \dot{x}_{des})$ are dynamic inversion controller states. The stability of the closed loop system will depend on stability of (6.4). If the dynamic system (6.4) has the following property - $\hat{g}(x_c, \hat{x}_c, \dot{x}_{des}, t) \to 0$ as $t \to \infty$, then its limiting system is described by the autonomous system

$$\dot{x}_i = f(x_i) \tag{6.5}$$

(see Reference 48, pages 57-62.) Furthermore, assume that $x(t)$, a solution of (6.4), is bounded and a solution $\overline{x}_i$ of (6.5) is a unique point, then the autonomous limiting system (6.5) can be used to establish the global stability result for the original closed loop system. Provided the solutions to both (6.4) and (6.5) satisfy the stated conditions, the global stability of the closed loop system can be established, as will be shown later in the chapter. The stated characteristics on the solutions are converted into algebraic conditions that will provide a test to determine whether the autonomous two-dimensional nonlinear system is globally stable. These conditions are vehicle dependent and so it makes sense to introduce aircraft equations of motion and to show how the closed loop dynamics are reduced to an autonomous system by the dynamic inversion controller. After determining the algebraic expressions for the abstract conditions on the solutions of (6.4) and (6.5), the global stability of the closed loop system is going to be presented.

6.3 System Equations of Motion

The system equations of motion used in the analysis are a modified version of (3.6) presented in Chapter 3. The modification involves limiting the number of flexible modes to one and using two-surface control effectors as described in the actual controller design in Chapter 5. Hence, the simplified longitudinal equations of motion are given below.

$$
\begin{bmatrix} \dot{u} \\ \dot{w} \\ \dot{q} \\ \dot{\theta} \\ \ddot{\eta} \\ \dot{\eta} \end{bmatrix} = \begin{pmatrix} -qw \\ qu \\ 0 \\ q \\ 0 \\ \dot{\eta} \end{pmatrix} + \begin{pmatrix} -g\sin\theta \\ g\cos\theta \\ 0 \\ 0 \\ 0 \\ 0 \end{pmatrix} + \begin{pmatrix} T/\mathrm{m} \\ 0 \\ 0 \\ 0 \\ 0 \\ 0 \end{pmatrix} + \frac{1}{2}\rho SV^2 \left\{ \begin{pmatrix} C_x(\alpha,M)/\mathrm{m} \\ C_z(\alpha,M)/\mathrm{m} \\ \bar{c}C_M(\alpha,M)/I_y \\ 0 \\ 0 \\ 0 \end{pmatrix} \right.
$$

$$
+ \begin{pmatrix} 0 \\ C_{z,\eta}(\alpha,M,GW^*)/\mathrm{m} \\ \bar{c}C_{M,\eta}(\alpha,M,GW^*)/I_y \\ 0 \\ \bar{q}C_{\eta\eta}(M,GW^*)/m_\eta \\ 0 \end{pmatrix} \eta + \begin{pmatrix} 0 \\ C_{z,\dot{\eta}}(\alpha,M,GW^*)/\mathrm{m} \\ \bar{c}C_{M,\dot{\eta}}(\alpha,M,GW^*)/I_y \\ 0 \\ \bar{q}C_{\eta\dot{\eta}}(M,GW^*)/m_\eta \\ 0 \end{pmatrix} \dot{\eta}
$$

$$
+ \frac{1}{m_\eta} \begin{pmatrix} 0 \\ 0 \\ 0 \\ 0 \\ C_{\eta u}(M,GW^*)u + C_{\eta w}(M,GW^*)w + C_{\eta q}(M,GW^*)q \\ 0 \end{pmatrix}
$$

$$
\left. + \begin{pmatrix} C_{x,\delta 1}(\alpha,M,GW^*)/\mathrm{m} \\ C_{z,\delta 1}(\alpha,M,GW^*)/\mathrm{m} \\ \bar{c}C_{M,\delta 1}(\alpha,M,GW^*)/I_y \\ 0 \\ C_{\eta\delta 1}(M,GW^*)/m_\eta \\ 0 \end{pmatrix} \delta_1 + \begin{pmatrix} 0 \\ C_{z,\delta 2}(\alpha,M,GW^*)/\mathrm{m} \\ \bar{c}C_{M,\delta 2}(\alpha,M,GW^*)/I_y \\ 0 \\ C_{\eta\delta 2}(M,GW^*)/m_\eta \\ 0 \end{pmatrix} \delta_2 \right\} \tag{6.6}
$$

where

m = vehicle mass, m_η = generalized mass associated with an elastic mode

GW^* = mass distibution, T = thrust, M = Mach number, V = speed

$\bar{c}$ = mean aerodynamic cord, S = planform area, $\bar{q}$ = dynamic pressure, ρ = density

The notation in the last equation, where $\dot{\eta} = \dot{\eta}$, may cause some confusion. Thus, please note that $\dot{\eta}$ on the left hand side of (6.6) is the time rate of change of the flexible deformation state η, while $\dot{\eta}$ on the right hand side is the flexible mode velocity state.

The system under investigation is considered to have two control surfaces as described in Chapter 5 in addition to a low-bandwidth control of thrust. Though not explicitly written as a control mass distribution, *GW** can certainly be considered one. The *GW** can be changed by shifting fuel around the vehicle as is done in the Concorde.

The intent is to explore the stability of aircraft undergoing rapid maneuvering, which implies that the behavior of the fast states and parameters affecting them is of primary concern. Also, this allows for a large time scale separation between the surfaces, slower changing thrust *T*, and still slower movement of c.g. through mass distribution *GW**. Moreover, such time scale separation allows the treatment of thrust as well as the parametric dependence on *GW** to be considered constant, which becomes advantageous in analysis as shown below. And as previously mentioned, the coefficient dependence on the Mach number can be legitimately dropped in the subsonic regime.

6.4 Equilibrium Set

The equilibrium and the associated equations for the system described by (6.6) are developed in this section. But first a more general approach to the equilibrium state is taken. Consider system equations of the form

$$\dot{x} = f(x,u) \tag{6.7}$$

where *x* is a vector in $\mathbf{R}^n$ and *u* is a vector in $\mathbf{R}^m$. Let $\bar{U}$ denote a set of allowed control values in $\mathbf{R}^m$. Define the equilibrium set

$$\bar{M} = \left\{ (x,u) \mid f(x,u) = 0,\ u \in \bar{U} \right\} \tag{6.8}$$

Projecting $\bar{M}$ onto the first factor *x* results in *M*, the set of equilibrium states for some δ

$$M = \left\{ x \mid f(x,\delta) = 0,\ \delta \in \bar{U} \right\} \tag{6.9}$$

Note that $\bar{M}$ and *M* depend on the specified control limits.

The equilibrium set of a system with m inputs is typically m-dimensional. The system modeled by (6.6) has four inputs $(T, GW^*, \delta_1, \delta_2)$ and its equilibrium set *M* is four-dimensional. The equilibrium set defined in (6.8) for equations of motion in (6.6) is simply an aircraft in steady state, straight, wings-level flight. Equilibrium in a more general dynamical sense corresponds to an equilibrium of all the external forces, *i.e.*, a state of zero acceleration $(\dot{u}, \dot{w}, \dot{q}) = \mathbf{0}$. Furthermore, in the aerodynamic steady state, the

Euler angle θ must be constant in addition to (u, w) being constant. From flexible mode dynamics, steady state implies that $(\ddot{\eta}, \dot{\eta}) = \mathbf{0}$. This leaves four states, (u, w, θ, η), with nontrivial solution on the equilibrium state manifold *M*. At equilibrium, the control surface deflections are determined by the need to balance the gravity and aerodynamic forces and moments. In particular, the need for the attitude dynamics to remain constant, *i.e.,* $(\dot{\theta}, \dot{q}, q) = \mathbf{0}$, defines the values the control deflections must assume in terms of the total pitching moment. Examining the equilibrium equations of motion (6.10) the controls (δ_1, δ_2) can be eliminated as follows.

$$\begin{bmatrix} 0 \\ 0 \\ 0 \\ 0 \\ 0 \\ 0 \end{bmatrix} = \begin{pmatrix} -g\sin\theta \\ g\cos\theta \\ 0 \\ 0 \\ 0 \\ 0 \end{pmatrix} + \begin{pmatrix} T/\mathrm{m} \\ 0 \\ 0 \\ 0 \\ 0 \\ 0 \end{pmatrix} + \frac{1}{2}\rho S V^2 \left\{ \begin{pmatrix} C_x(\alpha)/\mathrm{m} \\ C_z(\alpha)/\mathrm{m} \\ \bar{c}C_M(\alpha)/I_y \\ 0 \\ 0 \\ 0 \end{pmatrix} + \begin{pmatrix} 0 \\ C_{z,\eta}(\alpha, GW^*)/\mathrm{m} \\ \bar{c}C_{M,\eta}(\alpha, GW^*)/I_y \\ 0 \\ \bar{q}C_{\eta\eta}(GW^*)/m_\eta \\ 0 \end{pmatrix} \eta \right.$$

$$+ \begin{pmatrix} 0 \\ 0 \\ 0 \\ 0 \\ \dfrac{C_{\eta u}(GW^*)u}{m_\eta} + \dfrac{C_{\eta w}(GW^*)w}{m_\eta} \\ 0 \end{pmatrix} + \begin{pmatrix} \dfrac{C_{x,\delta 1}(\alpha, GW^*)}{\mathrm{m}} \\ \dfrac{C_{z,\delta 1}(\alpha, GW^*)}{\mathrm{m}} \\ \dfrac{\bar{c}C_{M,\delta 1}(\alpha, GW^*)}{I_y} \\ 0 \\ \dfrac{C_{\eta\delta 1}(GW^*)}{m_\eta} \\ 0 \end{pmatrix} \delta_1 + \left. \begin{pmatrix} 0 \\ \dfrac{C_{z,\delta 2}(\alpha, GW^*)}{\mathrm{m}} \\ \dfrac{\bar{c}C_{M,\delta 2}(\alpha, GW^*)}{I_y} \\ 0 \\ \dfrac{C_{\eta\delta 2}(GW^*)}{m_\eta} \\ 0 \end{pmatrix} \delta_2 \right\} \quad (6.10)$$

Solving the pitching moment and the flexible dynamics equations for the controls

$$\begin{bmatrix}0\\0\end{bmatrix}=\frac{1}{2}\rho SV^2\left\{\begin{pmatrix}\bar{c}C_M(\alpha)/I_y\\0\end{pmatrix}+\begin{pmatrix}\bar{c}C_{M,\eta}(\alpha,GW^*)/I_y\\\bar{q}C_{\eta\eta}(GW^*)/m_\eta\end{pmatrix}\eta\right.$$
$$+\frac{1}{m_\eta}\begin{pmatrix}0\\C_{\eta u}(GW^*)u+C_{\eta w}(GW^*)w\end{pmatrix} \qquad (6.11)$$
$$\left.+\begin{pmatrix}\bar{c}C_{M,\delta1}(\alpha,GW^*)/I_y\\C_{\eta\delta1}(GW^*)/m_\eta\end{pmatrix}\delta_1+\begin{pmatrix}\bar{c}C_{M,\delta2}(\alpha,GW^*)/I_y\\C_{\eta\delta2}(GW^*)/m_\eta\end{pmatrix}\delta_2\right\}$$

results in the following relation

$$\begin{bmatrix}\bar{\delta}_1\\\bar{\delta}_2\end{bmatrix}=\frac{-m_\eta I_y}{\bar{c}}\frac{1}{C_{M,\delta1}(\alpha)C_{\eta\delta2}-C_{\eta\delta1}C_{M,\delta2}(\alpha)}\begin{bmatrix}C_{\eta\delta2}/m_\eta & -\bar{c}C_{M,\delta2}(\alpha)/I_y\\-C_{\eta\delta1}/m_\eta & \bar{c}C_{M,\delta1}(\alpha)/I_y\end{bmatrix} \qquad (6.12)$$
$$\begin{bmatrix}\left(C_M(\alpha)+C_{M,\eta}(\alpha)\eta\right)\bar{c}/I_y\\\left(\bar{q}C_{\eta\eta}\eta+C_{\eta u}u+C_{\eta w}w\right)/m_\eta\end{bmatrix}$$

Substituting for the controls in (6.10) and simplifying gives

$$\begin{pmatrix} g\sin\theta - \dfrac{T}{\mathrm{m}} \\ -g\cos\theta \\ 0 \\ 0 \end{pmatrix} = \frac{1}{2}\rho SV^2 \left\{ \begin{pmatrix} \dfrac{C_x(\alpha)}{\mathrm{m}} \\ \dfrac{C_z(\alpha)}{\mathrm{m}} \\ \dfrac{\bar{c}C_M(\alpha)}{I_y} \\ 0 \end{pmatrix} + \begin{pmatrix} 0 \\ 0 \\ 0 \\ \dfrac{C_{\eta u}u + C_{\eta w}w}{m_\eta} \end{pmatrix} + \begin{pmatrix} 0 \\ \dfrac{C_{z,\eta}(\alpha)}{\mathrm{m}} \\ \dfrac{\bar{c}C_{M,\eta}(\alpha)}{I_y} \\ \dfrac{\bar{q}C_{\eta\eta}}{m_\eta} \end{pmatrix} \eta \right\}$$

$$-\frac{1}{2}\rho SV^2 \frac{m_\eta I_y}{\bar{c}} \frac{1}{C_{M,\delta 1}(\alpha)C_{\eta\delta 2} - C_{\eta\delta 1}C_{M,\delta 2}(\alpha)}$$

$$\begin{bmatrix} \dfrac{C_{x,\delta 1}(\alpha)C_{\eta\delta 2}}{\mathrm{m}m_\eta} & \dfrac{-\bar{c}C_{x,\delta 1}(\alpha)C_{M,\delta 2}(\alpha)}{\mathrm{m}I_y} \\ \dfrac{C_{z,\delta 1}(\alpha)C_{\eta\delta 2} - C_{z,\delta 2}(\alpha)C_{\eta\delta 1}}{\mathrm{m}m_\eta} & \dfrac{\bar{c}\left(C_{z,\delta 2}(\alpha)C_{M,\delta 1}(\alpha) - C_{z,\delta 1}(\alpha)C_{M,\delta 2}(\alpha)\right)}{\mathrm{m}I_y} \\ \dfrac{\bar{c}\left(C_{M,\delta 1}(\alpha)C_{\eta\delta 2} - C_{\eta\delta 1}C_{M,\delta 2}(\alpha)\right)}{m_\eta I_y} & 0 \\ 0 & \dfrac{\bar{c}\left(-C_{\eta\delta 1}C_{M,\delta 2}(\alpha) + C_{M,\delta 1}(\alpha)C_{\eta\delta 2}\right)}{m_\eta I_y} \end{bmatrix} \quad (6.13)$$

$$\begin{bmatrix} \left(C_M(\alpha) + C_{M,\eta}(\alpha)\eta\right)\bar{c}/I_y \\ \left(-\dfrac{2}{\rho SV^2}\omega^2\eta + \bar{q}C_{\eta\eta}\eta + C_{\eta u}u + C_{\eta w}w\right)/m_\eta \end{bmatrix}$$

which reduces to the following

$$\begin{pmatrix} \mathrm{m}g\sin\theta - T \\ -\mathrm{m}g\cos\theta \end{pmatrix} =$$

$$\frac{\rho SV^2}{2}\begin{pmatrix} C_x(\alpha) - \dfrac{C_{x,\delta 1}(\alpha)C_{\eta\delta 2}}{C_{M,\delta 1}(\alpha)C_{\eta\delta 2} - C_{\eta\delta 1}C_{M,\delta 2}(\alpha)}\left(C_M(\alpha) + C_{M,\eta}(\alpha)\eta\right) \\ C_z(\alpha) + C_{z,\eta}(\alpha)\eta - \dfrac{C_{z,\delta 1}(\alpha)C_{\eta\delta 2} - C_{z,\delta 2}(\alpha)C_{\eta\delta 1}}{C_{M,\delta 1}(\alpha)C_{\eta\delta 2} - C_{\eta\delta 1}C_{M,\delta 2}(\alpha)}\left(C_M(\alpha) + C_{M,\eta}(\alpha)\eta\right) \end{pmatrix} \quad (6.14)$$

$$+\frac{1}{2}\rho SV^2\begin{pmatrix} \dfrac{C_{x,\delta 1}(\alpha)C_{M,\delta 2}(\alpha)}{C_{M,\delta 1}(\alpha)C_{\eta\delta 2} - C_{\eta\delta 1}C_{M,\delta 2}(\alpha)}\left(\bar{q}C_{\eta\eta}\eta + C_{\eta u}u + C_{\eta w}w\right) \\ \dfrac{C_{z,\delta 1}(\alpha)C_{M,\delta 2}(\alpha) - C_{z,\delta 2}(\alpha)C_{M,\delta 1}(\alpha)}{C_{M,\delta 1}(\alpha)C_{\eta\delta 2} - C_{\eta\delta 1}C_{M,\delta 2}(\alpha)}\left(\bar{q}C_{\eta\eta}\eta + C_{\eta u}u + C_{\eta w}w\right) \end{pmatrix}$$

The equations in (6.14) govern the behavior of states on the equilibrium manifold defined in (6.10). These contain four states (u, w, θ, η) and two slow controls (T, GW^*). Since the manifold is four-dimensional, if four of the variables are chosen as coordinates, the behavior of the other two would be prescribed without a need for a specific solution if such a solution exists for the chosen values of the prescribed variables. In other words, if $(T_o, GW_o^*, \theta_o, \eta_o)$ are chosen as coordinates on *M*, then (u, w) are completely specified and define the rest of the equilibrium. The variables chosen as coordinates are a mixture of slow controls and position states, while surface positions have been determined by the restriction on the pitching moment they produce such that $q = 0$. The forces of thrust and gravity must be balanced by the aerodynamic forces and moments. Hence, for a given (T_o, θ_o), a solution to (6.14) exists wherever the aerodynamic coefficients, $C_{(\cdot)}(\alpha)$, are continuous and a (u, w) pair (or equivalently (V, α)) required to produce the equilibrium balance between competing forces is achievable. Both of these conditions are vehicle dependent and, in practice must be checked against the aerodynamic database and the flight envelope restrictions on (V, α).

In addition, the equilibrium equations (6.14) also allow for a natural separation of dynamics due to rigid body and elastic interactions. The equilibrium aerodynamic functions introduced are required to maintain equilibrium state and have direct connection to the aerodynamic forces in the limiting equations that govern dynamic behavior.

Definition: For a system represented by equation (6.14), the equilibrium aerodynamic functions due to rigid body effects are $\bar{C}_x(\alpha)$ and $\bar{C}_z(\alpha)$ defined by

$$\begin{pmatrix} \bar{C}_x(\alpha) \\ \bar{C}_z(\alpha) \end{pmatrix} = \begin{pmatrix} C_x(\alpha) - \dfrac{C_{x,\delta 1}(\alpha) C_{\eta \delta 2}}{C_{M,\delta 1}(\alpha) C_{\eta \delta 2} - C_{\eta \delta 1} C_{M,\delta 2}(\alpha)} C_M(\alpha) \\ C_z(\alpha) - \dfrac{C_{z,\delta 1}(\alpha) C_{\eta \delta 2} - C_{z,\delta 2}(\alpha) C_{\eta \delta 1}}{C_{M,\delta 1}(\alpha) C_{\eta \delta 2} - C_{\eta \delta 1} C_{M,\delta 2}(\alpha)} C_M(\alpha) \end{pmatrix}, \tag{6.15}$$

the equilibrium aerodynamic functions due to the rigid body effects on the elastic dynamics and control cross-coupling are $\bar{C}_x^{re}(\alpha)$ and $\bar{C}_z^{re}(\alpha)$ defined by

$$\begin{pmatrix} \bar{C}_x^{re}(\alpha) \\ \bar{C}_z^{re}(\alpha) \end{pmatrix} = \begin{pmatrix} \dfrac{C_{x,\delta 1}(\alpha) C_{M,\delta 2}(\alpha)}{C_{M,\delta 1}(\alpha) C_{\eta \delta 2} - C_{\eta \delta 1} C_{M,\delta 2}(\alpha)} \\ \dfrac{C_{z,\delta 1}(\alpha) C_{M,\delta 2}(\alpha) - C_{z,\delta 2}(\alpha) C_{M,\delta 1}(\alpha)}{C_{M,\delta 1}(\alpha) C_{\eta \delta 2} - C_{\eta \delta 1} C_{M,\delta 2}(\alpha)} \end{pmatrix} \left(C_{\eta u} \cos\alpha + C_{\eta w} \sin\alpha \right). \tag{6.16}$$

where $u = V\cos\alpha$ and $w = V\sin\alpha$, the equilibrium aerodynamic functions due to control cross coupling with the elastic dynamics are $\bar{C}_x^e(\alpha)$ and $\bar{C}_z^e(\alpha)$ defined by

$$\begin{pmatrix} \bar{C}_x^e(\alpha) \\ \bar{C}_z^e(\alpha) \end{pmatrix} = \begin{pmatrix} \dfrac{C_{x,\delta_1}(\alpha)}{C_{M,\delta_1}(\alpha) C_{\eta,\delta_2} - C_{\eta,\delta_1} C_{M,\delta_2}(\alpha)} \left(-C_{\eta,\delta_2} C_{M,\eta}(\alpha) + C_{M,\delta_2}(\alpha) \bar{q} C_{\eta\eta} \right) \\ C_{z,\eta}(\alpha) - \dfrac{C_{z,\delta_1}(\alpha) C_{\eta\delta_2} - C_{z,\delta_2}(\alpha) C_{\eta\delta_1}}{C_{M,\delta_1}(\alpha) C_{\eta,\delta_2} - C_{\eta,\delta_1} C_{M,\delta_2}(\alpha)} C_{M,\eta}(\alpha) \\ + \dfrac{C_{z,\delta_1}(\alpha) C_{M,\delta_2}(\alpha) - C_{z,\delta_2}(\alpha) C_{M,\delta_1}(\alpha)}{C_{M,\delta_1}(\alpha) C_{\eta,\delta_2} - C_{\eta,\delta_1} C_{M,\delta_2}(\alpha)} \bar{q} C_{\eta\eta} \end{pmatrix} \tag{6.17}$$

Hence the equilibrium aerodynamic force vector on the *M* manifold at any equilibrium state is

$$\begin{pmatrix} \bar{F}_x(u,w) + \bar{F}_x^{re}(u,w) + \bar{F}_x^e(u,w,\eta) \\ \bar{F}_z(u,w) + \bar{F}_z^{re}(u,w) + \bar{F}_z^e(u,w,\eta) \end{pmatrix} = \frac{1}{2}\rho V^2 S \begin{pmatrix} \bar{C}_x(\alpha) + \bar{C}_x^{re}(\alpha)V + \bar{C}_x^e(\alpha)\eta \\ \bar{C}_z(\alpha) + \bar{C}_z^{re}(\alpha)V + \bar{C}_z^e(\alpha)\eta \end{pmatrix}. \tag{6.18}$$

Under practical circumstances, an aircraft has a given flight envelope outside of which stability cannot be guaranteed or expected. This suggests dividing the analysis into two cases.

Assume unlimited control authority and work globally, or

Restrict analysis to a subset of states with adequate control authority.

The analysis of a global case does not require any specific numerical data unlike case two where specifics about the available control power must be available; hence, the initial analysis involves the global case only. The restriction on control authority simply confines the global results to a subset.

The equilibrium equations (6.14) are restated in terms of the equilibrium aerodynamic coefficients

$$\begin{pmatrix} 0 \\ 0 \end{pmatrix} = \begin{pmatrix} \mathrm{m}g\sin\theta_o - T_o \\ -\mathrm{m}g\cos\theta_o \end{pmatrix} + \frac{1}{2}\rho S V^2 \begin{pmatrix} \bar{C}_x(\alpha) + \bar{C}_x^{re}(\alpha)V + \bar{C}_x^{e}(\alpha)\eta_o \\ \bar{C}_z(\alpha) + \bar{C}_z^{re}(\alpha)V + \bar{C}_z^{e}(\alpha)\eta_o \end{pmatrix} \tag{6.19}$$

where $(T_o, GW_o^*, \theta_o, \eta_o)$ are parameters and $(\mathrm{m}, S, \rho, \omega, \mathrm{g})$ are fixed constants. Since $(T_o, GW_o^*, \theta_o, \eta_o)$ are chosen parameters, the remaining variables are (V, α). Since (V, α) are the wind axis or polar coordinate representation of the velocity components (u, w), and as previously mentioned, with $(T_o, GW_o^*, \theta_o, \eta_o)$ chosen, the (u, w) behavior is completely specified and defines the rest of the equilibrium. Then the solution (V, α) verifying (6.19) will completely define the equilibrium. The existence of such a solution, as mentioned above, depends on the continuous nature of the aerodynamic coefficients in the region where a specific (V, α) is required to balance the forces produced by $(T_o, GW_o^*, \theta_o, \eta_o)$.

6.1 Remark: For a given $(T_o, GW_o^*, \theta_o, \eta_o)$, the equilibrium of system (6.6) is formed by all points

$$(u, w, q, \theta, \eta, \dot{\eta}) = (\bar{u}, \bar{w}, 0, \theta_o, \eta_o, 0)$$

where

$$\bar{u} = \bar{V}\cos\bar{\alpha}, \quad \bar{w} = \bar{V}\sin\bar{\alpha},$$

and $(\bar{V}, \bar{\alpha})$ is a solution of (6.19) corresponding to the given $(T_o, GW_o^*, \theta_o, \eta_o)$. Thus, given $(T_o, GW_o^*, \theta_o, \eta_o)$ if (6.19) has a unique solution, then the system represented by (6.6) has a unique equilibrium point.

There are two parameters to consider when discussing the uniqueness of solution of (6.19) – thrust T and pitch attitude θ. For a fixed T_o, $\bar{V}$ is fixed and α becomes a function of θ_o. Recall the relationship $\theta = \alpha + \gamma$, where γ is flight path angle. Hence, for a given T_o, α is a single valued function of θ on some interval(s) and a multi value function on others. Typically, the multiple values occur for higher values of θ where the longitudinal and lateral-directional coupling becomes pronounced. Where these regions occur depends on the aerodynamic and structural characteristics of a specific aircraft; no generalization is available in literature.

6.5 Dynamic Inversion

The algebraic equations required to obtain system equilibrium independent of the control design have been established. Now a dynamic inversion controller to achieve a given equilibrium state is introduced. The control problem in general can be stated as follows:

Problem Statement: Given an equilibrium state $\bar{x}$, determine a controller $u = K(x, \bar{x})$ so that $\bar{x}$ is a global attractor for the system

$$\dot{x} = f\left(x, K\left(x, \bar{x}\right)\right) \tag{6.20}$$

Any global attractor must be an equilibrium state. Using dynamic inversion this problem is addressed for vehicle models having a unique equilibrium point for appropriately chosen engine thrust *T* and mass distribution *GW**.

The approach is to invert the rotational dynamics to a stable set of desired dynamics. Since the throttle is typically a low-bandwidth control that is not changed during dynamic maneuvers, it is left fixed throughout the construction of the controller K and the analysis.

The philosophy behind the control law is for the vehicle to follow the pitch rate commands and, for the purpose of this analysis, to directly control the elastic modes. The structure of the dynamic inversion controller K is given by the following expression

$$\begin{pmatrix} \dot{q} \\ \ddot{\eta} \end{pmatrix}^{des} = \begin{bmatrix} K1 & 0 \\ 0 & K3 \end{bmatrix} \begin{pmatrix} q_{cmd} - q \\ \Delta\phi' \left(\dot{\eta}_{cmd} - \dot{\eta} \right) \end{pmatrix} + \begin{bmatrix} K2 & 0 \\ 0 & K4 \end{bmatrix} \begin{pmatrix} \theta_{cmd} - \theta \\ \Delta\phi' \left(\eta_{cmd} - \eta \right) \end{pmatrix} \tag{6.21}$$

The desired dynamics are realized if the control surfaces conform to the following expression in the closed loop

$$\begin{bmatrix} \delta_1 \\ \delta_2 \end{bmatrix} = \frac{m_\eta I_y}{\bar{c}} \frac{1}{C_{M,\delta 1}(\alpha) C_{\eta \delta 2} - C_{\eta \delta 1} C_{M,\delta 2}(\alpha)} \begin{bmatrix} C_{\eta \delta 2} / m_\eta & -\bar{c} C_{M,\delta 2}(\alpha) / I_y \\ -C_{\eta \delta 1} / m_\eta & \bar{c} C_{M,\delta 1}(\alpha) / I_y \end{bmatrix}$$
$$\left\{ \frac{2}{\rho S V^2} \begin{pmatrix} \dot{q}^{des} \\ \ddot{\eta}^{des} \end{pmatrix} - \begin{bmatrix} \bar{c} \left(C_M(\alpha) + C_{M,\eta}(\alpha) \eta + C_{M,\dot{\eta}}(\alpha) \dot{\eta} \right) / I_y \\ \frac{1}{m_\eta} \left(\bar{q} C_{\eta\eta} \eta + \bar{q} C_{\eta\dot{\eta}} \dot{\eta} + C_{\eta u} u + C_{\eta w} w + C_{\eta q} q \right) \end{bmatrix} \right\} \tag{6.22}$$

Substituting the expression for controls (6.22) into the system equations (6.6) results in a closed loop system that readily separates into the following two subsystems. The controlled variables q and $\dot{\eta}$ and their associated equation give

$$\begin{pmatrix}\dot{q}\\ \dot{\theta}\\ \ddot{\eta}\\ \dot{\eta}\end{pmatrix} = \frac{1}{2}\rho SV^2 \left\{ \begin{pmatrix} \frac{\bar{c}C_M(\alpha)}{I_y} \\ 0 \\ 0 \\ 0 \end{pmatrix} + \begin{pmatrix} \frac{\bar{c}C_{M,\eta}(\alpha)}{I_y} \\ 0 \\ \frac{\bar{q}C_{\eta\eta}}{m_\eta} \\ 0 \end{pmatrix} \eta + \begin{pmatrix} \frac{\bar{c}C_{M,\dot{\eta}}(\alpha)}{I_y} \\ 0 \\ \frac{\bar{q}C_{\eta\dot{\eta}}}{m_\eta} \\ 0 \end{pmatrix} \dot{\eta} \right\} + \frac{1}{m_\eta} \begin{pmatrix} 0 \\ 0 \\ C_{\eta u}u + C_{\eta w}w + C_{\eta q}q \\ 0 \end{pmatrix}$$

$$-\frac{1}{2}\rho SV^2 \left\{ \begin{pmatrix} \frac{\bar{c}C_M(\alpha)}{I_y} \\ 0 \\ 0 \\ 0 \end{pmatrix} + \begin{pmatrix} \frac{\bar{c}C_{M,\eta}(\alpha)}{I_y} \\ 0 \\ \frac{\bar{q}C_{\eta\eta}}{m_\eta} \\ 0 \end{pmatrix} \eta + \begin{pmatrix} \frac{\bar{c}C_{M,\dot{\eta}}(\alpha)}{I_y} \\ 0 \\ \frac{\bar{q}C_{\eta\dot{\eta}}}{m_\eta} \\ 0 \end{pmatrix} \dot{\eta} \right\} + \begin{pmatrix} \dot{q}^{des} \\ 0 \\ \ddot{\eta}^{des} \\ 0 \end{pmatrix} + \frac{1}{m_\eta} \begin{pmatrix} 0 \\ 0 \\ C_{\eta u}u + C_{\eta w}w + C_{\eta q}q \\ 0 \end{pmatrix} \quad (6.23)$$

$$\begin{pmatrix}\dot{q}\\ \dot{\theta}\\ \ddot{\eta}\\ \dot{\eta}\end{pmatrix} = \begin{pmatrix}\dot{q}^{des}\\ q\\ \ddot{\eta}^{des}\\ \dot{\eta}\end{pmatrix}$$

$$= \begin{bmatrix} -K1 & -K2 & 0 & 0 \\ 1 & 0 & 0 & 0 \\ 0 & 0 & -\Delta\phi' K3 & -\Delta\phi' K4 \\ 0 & 0 & 1 & 0 \end{bmatrix} \begin{pmatrix} q \\ \theta \\ \dot{\eta} \\ \eta \end{pmatrix} + \begin{bmatrix} K1 & K2 & 0 & 0 \\ 0 & 0 & 0 & 0 \\ 0 & 0 & \Delta\phi' K3 & \Delta\phi' K4 \\ 0 & 0 & 0 & 0 \end{bmatrix} \begin{pmatrix} q_{cmd} \\ \theta_{cmd} \\ \dot{\eta}_{cmd} \\ \eta_{cmd} \end{pmatrix}$$

These equations are linear and decoupled from the *u*-*w* dynamics. The remaining dynamics of the *u*-*w* subsystem result in

$$\begin{pmatrix}\dot{u}\\ \dot{w}\end{pmatrix}=\begin{pmatrix}-qw\\ qu\end{pmatrix}+\begin{pmatrix}-g\sin\theta+\dfrac{T}{\mathrm{m}}\\ g\cos\theta\end{pmatrix}$$

$$+\frac{\rho SV^2}{2\mathrm{m}}\left\{\begin{pmatrix}C_x(\alpha)-\dfrac{C_{x,\delta1}(\alpha)C_{\eta\delta2}}{C_{M,\delta1}(\alpha)C_{\eta\delta2}-C_{\eta\delta1}C_{M,\delta2}(\alpha)}\left(C_M(\alpha)+C_{M,\eta}(\alpha)\eta+C_{M,\dot{\eta}}(\alpha)\dot{\eta}\right)\\ C_z(\alpha)+C_{z,\eta}(\alpha)\eta+C_{z,\dot{\eta}}(\alpha)\dot{\eta}\\ -\dfrac{C_{z,\delta1}(\alpha)C_{\eta\delta2}-C_{z,\delta2}(\alpha)C_{\eta\delta1}}{C_{M,\delta1}(\alpha)C_{\eta\delta2}-C_{\eta\delta1}C_{M,\delta2}(\alpha)}\left(C_M(\alpha)+C_{M,\eta}(\alpha)\eta+C_{M,\dot{\eta}}(\alpha)\dot{\eta}\right)\end{pmatrix}\right.$$

$$\left.+\begin{pmatrix}\dfrac{C_{x,\delta1}(\alpha)C_{M,\delta2}(\alpha)}{C_{M,\delta1}(\alpha)C_{\eta\delta2}-C_{\eta\delta1}C_{M,\delta2}(\alpha)}\left(\bar{q}C_{\eta\eta}\eta+\bar{q}C_{\eta\dot{\eta}}\dot{\eta}+C_{\eta u}u+C_{\eta w}w+C_{\eta q}q\right)\\ \dfrac{C_{z,\delta1}(\alpha)C_{M,\delta2}(\alpha)-C_{z,\delta2}(\alpha)C_{M,\delta1}(\alpha)}{C_{M,\delta1}(\alpha)C_{\eta\delta2}-C_{\eta\delta1}C_{M,\delta2}(\alpha)}\left(\bar{q}C_{\eta\eta}\eta+\bar{q}C_{\eta\dot{\eta}}\dot{\eta}+C_{\eta u}u+C_{\eta w}w+C_{\eta q}q\right)\end{pmatrix}\right\}$$

$$+\begin{bmatrix}\dfrac{I_yC_{x,\delta1}(\alpha)C_{\eta\delta2}}{\mathrm{m}\bar{c}\left(C_{M,\delta1}(\alpha)C_{\eta\delta2}-C_{\eta\delta1}C_{M,\delta2}(\alpha)\right)} & \dfrac{m_\eta}{\mathrm{m}}\dfrac{-C_{x,\delta1}(\alpha)C_{M,\delta2}(\alpha)}{\left(C_{M,\delta1}(\alpha)C_{\eta\delta2}-C_{\eta\delta1}C_{M,\delta2}(\alpha)\right)}\\ \dfrac{I_y\left(C_{z,\delta1}(\alpha)C_{\eta\delta2}-C_{z,\delta2}(\alpha)C_{\eta\delta1}\right)}{\mathrm{m}\bar{c}\left(C_{M,\delta1}(\alpha)C_{\eta\delta2}-C_{\eta\delta1}C_{M,\delta2}(\alpha)\right)} & \dfrac{m_\eta\left(-C_{z,\delta1}C_{M,\delta2}+C_{z,\delta2}C_{M,\delta1}\right)(\alpha)}{\mathrm{m}\left(C_{M,\delta1}(\alpha)C_{\eta\delta2}-C_{\eta\delta1}C_{M,\delta2}(\alpha)\right)}\end{bmatrix}\begin{pmatrix}\dot{q}^{des}\\ \ddot{\eta}^{des}\end{pmatrix}$$

Substituting the equilibrium aerodynamic functions to simplify the expression results in

$$\begin{pmatrix}\dot{u}\\ \dot{w}\end{pmatrix}=\begin{pmatrix}-qw\\ qu\end{pmatrix}+\begin{pmatrix}-g\sin\theta+T/\mathrm{m}\\ g\cos\theta\end{pmatrix}+\frac{\rho SV^2}{2\mathrm{m}}\left\{\begin{pmatrix}\bar{C}_x(\cdot)\\ \bar{C}_z(\cdot)\end{pmatrix}+\begin{pmatrix}\bar{C}_x^{re}(\cdot)\\ \bar{C}_x^{re}(\cdot)\end{pmatrix}V+\begin{pmatrix}\bar{C}_x^{e}(\cdot)\\ \bar{C}_x^{e}(\cdot)\end{pmatrix}\eta\right\}$$

$$+\frac{\rho SV^2}{2\mathrm{m}}\left\{\begin{pmatrix}\dfrac{C_{x,\delta1}(\cdot)C_{M,\delta2}(\cdot)}{C_{M,\delta1}(\cdot)C_{\eta\delta2}-C_{\eta\delta1}C_{M,\delta2}(\cdot)}\\ \dfrac{C_{z,\delta1}(\cdot)C_{M,\delta2}(\cdot)-C_{z,\delta2}(\cdot)C_{M,\delta1}(\cdot)}{C_{M,\delta1}(\cdot)C_{\eta\delta2}-C_{\eta\delta1}C_{M,\delta2}(\cdot)}\end{pmatrix}C_{\eta q}q+\right.$$

$$\left.\begin{pmatrix}-\dfrac{C_{x,\delta1}(\cdot)C_{\eta\delta2}}{C_{M,\delta1}(\cdot)C_{\eta\delta2}-C_{\eta\delta1}C_{M,\delta2}(\cdot)}C_{M,\dot{\eta}}(\cdot)+\dfrac{C_{x,\delta1}(\cdot)C_{M,\delta2}(\cdot)}{C_{M,\delta1}(\cdot)C_{\eta\delta2}-C_{\eta\delta1}C_{M,\delta2}(\cdot)}\bar{q}C_{\eta\dot{\eta}}\\ C_{z,\dot{\eta}}(\cdot)-\dfrac{C_{z,\delta1}(\cdot)C_{\eta\delta2}-C_{z,\delta2}(\cdot)C_{\eta\delta1}}{C_{M,\delta1}(\cdot)C_{\eta\delta2}-C_{\eta\delta1}C_{M,\delta2}(\cdot)}C_{M,\dot{\eta}}(\cdot)+\dfrac{\left(C_{z,\delta1}C_{M,\delta2}-C_{z,\delta2}C_{M,\delta1}\right)(\cdot)}{C_{M,\delta1}(\cdot)C_{\eta\delta2}-C_{\eta\delta1}C_{M,\delta2}(\cdot)}\bar{q}C_{\eta\dot{\eta}}\end{pmatrix}\dot{\eta}\right\}$$

$$+\frac{m_\eta I_y}{\mathrm{m}\bar{c}}\begin{bmatrix}\dfrac{C_{x,\delta1}(\cdot)C_{\eta\delta2}}{m_\eta\left(C_{M,\delta1}(\cdot)C_{\eta\delta2}-C_{\eta\delta1}C_{M,\delta2}(\cdot)\right)} & \dfrac{-\bar{c}C_{x,\delta1}(\cdot)C_{M,\delta2}(\cdot)}{I_y\left(C_{M,\delta1}(\cdot)C_{\eta\delta2}-C_{\eta\delta1}C_{M,\delta2}(\cdot)\right)}\\ \dfrac{C_{z,\delta1}(\cdot)C_{\eta\delta2}-C_{z,\delta2}(\cdot)C_{\eta\delta1}}{m_\eta\left(C_{M,\delta1}(\cdot)C_{\eta\delta2}-C_{\eta\delta1}C_{M,\delta2}(\cdot)\right)} & \dfrac{\bar{c}\left(-C_{z,\delta1}C_{M,\delta2}+C_{z,\delta2}C_{M,\delta1}\right)(\cdot)}{I_y\left(C_{M,\delta1}(\cdot)C_{\eta\delta2}-C_{\eta\delta1}C_{M,\delta2}(\cdot)\right)}\end{bmatrix}\begin{pmatrix}\dot{q}^{des}\\ \ddot{\eta}^{des}\end{pmatrix} \tag{6.24}$$

Consequently proving the stability of the *u*-*w* subsystem would prove the stability of the entire closed loop system (6.23) and (6.24), since the commanded variables are stable by design.

6.6 Stability of a 2-D System

This section derives explicit algebraic conditions that guarantee that the solutions of (6.4) and (6.5) satisfy the assumptions stated in Section 6.2. As was shown in the previous section, the dynamic inversion controller decomposes a six-dimensional system into a four-dimensional controlled dynamics and a two-dimensional internal dynamics. Furthermore, as observed earlier, the dynamics of $(q,\theta,\dot{\eta},\eta)$ are decoupled from the velocity dynamics (u,w). Therefore, while studying the internal dynamics, it may be assumed that $(q,\theta,\dot{\eta},\eta)$ are known functions; hence, (6.24) becomes a two-dimensional time-varying nonlinear system. The time dependence enters implicitly from the actions of the controls. The regulation of the closed loop system takes time and it asymptotically reaches the new state as $t \to \infty$.

Furthermore by design and physical limitation of the aircraft $q,\dot{\eta} \to 0$ and $\theta \to \theta_{cmd}, \eta \to \eta_{cmd}$ as $t \to \infty$, so the internal dynamics in (6.24) become

$$\begin{pmatrix} \dot{u} \\ \dot{w} \end{pmatrix} = \begin{pmatrix} -g\sin\theta_{cmd} + \dfrac{T}{\mathrm{m}} \\ g\cos\theta_{cmd} \end{pmatrix} + \frac{1}{\mathrm{m}} \begin{pmatrix} \bar{F}_x(u,w) + \bar{F}_x^{re}(u,w) + \bar{F}_x^{e}(u,w,\eta_{cmd}) \\ \bar{F}_z(u,w) + \bar{F}_z^{re}(u,w) + \bar{F}_z^{e}(u,w,\eta_{cmd}) \end{pmatrix} \tag{6.25}$$

where $\bar{F}_i, \bar{F}_i^{re}, \bar{F}_i^{e}$ for $i = x,z$ have been substituted from (6.19). Mathematically, the internal dynamics of the closed loop system in the limit, as $t \to \infty$, (6.25) are called the limiting system of (6.24); furthermore, their dynamic behavior determines that of (6.24)[48]. The idea behind limiting systems has been mentioned earlier in Section 6.2. The closed loop equations in (6.24) assume precisely the asymptotically autonomous form $\dot{x} = f(x) + \hat{g}(x,t)$ with perturbation $\hat{g}(x,t)$ describing direct control driven states, *i.e.*, as $t \to \infty$, $x \to x_{cmd}$. The details of limiting equations and stability of nonautonomous systems are discussed in Reference 48.

To this point, in the development of the global stability result, the n-dimensional system has been reduced to a two-dimensional nonautonomous one via a dynamic inversion controller. Earlier in this section, the nonautonomous system (6.24) was reduced to its limiting system (6.25), which is autonomous. The next step is to establish conditions for stability of the equilibrium of (6.25). The first of these is to prove the bound on a solution of (6.24). This is accomplished in the following lemma.

Lemma 6.1: Assume the total aerodynamic drag $\bar{C}_D^{re}(\alpha)$ is always positive.

Then there exists a finite neighborhood $D \subset \mathbf{R}^2$ on the *u*-*w* surface into which all trajectories enter and remain. And the dynamic system described by (6.24) is bounded.

Proof: Lyapunov's direct method of finding a Lyapunov function will show boundedness of the trajectories $\big(u(t), w(t)\big)$. Consider Lyapunov stability and the function $V^2 = u^2 + w^2$ as a candidate Lyapunov function. The variable *V* is speed of the vehicle and is directly proportional to the kinetic energy. (Recall that Lyapunov functions tend to be energy like.) If the candidate function proves to be a Lyapunov function, then a conclusion about the stability of the internal dynamics given by (6.24) can be made. The function is a quadratic, hence it is easy to verify that it will satisfy the first criteria of a Lyapunov function, $V(0) = 0$ and $V(x) > 0, \quad \forall x \in D - \{0\}$. Since the original equations do not have the equilibrium at the origin, a change of variable $\hat{u} = u - u_o$ and $\hat{w} = w - w_o$ is applied to (6.24) and $V(0)$ is computed. Let $V(0) = V(\hat{u}, \hat{w})_{(0,0)}$, then

$V(\hat{u}, \hat{w})_{(0,0)} = (u - u_o)^2_{u=u_o} + (w - w_o)^2_{w=w_o}$, $V(\hat{u}, \hat{w})_{(0,0)} = 0$, and

$V(\hat{u}, \hat{w}) \neq 0, \forall \hat{u}, \hat{w} \in D - \{0\}$

To satisfy the second criteria, from (6.24) compute the time rate of change of $dV(\hat{u}, \hat{w})/dt$ along the trajectory with new variables $(\hat{u}, \hat{w})$. For convenience of algebraic manipulations define new variables. These can be also considered to form elements of a closed loop "control effectiveness" matrix and are defined as follows:

$$\bar{C}_{x,\delta 1}(\alpha)=\frac{C_{x,\delta 1}(\alpha)C_{\eta\delta 2}}{\left(C_{M,\delta 1}(\alpha)C_{\eta\delta 2}-C_{\eta\delta 1}C_{M,\delta 2}(\alpha)\right)}$$

$$\bar{C}_{x,\delta 2}(\alpha)=\frac{-C_{x,\delta 1}(\alpha)C_{M,\delta 2}(\alpha)}{\left(C_{M,\delta 1}(\alpha)C_{\eta\delta 2}-C_{\eta\delta 1}C_{M,\delta 2}(\alpha)\right)}$$

$$\bar{C}_{z,\delta 1}(\alpha)=\frac{C_{z,\delta 1}(\alpha)C_{\eta\delta 2}-C_{z,\delta 2}(\alpha)C_{\eta\delta 1}}{\left(C_{M,\delta 1}(\alpha)C_{\eta\delta 2}-C_{\eta\delta 1}C_{M,\delta 2}(\alpha)\right)}$$

$$\bar{C}_{z,\delta 2}=\frac{-C_{z,\delta 1}(\alpha)C_{M,\delta 2}(\alpha)+C_{z,\delta 2}(\alpha)C_{M,\delta 1}(\alpha)}{\left(C_{M,\delta 1}(\alpha)C_{\eta\delta 2}-C_{\eta\delta 1}C_{M,\delta 2}(\alpha)\right)}$$

Then the equations in (6.24) can be rewritten as

$$\begin{pmatrix}\dot{\hat{u}}\\ \dot{\hat{w}}\end{pmatrix}=\begin{pmatrix}-q(\hat{w}+w_o)\\ q(\hat{u}+u_o)\end{pmatrix}+\begin{pmatrix}-g\sin\theta+\dfrac{T}{\mathrm{m}}\\ g\cos\theta\end{pmatrix}+\frac{m_\eta I_y}{\mathrm{m}\bar{c}}\begin{bmatrix}\dfrac{\bar{C}_{x,\delta 1}(\alpha)}{m_\eta} & \dfrac{\bar{c}\bar{C}_{x,\delta 2}(\alpha)}{I_y}\\ \dfrac{\bar{C}_{z,\delta 1}(\alpha)}{m_\eta} & \dfrac{\bar{c}\bar{C}_{z,\delta 2}(\alpha)}{I_y}\end{bmatrix}\begin{pmatrix}\dot{q}^{des}\\ \ddot{\eta}^{des}\end{pmatrix}$$

$$+\frac{\rho S}{2\mathrm{m}}(\hat{V}+V_o)^2\left\{\begin{pmatrix}\bar{C}_x(\alpha)+\bar{C}_x^e(\alpha)\eta+\bar{C}_x^{re}(\alpha)(\hat{V}+V_o)\\ \bar{C}_z(\alpha)+\bar{C}_z^e(\alpha)\eta+\bar{C}_z^{re}(\alpha)(\hat{V}+V_o)\end{pmatrix}\right.$$

$$\left.+\begin{pmatrix}-\bar{C}_{x,\delta 1}(\alpha)C_{M,\dot{\eta}}(\alpha)\dot{\eta}-\bar{C}_{x,\delta 2}(\alpha)\left(\bar{q}C_{\eta\dot{\eta}}\dot{\eta}+C_{\eta q}q\right)\\ C_{z,\dot{\eta}}(\alpha)\dot{\eta}-\bar{C}_{z,\delta 1}(\alpha)C_{M,\dot{\eta}}(\alpha)\dot{\eta}-\bar{C}_{z,\delta 2}(\alpha)\left(\bar{q}C_{\eta\dot{\eta}}\dot{\eta}+C_{\eta q}q\right)\end{pmatrix}\right\}$$

Using the above equation, the time rate of change of $V(\hat{u},\hat{w})$ becomes

$$\frac{d\hat{V}^2}{dt}=2\hat{u}\left(\begin{array}{l}-q(\hat{w}+w_o)-g\sin\theta+\dfrac{T}{\mathrm{m}}+\dfrac{\rho S}{2\mathrm{m}}(\hat{V}+V_o)^2\left\{\left(\bar{C}_x+\bar{C}_x^e\eta+\bar{C}_x^{re}(\hat{V}+V_o)\right)(\alpha)\right.\\ \left.+\left(-\bar{C}_{x,\delta 1}(\alpha)C_{M,\dot{\eta}}(\alpha)\dot{\eta}-\bar{C}_{x,\delta 2}(\alpha)\left(\bar{q}C_{\eta\dot{\eta}}\dot{\eta}+C_{\eta q}q\right)\right)\right\}\\ +\dfrac{m_\eta I_y}{\mathrm{m}\bar{c}}\begin{bmatrix}\dfrac{\bar{C}_{x,\delta 1}(\alpha)}{m_\eta} & \dfrac{\bar{c}\bar{C}_{x,\delta 2}(\alpha)}{I_y}\end{bmatrix}\begin{pmatrix}\dot{q}^{des}\\ \ddot{\eta}^{des}\end{pmatrix}\end{array}\right)$$

$$+2\hat{w}\left(\begin{array}{l}q(\hat{u}+u_o)+g\cos\theta+\dfrac{\rho S}{2\mathrm{m}}(\hat{V}+V_o)^2\left\{\left(\bar{C}_z(\alpha)+\bar{C}_z^e(\alpha)\eta+\bar{C}_z^{re}(\alpha)(\hat{V}+V_o)\right)\right.\\ \left.+\left(C_{z,\dot{\eta}}(\alpha)\dot{\eta}-\bar{C}_{z,\delta 1}(\alpha)C_{M,\dot{\eta}}(\alpha)\dot{\eta}-\bar{C}_{z,\delta 2}(\alpha)\left(\bar{q}C_{\eta\dot{\eta}}\dot{\eta}+C_{\eta q}q\right)\right)\right\}\\ +\dfrac{m_\eta I_y}{\mathrm{m}\bar{c}}\begin{bmatrix}\dfrac{\bar{C}_{z,\delta 1}(\alpha)}{m_\eta} & \dfrac{\bar{c}\bar{C}_{z,\delta 2}(\alpha)}{I_y}\end{bmatrix}\begin{pmatrix}\dot{q}^{des}\\ \ddot{\eta}^{des}\end{pmatrix}\end{array}\right)$$

where $\dot{q}^{des}$ and $\ddot{\eta}^{des}$ are defined in (6.21). Changing the coordinate system to polar coordinates and expressing aerodynamic coefficients in terms of lift and drag necessitates the following expressions

$$\bar{C}_x^{(\bullet)} = \sin\alpha \bar{C}_L^{(\bullet)} - \cos\alpha \bar{C}_D^{(\bullet)} \qquad \bar{C}_z^{(\bullet)} = -\cos\alpha \bar{C}_L^{(\bullet)} - \sin\alpha \bar{C}_D^{(\bullet)}$$

$$\frac{d\hat{V}^2}{dt} = 2\hat{V}\cos\alpha \left(\begin{array}{l} -q(\hat{V}+V_o)\sin\alpha - g\sin\theta + \frac{T}{\mathrm{m}} + \frac{m_\eta I_y}{\mathrm{m}\bar{c}} \begin{bmatrix} \frac{\bar{C}_{x,\delta 1}(\alpha)}{m_\eta} & \frac{\bar{c}\bar{C}_{x,\delta 2}(\alpha)}{I_y} \end{bmatrix} \begin{pmatrix} \dot{q}^{des} \\ \ddot{\eta}^{des} \end{pmatrix} \\ + \frac{\rho S}{2\mathrm{m}}(\hat{V}+V_o)^2 \left\{ \left(\bar{C}_x(\alpha) + \bar{C}_x^e(\alpha)\eta + \bar{C}_x^{re}(\alpha)(\hat{V}+V_o) \right) \right. \\ \left. - \left(\bar{C}_{x,\delta 1}(\alpha) C_{M,\dot{\eta}}(\alpha)\dot{\eta} + \bar{C}_{x,\delta 2}(\alpha)\left(\bar{q} C_{\eta\dot{\eta}}\dot{\eta} + C_{\eta q} q \right) \right) \right\} \end{array} \right)$$

$$+2\hat{V}\sin\alpha \left(\begin{array}{l} q(\hat{V}+V_o)\cos\alpha + g\cos\theta + \frac{m_\eta I_y}{\mathrm{m}\bar{c}} \begin{bmatrix} \frac{\bar{C}_{z,\delta 1}(\alpha)}{m_\eta} & \frac{\bar{c}\bar{C}_{z,\delta 2}(\alpha)}{I_y} \end{bmatrix} \begin{pmatrix} \dot{q}^{des} \\ \ddot{\eta}^{des} \end{pmatrix} \\ + \frac{\rho S}{2\mathrm{m}}(\hat{V}+V_o)^2 \left\{ \left(\bar{C}_z(\alpha) + \bar{C}_z^e(\alpha)\eta + \bar{C}_z^{re}(\alpha)(\hat{V}+V_o) \right) \right. \\ \left. + \left(C_{z,\dot{\eta}}(\alpha)\dot{\eta} - \bar{C}_{z,\delta 1}(\alpha) C_{M,\dot{\eta}}(\alpha)\dot{\eta} - \bar{C}_{z,\delta 2}(\alpha)\left(\bar{q} C_{\eta\dot{\eta}}\dot{\eta} + C_{\eta q} q \right) \right) \right\} \end{array} \right)$$

Collecting terms and simplifying

$$\frac{d\hat{V}^2}{dt} = 2\left(-g\left(\cos\alpha\sin\theta + \sin\alpha\cos\theta\right) + \frac{T}{\mathrm{m}}\cos\alpha - \frac{I_y}{\mathrm{m}\bar{c}}\bar{C}_{D,\delta 1}(\alpha)\dot{q}^{des} - \frac{m_\eta}{\mathrm{m}}\bar{C}_{D,\delta 2}(\alpha)\ddot{\eta}^{des} \right)\hat{V}$$
$$+ \frac{\rho S}{\mathrm{m}}(\hat{V}+V_o)^2\hat{V}\left\{ -\bar{C}_D(\alpha) - \bar{C}_D^e(\alpha)\eta - \bar{C}_D^{re}(\alpha)(\hat{V}+V_o) + \bar{C}_{D,\delta 1}(\alpha)C_{M,\dot{\eta}}(\alpha)\dot{\eta} \right.$$
$$\left. + \sin\alpha C_{z,\dot{\eta}}(\alpha)\dot{\eta} + \bar{C}_{D,\delta 2}(\alpha)\left(\bar{q}C_{\eta\dot{\eta}}\dot{\eta} + C_{\eta q}q\right)\right\}$$
$$= 2\left(-g\left(\cos\alpha\sin\theta + \sin\alpha\cos\theta\right) + \frac{T}{\mathrm{m}}\cos\alpha - \frac{I_y}{\mathrm{m}\bar{c}}\bar{C}_{D,\delta 1}(\alpha)\dot{q}^{des} - \frac{m_\eta}{\mathrm{m}}\bar{C}_{D,\delta 2}(\alpha)\ddot{\eta}^{des} \right)\hat{V}$$
$$+ \frac{\rho S}{\mathrm{m}}\hat{V}V_o^2\begin{pmatrix} -\bar{C}_D(\alpha) - \bar{C}_D^e(\alpha)\eta + \bar{C}_{D,\delta 1}(\alpha)C_{M,\dot{\eta}}(\alpha)\dot{\eta} + \sin\alpha C_{z,\dot{\eta}}(\alpha)\dot{\eta} \\ + \bar{C}_{D,\delta 2}(\alpha)\left(\bar{q}C_{\eta\dot{\eta}}\dot{\eta} + C_{\eta q}q\right) \end{pmatrix}$$
$$+ \frac{\rho S}{\mathrm{m}}2\hat{V}^2V_o\begin{pmatrix} -\bar{C}_D(\alpha) - \bar{C}_D^e(\alpha)\eta + \bar{C}_{D,\delta 1}(\alpha)C_{M,\dot{\eta}}(\alpha)\dot{\eta} + \sin\alpha C_{z,\dot{\eta}}(\alpha)\dot{\eta} \\ + \bar{C}_{D,\delta 2}(\alpha)\left(\bar{q}C_{\eta\dot{\eta}}\dot{\eta} + C_{\eta q}q\right) \end{pmatrix}$$
$$+ \frac{\rho S}{\mathrm{m}}\hat{V}^3\begin{pmatrix} -\bar{C}_D(\alpha) - \bar{C}_D^e(\alpha)\eta + \bar{C}_{D,\delta 1}(\alpha)C_{M,\dot{\eta}}(\alpha)\dot{\eta} + \sin\alpha C_{z,\dot{\eta}}(\alpha)\dot{\eta} \\ + \bar{C}_{D,\delta 2}(\alpha)\left(\bar{q}C_{\eta\dot{\eta}}\dot{\eta} + C_{\eta q}q\right) \end{pmatrix}$$
$$- \frac{\rho S}{\mathrm{m}}\left(\hat{V}^4 + 3\hat{V}^3V_o + 3\hat{V}^2V_o^2 + \hat{V}V_o^3\right)\bar{C}_D^{re}(\alpha)$$

$$\frac{d\hat{V}^2}{dt} = 2\left(g\sin(\theta-\alpha) + \frac{T}{\mathrm{m}}\cos\alpha - \frac{I_y}{\mathrm{m}\bar{c}}\bar{C}_{D,\delta 1}(\alpha)\dot{q}^{des} - \frac{m_\eta}{\mathrm{m}}\bar{C}_{D,\delta 2}(\alpha)\ddot{\eta}^{des} \right)\hat{V}$$
$$+ \frac{\rho S}{\mathrm{m}}\left(\hat{V}V_o^2 + 2\hat{V}^2V_o\right)\begin{pmatrix} -\bar{C}_D(\alpha) - \bar{C}_D^e(\alpha)\eta + \bar{C}_{D,\delta 1}(\alpha)C_{M,\dot{\eta}}(\alpha)\dot{\eta} + \sin\alpha C_{z,\dot{\eta}}(\alpha)\dot{\eta} \\ + \bar{C}_{D,\delta 2}(\alpha)\left(\bar{q}C_{\eta\dot{\eta}}\dot{\eta} + C_{\eta q}q\right) \end{pmatrix} \quad (6.26)$$
$$+ \frac{\rho S}{\mathrm{m}}\hat{V}^3\begin{pmatrix} -\bar{C}_D(\alpha) - \bar{C}_D^e(\alpha)\eta + \bar{C}_{D,\delta 1}(\alpha)C_{M,\dot{\eta}}(\alpha)\dot{\eta} + \sin\alpha C_{z,\dot{\eta}}(\alpha)\dot{\eta} \\ + \bar{C}_{D,\delta 2}(\alpha)\left(\bar{q}C_{\eta\dot{\eta}}\dot{\eta} + C_{\eta q}q\right) \end{pmatrix}$$
$$- \frac{\rho S}{\mathrm{m}}\left(3\hat{V}^2V_o^2 + \hat{V}V_o^3\right)\bar{C}_D^{re}(\alpha) - \frac{\rho S}{\mathrm{m}}3V_o\bar{C}_D^{re}(\alpha)\hat{V}^3 - \frac{\rho S}{\mathrm{m}}\bar{C}_D^{re}(\alpha)\hat{V}^4$$

where

$$
\begin{aligned}
\bar{C}_D^{re}(\alpha) &= -\cos\alpha \bar{C}_x^{re}(\alpha) - \sin\alpha \bar{C}_z^{re}(\alpha) \\
&= -\cos\alpha \frac{C_{x,\delta 1}(\alpha) C_{M,\delta 2}(\alpha)}{C_{M,\delta 1}(\alpha) C_{\eta\delta 2} - C_{\eta\delta 1} C_{M,\delta 2}(\alpha)} \left(C_{\eta u} \cos\alpha + C_{\eta w} \sin\alpha \right) \\
&\quad -\sin\alpha \frac{C_{z,\delta 1}(\alpha) C_{M,\delta 2}(\alpha) - C_{z,\delta 2}(\alpha) C_{M,\delta 1}(\alpha)}{C_{M,\delta 1}(\alpha) C_{\eta\delta 2} - C_{\eta\delta 1} C_{M,\delta 2}(\alpha)} \left(C_{\eta u} \cos\alpha + C_{\eta w} \sin\alpha \right) \quad (6.27) \\
&= \left(-\cos\alpha \bar{C}_{x,\delta 1}(\alpha) - \sin\alpha \bar{C}_{z,\delta 1}(\alpha) \right) \left(C_{\eta u} \cos\alpha + C_{\eta w} \sin\alpha \right) \\
&= \bar{C}_{D,\delta 1}(\alpha) \left(C_{\eta u} \cos\alpha + C_{\eta w} \sin\alpha \right)
\end{aligned}
$$

The expression for $\bar{C}_D^{re}(\alpha)$ denotes the total equilibrium drag due to the elastic effects on the rigid body including direct surface effects. The coefficient of $\hat{V}$ consists of functions of thrust and gravity as well as of desired dynamic variables all of which are bounded by physics, gravity, or design. For sufficiently large *V*, the $\hat{V}^4$ term will dominate the candidate Lyapunov function. (In fact, all of the $\hat{V}^3 V_o, \hat{V} V_o^3, \hat{V}^2 V_o^2$ coefficients are $\bar{C}_D^{re}(\alpha)$.) Hence, if the coefficient of $\hat{V}^4$ is positive, the time rate of change of $\hat{V}^2 = \hat{u}^2 + \hat{w}^2$ is negative and the conclusion of boundedness of (6.24) from above follows. □

The expression for $\bar{C}_D^{re}(\alpha)$ can also be considered in terms of feedback control cross-coupling and the flexible mode excitation due to velocity in the direction of drag. The requirement that $\bar{C}_D^{re}(\alpha) > 0$ sets limitations on the size of the elastic dynamic excitation due to velocity and the rigid body control effectiveness cross-coupling. This condition ensures that a solution $(u(t), w(t))$ of (6.24) is bounded, and is based on the physics on the problem. It is reassuring when the mathematics reassert the understanding of the physical behavior.

Now given the boundedness of solution $(u(t), w(t))$ of (6.24), the equilibrium of a two-dimensional autonomous system (6.25) is either a point or a limit cycle and is either stable or not. Here the physics of the problem are used to create appropriate conditions for stability. For straight and level flight equilibrium, the aerodynamic forces must balance the force of gravity and thrust. For a given value of thrust T, if the vehicle is too fast for its equilibrium, the pitch angle would increase, thus increasing drag to slow the

vehicle down. If, on the other hand, the aircraft is slower than its equilibrium velocity, the pitch angle would be decreased to increase the gravitational acceleration and potentially decrease drag in order to speed up. This is not an optimum approach in practice, especially at low altitude, but it is a legitimate maneuver to achieve desired speed. Notice that in both cases, drag, and implicitly its companion lift, would play a role, so it would be natural to suppose that they would play a role in describing stability conditions. It can be further argued that the aerodynamic force of drag would be dissipative for any speed greater than zero. Appropriate amount of thrust balanced with gravitational force is what overcomes this dissipative effect in actual flight. The following lemma codifies this relationship.

Lemma 6.2: Define *G* as the right hand side of (6.25). Assume that the aerodynamic forces have a dissipative effect, that is

$$div(G) < 0$$

where

$$div(G) = \frac{\rho SV}{2\mathrm{m}}\left\{-\left(3\bar{C}_D(\alpha)+\frac{d\bar{C}_L(\alpha)}{d\alpha}\right)-\left(4\bar{C}_D^{re}(\alpha)+\frac{d\bar{C}_L^{re}(\alpha)}{d\alpha}\right)V-\left(3\bar{C}_D^{e}(\alpha)+\frac{d\bar{C}_L^{e}(\alpha)}{d\alpha}\right)\eta_{cmd}\right\} \tag{6.28}$$

for all (u,w) not equal to (0,0). Then the only possible closed orbits of the limiting system (6.25) are equilibria.

This lemma is a restatement of the Bendixson's criterion.

Proof: The proof is by contradiction and application of the Green's Theorem. Assume that there exists some closed orbit *C* and let *R* define the interior region, then by the Green's Theorem

$$\int_C G \cdot n d\sigma = \iint_R divG d\ Area$$

where $\boldsymbol{n}d\sigma$ is a vector element on a plane directed along the unit outer normal vector ***n*** to *C*. The inner product on the left side is thus zero by construction, while *divG* on the right is negative by assumption. Hence, there exists a contradiction that proves the lemma. (This Lemma is an extension of the

theorem in Hale (1980) Chapter 2, Exercise 1.3.) The detailed calculation of *divG* is shown in detail in Appendix D. □

Prior to proceeding, a definition of an *ω-limit set* and an associated invariance property are introduced here for background purposes. These will be used in upcoming technical developments.

Definition: The *ω-limit set* of a solution $x(t, x_o, t_o) \in \mathbf{R}^n$ of (6.5), denoted $\Omega(x) \subset \mathbf{R}^n$, consists of all points *y* such that there exists a strictly increasing sequence t_k such that $x(t_k, x_o, t_o) \to y$ as $t_k \to \infty$.

For convenience, a well known invariance property of ω-limit set of the autonomous system is restated here. The proof can be found any standard text, *e.g.* References 34 or 48

Lemma 6.3: If a solution $x(t)$ of (6.5) is bounded and belongs to $D \subset \mathbf{R}^n$, a domain containing the equilibrium point, for $t \geq 0$, then its ω-limit set $\Omega(x)$ is a nonempty, compact, invariant set. In other words, for any $y \in \Omega(x)$, the solution $x(t)$ through *y* stays in $\Omega(x)$ whenever it is defined. Moreover, the trajectory actually approaches its limit set, $x(t) \to \Omega(x)$, as $t \to \infty$.

As a corollary of the above dissipative condition lemma 6.2, the following stability result applies to the limiting system (6.25).

Corollary 6.1: Assume that

(1) the limiting system (6.25) has a unique equilibrium $(\overline{u}, \overline{w})$ for given $(T_o, GW_o^*, \theta_{cmd}, \eta_{cmd})$;

(2) the forces defined by vector G that includes the equilibrium aerodynamic forces F satisfy the divergent condition (6.28).

Then the unique equilibrium is a global attractor for the limiting system (6.25), *i.e.,* any solution $\left(u(t), w(t)\right)$ of the limiting system (6.25) satisfies

$$\lim_{t\to\infty} u(t) = \bar{u}, \quad \lim_{t\to\infty} w(t) = \bar{w}$$

Proof: Since the asymptotically limiting behavior of (6.24) is expressed by (6.25) and since a solution of (6.24) is bounded by Lemma 6.1, then any solution $\left(u(t), w(t)\right)$ of (6.25) is bounded. Thus, its ω-limit set $\Omega(x)$ is either equilibria or a periodic orbit. But Lemma 6.2 excludes the periodic closed orbit case and Assumption 1 excludes a union of equilibria and connecting trajectories. Hence, by the invariance property stated in Lemma 6.3, the ω-limit set $\Omega(x)$ of any solution consists of one point $\left(\bar{u}, \bar{w}\right)$, which is the unique equilibrium of (6.25) by assumption. This is equivalent of saying that $\left(\bar{u}, \bar{w}\right)$ is the global attractor of the system (6.25). □

Remark 6.2: For a given $(T_o, GW_o^*, \theta_{cmd}, \eta_{cmd})$, the limiting system (6.25) has a unique equilibrium if and only if the equations

$$\begin{pmatrix} 0 \\ 0 \end{pmatrix} = \begin{pmatrix} -\mathrm{m}g\sin\theta_{cmd} + T \\ \mathrm{m}g\cos\theta_{cmd} \end{pmatrix} + \frac{1}{2}\rho S V^2 \begin{pmatrix} \bar{C}_x(\alpha) + \bar{C}_x^e(\alpha)\eta + \bar{C}_x^{re}(\alpha)V \\ \bar{C}_z(\alpha) + \bar{C}_z^e(\alpha)\eta - \bar{C}_z^{re}(\alpha)V \end{pmatrix} \tag{6.29}$$

have only one solution $(\bar{\alpha}, \bar{V})$ for given $(T_o, GW_o^*, \theta_{cmd}, \eta_{cmd})$.

The solution can be found by looking for an intersection of contour plots of each equation. For a given mass distribution GW_o^* and flight condition specified by $(T_o, \theta_{cmd}, \bar{\alpha}, \bar{V})$, the aircraft will assume a unique quasi-static deformation η_{cmd}. The uniqueness of solution $(\bar{\alpha}, \bar{V})$ depends on where for a given value of T_o / mg, α is a single valued function of θ_{cmd} as well as where α is a singled valued function of T_o / mg for a given value of θ_{cmd}. The size of these regions depends on the thrust-to-weight ratio for an aircraft and its controllability across the α range. The higher the T_o / mg, the larger the α range where $(\bar{\alpha}, \bar{V})$ is a unique solution. Furthermore, bifurcation analysis,

given a specific aircraft, can determine regions of a unique solution versus multiple solutions. As previously mentioned, there are no generalizations available to determine these regions without actual aircraft aerodynamics being employed in the analysis.

In summary, the lemmas and corollary have shown that there is a unique, stable global attractor for the limiting system (6.25), provided it has a unique equilibrium (see Remark 6.2), the equilibrium is not a limit cycle (see Lemma 6.2), and the solution of the nonautonomous two-dimensional system is bounded (see Lemma 6.1). At this juncture the global stability theorem that relates the stability of the autonomous limiting system (6.25) to that of the internal dynamics (6.24) is stated in terms of the required algebraic conditions.

Theorem 6.1: Assume that

(1) the total drag coefficient

$$\bar{C}_D^{re}(\alpha) > 0$$

(2) the aerodynamic functions satisfy the dissipative condition

$$div(G) < 0$$

with *G* defined as the right side of limiting equation (6.25),

(3) for a given $(T_o, GW_o^*, \theta_{cmd}, \eta_{cmd})$, the equations (6.29)

$$\begin{pmatrix} 0 \\ 0 \end{pmatrix} = \begin{pmatrix} -\mathrm{m}g\sin\theta_{cmd} + T \\ \mathrm{m}g\cos\theta_{cmd} \end{pmatrix} + \frac{1}{2}\rho SV^2 \begin{pmatrix} \bar{C}_x(\alpha) + \bar{C}_x^e(\alpha)\eta + \bar{C}_x^{re}(\alpha)V \\ \bar{C}_z(\alpha) + \bar{C}_z^e(\alpha)\eta - \bar{C}_z^{re}(\alpha)V \end{pmatrix}$$

have a unique solution $(\bar{\alpha}, \bar{V})$,

Then, for a given $(T_o, GW_o^*, \theta_{cmd}, \eta_{cmd})$, the closed loop system (6.23) and (6.24) has a unique equilibrium $(\bar{u}, \bar{w}, \bar{q}, \bar{\theta}, \bar{\eta}, \dot{\bar{\eta}})$ given by

$$\bar{u} = \cos\bar{\alpha}\bar{V}, \quad \bar{w} = \sin\bar{\alpha}\bar{V}, \quad \bar{q} = 0, \quad \bar{\theta} = \theta_{cmd}, \quad \dot{\bar{\eta}} = 0, \quad \bar{\eta} = \eta_{cmd}$$

where $(\bar{\alpha}, \bar{V})$ is the unique solution of the equations (6.29).

Furthermore, any solution $(u(t), w(t), q(t), \theta(t), \eta(t), \dot{\eta}(t))$ of the closed loop system (6.23) and (6.24) satisfies

$$u(t) \to \bar{u}, \quad w(t) \to \bar{w}, \quad q(t) \to 0, \quad \theta(t) \to \theta_{cmd}, \quad \eta(t) \to \eta_{cmd}, \quad \dot{\eta}(t) \to 0$$

as $t \to \infty$. In other words $(\bar{u}, \bar{w}, 0, \theta_{cmd}, 0, \eta_{cmd})$ is a global attractor of the closed loop system (6.23) and (6.24).

Proof Outline: A basic sketch of the proof is given here. A more rigorous and detailed version is presented in the following section along with the necessary background theorems. By the design of the feedback control the closed loop system is decoupled into internal dynamics (6.24) and stable controlled dynamics (6.23). Furthermore, since $q, \dot{\eta} \to 0$ and $\theta \to \theta_{cmd}, \eta \to \eta_{cmd}$ as $t \to \infty$, internal dynamics system (6.24) is asymptotically autonomous and its limiting equation is given by an autonomous system (6.25). A corollary to the Markus theorem[49] is invoked to relate the stability of (6.24) to that of (6.25), which establishes that $(\bar{u}, \bar{w})$ is the local attractor to the nonautonomous system (6.24). It is possible to apply this extension of the Poincare Theorem only because the system is two-dimensional. The Yoshizawa theorem[50] is then applied to show that $(\bar{u}, \bar{w})$ is also a global attractor of (6.24).

The first two assumptions are based on the physical characteristics of the vehicle under consideration. Furthermore, a variation of these assumptions that does not include the flexible vehicle dynamics, have been shown by Morton, *et al.* to hold for a variety of fighter aircraft. Hence, the stability of the closed loop system depends on whether equations (6.29) have a unique solution $(\bar{\alpha}, \bar{V})$. This in turn depends on the uniqueness of α for a given engine thrust *T* and the commanded attitude θ.

The next section reverts to addressing the stability in a more general form of nonlinear system representation.

6.7 Stability of a Standard Dynamic Inversion Controlled System

This section establishes the connection between the behavior of a nonautonomous two-dimensional nonlinear system and it limiting system. Furthermore, the reduction from n-dimensional to two-dimensional system by control and why that is necessary for the global stability result is discussed.

The basics of standard dynamic inversion or feedback linearization are introduced in Chapter 2. For exact feedback linearization, all original dynamics are cancelled and converted to a string of integrators. These are then assigned desired dynamics by the controller and the system is stable by design. All of this, of course, occurs for a nominal system that is known exactly and the issue of robust stability is not considered. In the case that the system relative degree *r* is not equal to the number of states *n,* feedback linearization results in a system with linearized dynamics, a string of integrators, and internal dynamics that are unobservable in the output. The system stability then depends on the stability of its internal dynamics. However, the standard feedback linearization stability results are local in nature, in the sense that they lead to a design of feedback laws which are defined only in a neighborhood of a given equilibrium point[15].

The interest in this work is in global stability of the aircraft dynamical system, which the standard feedback linearization results do not accommodate. Fortuitously, the dynamic inversion controller reduces the problem such that the internal dynamics are two-dimensional and a special tool available only in two-dimensional can be used to establish global stability result as will be shown in this section.

Consider a nonlinear system representative of aircraft dynamics given by

$$\begin{aligned} \dot{x} &= f(x) + g(x)\delta, \quad x = (x_i, x_c) \in \mathbf{R}^n \\ y &= h(x) \end{aligned} \tag{6.30}$$

where x_c are the states that are controlled in the output and x_i are internal states that are not controlled. In certain cases, there exists an input-output feedback linearizing controller $\delta = u\left(\hat{x}_c, \dot{x}_{des}, t\right)$ where

$$u\left(\hat{x}_c, \dot{x}_{des}, t\right) = \left(h(x_c)g(x_c)\right)^{-1}\left(\dot{x}_{des} - f(x_c)\right)$$

such that the closed loop system assumes a special structure

$$\begin{pmatrix} \dot{x}_i \\ \dot{x}_c \end{pmatrix} = \begin{pmatrix} f(x_i) + \hat{g}(x_c, \hat{x}_c, \dot{x}_{des}, t) \\ \dot{x}_{des} \end{pmatrix} \qquad \begin{matrix} x_i \in \mathbf{R}^2 \\ \left(x_c, \hat{x}_c, \dot{x}_{des}\right) \in \mathbf{R}^{n-2} \end{matrix} \tag{6.31}$$

The time dependence arises implicitly from the control action as the system reaches a new commanded value. The stability of the system, as been alluded to before, depends on the stability of it internal dynamics, $x_i(t)$. What makes this case special is that the

internal dynamics belong to two-dimensional space, $\mathbf{R}^2$, which enables a proof of global stability by introducing certain mathematical tools available only in this space. An example of just such a system is the integrated flight/SMC controller closed loop discussed in Section 6.5.

The desired dynamics of the controlled states are expressed as a difference between the commanded and actual measurement of the state, $\dot{x}_{des} = f(x_{cmd} - x_c)$; so as $t \to \infty$, the controlled states reach their commanded value $x_c \to x_{cmd}$. Consider the dynamic behavior of the internal dynamics, also represented by (6.4), in the limit, *i.e.*, as $t \to \infty$. As mentioned in the earlier section of this chapter, the nonlinear autonomous dynamic system that describes the behavior of (6.4) as $t \to \infty$ is a limiting system of (6.4). Hence, as $t \to \infty$, the controlled states go to their commanded values $x_c \to x_{cmd}$ and the desired dynamics $\dot{x}_{des} = f(x_{cmd} - x_c)$ go to $\dot{x}_{des} = f(0) \to 0$. Consider the behavior of the controller $u(\hat{x}_c, \dot{x}_{des}, t)$ in this situation. First there is no longer time dependence in the control action since the commanded value has been reached, hence as $t \to \infty$

$$u(\hat{x}_c, \dot{x}_{des}, t) \to u(\hat{x}_{cmd}, 0) = \left(h(x_{cmd})g(x_{cmd})\right)^{-1}\left(-f(x_{cmd})\right)$$

with $\hat{x}_{cmd}$ constant. Since the perturbation $\hat{g}(x_c, \hat{x}_c, \dot{x}_{des}, t)$ of (6.4) is the result of the controller influence on the internal dynamics, $\hat{g}(x_c, \hat{x}_c, \dot{x}_{des}, t) \to \hat{g}(x_{cmd}, \hat{x}_{cmd}, 0)$. Moreover, $\hat{g}(x_{cmd}, \hat{x}_{cmd}, 0) \to c$ where *c* is a constant. Hence, without loss of generality, $\hat{g}(x_c, \hat{x}_c, \dot{x}_{des}, t) \to 0$ as $t \to \infty$ and(6.4) becomes (6.5). When a nonlinear system assumes the characteristics exhibited by (6.4), it is called an asymptotically autonomous system with $\dot{x}_i = f(x_i)$ as the limiting equation. Recall from Lemma 6.3 that the ω-limit set $\Omega(x_i)$ of the solution $x_i(t)$ is invariant. In other words, for any $y \in \Omega(x_i)$, the solution $x_i(t)$ through *y* stays in $\Omega(x_i)$ whenever it is defined. Moreover, the trajectory actually approaches its limit set, $x_i(t) \to \Omega(x_i)$, as $t \to \infty$.

The limiting system and the asymptotically autonomous form of the internal dynamics allow for two-dimensional specific tools to be used to prove global stability of the closed loop system (6.31). There are two theorems that are stated for convenience and are used in the proof prior to the statement of the global stability result.

Theorem (Markus)[48, 49]**:** Let in $\mathbf{R}^2$ system (6.4) be asymptotically autonomous (*i.e.*, $\hat{g}(x_c, \hat{x}_c, \dot{x}_{des}, t) \to 0$ uniformly on compact sets as $t \to \infty$, as in Markus[49] (see also LaSalle[48]). Let a solution $x_i = x_i(t)$ of (6.4) lie in a compact set $K \subset \mathbf{R}^2$ and suppose $\Omega(x)$ does not contain any critical points of $\dot{x}_i = f(x_i)$. Also assume that $\dot{x}_i = f(x_i)$ has the uniqueness property. Then $\Omega(x)$ is the union of closed orbits of $\dot{x}_i = f(x_i)$.

The direct corollary to the Markus theorem is given below.

Corollary 6.2: Assume

(1) limiting system (6.5) has a unique equilibrium $\overline{x}_i$ for a given x_o,

(2) limiting system (6.5) has a stable equilibrium that is not a limit cycle.

Then there is a neighborhood *D* of $\overline{x}_i$ such that for any $x_o \in D$, the solution $x_i(t)$ of the original system (6.4) with $x(0) = x_o$ satisfies

$$\lim_{t \to \infty} x_i(t) = \overline{x}_i$$

Proof: This is a direct corollary of the Markus' Theorem and the fact that $\overline{x}_i$ is not only a global attractor for the limiting system, but also a stable equilibrium. The algebraic conditions that make $\overline{x}_i$ the global attractor and stable equilibrium are given in Corollary 6.1 in terms of aircraft parameters. □

The above corollary states that $\overline{x}_i$ is a local attractor of the original system (6.4), which is asymptotically autonomous. The goal is to show that $\overline{x}_i$ is also a global attractor to original system, which is achieved by using the following Yoshizawa's theorem, modified for the system under consideration.

Theorem (Yoshizawa)[50]**:** Let D be a nonempty closed set in the space Q. Assume that as $t \to \infty$, $\dot{x} = f(x,t) + g(x,t)$ evolves such that $f(x,t) \to f(x)$ and $g(x,t)$ is bounded; and, corresponding to each $\varepsilon > 0$ and each $y \in D$, there exists a $\delta(\varepsilon, y) > 0$ and a $T(\varepsilon, y) > 0$ such that if $|x - y| < \delta(\varepsilon, y)$ and $t \geq T(\varepsilon, y)$, then $|f(x,t) - f(y,t)| < \varepsilon$.

Suppose that a solution $x_i(x_o, t_o, t)$ of (6.4) is bounded and approaches a closed set D in the space Q. If $f(x_i)$ satisfies the assumption, then the ω-limit set $\Omega(x_i)$ is an invariant set contained in D of the equation (6.5) contained in D.

The global stability result for the nonlinear system described in this section can now be stated.

Theorem 6.2: Assume that

(1) the solution $x_i(t)$ of (6.4) is bounded

(2) the limiting system (6.5) has a unique equilibrium $\overline{x}_i$ for a given x_o

(3) the equilibrium $\overline{x}_i$ of the limiting system (6.5) is a point and not a limit cycle

Then, for a given x_o, the closed loop system (6.31) has a unique equilibrium $\overline{x}$ given by

$$\overline{x} = (\overline{x}_i, \overline{x}_c)$$

where $\overline{x}_i$ is a unique solution of $0 = f(x_i)$ (equilibrium form of (6.5)) and $\overline{x}_c = x_{cmd}$.

Furthermore, any solution $(x_i(t), x_c(t))$ of the closed loop system (6.31) satisfies

$$x_i(t) \to \overline{x}_i, \quad x_c(t) \to x_{cmd}$$

as $t \to \infty$. In other words, $(\overline{x}_i, x_{cmd})$ is a global attractor of the closed loop system (6.31).

Proof: The system (6.4) satisfies the assumptions of the Yoshizawa's theorem by inspection (see Note below for aircraft application).

(1) It follows from the Yoshizawa's theorem, that the ω-limit set $\Omega(x_i)$ of $x_i(t)$ is an invariant set of the equation (6.5). From Corollary 6.1, the unique equilibrium $\overline{x}_i$ of the limiting system (6.5) is contained inside the closure of any ω-limit set of (6.5), in particular $\overline{x}_i \in \Omega(x_i)$.

(2) By Corollary 6.2, there is a neighborhood D of $\overline{x}_i$ such that if the solution $x_i(t)$ enters into D, then $x_i(t) \to \overline{x}_i$ as $t \to \infty$.

From (1), $\overline{x}_i$ is a limit point of $x_i(t)$, which guarantees that $x_i(t)$ will enter into D at some time $t_o > 0$. By (2) $x_i(t) \to \overline{x}_i$ as $t \to \infty$ making $\overline{x}_i$, a unique equilibrium, the global attractor of (6.4). This completes the proof.

Note: For the aircraft equations of motion (6.24), the assumptions of the Yoshizawa's Theorem are satisfied if $\Omega(x_i) = \mathbf{R}^2$ and

$$f(x,t) = \begin{pmatrix} -qw \\ qu \end{pmatrix} + \begin{pmatrix} -g\sin\theta + T/\mathrm{m} \\ g\cos\theta \end{pmatrix} + \frac{\rho SV^2}{2\mathrm{m}} \left\{ \begin{pmatrix} \overline{C}_x(\cdot) \\ \overline{C}_z(\cdot) \end{pmatrix} + \begin{pmatrix} \overline{C}_x^{re}(\cdot) \\ \overline{C}_x^{re}(\cdot) \end{pmatrix} V + \begin{pmatrix} \overline{C}_x^{e}(\cdot) \\ \overline{C}_x^{e}(\cdot) \end{pmatrix} \eta \right\}$$

and

$$g(x,t) = \frac{\rho SV^2}{2\mathrm{m}} \left\{ \begin{pmatrix} \dfrac{C_{x,\delta 1}(\cdot)C_{M,\delta 2}(\cdot)}{C_{M,\delta 1}(\cdot)C_{\eta\delta 2} - C_{\eta\delta 1}C_{M,\delta 2}(\cdot)} \\ \dfrac{C_{z,\delta 1}(\cdot)C_{M,\delta 2}(\cdot) - C_{z,\delta 2}(\cdot)C_{M,\delta 1}(\cdot)}{C_{M,\delta 1}(\cdot)C_{\eta\delta 2} - C_{\eta\delta 1}C_{M,\delta 2}(\cdot)} \end{pmatrix} C_{\eta q} q + \right.$$

$$\left. \begin{pmatrix} -\dfrac{C_{x,\delta 1}(\cdot)C_{\eta\delta 2}}{C_{M,\delta 1}(\cdot)C_{\eta\delta 2} - C_{\eta\delta 1}C_{M,\delta 2}(\cdot)} C_{M,\dot{\eta}}(\cdot) + \dfrac{C_{x,\delta 1}(\cdot)C_{M,\delta 2}(\cdot)}{C_{M,\delta 1}(\cdot)C_{\eta\delta 2} - C_{\eta\delta 1}C_{M,\delta 2}(\cdot)} \overline{q} C_{\eta\dot{\eta}} \\ C_{z,\dot{\eta}}(\cdot) - \dfrac{C_{z,\delta 1}(\cdot)C_{\eta\delta 2} - C_{z,\delta 2}(\cdot)C_{\eta\delta 1}}{C_{M,\delta 1}(\cdot)C_{\eta\delta 2} - C_{\eta\delta 1}C_{M,\delta 2}(\cdot)} C_{M,\dot{\eta}}(\cdot) + \dfrac{\left(C_{z,\delta 1}C_{M,\delta 2} - C_{z,\delta 2}C_{M,\delta 1}\right)(\cdot)}{C_{M,\delta 1}(\cdot)C_{\eta\delta 2} - C_{\eta\delta 1}C_{M,\delta 2}(\cdot)} \overline{q} C_{\eta\dot{\eta}} \end{pmatrix} \dot{\eta} \right\}$$

$$+ \frac{m_\eta I_y}{\mathrm{m}\overline{c}} \begin{bmatrix} \dfrac{C_{x,\delta 1}(\cdot)C_{\eta\delta 2}}{m_\eta \left(C_{M,\delta 1}(\cdot)C_{\eta\delta 2} - C_{\eta\delta 1}C_{M,\delta 2}(\cdot)\right)} & \dfrac{-\overline{c}C_{x,\delta 1}(\cdot)C_{M,\delta 2}(\cdot)}{I_y \left(C_{M,\delta 1}(\cdot)C_{\eta\delta 2} - C_{\eta\delta 1}C_{M,\delta 2}(\cdot)\right)} \\ \dfrac{C_{z,\delta 1}(\cdot)C_{\eta\delta 2} - C_{z,\delta 2}(\cdot)C_{\eta\delta 1}}{m_\eta \left(C_{M,\delta 1}(\cdot)C_{\eta\delta 2} - C_{\eta\delta 1}C_{M,\delta 2}(\cdot)\right)} & \dfrac{\overline{c}\left(-C_{z,\delta 1}C_{M,\delta 2} + C_{z,\delta 2}C_{M,\delta 1}\right)(\cdot)}{I_y \left(C_{M,\delta 1}(\cdot)C_{\eta\delta 2} - C_{\eta\delta 1}C_{M,\delta 2}(\cdot)\right)} \end{bmatrix} \begin{pmatrix} \dot{q}^{des} \\ \ddot{\eta}^{des} \end{pmatrix}$$

So that as $t \to \infty$

$$f(x,t) \to f(x) = \begin{pmatrix} -g\sin\theta_{cmd} + T/\mathrm{m} \\ g\cos\theta_{cmd} \end{pmatrix} + \frac{\rho S V^2}{2\mathrm{m}} \left\{ \begin{pmatrix} \bar{C}_x(\cdot) \\ \bar{C}_z(\cdot) \end{pmatrix} + \begin{pmatrix} \bar{C}_x^{re}(\cdot) \\ \bar{C}_x^{re}(\cdot) \end{pmatrix} V + \begin{pmatrix} \bar{C}_x^{e}(\cdot) \\ \bar{C}_x^{e}(\cdot) \end{pmatrix} \eta_{cmd} \right\}$$

and

$$g(x,t) \to 0$$

6.8 Summary

The results of this chapter show how a complicated dynamical problem of establishing system stability reduces to checking algebraic conditions that are manageably complex. This is accomplished by reducing the determination of stability of an n-dimensional system to that of a two-dimensional one via a dynamic inversion controller. The resulting nonautonomous system is then reduced to its autonomous limiting system and the stability of the limiting system is established. The stability of the autonomous system is shown in two steps that produce vehicle specific conditions.

The established algebraic conditions provide an initial test that can guarantee global stability when applied to a real world problem that involves highly coupled flight and aeroelastic dynamics as well as an integrated flight/SMC control MIMO system. The initial approach is to simplify the problem, address the pitch axis dynamics with only a single mode and no actuator dynamics, and then assess the ramifications of aeroelasticity on the stability results. The role played by flexible dynamics is immediately apparent from consideration of the internal dynamics of the system. Furthermore, these flexible dynamics play a role in establishing stability guarantees for the closed loop system. While the analysis represents a somewhat idealized case, the insight provided has immediate real world application with respect to the influence of flexible dynamics on the system as a whole.

The results presented are the first to include flexible dynamics in stability analysis of dynamic inversion methodology. These form an initial basis to more complicated control problem formulation that includes a modified dynamic inversion methodology employed to design an integrated flight/SMC controller for a high fidelity model discussed earlier. The next step undertaken in the following chapter is to introduce the modified dynamic

inversion into the analysis performed here and then establish stability guarantees that are still possible with this complication.

Chapter 7 – Stability for Novel Dynamic Inversion

There is a need to make a connection between the case of standard dynamic inversion applied to a system with substantial rigid body/flexible mode interaction and novel dynamic inversion applied to a high fidelity model of highly flexible aircraft. In the former case, a global stability result is derived that imposes limitations on the relative magnitude of dynamic rigid/flexible body dynamics. In the latter case, the novel dynamic inversion is applied to a high fidelity dynamic model and achieves decoupling control results in the rigid body pitch loop while modifying the flexible dynamics without their cancellation. This case is too complicated to establish an analytically based stability result, which leaves only simulation to show stability of the controlled system. The goal of this chapter is to establish a link between these two cases, by utilizing the simplicity of the analytical model that still reflects the complexity of the rigid/flexible dynamic interactions and then introduce the fundamental changes of the modified dynamic inversion. The simplest model that still reflects the complexity of the rigid body / flexible mode interactions requiring an integrated flight/SMC control consists of longitudinal plus one flexible mode dynamics. This model structure has been used for most analytical analysis in this thesis and will again be employed throughout this chapter.

The stability analysis once again is based on the Lyapunov's method since it is the only mathematical framework available for a nonlinear system. The work discussed in Chapter 6 is based on the premise that determination of stability of an n-dimensional system is reduced to a 2-dimensional one. This is accomplished via a standard dynamic inversion controller that results in 2-dimensional internal dynamics. This dimensionality is what allows the use of special tools available in $\mathbf{R}^2$. The application of the novel dynamic inversion controller to the same system destroys the separation between controlled and internal dynamics (as shown in Chapter 4), thus removing the advantage of $\mathbf{R}^2$. The problem of establishing stability then reverts to use of a more general method for nonlinear systems – the construction of a Lyapunov function. Two methodologies are considered. One considers a candidate function similar to the one used in Chapter 6 to show boundedness, and the other uses algorithmic techniques to find a Lyapunov function.

7.1 Stability - Analytical

Assessing stability of the closed loop system with a filter in a flexible dynamics loop analytically is more complicated than might appear on the surface. The lack of separation between the internal dynamic states and those of the controlled variables precludes the use of analysis similar to those of Chapter 6. This leaves trying to find a Lyapunov function in a traditional way; which, as shown in Appendix E, results in constraints that are very difficult if not impossible to verify theoretically for a general case. The other approach explored in this chapter is to find a Lyapunov function algorithmically. A new tool, called SOSTOOLS, which has recently been developed at Caltech[51, 52] to perform precisely such function, is introduced and its applicability to a system of equations representing a flexible aircraft is investigated.

7.2 SOSTOOLS – Background

This section provides a brief overview of the underlying ideas that govern stability analysis using Sum of Squares tools[53]. For convenience, fundamental ideas about Lyapunov functions and the role they play in establishing stability for nonlinear systems are recalled. Then some concepts are introduced that utilize Sum of Squares decomposition to created a framework where an algorithmic computation of a Lyapunov function is feasible.

In 1892 A. M. Lyapunov developed a very powerful theorem that basically says if one can construct a function which is zero at the equilibrium, positive everywhere else, and whose time derivative along the system's trajectories is non-increasing the stability of the equilibrium point follows. This function resembles an energy function for a dynamical system since its minimum is at the equilibrium (the point of rest) and it is non-increasing as the system evolves from a state other than equilibrium. However, Lyapunov functions are far more general than simple energy functions. However, while providing a powerful analysis framework, one of its practical limitations is that no method is given to construct such a function. Total energy of a system is a good candidate but it has limitations such as total energy may not be known or the system analyzed is an approximation of a higher order system and there is no intuition as to what the structure of its energy function should look like.

Now the Lyapunov stability theorem, which serves as a basis for the SOSTOOLS analysis can be formally stated. Consider the equilibrium of interest of the system $\dot{x} = f(x)$ to be at the origin, *i.e.*, $f(0) = 0$. Then a Lyapunov function is given by the following theorem:

Lyapunov Theorem 7.3[34]: Let $x = 0$ be an equilibrium point for $\dot{x} = f(x)$ and $D \subset \mathbf{R}^n$ be a domain containing $x = 0$. Let $V : D \to \mathbf{R}$ be a continuously differentiable function, such that

$$V(0) = 0 \text{ and } V(x) > 0 \text{ in } D - \{0\} \tag{7.1}$$

$$\dot{V}(x) \le 0 \text{ in } D \tag{7.2}$$

Then, $x = 0$ is stable. Moreover, if

$$\dot{V}(x) < 0 \text{ in } D - \{0\} \tag{7.3}$$

then $x = 0$ is asymptotically stable.

Condition (7.1) is the positive definiteness condition on $V(x)$ and condition (7.2) is the negative semidefiniteness of its time derivative $\dot{V}(x)$.

Intuitively Theorem 7.3 can be explained by introducing a concept of a *Lyapunov surface* or *level set*, which is simply the surface $V(x) = c$, for some $c > 0$. For decreasing values of *c*, the level sets form nested regions that restrict the flow of the system to within their boundaries. The region *D* in the above theorem can be used to produce results that are not global in space. This is typically the case for systems, for example, that possess multiple equilibria. Region *D* defines the section of space around the equilibrium where the constructed Lyapunov function is valid. The construction of Lyapunov functions in some region of the equilibrium reveals estimates of its region of attraction, *i.e.,* the initial conditions that will lead to that equilibrium. In order to provide an estimate, the concept of level sets is introduced. A level set is simply the surface $V(x) = c$, for some $c > 0$. The condition $\dot{V}(x) \le 0$ implies that when a trajectory crosses a level set $V(x) = c$, it moves inside the set $\Omega_c = \{x \in \mathbf{R}^n \mid V(x) \le c\}$ and can never come out again. Hence, an estimate of the region of attraction is Ω_c, the maximal level

set of a Lyapunov function that can fit in *D*. The region *D* can be described fully by making use of inequality constraints in the state-space.

The framework that would encapsulate the inequality constraints using Lyapunov functions is the following. Consider the system

$$\dot{x} = f(x) \tag{7.4}$$

with the following constraints

$$a_{i_1}(x) \le 0, \qquad \text{for } i_1 = 1, \ldots, N_1 \tag{7.5}$$

Here $x \in \mathbf{R}^n$ is the state of the system. We assume that the a_{i_1}'s , are polynomial functions in *x*, and $f(x)$ is a vector polynomial or rational functions in *x* with no singularity in *D*, where $D \subset \mathbf{R}^n$ is defined as

$$D = \left\{ x \in \mathbf{R}^n \mid a_{i_1}(x) \le 0, \text{ for all } i_1 \right\}.$$

Without loss of generality, it is assumed that $f(x) = 0$ for $x = 0$. The following theorem is an extension of Lyapunov's stability theorem, and can be used to prove that the origin is a stable equilibrium of $\dot{x} = f(x)$. The inequality constraints (7.5) are adjoined to the corresponding Lyapunov conditions using a technique reminiscent of the well known S-procedure[54] in nonlinear and robust control theory.

Theorem 7.4[55]: Suppose that for the above system there exist polynomial functions $V(x)$, $w(x) > 0, p_i(x) \ge 0$ in D, such that $V(x)$ is positive definite in a neighborhood of the origin. Then

$$-w(x)\frac{\partial V}{\partial x} f(x) + \sum p_{i_1}(x) a_{i_1}(x) \ge 0 \tag{7.6}$$

will guarantee that the origin of the state space is a stable equilibrium of the system.

The proof of this can be found in Reference 55. In the case in which $f(x)$ is a rational vector field, the multiplier $w(x)$ should be chosen such that $w(x)\frac{\partial V}{\partial x} f(x)$ is a polynomial. Indeed, rational vector fields are very common, and the denominators do not

change sign as the system evolves; otherwise the vector field would be infinite at that point. The above framework is also ideal for robust stability analysis, etc.

Observe that the construction of Lyapunov functions involves constructing and testing positivity of a function. Testing polynomial nonnegativity is known to be NP-hard when the order of the polynomial is greater than or equal to 4[56]: given a polynomial, test that it takes nonnegative values for all values in the domain over which it is defined. This is an absolutely crucial element in using Lyapunov methods for nonlinear dynamical systems. In fact, there is no algorithm that will efficiently answer the question "Does this polynomial take only nonnegative values when evaluated at every point in its domain?" Altering the question to "Can this polynomial be expressed as a sum of other polynomials squared?", *i.e.*, trying to construct a *Sum of Squares* decomposition for it – finding other polynomials that squared and added together result in the original polynomial – *can* be solved efficiently. This idea is indeed the step that opened up the way to an algorithmic analysis of nonlinear systems. If a Sum of Squares decomposition is found, this implies that the polynomial is nonnegative. The converse is not true: there are polynomials that are nonnegative but for which there is no Sum of Squares decomposition. If the two were equivalent, then this would imply that P=NP. Thus, Lyapunov functions can now be constructed through the Sum of Squares decomposition algorithmically[51].

It is believed that the Sum of Square decomposition is an efficient and accurate *relaxation* of nonnegativity. But how does one compute the Sum of Squares decomposition? The following attempts to illustrate the algorithmic methodology. A multivariate polynomial $p(x_1,\ldots,x_n) \triangleq p(x)$ is a sum of squares (SOS), if there exist polynomials $f_1(x),\ldots, f_m(x)$ such that

$$p(x) = \sum_{i=1}^{m} f_i^2(x)$$

This in turn is equivalent to the existence of a positive semidefinite matrix Q[51], and a properly chosen vector of monomials $Z(x)$ such that

$$p(x) = Z(x)^T QZ(x).$$

Finding Q can now be cast as a Semidefinite Program SDP[54], which uses an algorithm with a worst-case polynomial time complexity. The conversion of the question "Does there exist a Sum of Squares decomposition for $p(x)$?" to the question "Does there exist a matrix Q?" is done automatically using SOSTOOLS[51], which solves the Semidefinite Program using SeDuJMi[57], a semidefinite programming solver. The details of the conversion are abstracted from the user, who only has to work at the polynomial formulation level.

The challenge now lies in how the conditions in Theorem 7.4 can be verified algorithmically. To this end, advantage can be taken of the computational tractability of the Sum of Squares decomposition in order to avoid the NP hardness of testing that a polynomial function is positive definite or positive semidefinite. It has already been stressed that the condition $p(x)$ is a sum of squares is stricter, yet more verifiable, than $p(x) \geq 0$. Therefore, by deliberately choosing to work with polynomial and rational functions, the positive definite conditions in Theorem 7.4 can be relaxed to the existence of SOS decomposition, and the problem can be cast as an SOS program[52]. Under this relaxation, the search for a bounded degree Lyapunov function $V(x)$ and multipliers $p_{i_1}(x)$ can be efficiently performed. The SOS program can therefore be formulated as follows.

Program: Suppose that we are given the system (7.4-7.5). For a polynomial function $W(x)$ with a predetermined form that is locally positive definite, find bounded degree polynomials $V(x)$ and $p_{i_1}(x)$'s

1. $V(x) - W(x)$ is sum of squares (implying ≥ 0,
2. The left-hand side of inequality (7.5) is a sum of squares,
3. $p_{i_1}(x)$ are sums of squares.

In this SOS program, Condition 2 is a computational relaxation of inequality (7.5) in Theorem 7.4, whereas Condition 1 is required to impose strict positive definiteness on $V(x)$, as required by Theorem 7.4. Using $W(x)$ restricts $V(x)$ to be positive definite, or

at least have a local minimum at the origin. $W(x)$ may be parameterized by some decision variables, on which restrictions may be applied to render it positive definite.

If such a $V(x)$ that fulfills the required conditions is not found, one of higher order will be sought. Failure to find a Lyapunov function does not necessarily mean that the equilibrium is unstable, as all the above conditions are sufficient.

The next section presents an attempt to use Sum of Squares techniques outlined above to analyze coupled longitudinal/flexible dynamics of a highly flexible aircraft.

7.3 Model for SOSTOOLS

The novel dynamic inversion is applied to the aircraft longitudinal dynamics as described in Chapter 4.6.2. In terms of specific aerodynamic force and moment coefficients nonlinear closed loop system (4.31) becomes

$$\begin{pmatrix} \dot{u} \\ \dot{w} \\ \dot{q} \\ \dot{\theta} \\ \ddot{\eta} \\ \dot{\eta} \\ \dot{x}_f \end{pmatrix} = \begin{pmatrix} -qw - g\sin\theta + \dfrac{T}{m} \\ qu + g\cos\theta \\ 0 \\ q \\ \dfrac{-2\zeta\omega\dot{\eta} - \omega^2\eta}{m_\eta} \\ \dot{\eta} \\ 0 \end{pmatrix} + \frac{\rho S V^2}{2} \left\{ \begin{pmatrix} \dfrac{1}{m}\left(C_x + C_{x,\eta}\eta + C_{x,\dot{\eta}}\dot{\eta}\right)(\alpha) \\ \dfrac{1}{m}\left(C_z + C_{z,\eta}\eta + C_{z,\dot{\eta}}\dot{\eta}\right)(\alpha) \\ \dfrac{\bar{c}}{I_y}\left(C_M + C_{M,\eta}\eta + C_{M,\dot{\eta}}\dot{\eta}\right)(\alpha) \\ 0 \\ \dfrac{1}{m_\eta}\left(\bar{q}C_{\eta\eta}\eta + \bar{q}C_{\eta\dot{\eta}}\dot{\eta}\right) \\ 0 \\ 0 \end{pmatrix} + \begin{bmatrix} 0 & 0 & 0 \\ 0 & 0 & 0 \\ 0 & 0 & 0 \\ 0 & 0 & 0 \\ \dfrac{C_{\eta u}}{m_\eta} & \dfrac{C_{\eta w}}{m_\eta} & \dfrac{C_{\eta q}}{m_\eta} \\ 0 & 0 & 0 \\ 0 & 0 & 0 \end{bmatrix} \begin{pmatrix} u \\ w \\ q \end{pmatrix} \right\} +$$

$$
\begin{pmatrix}
\frac{1}{2}\rho SV^2\frac{1}{m}\frac{C_{x,\delta_1}(\alpha)C_{\eta,\delta 2}}{\left(C_{M,\delta_1}(\alpha)C_{\eta,\delta 2}-C_{\eta,\delta_1}C_{M,\delta 2}(\alpha)\right)}\left(C_M(\alpha)+C_{M,\eta}(\alpha)\eta+C_{M,\dot{\eta}}(\alpha)\dot{\eta}\right)+ \\
\frac{\frac{\phi'}{m}C_{x,\delta_1}(\alpha)C_{\eta,\delta 2}}{\frac{\bar{c}}{I_y}\left(C_{M,\delta_1}(\alpha)C_{\eta,\delta 2}-C_{\eta,\delta_1}C_{M,\delta 2}(\alpha)\right)}\left(\begin{array}{l}\frac{\rho SV^2}{2}\left(\frac{\bar{q}C_{\eta\eta}\eta+\bar{q}C_{\eta\dot{\eta}}\dot{\eta}+C_{\eta u}u+C_{\eta w}w+C_{\eta q}q}{m_\eta}\right) \\ +\frac{-2\zeta\omega\dot{\eta}-\omega^2\eta}{m_\eta}\end{array}\right) \\
\frac{\rho SV^2}{2m}\frac{\left(C_{z,\delta_1}(\alpha)C_{\eta,\delta 2}-C_{z,\delta_2}(\alpha)C_{\eta,\delta_1}\right)}{\left(C_{M,\delta_1}(\alpha)C_{\eta,\delta 2}-C_{\eta,\delta_1}C_{M,\delta 2}(\alpha)\right)}\left(C_M(\alpha)+C_{M,\eta}(\alpha)\eta+C_{M,\dot{\eta}}(\alpha)\dot{\eta}\right)+ \\
\frac{\frac{\phi'}{m}\frac{1}{m}\left(C_{z,\delta_1}(\alpha)C_{\eta,\delta 2}-C_{z,\delta_2}(\alpha)C_{\eta,\delta_1}\right)}{\frac{\bar{c}}{I_y}\left(C_{M,\delta_1}(\alpha)C_{\eta,\delta 2}-C_{\eta,\delta_1}C_{M,\delta 2}(\alpha)\right)}\left(\begin{array}{l}\frac{\rho SV^2}{2}\left(\frac{\bar{q}C_{\eta\eta}\eta+\bar{q}C_{\eta\dot{\eta}}\dot{\eta}+C_{\eta u}u+C_{\eta w}w+C_{\eta q}q}{m_\eta}\right) \\ +\frac{-2\zeta\omega\dot{\eta}-\omega^2\eta}{m_\eta}\end{array}\right) \\
-\phi'\frac{1}{m_\eta}\left(-2\zeta\omega\dot{\eta}-\omega^2\eta+\frac{1}{2}\rho SV^2\left(\bar{q}C_{\eta\eta}\eta+\bar{q}C_{\eta\dot{\eta}}\dot{\eta}+C_{\eta u}u+C_{\eta w}w+C_{\eta q}q\right)\right) \\
0 \\
0 \\
0 \\
b_f\Delta\phi'\frac{1}{m_\eta}\left(-2\zeta\omega\dot{\eta}-\omega^2\eta+\frac{1}{2}\rho SV^2\left(\bar{q}C_{\eta\eta}\eta+\bar{q}C_{\eta\dot{\eta}}\dot{\eta}+C_{\eta u}u+C_{\eta w}w+C_{\eta q}q\right)\right)
\end{pmatrix}
$$

$$
+\begin{pmatrix}
\dfrac{1}{\Delta\phi'}\dfrac{1}{m}\dfrac{-C_{x,\delta_1}(\alpha)\left(\dfrac{\bar{c}}{I_y}C_{M,\delta 2}(\alpha)+\dfrac{\phi'}{m_\eta}C_{\eta,\delta 2}\right)}{\dfrac{\bar{c}}{I_y}\dfrac{1}{m_\eta}\left(C_{M,\delta_1}(\alpha)C_{\eta,\delta 2}-C_{\eta,\delta_1}C_{M,\delta 2}(\alpha)\right)} \\
\dfrac{1}{\Delta\phi'}\dfrac{1}{m}\dfrac{-C_{z,\delta_1}(\alpha)\left(\dfrac{\bar{c}}{I_y}C_{M,\delta 2}(\alpha)+\dfrac{\phi'}{m_\eta}C_{\eta,\delta 2}\right)+C_{z,\delta_2}(\alpha)\left(\dfrac{\bar{c}}{I_y}C_{M,\delta_1}(\alpha)+\dfrac{\phi'}{m_\eta}C_{\eta,\delta_1}\right)}{\dfrac{\bar{c}}{I_y}\dfrac{1}{m_\eta}\left(C_{M,\delta_1}(\alpha)C_{\eta,\delta 2}-C_{\eta,\delta_1}C_{M,\delta 2}(\alpha)\right)} \\
-\dfrac{\phi'}{\Delta\phi'} \\
0 \\
\dfrac{1}{\Delta\phi'} \\
0 \\
A_f
\end{pmatrix} x_f
$$

$$
+\begin{pmatrix}
\dfrac{\dfrac{1}{m}C_{x,\delta_1}(\alpha)C_{\eta,\delta 2}}{\dfrac{\bar{c}}{I_y}\left(C_{M,\delta_1}(\alpha)C_{\eta,\delta 2}-C_{\eta,\delta_1}C_{M,\delta 2}(\alpha)\right)}\dot{y}_1^{des} \\
\dfrac{\dfrac{1}{m}\left(C_{z,\delta_1}(\alpha)C_{\eta,\delta 2}-C_{z,\delta_2}(\alpha)C_{\eta,\delta_1}\right)}{\dfrac{\bar{c}}{I_y}\left(C_{M,\delta_1}(\alpha)C_{\eta,\delta 2}-C_{\eta,\delta_1}C_{M,\delta 2}(\alpha)\right)}\dot{y}_1^{des} \\
\dot{y}_1^{des} \\
0 \\
0 \\
b_f\dot{y}_2^{des}
\end{pmatrix}
\tag{7.7}
$$

If the force and moment coefficients in the equations of motion can be written explicitly in terms of state variables, then the stability of the closed loop can be checked via a Lyapunov function. Typically force and moment coefficients are calculated as a

function of Mach and α, which require a conversion of (7.7) into polar coordinates, (V,α). The flexible dynamics model can assume one of two forms - m_η is either absorbed into the coefficients or is $m_\eta = 1$ by model development definition. The numbers used for the model are based on the later. Taking into consideration the linear nature of the flexible dynamics model, the elastic coefficients become

$$Z_\eta = \frac{1}{2}\rho SV^2 C_{z,\eta}(\alpha) \qquad Z_{\dot\eta} = \frac{1}{2}\rho SV^2 C_{z,\dot\eta}(\alpha)$$

$$M_\eta = \frac{1}{2}\rho SV^2 \bar{c} C_{M,\eta}(\alpha) \qquad M_{\dot\eta} = \frac{1}{2}\rho SV^2 \bar{c} C_{M,\dot\eta}(\alpha)$$

$$E_\eta = \frac{1}{2}\rho SV^2 \bar{q} C_{\eta\eta} - \omega^2 \qquad E_{\dot\eta} = \frac{1}{2}\rho SV^2 \bar{q} C_{\eta\dot\eta} - 2\zeta\omega$$

$$E_u u + E_w w + E_q q = \frac{1}{2}\rho SV^2 \left(C_{\eta u} u + C_{\eta w} w + C_{\eta q} q\right)$$

$$E_{\delta 1} = \frac{1}{2}\rho SV^2 C_{\eta\delta 1} \qquad E_{\delta 2} = \frac{1}{2}\rho SV^2 C_{\eta\delta 2}$$

that makes (7.7) assume the linear-nonlinear hybrid system form

$$\begin{pmatrix} \dot{u} \\ \dot{w} \\ \dot{q} \\ \dot{\theta} \\ \ddot{\eta} \\ \dot{\eta} \\ \dot{x}_f \end{pmatrix} = \begin{pmatrix} -qw - g\sin\theta + \dfrac{T}{m} \\ qu + g\cos\theta \\ 0 \\ q \\ 0 \\ \dot{\eta} \\ 0 \end{pmatrix} + \frac{1}{2m}\rho SV^2 \begin{pmatrix} C_x(\alpha) - \dfrac{-C_{x,\delta_1}(\alpha)E_{\delta 2}}{\left(C_{M,\delta_1}(\alpha)E_{\delta 2} - E_{\delta_1}C_{M,\delta 2}(\alpha)\right)}C_M(\alpha) \\ C_z(\alpha) - \dfrac{\left(C_{z,\delta_1}(\alpha)E_{\eta 2} - C_{z,\delta_2}(\alpha)E_{\delta_1}\right)}{\left(C_{M,\delta_1}(\alpha)E_{\delta 2} - E_{\delta_1}C_{M,\delta 2}(\alpha)\right)}C_M(\alpha) \\ 0 \\ 0 \\ 0 \\ 0 \\ 0 \end{pmatrix}$$

$$+\frac{1}{m}\begin{pmatrix} \left(X_\eta\eta + X_{\dot\eta}\dot\eta\right) - \dfrac{C_{x,\delta_1}(\alpha)E_{\delta 2}}{\overline{c}\left(C_{M,\delta_1}(\alpha)E_{\delta 2} - E_{\delta_1}C_{M,\delta 2}(\alpha)\right)}\left(M_\eta\eta + M_{\dot\eta}\dot\eta\right) \\ \left(Z_\eta\eta + Z_{\dot\eta}\dot\eta\right) - \dfrac{\left(C_{z,\delta_1}(\alpha)E_{\eta 2} - C_{z,\delta_2}(\alpha)E_{\delta_1}\right)}{\overline{c}\left(C_{M,\delta_1}(\alpha)E_{\delta 2} - E_{\delta_1}C_{M,\delta 2}(\alpha)\right)}\left(M_\eta\eta + M_{\dot\eta}\dot\eta\right) \\ 0 \\ 0 \\ 0 \\ 0 \\ 0 \end{pmatrix}$$

$$+\begin{pmatrix} -\dfrac{\phi'}{m}\dfrac{I_y}{\overline{c}}\dfrac{C_{x,\delta_1}(\alpha)E_{\delta 2}}{\left(C_{M,\delta_1}(\alpha)E_{\delta 2} - E_{\delta_1}C_{M,\delta 2}(\alpha)\right)}\left(E_\eta\eta + E_{\dot\eta}\dot\eta + E_u u + E_w w + E_q q\right) \\ -\dfrac{\phi'}{m}\dfrac{I_y}{\overline{c}}\dfrac{\left(C_{z,\delta_1}(\alpha)E_{\eta 2} - C_{z,\delta_2}(\alpha)E_{\delta_1}\right)}{\left(C_{M,\delta_1}(\alpha)E_{\delta 2} - E_{\delta_1}C_{M,\delta 2}(\alpha)\right)}\left(E_\eta\eta + E_{\dot\eta}\dot\eta + E_u u + E_w w + E_q q\right) \\ -\phi'\left(E_\eta\eta + E_{\dot\eta}\dot\eta + E_u u + E_w w + E_q q\right) \\ 0 \\ \left(E_\eta\eta + E_{\dot\eta}\dot\eta + E_u u + E_w w + E_q q\right) \\ 0 \\ b_f\Delta\phi'\left(E_\eta\eta + E_{\dot\eta}\dot\eta + E_u u + E_w w + E_q q\right) \end{pmatrix}$$

$$\begin{pmatrix} \frac{\rho SV^2}{2\Delta\phi' m}\frac{-C_{x,\delta_1}(\alpha)C_{M,\delta 2}(\alpha)}{\left(C_{M,\delta_1}(\alpha)E_{\delta 2}-E_{\delta_1}C_{M,\delta 2}(\alpha)\right)}+\frac{\phi'}{\Delta\phi' m}\frac{I_y}{\bar{c}}\frac{-C_{x,\delta_1}(\alpha)E_{\delta 2}}{\left(C_{M,\delta_1}(\alpha)E_{\delta 2}-E_{\delta_1}C_{M,\delta 2}(\alpha)\right)} \\ \frac{\rho SV^2}{2\Delta\phi' m}\frac{\left(-C_{z,\delta_1}C_{M,\delta 2}+C_{z,\delta_2}C_{M,\delta_1}\right)(\alpha)}{\left(C_{M,\delta_1}(\alpha)E_{\delta 2}-E_{\delta_1}C_{M,\delta 2}(\alpha)\right)}+\frac{\phi'}{\Delta\phi' m}\frac{I_y}{\bar{c}}\frac{-C_{z,\delta_1}(\alpha)E_{\delta 2}+C_{z,\delta_2}(\alpha)E_{\delta_1}}{\left(C_{M,\delta_1}(\alpha)E_{\delta 2}-E_{\delta_1}C_{M,\delta 2}(\alpha)\right)} \\ -\frac{\phi'}{\Delta\phi'} \\ 0 \\ \frac{1}{\Delta\phi'} \\ 0 \\ A_f \end{pmatrix} x_f$$

$$+\begin{pmatrix} \frac{1}{m}\frac{I_y}{\bar{c}}\frac{C_{x,\delta_1}(\alpha)E_{\delta 2}}{\left(C_{M,\delta_1}(\alpha)E_{\delta 2}-E_{\delta_1}C_{M,\delta 2}(\alpha)\right)}\dot{y}_1^{des} \\ \frac{1}{m}\frac{I_y}{\bar{c}}\frac{\left(C_{z,\delta_1}(\alpha)E_{\delta 2}-C_{z,\delta_2}(\alpha)E_{\delta_1}\right)}{\left(C_{M,\delta_1}(\alpha)E_{\delta 2}-E_{\delta_1}C_{M,\delta 2}(\alpha)\right)}\dot{y}_1^{des} \\ \dot{y}_1^{des} \\ 0 \\ 0 \\ 0 \\ b_f\dot{y}_2^{des} \end{pmatrix}$$

Converting these equations into polar coordinates produces

$$\begin{pmatrix} \dot{V} \\ \dot{\alpha} \\ \dot{q} \\ \dot{\theta} \\ \ddot{\eta} \\ \dot{\eta} \\ \dot{x}_f \end{pmatrix} = \frac{1}{2}\rho S V^2 \frac{1}{m} \begin{pmatrix} -C_D + \dfrac{C_{D,\delta_1} E_{\delta 2} - \left(\cos\alpha \sin\alpha C_{L,\delta_2} + \sin^2\alpha\, C_{D,\delta_2}\right) E_{\delta_1}}{\left(C_{M,\delta_1}(\alpha) E_{\delta 2} - E_{\delta_1} C_{M,\delta 2}(\alpha)\right)} C_M(\alpha) \\ -\dfrac{1}{V} C_L + \dfrac{1}{V} \dfrac{C_{L,\delta_1} E_{\delta 2} - \left(\cos^2\alpha\, C_{L,\delta_2} + \cos\alpha \sin\alpha\, C_{D,\delta_2}\right) E_{\delta_1}}{\left(C_{M,\delta_1}(\alpha) E_{\delta 2} - E_{\delta_1} C_{M,\delta 2}(\alpha)\right)} C_M(\alpha) \\ 0 \\ 0 \\ 0 \\ 0 \\ 0 \end{pmatrix}$$

$$+ \frac{1}{m} \begin{pmatrix} \left(X_\eta \cos\alpha + Z_\eta \sin\alpha\right)\eta + \left(X_{\dot\eta} \cos\alpha + Z_{\dot\eta} \sin\alpha\right)\dot\eta \\ + \dfrac{C_{D,\delta_1} E_{\delta 2} - \left(\cos\alpha \sin\alpha C_{L,\delta_2} + \sin^2\alpha\, C_{D,\delta_2}\right) E_{\delta_1}}{\bar{c}\left(C_{M,\delta_1}(\alpha) E_{\delta 2} - E_{\delta_1} C_{M,\delta 2}(\alpha)\right)} \left(M_\eta \eta + M_{\dot\eta} \dot\eta\right) \\ \left(-X_\eta \dfrac{\sin\alpha}{V} + Z_\eta \dfrac{\cos\alpha}{V}\right)\eta + \left(-X_{\dot\eta} \dfrac{\sin\alpha}{V} + Z_{\dot\eta} \dfrac{\cos\alpha}{V}\right)\dot\eta \\ + \dfrac{1}{V} \dfrac{C_{L,\delta_1} E_{\delta 2} - \left(\cos^2\alpha\, C_{L,\delta_2} + \cos\alpha \sin\alpha\, C_{D,\delta_2}\right) E_{\delta_1}}{\bar{c}\left(C_{M,\delta_1}(\alpha) E_{\delta 2} - E_{\delta_1} C_{M,\delta 2}(\alpha)\right)} \left(M_\eta \eta + M_{\dot\eta} \dot\eta\right) \\ 0 \\ 0 \\ 0 \\ 0 \\ 0 \end{pmatrix}$$

$$+ \begin{pmatrix} -g \sin\left(\theta - \alpha\right) + \dfrac{T}{m} \cos\alpha \\ q + \dfrac{1}{V} g \cos\left(\theta - \alpha\right) - \sin\alpha \dfrac{T}{m} \dfrac{1}{V} \\ 0 \\ q \\ 0 \\ \dot\eta \\ 0 \end{pmatrix} +$$

$$
\begin{pmatrix}
\dfrac{\phi'}{m}\dfrac{I_y}{\bar{c}}\dfrac{C_{D,\delta_1}E_{\delta 2}-\left(\cos\alpha\sin\alpha C_{L,\delta_2}+\sin^2\alpha\, C_{D,\delta_2}\right)E_{\delta_1}}{\left(C_{M,\delta_1}(\alpha)E_{\delta 2}-E_{\delta_1}C_{M,\delta 2}(\alpha)\right)}\left(E_u u+E_w w+E_q q+E_\eta \eta+E_{\dot\eta}\dot\eta\right)\\
\dfrac{1}{V}\dfrac{\phi'}{m}\dfrac{I_y}{\bar{c}}\dfrac{C_{L,\delta_1}E_{\delta 2}-\left(\cos^2\alpha\, C_{L,\delta_2}+\cos\alpha\sin\alpha\, C_{D,\delta_2}\right)E_{\delta_1}}{\left(C_{M,\delta_1}(\alpha)E_{\delta 2}-E_{\delta_1}C_{M,\delta 2}(\alpha)\right)}\left(E_u u+E_w w+E_q q+E_\eta \eta+E_{\dot\eta}\dot\eta\right)\\
-\phi'\left(E_u u+E_w w+E_q q+E_\eta \eta+E_{\dot\eta}\dot\eta\right)\\
0\\
\left(E_u u+E_w w+E_q q+E_\eta \eta+E_{\dot\eta}\dot\eta\right)\\
0\\
b_f\Delta\phi'\left(E_u u+E_w w+E_q q+E_\eta \eta+E_{\dot\eta}\dot\eta\right)
\end{pmatrix}
$$

$$
+\begin{pmatrix}
\dfrac{1}{\Delta\phi' m}\left(\dfrac{\rho SV^2}{2}\dfrac{C_{D,\delta_1}(\alpha)C_{M,\delta 2}(\alpha)-\left(\sin\alpha\cos\alpha C_{L,\delta_2}+\sin^2\alpha C_{D,\delta_2}\right)(\alpha)C_{M,\delta_1}(\alpha)}{\left(C_{M,\delta_1}(\alpha)E_{\delta 2}-E_{\delta_1}C_{M,\delta 2}(\alpha)\right)}\right.\\
\left.+\dfrac{\phi' I_y}{\bar{c}}\dfrac{C_{D,\delta_1}(\alpha)E_{\delta 2}+\left(\sin\alpha\cos\alpha C_{L,\delta_2}(\alpha)+\sin^2\alpha C_{D,\delta_2}(\alpha)\right)E_{\delta_1}}{\left(C_{M,\delta_1}(\alpha)E_{\delta 2}-E_{\delta_1}C_{M,\delta 2}(\alpha)\right)}\right)\\
\dfrac{1}{V\Delta\phi' m}\left(\dfrac{\rho SV^2}{2}\dfrac{C_{L,\delta_1}(\alpha)C_{M,\delta 2}(\alpha)-\left(\cos^2\alpha C_{L,\delta_2}+\cos\alpha\sin\alpha C_{D,\delta_2}\right)(\alpha)C_{M,\delta_1}(\alpha)}{\left(C_{M,\delta_1}(\alpha)E_{\delta 2}-E_{\delta_1}C_{M,\delta 2}(\alpha)\right)}\right.\\
\left.+\dfrac{\phi' I_y}{\bar{c}}\dfrac{C_{L,\delta_1}(\alpha)E_{\delta 2}-\left(\cos^2\alpha C_{L,\delta_2}+\cos\alpha\sin\alpha C_{D,\delta_2}\right)(\alpha)E_{\delta_1}}{\left(C_{M,\delta_1}(\alpha)E_{\delta 2}-E_{\delta_1}C_{M,\delta 2}(\alpha)\right)}\right)\\
-\dfrac{\phi'}{\Delta\phi'}\\
0\\
\dfrac{1}{\Delta\phi'}\\
0\\
A_f
\end{pmatrix}x_f
$$

$$+\begin{pmatrix} \dfrac{1}{m}\dfrac{I_y}{\bar{c}}\dfrac{-C_{D,\delta_1}(\alpha)E_{\delta 2}+\left(\sin\alpha\cos\alpha C_{L,\delta_2}(\alpha)+\sin^2\alpha C_{D,\delta_2}(\alpha)\right)E_{\delta_1}}{\left(C_{M,\delta_1}(\alpha)E_{\delta 2}-E_{\delta_1}C_{M,\delta 2}(\alpha)\right)} \\ \dfrac{1}{V}\dfrac{1}{m}\dfrac{I_y}{\bar{c}}\left(\dfrac{-C_{L,\delta_1}(\alpha)E_{\delta 2}+\left(\cos^2\alpha C_{L,\delta_2}(\alpha)+\cos\alpha\sin\alpha C_{D,\delta_2}(\alpha)\right)E_{\delta_1}}{\left(C_{M,\delta_1}(\alpha)E_{\delta 2}-E_{\delta_1}C_{M,\delta 2}(\alpha)\right)}\right)\dot{y}_1^{des} \\ \dot{y}_1^{des} \\ 0 \\ 0 \\ 0 \\ b_f\dot{y}_2^{des} \end{pmatrix} \tag{7.8}$$

Choosing worse case flexible dynamic interaction, which is a light aircraft at the end of cruise and low altitude (increased dynamic pressure). This assumption provides the following constant values in the equations

$$I_y = 43953900.0 \quad \bar{c} = 86.023 \quad \phi' = 0.1673$$

$$\frac{1}{m} = 2.5995e^{-6} \quad \frac{1}{2}\rho S = 8.1939 \quad \Delta\phi' = -0.5430$$

$$A_f = -10 \quad b_f = 10$$

with the filter given as

$$\begin{aligned} \dot{x}_f &= A_f x_f + \begin{bmatrix} 0 & b_f \end{bmatrix}\begin{pmatrix} \bar{u}_1 \\ \bar{u}_2 \end{pmatrix} \\ y_f &= \begin{bmatrix} 0 \\ 1 \end{bmatrix} x_f + \begin{bmatrix} 1 & 0 \\ 0 & 0 \end{bmatrix}\begin{pmatrix} \bar{u}_1 \\ \bar{u}_2 \end{pmatrix} \end{aligned} \Rightarrow \begin{aligned} \dot{x}_f &= -10x_f + \begin{bmatrix} 0 & 10 \end{bmatrix}\begin{pmatrix} \bar{u}_1 \\ \bar{u}_2 \end{pmatrix} \\ y_f &= \begin{bmatrix} 0 \\ 1 \end{bmatrix} x_f + \begin{bmatrix} 1 & 0 \\ 0 & 0 \end{bmatrix}\begin{pmatrix} \bar{u}_1 \\ \bar{u}_2 \end{pmatrix} \end{aligned}$$

and desired dynamics as

$$\begin{aligned} \begin{pmatrix} \dot{y}_1^{des} \\ \dot{y}_2^{des} \end{pmatrix} &= \begin{pmatrix} k1\left(q_{cmd}-q\right)+k2\left(\int q_{cmd}-\theta\right) \\ k3\left(\dot{\eta}_{cmd}-\Delta\phi'\dot{\eta}\right)+k4\int\left(\dot{\eta}_{cmd}-\Delta\phi'\dot{\eta}\right) \end{pmatrix} \\ &= \begin{pmatrix} 3.6\left(q_{cmd}-q\right)+10\left(\theta_{cmd}-\theta\right) \\ 10\left(\dot{\eta}_{cmd}-\Delta\phi'\dot{\eta}\right)+100\left(\eta_{cmd}-\Delta\phi'\eta\right) \end{pmatrix} \end{aligned}$$

In the absence of sensed variables, *i.e.*, without the full simulation, and for the purposes of analytical analysis, the state feedback variables that approximate the measured ones can be used. The polynomial coefficient equations are

$$
\begin{aligned}
C_D &= 0.0595 + 8.6325e^{-4}\alpha - 1.2877e^{-4}\alpha^2 \\
C_L &= 0.2976 + 0.0984\alpha - 4.8342e^{-4}\alpha^2 \\
C_M &= 0.2533 - 0.0011\alpha - 2.7070e^{-5}\alpha^2 \\
C_{D,\delta_1} &= 5.9718e^{-5}\delta_1 + 2.0928e^{-4}\delta_1\alpha + 1.2170e^{-4}\delta_1^2 - 2.8589e^{-7}\delta_1^2\alpha \\
C_{L,\delta_1} &= -6.1452e^{-3} + 0.0111\delta_1 - 8.0998e^{-6}\delta_1\alpha - 1.9860e^{-5}\delta_1^2 \\
C_{M,\delta_1} &= -0.5895 \\
E_{\ddot{\eta},\delta_1} &= -7.7607 \\
C_{D,\delta_2} &= -3.4321e^{-6}\delta_2 - 1.2028e^{-5}\delta_2\alpha - 6.9943e^{-6}\delta_2^2 + 1.6430e^{-8}\delta_2^2\alpha \\
C_{L,\delta_2} &= 3.5317e^{-4} - 6.3793e^{-4}\delta_2 + 4.6551e^{-7}\delta_2\alpha + 1.1414e^{-6}\delta_2^2 \\
C_{M,\delta_2} &= 0.0334 \\
E_{\ddot{\eta},\delta_2} &= -0.4240
\end{aligned}
$$

where $e^x \triangleq 10^x$ for convenience.

The trim condition is level flight at Mach = 0.24 and altitude of 1000 ft (see Fig. 7.1). All the state variables are allowed to vary within the constraint of the relationship of $\alpha \approx \theta$ for level flight while the initial conditions are set from the complete model trim at this condition (all accelerations and angular velocities are zero). The initial value for η

Mach	0.24
Altitude	1000 ft
Mass	384,862 lbs

Trim variables	Resultant values for level flight trim
$q,\ \dot{\eta}$	0
theta	7.5846 deg
alpha	7.6668 deg
η	-0.8458

Figure 7.1: Trim Conditions.

should be maintained since it has very little bearing in steady state on the aerodynamic forces and moments. The system is trimmed in open loop and then is checked for closed loop with commanded variables $(q_{cmd}, \theta_{cmd}, \dot{\eta}_{cmd}, \eta_{cmd}) = (q_0, \theta_0, \dot{\eta}_0, \eta_0)$. Once nontrim commands are applied the system moves from level flight and is no longer in static

equilibrium. It is the stability of this new dynamic status of the system that SOSTOOLS is attempting to establish.

One point of note about trim is that the condition of interest is at the section of the flight envelope where the aircraft has very poor Lift characteristics, *i.e.*, high speed aircraft operating at very low speed. Since the model used is a simplified representation that does not have all the surfaces that provide additional Lift, the model could not be trimmed for reasonable values of angle of attack at the speed and thrust of the full nonlinear simulation. The speed and thrust were allowed to change their value considerably to achieve trim, but the qualitative sensitivity of the aircraft to these variables from high fidelity simulation has been retained. So the model while not a precise replica of the high fidelity dynamic response, nevertheless maintains the same qualitative characteristics both in time response and linearized system eigenvalues as the high fidelity aircraft.

Combining the trim values and polynomial expressions for aerodynamic force and moment coefficients with the system given by (7.8) results in a model used by SOSTOOLS for stability analysis.

7.4 SOSTOOLS Stability Analysis Results

Nonlinear system in analytic form was initially evaluated for stability by taking the Jacobian at trim condition specified in the above section and evaluating the eigenvalues for a range of command parameters $\left(q_{cmd}, \theta_{cmd}\right)$. The region where the linearized form of the system in (7.8) is stable is illustrated in Figure 7.2.

In order to apply the SOSTOOLS the system equilibrium was translated to the origin and the variables were appropriately rescaled using $x = x_o(x+1)$ variable substitution, with x_o trim value (equilibrium) and $\bar{x}$ the new normalized state. The rescaling of the translated state is done to improve the numerical condition of the problem. This transformation cannot be applied if $x_o = 0$, which occurs in level flight for q and $\dot{\eta}$ states. In this, no translation to the origin is necessary and the rescaling, if any, uses an appropriate value.

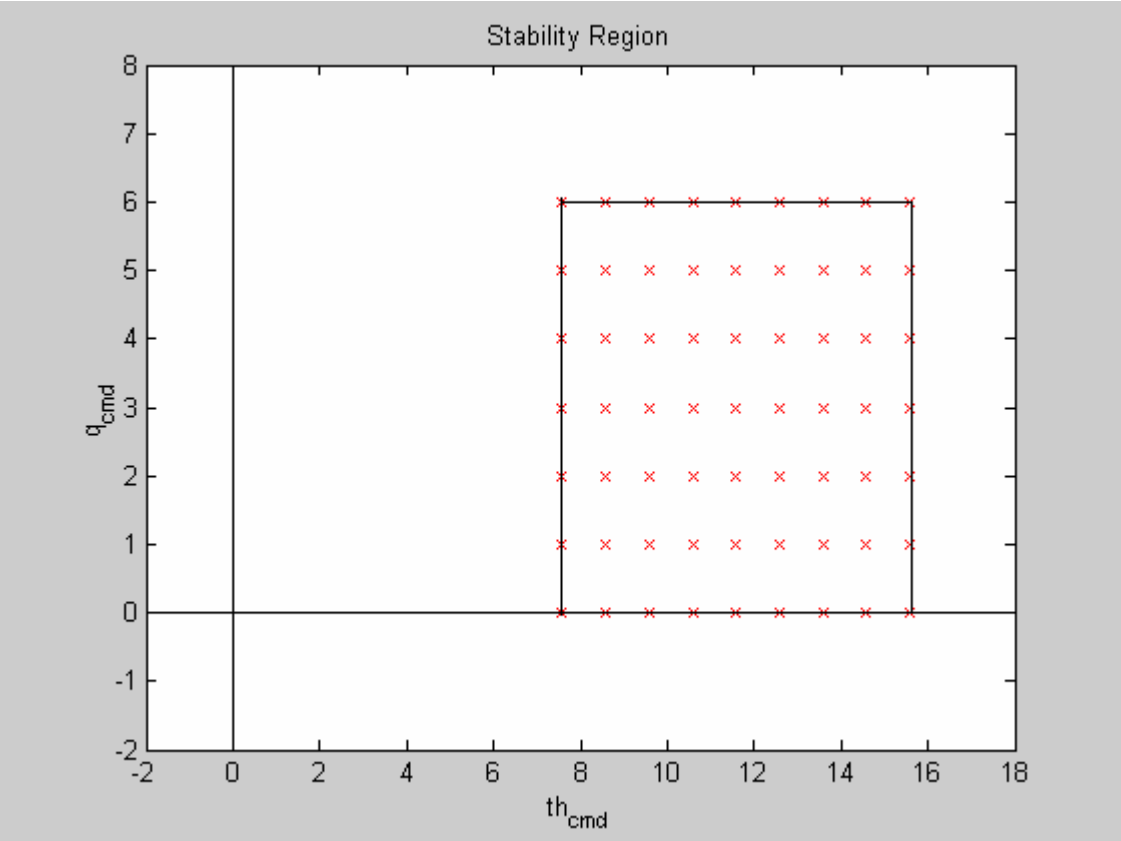

Figure 7.2: Stability region of (7.8) for variation in control command parameters (q_{cmd}, θ_{cmd}).

The translated and normalized version of the nonlinear system (7.8) can now be analyzed using SOSTOOLS. Even though the vector field is rational, the framework of Theorem 7.4 can be used with polynomial $w(x)$ defined as the least common multiple of the denominators in the vector field.

The region D defined in Lyapunov's Stability Theorem 7.3 can be described by the inequalities a_i as a ball around the equilibrium. Therefore we can use

$$a \triangleq \sum_i x_i^2 - \gamma^2 \leq 0 \tag{7.9}$$

where γ is the radius of the sphere and x_i denotes the normalized aircraft states. The $W(x)$ described in Program is chosen to be $W(x) = \varepsilon \sum_i x_i^2$, with ε a small positive constant, which ensures that $W(x)$ is positive definite.

There were a number of issues that arose in application of SOSTOOLS to the system described by (7.8) documented in Reference 58. The major issue was the complexity of the system. Even in simplified form the equations were too cumbersome, primarily due to the fact that the numerator of the system is 17^{th} order with 6^{th} order denominator. If the Lyapunov function is 2^{nd} order, then the derivative condition in Theorem 7.4 will be 24^{th} order polynomial in 7 variables. The Semidefinite program is intractably large with any current solver.

A promising solution to the complexity problem was to use Taylor series expansion about the equilibrium and to apply the analysis tools to the expansion. A preliminary analysis has been performed to compare the linearized system, third-order Taylor series expansion and original nonlinear system (7.8) dynamics using simulation for initial conditions close to the equilibrium. The results in Figures 7.3 and 7.4 indicate qualitative convergence of third-order Taylor series expansion dynamics to those of the nonlinear system. This implies that third-order expansion makes a good approximation to the nonlinear system in the region considered. Hence we can conclude that since the Taylor series expansion has local Lyapunov function and is stable, the equilibrium of the system (7.8) to which it converges will also be locally stable.

The third-order Taylor series approximation was used on SOSTOOLS and a Lyapunov function was constructed for $\gamma = 0.1$. The Lyapunov function is given by

$$\begin{aligned} V(x) = {} & 1261.8\bar{\theta}^2 - 36.259\bar{\alpha}\dot{\bar{\eta}} + 2.6904\bar{\alpha}\bar{x}_f - 1.2431\bar{q}\bar{\eta} + 341.3\bar{\alpha}^2 + 0.14323\bar{q}\bar{x}_f \\ & + 191.28\bar{\eta}^2 - 1.7648\bar{q}\dot{\bar{\eta}} + 3.4655\bar{q}^2 + 7.1676\dot{\bar{\eta}}^2 - 327.33\bar{\alpha}\bar{\theta} \\ & + 17.265\bar{\alpha}\bar{q} + 71.045\bar{V}\bar{\eta} + 0.58969\bar{\eta}\bar{x}_f + 0.14927\bar{\theta}\bar{x}_f \\ & + 0.011155\bar{x}_f^2 - 36.415\bar{V}\dot{\bar{\eta}} - 20.193\bar{\eta}\dot{\bar{\eta}} - 0.30079\bar{x}_f\dot{\bar{\eta}} \\ & + 133.31\bar{V}\bar{\theta} + 205.88\bar{V}\bar{\alpha} + 1048.1\bar{V}^2 + 70.639\bar{\alpha}\bar{\eta} + 23.687\bar{q}\bar{\theta} \\ & + 50.744\bar{\theta}\bar{\eta} + 2.6975\bar{x}_f\bar{V} - 13.214\bar{\theta}\dot{\bar{\eta}} + 17.278\bar{q}\bar{V} \end{aligned}$$

where each of the bared variables is the translated and normalized version of the original state. In addition, a maximal level set was computed for this Lyapunov function to give an approximation to the region of attraction described by

$$V(x) - (0.006)^2 < 0$$

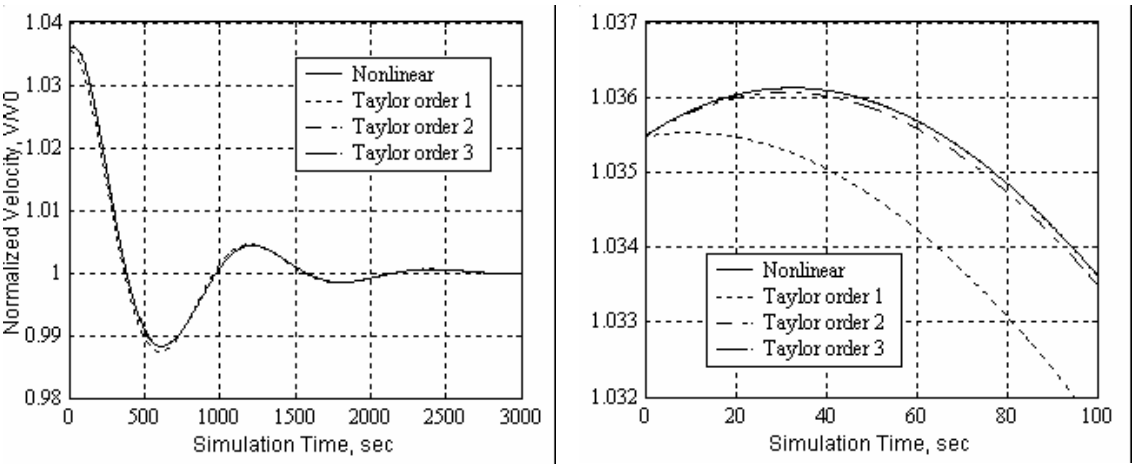

Figure 7.3: Velocity response of nonlinear system and its Taylor series expansions of linear, quadratic, and third-order. Figure on the right is an extract from the left.

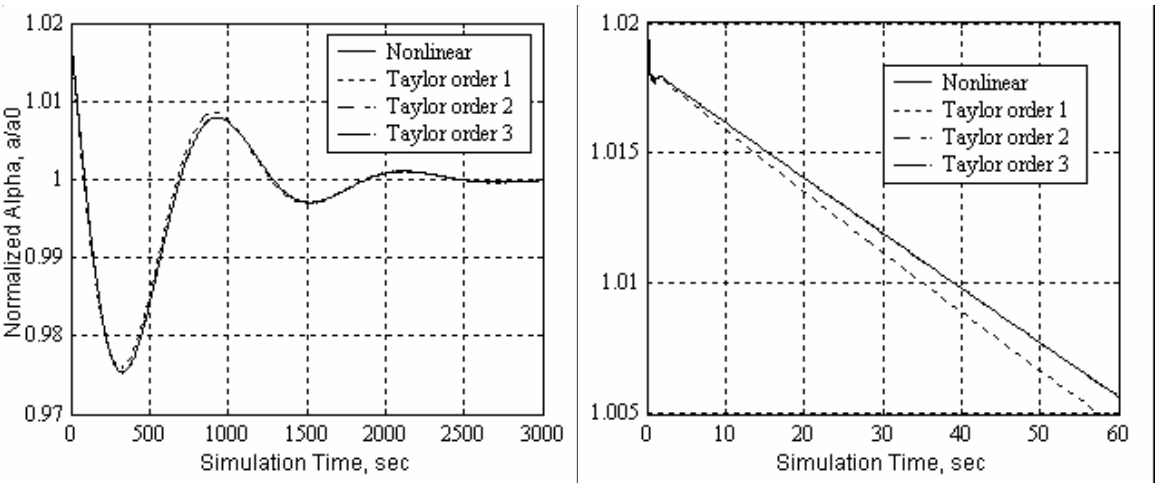

Figure 7.4: Angle of attack response of nonlinear system and its Taylor series expansions of linear, quadratic, and third-order. Figure on the right is an extract from the left.

7.5 Conclusions

This chapter attempts to bridge the stability results obtained for the novel dynamic inversion integrated flight/SMC controller on a high fidelity, high complexity aircraft model and the global stability analytical results for an integrated flight/SMC standard dynamic inversion controller in the presence of highly coupled flexible dynamics. The former were constrained to simulation due to the complexity of the problem, while the later addressed the flexible dynamics issue but for a standard dynamic inversion. The tools used to establish the global stability results are not available for the novel dynamic

inversion controller since the closed loop does not subdivide into a string of integrators and internal dynamics; and the question of stability cannot be reduced to evaluating the stability of the internal dynamics only. Thus, determination of stability was based on finding a local Lyapunov function for the closed loop system driven by the novel dynamic inversion controller.

A new tool was introduced in an attempt to find Lyapunov functions. The tool, called SOSTOOLS, is based on the Sum of Squares decomposition for finding a Lyapunov function algorithmically. In order to use the tool, the aircraft system model had to be expressed in terms of polynomials. The system model also had to be simplified while retaining the critical interaction to enable the application of the SOSTOOLS. While SOSTOOLS was unable to handle the complexity of the closed loop model, it was able to generate local Lyapunov function for a third-order Taylor series expansion of the system. The Taylor series expansion has been shown to qualitatively converge using a simulation to the nonlinear system and hence the equilibrium of the system to which it converges will also be locally stable.

Chapter 8 – Conclusions and Future Research Recommendations

High performance aircraft of the future will be designed to be lighter, more maneuverable, and operate over an ever expanding flight envelope[1]. This set of conditions will necessarily mean highly flexible vehicles operating in nonlinear regimes. In order to control these vehicles, new methods are being sought to better optimize their responses to both pilot input and external disturbances, as well as to decrease the cost of vehicle design. The methodology that has been proposed here is modified dynamic inversion. The attractiveness of this methodology lies in the fact that the inherent nonlinearities of the problem as well as the coupled nature of flexible dynamics are explicitly considered.

One of the largest differences from the flight control perspective between current and future advance aircraft is elasticity. All of the aircraft to which dynamic inversion had been applied to date are considered rigid vehicles. In the context of flight control, this means that the frequency separation between the fastest aerodynamic modes and the slowest body deforming mode is typically on the order of 60 rad/sec (10 Hz)[10]. The aircraft of the future will not have this luxury. One type of such an aircraft that has gained prominence in recent years is an Uninhabited Aerial Vehicle (UAV). These vehicles span a great variety of missions and hence have a number of very different configurations including highly flexible ones. The aircraft of choice for this research has been an HSCT chosen based on its aeroelastic characteristics and the high fidelity of available models.

8.1 Model

The importance of the model utilized in this research comes from the fact that it is physically the highest fidelity model used to represent a highly flexible aircraft. This model was formulated in the following way. The general nonlinear equations of unsteady motion for an aircraft are expanded to include the coupling between rigid body and quasi-steady aeroelastic modes. These equations are further augmented with dynamic aeroelastic equations that are required for an aircraft whose flexible modes are low enough frequency to start impacting rigid body flight dynamics and hence are no longer validly represented as quasi-static states. Continuing this development the dynamics associated with the specific vehicle under study are presented and discussed in detail at a

flight condition that make the flexible mode interaction with the rigid flight dynamics most pronounced. The specific issues highlighted that make this a very challenging problem include the vehicle dynamic response to control surfaces as well as the dynamic modeling fidelity and encroachment of the first few flexible modes into the pilot's bandwidth.

Since the model contains closely spaced flexible modes in proximity to rigid body dynamics, the actuator dynamics invariably play a significant role in their response. The presence of actuator dynamics continues excitation of high frequency modes while their absence allows for the dynamic roll off and modal attenuation. This observation is very important for control design purposes since typically actuator dynamics are not considered during the design process. The implication here is that the controller must roll off significantly before the excitation of flexible modes due to actuator dynamics comes into play. In addition, it is interesting to note how the HSCT vehicle would respond to a surface deflection at its tail generating a pitching moment. The initial response to nose down moment for the elastic vehicle is nonminimum phase, *i.e.*, response is in direction opposite of that commanded. This type of response has implications for flight control design.

8.1.1 Novel Dynamic Inversion Model Analysis

The novel dynamic inversion methodology introduces additional dynamics, $W(x)$, into the inversion loop to alter the controlled dynamics in a more intelligent manner than canceling dynamics very close to the jω-axis. This modification alters the internal dynamics of the system and destroys the separation between internal dynamics and controlled dynamics that was present for the standard inversion case. However, when additional dynamics of $W(x)$ are present in one loop, the input-output dynamics reflect the modification in the altered loop and recover the standard integrator in the nominal one. This work has added to both analytical and physical insight regarding the nature of the novel dynamic inversion applied to an integrated flight/SMC control for a highly flexible aircraft.

Another part of this work focused on specific effects that the additional dynamics associated with the novel dynamic inversion have on the response of the closed loop aircraft system. The additional dynamics have been analytically explored on longitudinal

and symmetric flexible dynamics of varying complexity. While the model used here is much simpler than the full model for which the controller was designed, the results are revealing nonetheless. These results provide some analytical basis and further insight into the workings of dynamic inversion methodology that has been modified to address the problem associated with large, flexible aircraft.

There exists a large degree of freedom to control rigid body and flexible dynamics independently of one another in the novel dynamic inversion context. The apparent separation in controlling the short period and elastic mode dynamics through novel dynamic inversion is valuable when control of disturbances is as important as control of commanded variable. Specifically, the ability to alter the damping of elastic modes as well as cancel their response to the commanded vehicle motion is the main objective of an integrated flight/SMC control that is required for advanced, large, flexible aircraft.

The increased complexity of system dynamics that included full longitudinal as well as multiple symmetric flexible mode dynamics showed that a certain degree of separation in controlling rigid body and flexible dynamics still exists. However, the introduction of parametric uncertainty into frequency and damping of the dominant flexible mode also showed the coupling between very low frequency rigid body and flexible dynamics. This coupling must be carefully considered during a controller design process since in the real world application there is always uncertainty present in the system.

8.1.2 Novel Dynamic Inversion for Integrated Flight/SMC Controller Design

An initial application of the novel dynamic inversion control methodology to a flexible vehicle is presented here. While the standard dynamic inversion has been applied to aircraft that could be treated as rigid, it never has had to contend with a piloted aircraft whose first few flexible modes resided well within the pilot's bandwidth. The associated problems as well as the proposed modifications to the standard dynamic inversion to deal with them have been presented. The resulting novel dynamic inversion controller was assessed in a high fidelity nonlinear simulation under a variety of conditions including severe turbulence, saturated control surfaces, and uncertainty in the flexible modes.

The results obtained in this initial application are very promising. The novel dynamic inversion controller makes a highly flexible aircraft appear as essentially rigid to pilot in

response to his commands. In addition, the damping ratio of the primary fuselage structural mode has been increased from around 5% to close to 20%. The second fuselage flexible mode damping was improved as well, and the higher frequency mode dynamics either remained the same or slightly improved. Furthermore, the aircraft had a favorable response to moderate an severe turbulence. The vehicle was robust to 50% variation in damping and 15% uncertainty in the frequency of the first two flexible modes as well as remained stable for saturated control surfaces.

The obtained results were compared to a controller designed on a QSAE aircraft model and tuned for performance in extensive piloted simulations. While the dynamic inversion controller has not yet been tuned in piloted simulation, the response at lower frequency is similar to that of the QSAE controller. Although it is expected that the QSAE controller would not attenuate the flexible modes since it is not designed on a flexible model, it exacerbates the problem of flexible mode control by a separately designed SMC. Thus, the results of this work also advocate the integrated design of the SAS/SMC controller to maximize the performance of the aircraft.

Another interesting observation is that a number of flexible modes are primarily wing modes and require wing surfaces to attenuate them. While fuselage mounted control effectors do a good job on the fuselage bending modes they have little to no effect on the wing modes which in turn contribute to the excitation of fuselage modes and to a slight heave of the entire aircraft.

8.1.3 Integrated Dynamic Inversion Controller Closed Loop Stability

This research started to establish conditions under which the standard dynamic inversion control methodology can be guaranteed global stability when applied to a real world problem that involves highly coupled flight and aeroelastic dynamics as well as an integrated flight/structural mode control MIMO system.

From a mathematical perspective, the results show how a complicated dynamical problem of establishing system stability reduces to checking algebraic conditions that are manageably complex. This is accomplished by reducing the determination of stability of an n-dimensional system to that of a two-dimensional one via a dynamic inversion controller. The resulting nonautonomous system is then reduced to its autonomous

limiting system and the stability of the limiting system is established. The stability of the autonomous system is shown in two steps that produce vehicle specific conditions.

The established algebraic conditions provide an initial test that can guarantee global stability when applied to a real world problem that involves highly coupled flight and aeroelastic dynamics as well as an integrated flight/SMC control MIMO system. The initial approach is to simplify the problem, address the pitch axis dynamics with only a single mode and no actuator dynamics, and then assess the ramifications of aeroelasticity on the stability results. The role played by flexible dynamics is immediately apparent from consideration of the internal dynamics of the system. Furthermore, these flexible dynamics play a role in establishing stability guarantees for the closed loop system. While the analysis represents a somewhat idealized case, the insight provided has immediate real world application with respect to the influence of flexible dynamics on the system as a whole.

The results presented are the first to include flexible dynamics in stability analysis of dynamic inversion methodology. These form an initial basis to more complicated control problem formulation that includes a modified dynamic inversion methodology employed to design an integrated flight/SMC controller for a high fidelity model discussed earlier. The next step undertaken in the following chapter is to introduce the modified dynamic inversion into the analysis performed here and then establish stability guarantees that are still possible with this complication.

8.1.4 Integrated Novel Dynamic Inversion Controller Closed Loop Stability

The next step is to introduce the novel dynamic inversion into the analysis and then establish stability guarantees that are still possible with this complication. This next step attempts to bridge the stability results obtained for the novel dynamic inversion integrated flight/SMC controller on a high fidelity, high complexity aircraft model and the global stability analytical results for an integrated flight/SMC standard dynamic inversion controller in the presence of highly coupled flexible dynamics. The former were constrained to simulation due to the complexity of the problem, while the later addressed the flexible dynamics issue but for a standard dynamic inversion. The tools used to establish the global stability results are not available for the novel dynamic inversion controller since the closed loop does not subdivide into a string of integrators and internal

dynamics; and the question of stability cannot be reduced to evaluating the stability of the internal dynamics only. Thus, determination of stability was based on finding a local Lyapunov function for the closed loop system driven by the novel dynamic inversion controller.

A new tool was introduced in an attempt to find Lyapunov functions. The tool, called SOSTOOLS, is based on the Sum of Squares decomposition for finding a Lyapunov function algorithmically. In order to use the tool, the aircraft system model had to be expressed in terms of polynomials. The system model also had to be simplified while retaining the critical interaction to enable the application of the SOSTOOLS. While SOSTOOLS was unable to handle the complexity of the closed loop model, it was able to generate local Lyapunov function for a third-order Taylor series expansion of the system. The Taylor series expansion has been shown to qualitatively converge using a simulation to the nonlinear system and hence the equilibrium of the system to which it converges will also be locally stable.

8.2 Contribution of This Work

The contribution of this work to the state of the art is predicated on the development and application of dynamic inversion methodology to handle highly flexible aircraft in an integrated flight/SMC control manner. The development and evaluation are performed on a sophisticated, high fidelity, nonlinear dynamic model across the frequency spectrum. The dynamic nature of structural modes and the flight control reciprocal interaction with flexible modes because of unprecedented small separation between rigid body and flexible modes are the key elements of the aircraft model. The standard methodology of dynamic inversion has been modified in the manner described in this work to accommodate the nature of the vehicle and fulfill the dual objectives of integrated flight/SMC control. These objectives constituted command following, disturbance rejection in the rigid body and improved structural dynamic damping to minimize excitation from turbulence and render the aircraft rigid from the pilot station perspective.

The structural nature of the modification to the standard dynamic inversion methodology and its effect on the necessary level model complexity for design has been established with particular attention given to establishing physical understanding of the

control design process. Furthermore, the effect of uncertainty in the structural mode dynamics has been addressed as well.

Further contribution of this work is addressing the issue of dynamic inversion and stability of highly flexible aircraft studied in this work from the mathematical perspective. The results presented are the first to include flexible dynamics in stability analysis of dynamic inversion methodology. These form an initial basis to more complicated control problem formulation that includes a modified dynamic inversion methodology employed to design an integrated flight/SMC controller for a high fidelity model discussed earlier.

The changes in dynamics attributed to the modification in the inversion methodology have been traced for both linear and nonlinear systems. This work has added to both analytical and physical insight regarding the nature of modified dynamic inversion applied to an integrated flight/structural mode control for a high flexible aircraft.

Furthermore, a new tool was introduced in an attempt to find Lyapunov functions that would guarantee local stability for the nonlinear system with modified dynamic inversion controller alluded to above. The tool, called SOSTOOLS, is based on the Sum of Squares decomposition for finding a Lyapunov function algorithmically. While SOSTOOLS were unable to handle the complexity of the closed loop model, it was able to generate local Lyapunov function for a Taylor series expansion of the system up to order 3. The Taylor series expansion has been shown to converge using a simulation to the nonlinear system and hence the results found apply to the nonlinear system as well.

Portions of this work have been published in publicly available forums and are included in the reference section[31-33].

8.3 Future Research

There are a number of areas for fruitful research that would build on this work. One such area would incorporate adaptive control techniques to reduce the model fidelity necessary for integrated controller design. This approach would potentially significantly reduce vehicle development cost. The adaptation part of the controller would operate on the error between desired behavior based on the assumed model and actual behavior. This would enable both decoupled rigid body response as well as altering the damping of the flexible dynamics without precise knowledge of these dynamics. The research issue

is not only how to do this in an intelligent way but also how to preserve the stability guarantees for such a system.

Another area of important research is the maturation of the SOSTOOLS that would allow the algorithm to deal with complicated systems that describe the flexible aircraft dynamics. The ability to find Lyapunov functions for aircraft becomes increasingly important as the flight envelope is extended to highly nonlinear regimes and certification issues require analytical guarantee of stability for operational vehicles.

The third area of research that indirectly suggests itself, is how to incorporate nontraditional control effectors into a more traditional control analysis and design framework. Certain vehicles in the future are expected to have 100's and then 1000's control effectors, whether these are fluidic like synthetic jets or a wing that continuously changes shape to provide optimal maneuverability and mission performance. Can the research into integrated flight/structural mode control presented here serve to further the understanding of this new control problem, particularly in the latter case?

The future awaits and it is full of challenges and opportunities.

Bibliography

[1] New World Vistas Study: Aircraft and Propulsion Technologies. United States Air Force Scientific Advisory Board. 1995.

[2] Bugajski, Daniel, Dale Enns, and Russ Hendrick. Multi-Application Control (MACH): F-18 High Angle-of-Attack Research Vehicle (HARV) Reports. Honeywell Technology Center. November 1994.

[3] Application of Multivariable Control Theory to Aircraft Control Laws. Final Report: Multivariable Control Design Guidelines. WL-TR-96-3099. May 1996.

[4] Bugajski, Daniel and Dale Enns. "Nonlinear Control Law with Application to High Angle-of-Attack Flight." J. of Guidance, Control, and Dynamics, Vol. 15, No. 3, May-June 1992.

[5] Enns, Dale, Dan Bujaski, Russ Hendrick, and Gunter Stein. "Dynamic Inversion: An Evolving Methodology for Flight Control Design." Int. J. Control, Vol. 59, No. 1, 1994. pp. 71-91.

[6] Calise, A. J., S. Lee, and M. Sharma. "Development of a Reconfigurable Flight Control Law for the X-36 Tailless Fighter Aircraft." AIAA-2000-3940.

[7] Schumacher, C. J. and J. D. Johnson. "PI Control of a Tailless Fighter Aircraft with Dynamic Inversion and Neural Networks." Proceedings of the American Control Conference, San Diego, CA, June 1999.

[8] Bacon, B. J. and A. J. Ostroff. "Reconfigurable Flight Control Using a Special Accelerometer Implementation." AIAA-2000-4565.

[9] Bacon, B. J., A. J. Ostroff, and S.M. Joshi. "Reconfigurable NDI Controller Using Inertial Sensor Failure Detection and Isolation." IEEE Trans. On Aerospace and Electronic Systems, Vol. 37, No. 4, October 2001. pp.1373-1383.

[10] Application of Multivariable Control Theory to Aircraft Control Laws. 8th Quarterly Review. July 1995.

[11] HELIOS Prototype. NASA Facts. NASA Dryden Flight Test Center. www.dfrc.nasa.gov/Newsroom/FactSheets/FS-068-DFRC.html.

[12] Edberg, Don. "Structures, Design and Test." Aerospace America. December 2003. p. 78.

[13] "New Aero-Elastic UAV Design." UAV Rolling News. www.uavworld.com, January 2004.

[14] Morton, B., D. Enns, and B. Y. Zhang. "Stability of Dynamic Inversion Control Laws Applied to Nonlinear Aircraft Pitch-Axis Models." International Journal of Control, Volume 63, Issue: 1, January 1996. pp. 1-25.

[15] Isidori, Alberto. Nonlinear Control Systems: An Introduction, 2nd ed. Springer-Verlag, 1985.

[16] Military Specifications - Flying Qualities of Piloted Vehicles. MIL-STD-1797A. March 1987.

[17] Enns, Dale. Conversations. Honeywell Technology Research Center, Minneapolis, MN. March 24-28, 1996.

[18] Doyle, John, and Gunter Stein. "Multivariable Feedback Design: Concepts for a Classical/Modern Synthesis." IEEE Trans. on Automatic Control, 26. 1981. pp. 4-16.

[19] Stein, Gunter, and John Doyle. "Beyond Singular Values and Loop Shapes." J. of Guidance, Control, and Dynamics, 14. Jan-Feb 1991. pp. 5-16.

[20] Packard, Andy, John Doyle, and Gary Balas. "Linear, Multivariable, Robust Control with a μ Perspective." ASME J. of Dynamics, Measurement, and Control, 115. June 1993. pp. 426-438.

[21] Etkin, B. Dynamics of Atmospheric Flight. John Wiley & Sons, Inc., New York. 1972.

[22] Wykes, John, Thomas Byar, Cary MacMiller, and David Greek. Analyses and Tests of the B-1 Aircraft Structural Mode Control System. NASA CR 144887. 1980.

[23] Newman, Brett, and Carey Buttrill. "Conventional Control for an Aeroelastic, Relaxed Static Stability high-Speed Transport." AIAA paper 95-3250-CP.

[24] Schmidt, D. K. "On Integrated Control of Flexible Supersonic Transport Aircraft." AIAA-95-3200.

[25] Hess, R. A., and D. K. Henderson. "Flexible Vehicle Control Using Quantitative Feedback Theory." Journal of Guidance, Control, and Dynamics, Vol. 18, No. 5. September-October 1995.

[26] Kubica, F., and T. Livet. "Flight Control Law Synthesis for a Flexible Aircraft." AIAA-94-3630.

[27] Newman, B. "Multivariate Techniques for High-Speed Research Flight Control Systems." NASA CR-1999-209528. NASA Langley Research Center. December 1999.

[28] Calise, A. J., N. Kim, and J. M. Buffington. "Adaptive Compensation for Flexible Dynamics." AIAA-02-4917.

[29] Calise, A. J., N. Hovakimyan, and M. Idan. "Adaptive Output Feedback Control of Nonlinear Systems Using Neural Networks." Automatica Special Issue on Neural Networks for Feedback Control. Vol. 37, No. 8. 2001.

[30] Novakimyan, N., F. Nard, and A. J. Calise. "A Novel Observer Based Output Feedback Approach for Control of Uncertain Systems." Proceeding of the American Control Conference. 2001.

[31] Gregory, Irene M. "Dynamic Inversion to Control Large Flexible Transport Aircraft." 1998 AIAA Guidance, Navigation, and Controls Conference, Boston, MA. AIAA paper 98-4323. 1998.

[32] Gregory, Irene M. “Modified Dynamic Inversion to Control Large Flexible Aircraft – What’s Going On?” 1999 AIAA Guidance, Navigation, and Controls Conference, Portland, OR. AIAA paper 99-3998. 1999.

[33] Gregory, Irene M. “Stability Result for Dynamic Inversion Devised to Control Large Flexible Aircraft.” 2001 AIAA Guidance, Navigation, and Controls Conference, Montreal, Quebec, Cananda. AIAA-01-4284. 2001.

[34] Khalil, H. K. Nonlinear Systems. Macmillan Publishing Company, New York. 1992.

[35] Rosenbrock, H. H. State-Space and Multivariable Theory. Nelson, London. 1970

[36] Enns, Dale. “Control Allocation Approaches.” AIAA Paper 98-4109.

[37] Bordington, Kenneth A. and Wayne C. Durham. “Closed-Form Solutions to Constrained Control Allocation Problem.” Journal of Guidance, Control, and Dynamics Vol. 18, No. 5. September-October 1995.

[38] McRuer, D., I. Ashkenas, and D. Graham. Aircraft Dynamics and Automatic Control. Princeton University Press, Princeton, NJ. 1973.

[39] AGARD. “Aeroelastic Effects from a Flight Mechanics Standpoint.” Conference Proceedings, No. 46. March 1970.

[40] Milne, R. D. “Dynamics of the Deformable Airplane.” ARC R&M 3345. 1964.

[41] McLaughlin, M. D. “A Theoretical Investigation of the Short-Period Dynamic Longitudinal Stability of Airplanes Having Elastic Wings of 0° to 60° Sweepback.” NACA TN3251. 1954.

[42] DAMWG. “Proceedings of a Workshop of the Dynamic Aeroelastic Modeling Working Group.” NASA Langley Research Center, Hampton, VA. August 13-15, 1997.

[43] Tiffany, Sherwood, and William Adams. Nonlinear Programming Extensions to Rational Function Approximation Methods for Unsteady Aerodynamic Forces. NASA TP-2776. July 1988.

[44] Adams, W. M. “Coupling of Linear Dynamic Aeroelastic Effects with Nonlinear Quasi-Static Simulation.” Unpublished.

[45] Winther, B. A., P. J. Goggin, and J. R. Dykman. “Reduced Order Dynamic Aeroelastic Model Development and Integration with Nonlinear Simulation.” AIAA paper 98-1897.

[46] Johnson, D. L. Terrestrial Environment (Climatic) Criteria Guidelines for Use in Aerospace Vehicle Development, 1993 Revision. NASA TM 4511. August 1993.

[47] 1997 NASA High-Speed Research Program Aerodynamic Performance Workshop, Volume IV-Flight Controls. Hampton VA. February 25-28, 1997.

[48] La Salle, J. P. The Stability of Dynamical Systems. Regional Conference Series in Applied Mathematics, Vol. 25. 1976.

[49] Markus, L. "Asymptotically Autonomous Differential Systems." Contributions to the Theory of Nonlinear Oscillations, Vol. III. S. Lefschetz ed., Princeton University Press. 1956. pp. 17-29.

[50] Yoshizawa, T. Stability Theory and the Existence of Periodic Solutions and Almost Periodic Solutions. Springer-Verlag. 1975.

[51] Parrilo, P. A. Structured Semidefinite Programs and Semialgebraic Geometry Methods in Robustness and Optimization. PhD. Thesis, California Institute of Technology, Pasadena, CA. 2000. Available at www.control.ethz.ch/~parrilo/pubs/index.html.

[52] Prajna, S., A. Papachristodoulou, and P. A. Parrilo. "Introducing SOSTOOLS: A General Purpose Sum of Squares Programming Solver." In Proceedings IEEE Conference on Decision and Control. 2002.

[53] Papachristodoulou, A. "Nonlinear Analysis of High-Speed Aircraft Dynamics Using SOSTOOLS." Memo. April 4, 2004.

[54] Vandenberghe, L and S. Boyd. "Semidefinite Programming." SIAM Review 38(1). pp. 49-95.

[55] Papachristodoulou, A. and S. Prajna. "On the Construction Lyapunov Functions Using the Sum of Squares Decomposition." In Proceedings IEEE Conference on Decision and Control. 2002.

[56] Murty, K. G. and S. N. Kabadi. "Some NP-complete Problems in Quadratic and Nonlinear Programing." Mathematical Programming, 39. 1987. pp. 117-129.

[57] Sturm, J. F. "Using SeDuMi 1.02 , a MATLAB Toolbox for Optimization Over Symmetric Cones." Optimization Methods and Software 11-12. pp. 625-653. Available at http://fewcal.kub.nl/sturm/software/sedumi.html.

[58] Kogan, D. L. "A Stability Analysis of High-Speed Aircraft Using SOSTOOLS." from CDS213 Final Project. March 17, 2004.

[59] High Speed Civil Transport Reference H – Cycle 5 Simulation Data Base and Models. NASA Contract NAS1-20220. January 1999.

Appendix A – Aerodynamic Coefficients

The aerodynamic force and moment coefficient buildup in the simulation for all the major parts are given below[59].

The Lift coefficient is build up from individual surface parts and structural deformation in quasi-static flow corrections. The model used in simulation for controller design and analysis contains all of these dependencies. The equations used for symbolic analysis are simplified as indicated in Chapter 3.

$$C_L = C_L(Tail\_clean) + C_L(surfaces) + C_L(canard) + C_L(tail) + C_L(q) + C_L(\dot{q}) + C_L(\dot{\alpha})$$

$$C_L^R(TOC) = f(\alpha, M)$$

$$\Delta^E C_L(TOC) = f(\alpha, M, \bar{q}, GW^*)$$

$$C_L^R(surfaces) = f(\alpha, M, \delta surf)$$

$$C_L^{E/R}(surfaces) = f(\alpha, M, \bar{q}, GW^*)$$

$$C_L^R(tail) = f(\alpha, M, \delta tail)$$

$$\Delta^E C_L(tail) = f(\alpha, M, \bar{q}, GW^*, \delta tail)$$

$$C_L^R(q) = f(\alpha, M)$$

$$\Delta^E C_L(q) = f(M, \bar{q}, GW^*)$$

$$C_L^R(\dot{q}) = f(M)$$

$$\Delta^E C_L(\dot{q}) = f(M, \bar{q}, GW^*)$$

$$C_L^R(\dot{\alpha}) = f(M)$$

$$\Delta^E C_L(\dot{\alpha}) = f(M, \bar{q}, GW^*)$$

$$= f(\alpha, M)_{rigid} + f(\alpha, M, \bar{q}, GW^*)_{elastic\ increments} + C_{Lq}(\alpha, M)_r + C_{Lq}(M, \bar{q}, GW^*)_e + \ldots$$
$$+ C_{L\dot{q}}(M)_r + C_{L\dot{q}}(M, \bar{q}, GW^*)_e + C_{L\dot{\alpha}}(M)_r + C_{L\dot{\alpha}}(M, \bar{q}, GW^*)_e + \ldots$$
$$+ C_{L\eta}(M, GW^*)\ \eta + C_{L\dot{\eta}}(M, \bar{q}, GW^*)\ \dot{\eta} + \ldots$$
$$+ C_{L\delta}(\alpha, M, \delta)_r + C_{L\delta}(\alpha, M, \bar{q}, GW^*, \delta)_e$$

The Drag coefficient is treated in a similar manner as Lift.

$$C_D = C_D(TailClean) + C_D(surfaces) + C_D(canard) + C_D(tail) + C_D(q) + C_D(\dot{q}) + C_D(\dot{\alpha})$$

$$C_D^R(TOC) = f(\alpha, M)$$

$$\Delta^E C_D(TOC) = f(\alpha, M, \bar{q}, GW^*)$$

$$C_D^R(surfaces) = f(\alpha, M, \delta surf)$$

$$\Delta^E C_D(surfaces) = f(\alpha, M, \bar{q}, GW^*, \delta surf)$$

$$C_D^R(tail) = f(\alpha, M, \delta tail)$$

$$\Delta^E C_D(tail) = f(\alpha, M, \bar{q}, GW^*)$$

$$C_D^R(q) = f(\alpha, M)$$

$$\Delta^E C_D(q) = f(\alpha, M, \bar{q}, GW^*)$$

$$C_D^R(\dot{q}) = f(\alpha, M)$$

$$\Delta^E C_D(\dot{q}) = f(\alpha, M, \bar{q}, GW^*)$$

$$C_D^R(\dot{\alpha}) = f(\alpha, M)$$

$$\Delta^E C_D(\dot{\alpha}) = f(\alpha, M, \bar{q}, GW^*)$$

$$= f(\alpha, M)_{rigid} + f(\alpha, M, \bar{q}, GW^*)_e + C_{Dq}(\alpha, M)_r + C_{Dq}(\alpha, M, \bar{q}, GW^*)_e + \ldots$$
$$+ C_{D\dot{q}}(\alpha, M)_r + C_{D\dot{q}}(\alpha, M, \bar{q}, GW^*)_e + C_{D\dot{\alpha}}(\alpha, M)_r + C_{D\dot{\alpha}}(\alpha, M, \bar{q}, GW^*)_e + \ldots$$
$$+ C_{D\eta}(M, GW^*)\ \eta + C_{D\dot{\eta}}(M, \bar{q}, GW^*)\ \dot{\eta} + \ldots$$
$$+ C_{D\delta}(\alpha, M, \delta)_r + C_{D\delta}(\alpha, M, \bar{q}, GW^*)_e \delta$$

The pitching moment coefficient is given by

$$C_M = C_M(TailCl) + C_M(surfaces) + C_M(canard) + C_M(tail) + C_M(q) + C_M(\dot{q}) + C_M(\dot{\alpha})$$

$$C_M^R(TOC) = f(\alpha, M)$$

$$\Delta^E C_M(TOC) = f(\alpha, M, \bar{q}, GW^*)$$

$$C_M^R(surfaces) = f(\alpha, M, \delta surf)$$

$$\Delta^E C_M(surfaces) = f(M, \bar{q}, GW^*, \delta surf)$$

$$C_M^R(tail) = f(\alpha, M, \delta tail)$$

$$\Delta^E C_M(tail) = f(\alpha, M, \bar{q}, GW^*, \delta tail)$$

$$C_M^R(q) = f(\alpha, M)$$

$$\Delta^E C_M(q) = f(\alpha, M, \bar{q}, GW^*)$$

$$C_M^R(\dot{q}) = f(M)$$

$$\Delta^E C_M(\dot{q}) = f(M, \bar{q}, GW^*)$$

$$C_M^R(\dot{\alpha}) = f(M)$$

$$\Delta^E C_M(\dot{\alpha}) = f(M, \bar{q}, GW^*)$$

$$= f(\alpha, M)_{rigid} + f(\alpha, M, \bar{q}, GW^*)_e + C_{Mq}(\alpha, M)_r + C_{Mq}(\alpha, M, \bar{q}, GW^*)_e + \ldots$$
$$+ C_{M\dot{q}}(M)_r + C_{M\dot{q}}(M, \bar{q}, GW^*)_e + C_{M\dot{\alpha}}(M)_r + C_{M\dot{\alpha}}(M, \bar{q}, GW^*)_e + \ldots$$
$$+ C_{M\eta}(M, GW^*)\ \eta + C_{M\dot{\eta}}(M, \bar{q}, GW^*)\ \dot{\eta} + \ldots$$
$$+ C_{M\delta}(\alpha, M, \delta)_r + C_{M\delta}(\alpha, M, \bar{q}, GW^*, \delta)_e$$

The dynamic aeroelastic part coefficient is given by

$$C_\eta = C_{\eta u}(M, GW^*) + C_{\eta w}(M, GW^*) + C_{\eta q}(M, GW^*) + \ldots$$
$$+ C_{\eta \dot{u}}(M, GW^*) + C_{\eta \dot{w}}(M, GW^*) + C_{\eta \dot{q}}(M, GW^*) + \ldots$$
$$+ C_{\eta\eta}(M, GW^*) + C_{\eta\dot{\eta}}(M, GW^*) + C_{\eta\ddot{\eta}}(M, GW^*) + \ldots$$
$$+ C_{\eta\delta}(M, GW^*)\ \delta + C_{\eta\dot{\delta}}(M, GW^*)\ \dot{\delta} + C_{\eta\ddot{\delta}}(M, GW^*)\ \ddot{\delta}$$

The apparent mass is given by

$$-M\omega_\eta^2 + \bar{q}Q_D \rightarrow \eta$$
$$-aMs\omega_\eta + \bar{q}Q_R \rightarrow \dot{\eta}$$
$$M = \mathrm{M} + \rho \begin{bmatrix} 0 & \\ & Q_A \end{bmatrix} \approx \mathrm{M}$$

Appendix A – Aero Coefficients

Appendix B – Flexible Modes

The symmetric bending modes of the aircraft are illustrated in Figure B1. Only the first three modes are shown since the shape gets more complicated and more difficult to discern on a full vehicle profile. Of the first three modes note that mode 1 and 3 are predominantly wing modes, while mode 2 is the classic first fuselage bending mode. In designing a controller for this vehicle, controlling the fuselage bending modes and especially the first bending mode was one of the primary objectives.

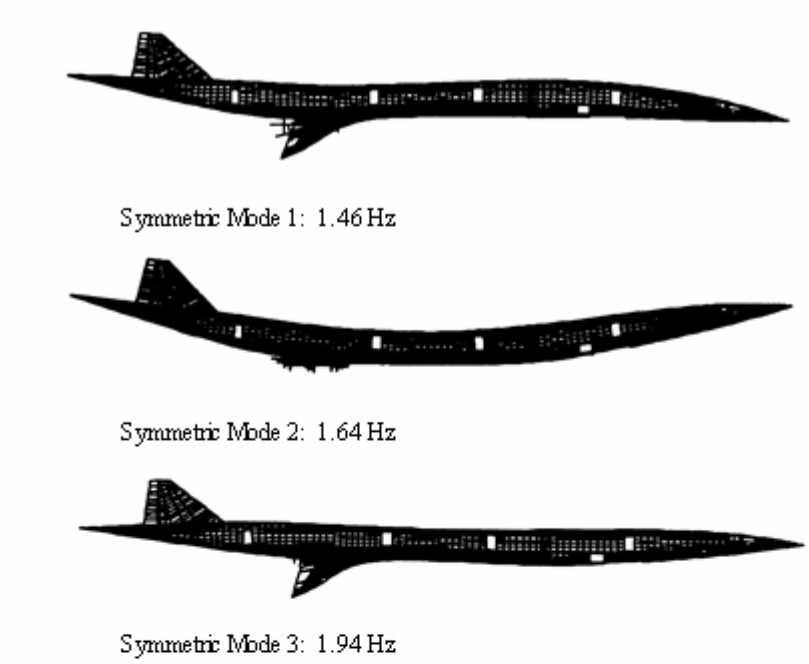

Figure B1: Symmetric flexible modes of an HSCT vehicle.

The *in vacuo* symmetric mode shapes for the first ten modes are presented in the Figures B2 and B3 below. Note that the first eight modes are at lower frequency, or right at it for mode eight, than the first break frequency for the slowest control surface, the stabilator. This means that all of these modes get the full energy transmission without attenuation every time the stabilator moves. Furthermore, the first frequency breakpoint for the elevator and other surfaces is at 75 rad/sec which is higher than all of the 20 flexible modes modeled. Thus, unlike more traditional vehicles where the flexible modes

are typically at frequencies where control activity energy is already attenuated so their excitation is not that severe and certainly not at frequencies that interfere with flight control.

Figure B2 gives symmetric mode shapes and their associated frequencies for the first 5 modes. The *in vacuo* mode displacements were calculated such that the associated generalized mass equal to 1, hence, the z displacement axis is for relative displacement comparison not an absolute vehicle displacement.

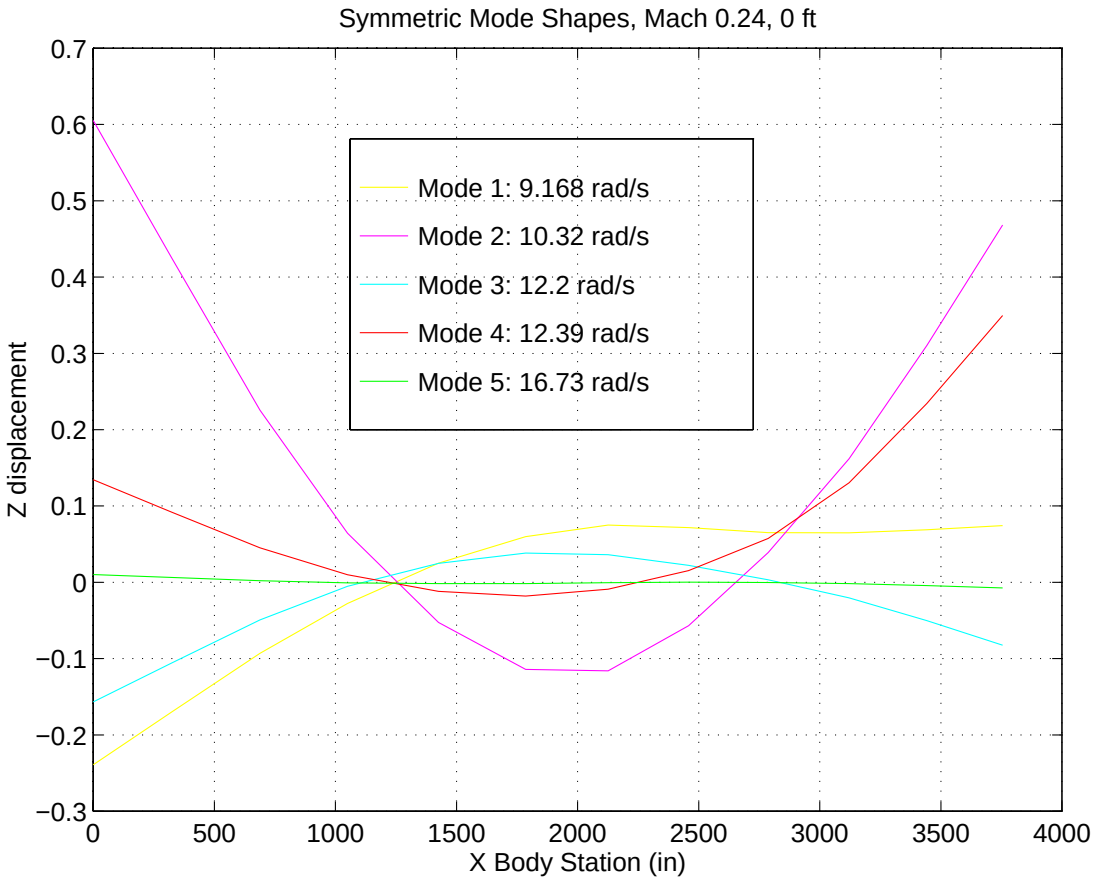

Figure B2: Symmetric mode shapes 1 through 5 and their respective frequencies.

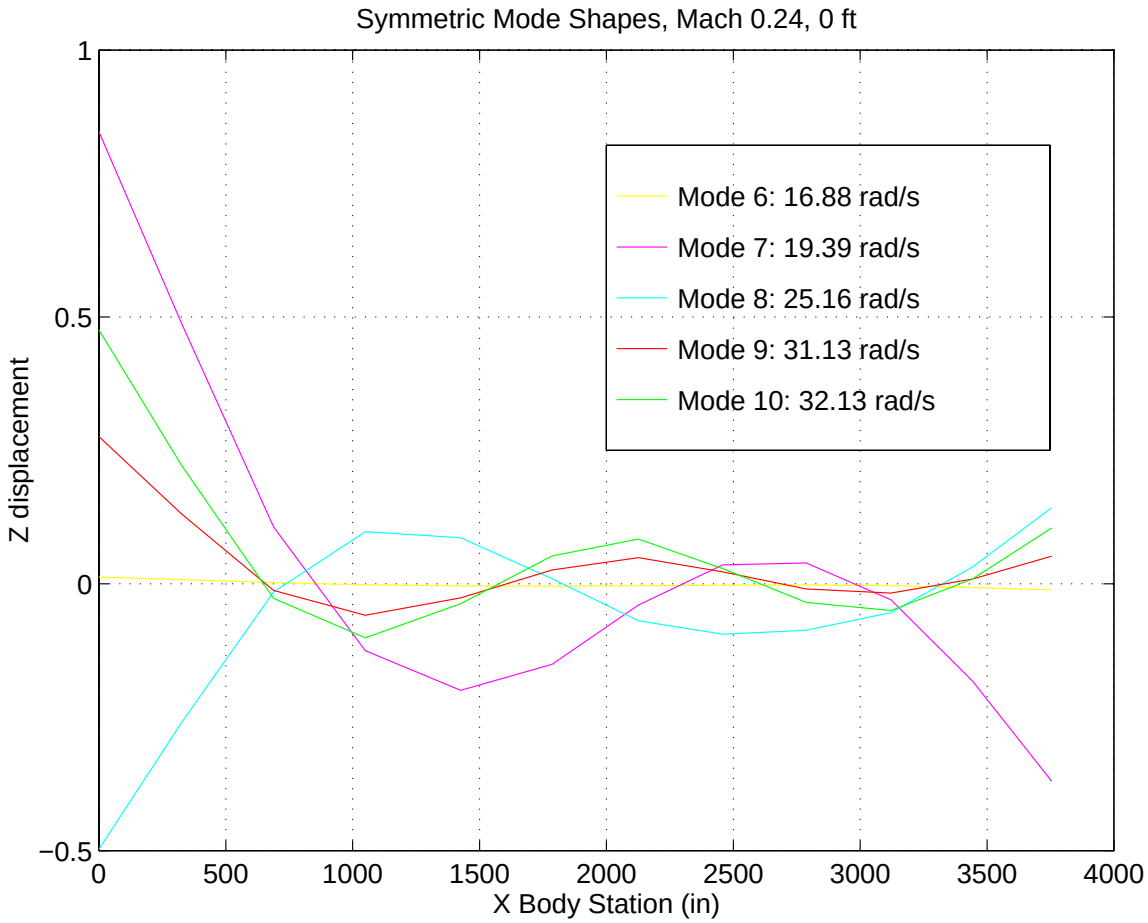

Figure B3: Symmetric mode shapes 6 through 10 and their respective frequencies.

Appendix B

Appendix C – Alternative Dynamic Inversion Controller Strategies

C.1 Introduction

Without RCV availability, longitudinal control has at its disposal stabilator, elevon, and trailing edge flaps. The stabilator is the slowest of the surfaces and is inappropriate for structural mode control, even though it is used in conjunction with the elevon for flight control in order to provide increased control power in the longitudinal axis. Alternative control strategies described in this appendix involve using the all-moving horizontal tail, *i.e.*, stabilator+ elevon, as well as available trailing edge flaps to provide integrated flight/structural mode control. However, before these are presented a short result on trying to use only the elevon for integrated flight/SMC is discussed.

C.2 One Actuator Multi-Objective Control

Rotational motion of the airplane in the longitudinal axis is typically controlled by one set of actuators, the elevator. The primary mode of rotational motion is known as the short period mode and is typically the fastest mode in the longitudinal motion of a rigid airplane. Hence if pitch rate is commanded, an elevator deflection is used to follow that command in a rigid vehicle.

Now to make the problem more complicated, consider a flexible vehicle. Theoretically it is possible to control flexible motion and short period motion by using only one actuator, the elevator, provided there is sufficiently large frequency separation between short period and the flexible mode to be controlled. The idea here is based strictly on the principle of superposition, the actuator dynamics, and the physics of the aircraft. Provided that the speed of the elevator is fast enough to be effective, the elevator action to dampen out elastic oscillations would be superimposed on the action to change the attitude of the mean axis of the airplane. An example of such elevator response is illustrated in Figures C1, C2, and C3 where the vehicle is subject to external gust disturbance simulated by impulse elevator while trying to track pitch rate command. The controller is a PI filter that attempts to track a commanded pitch rate while minimizing the error between the mean axis and the pilot station response. The results of this multi-objective vehicle control are very dependent on the frequency of the elastic mode, and hence a function of the separation between it and the short period.

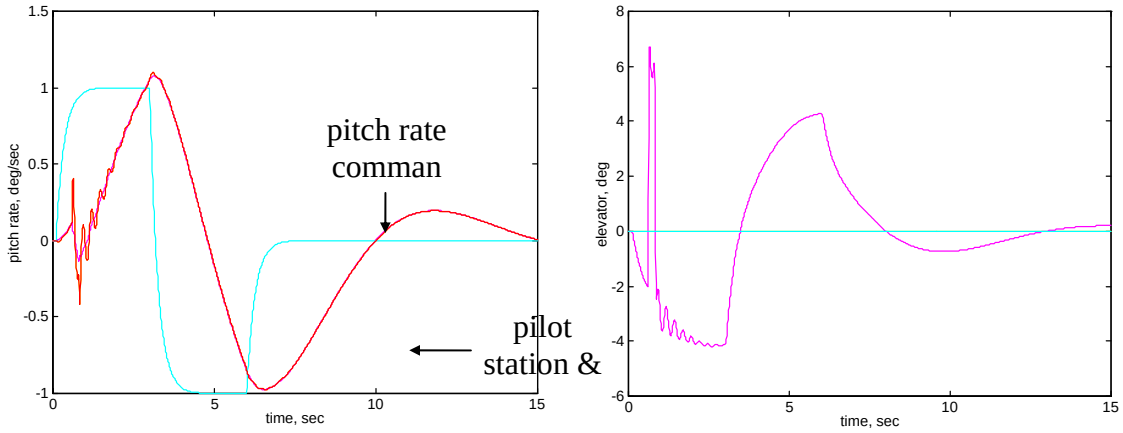

Figure C1: Pitch rate response, at mean axis and pilot station sensors, and elevator response to pitch rate command and impulse disturbance in elevator – elastic mode frequency ω_e=23.1 rad/sec.

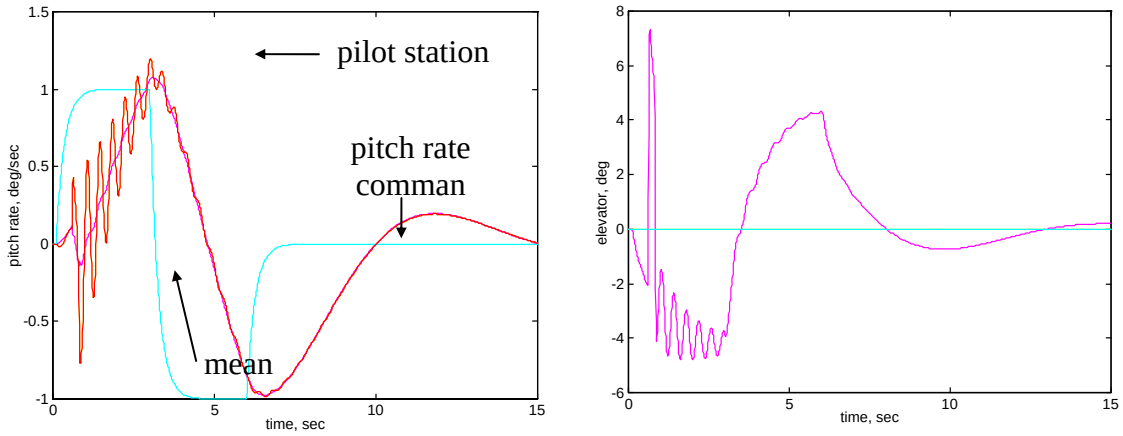

Figure C2: Pitch rate response, at mean axis and pilot station sensors, and elevator response to pitch rate command and impulse disturbance in elevator - elastic mode frequency ω_e=15.4 rad/sec.

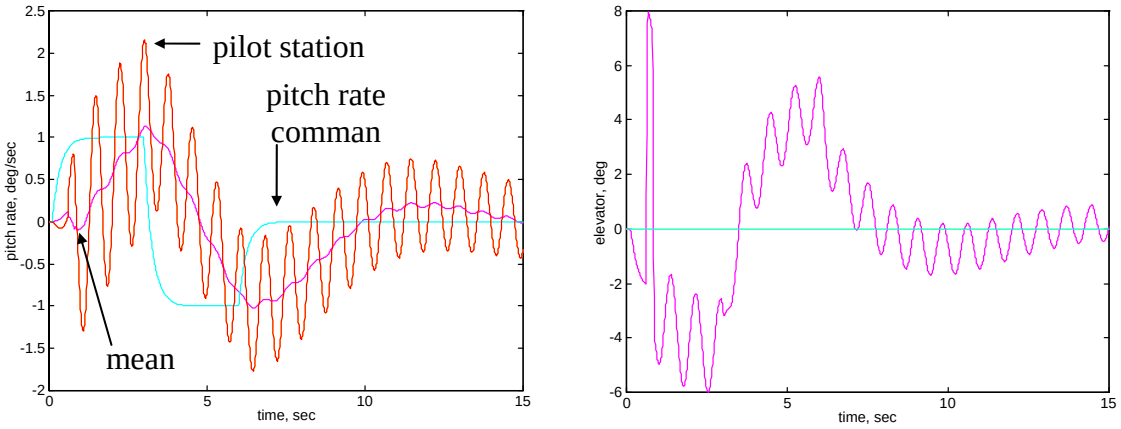

Figure C3: Pitch rate response, at mean axis and pilot station sensors, and elevator response to pitch rate command and impulse disturbance in elevator - elastic mode frequency ω_e=7.7 rad/sec.

As demonstrated in Figure C4, commanding a pitch rate, without additional external excitation, for a vehicle excites the first elastic mode, which the elevator cannot control while also trying to track a commanded pitch rate, and results in an unacceptable performance at the pilot station. The disturbance rejection results, in addition to a commanded pitch rate, are considerably worse (see Fig. C3). As the frequency of the first elastic mode is increased by 2X, the elevator no longer appreciably excites the first elastic mode due to a sufficient closed loop system roll off. The disturbance results also improve as the elevator is beginning to handle both command to the vehicle and disturbance caused excitation to the first elastic mode (see Fig. C2). As the elastic mode frequency is increased to 3X the original, the effects of the closed loop system roll off and the ability of the elevator to handle two objectives becomes even more apparent (see Fig. C1).

One of the characteristics of a large frequency separation between short period and elastic modes that is very beneficial is the fact that the closed loop system has significant rolled-off to attenuate any excitation to the elastic modes from mean axis pitch rate command (see Fig. C5) or to disturbances (see Fig. C6). The increase in the gain of the

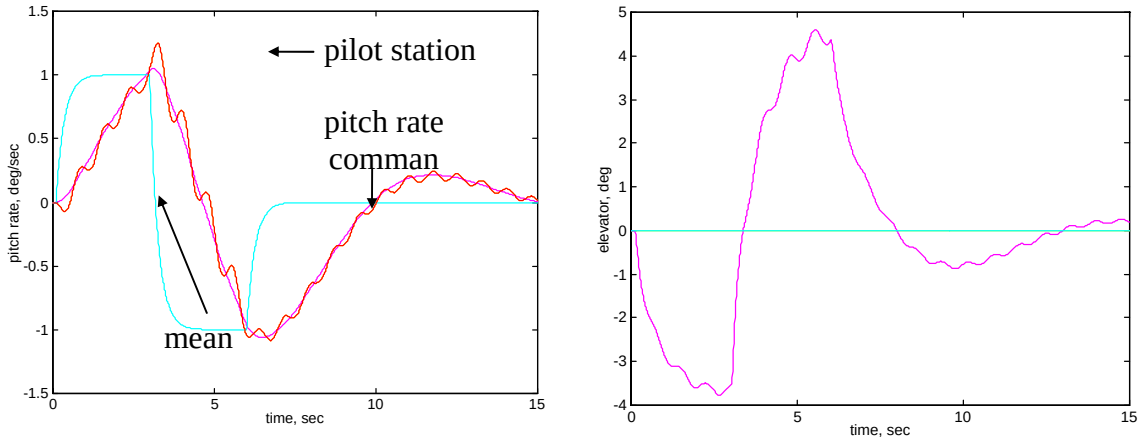

Figure C4: Pitch rate response, at mean axis and pilot station sensors, and elevator response to pitch rate command - elastic mode frequency ω_e=7.7 rad/sec.

flexible mode peak as the frequency decreases from 23.1 rad/sec to 15.4 rad/sec to 7.7 rad/sec is evident both at the mean axis approximating sensor and at the pilot station. The elevator controlling the pilot station flexible response is the extreme case of noncollocated sensor/actuator pair on this vehicle and the most difficult arrangement to control. The effect of the increased flexible mode peaks in the frequency response is directly illustrated in the high frequency oscillatory response, especially at the pilot station, superimposed on the lower frequency command following response as seen in figures C1-C3.

As the elastic mode frequency decreases, superimposing the flexible mode controller elevator command on the mean axis command becomes less and less effective since the oscillatory speed of the actuator must diminish in order to match the elastic mode frequency thus having greater impact on the mean axis vehicle response. From the elevator time response it is still apparent that superposition of two actuator commands is present but the pitch rate response at the pilot station and at the sensor approximating mean axis response illustrate the inability to fulfill the control objectives with a single actuator.

These results, support the conclusion that given the dynamics of this particular aircraft a single actuator cannot fulfill the dual objectives of controlling the vehicle, *i.e.*, its short period motion, and dampening the elastic mode excitation due to vehicle motion and external disturbances. The required frequency separation between the short period and the first elastic mode that would allow a single actuator to fulfill the dual objectives depends on the requirements placed on both the vehicle response and the response of the elastic modes. It would appear that the least acceptable separation would be 25 times the short period frequency or more than 10Hz.

C.3 Dual Actuator Multi-Objective Control

Recall the aircraft model discussed in Chapter 3. The early configuration of the HSCT vehicle did not have the RCV surfaces and, hence, the trailing edge flaps were used in conjunction with all-movable tail for an integrated flight/SMC control. The development of this control law is described in the following sections.

C.4 Control Development

The philosophy behind the design of the modified dynamic inversion controller is the same as described in Chapter 4. In developing this controller aircraft models of increasing complexity were used and the results are presented below. The results provide a good indication of the necessary dynamics that the design model must posses in order to have a successful design. Initial designs were also performed on the linear models in order to obtain a better understanding of the underlying dynamics. The subsequent design for the final HSCT configuration that had the RCV surfaces proceeded on the nonlinear models.

C.4.1 Control Design - 1 Degree of Freedom Problem

The fundamental function of the control law is to stabilize the vehicle and enable precise command tracking. For the specific flight condition under consideration, the vehicle is has benign rigid body instability and three lightly damped elastic modes. The open loop eigenvalues of the model under investigation are given in Figures C7 and C8. Hence, the role of the control system is to stabilize the instability and to track a commanded pitch rate, whether it is initiated by the pilot or by a guidance autopilot.

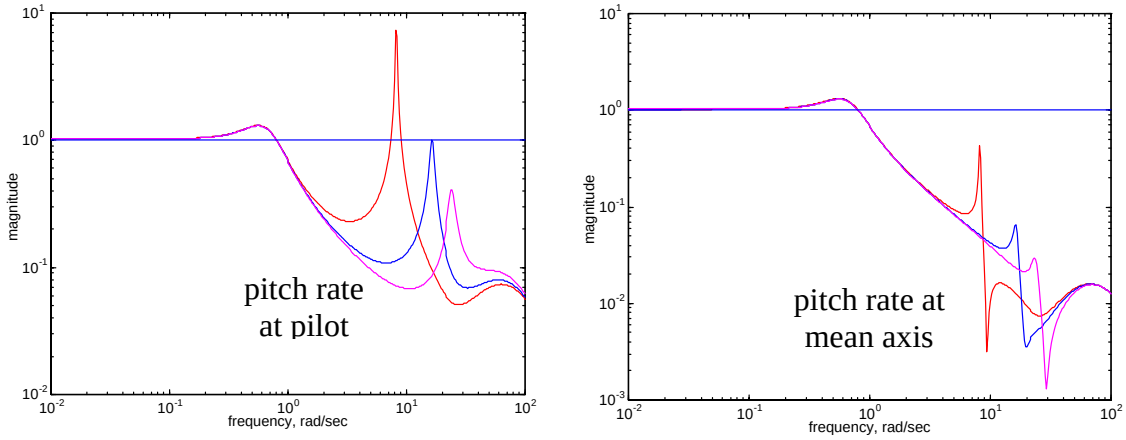

Figure C5: Pitch rate at pilot station and mean axis to pitch rate command loop frequency response for 3 different elastic mode frequencies.

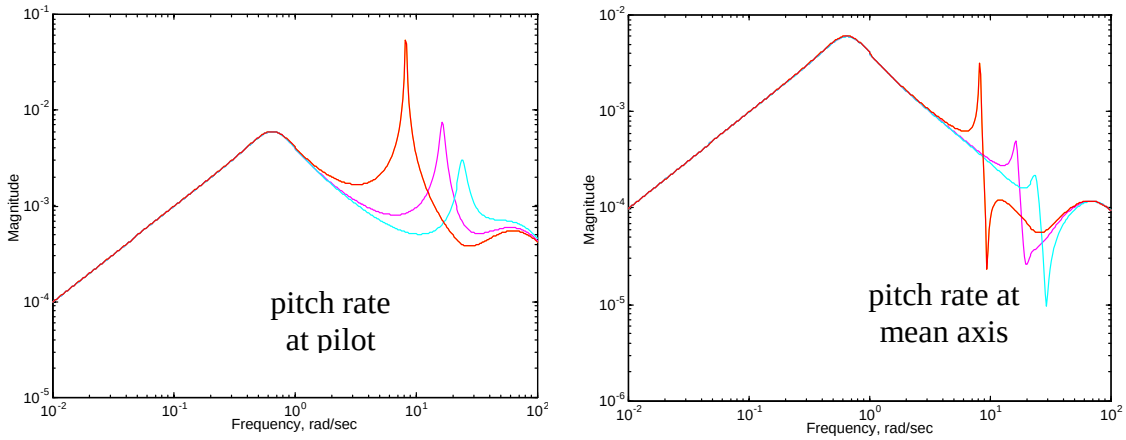

Figure C6: Pitch rate at pilot station and mean axis to input disturbance loop frequency response for 3 different elastic mode frequencies.

Nominal 3 elastic mode model

	Eigenvalue	Damping	Freq. (rad/sec)
	0.0117	-1.0000	0.0117
rigid body	-0.4297 + 0.3280i	0.7949	0.5406
	-0.4297 - 0.3280i	0.7949	0.5406
1st mode	-0.3430 + 7.7098i	0.0444	7.7175
	-0.3430 - 7.7098i	0.0444	7.7175
2nd mode	-0.7117 +12.7449i	0.0558	12.7647
	-0.7117 -12.7449i	0.0558	12.7647
3rd mode	-0.9873 +16.8986i	0.0583	16.9275
	-0.9873 -16.8986i	0.0583	16.9275
actuator dynamics	-20.0000	1.0000	20.0000
	-56.5680 +56.5691i	0.7071	80.0000
	-56.5680 -56.5691i	0.7071	80.0000

Figure C7: Open loop nominal 3 mode system eigenvalues. Modes enclosed in the box used for controller design.

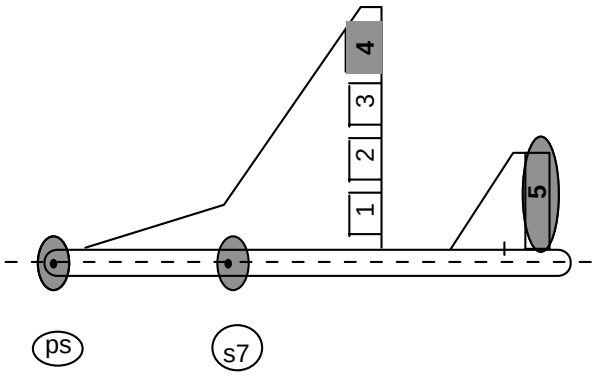

Figure C8: Sensors and actuators used in the study.

The controller is designed based on the short period and 1st elastic mode, outlined in a box in Figure C7. To facilitate better understanding of the results a linear model of the aerodynamics at a fixed flight condition is used. The control law from (23) with weighted control effectiveness and linear system representation becomes (C1). In this formulation the controller is an integrator of a degree equivalent to the number of the different desired CV dynamics. In this application, the controller is a single and a double integrator respectively.

$$u^{cmd} = (WCB)^{-1}\left[\dot{y}^{des} - CAx\right]$$
$$with\ \ \dot{y}^{des} = b\left[F_c\, y^{cmd} - y^{meas} + bF_i \int (y^{cmd} - y^{meas})dt\right] \tag{C1}$$

Moreover, only the 1st elastic mode is included in the design in order to evaluate the controller effect on the adjacent modes not explicitly considered. This, in fact, was the first controller design for the dynamic inversion methodology on an HSCT class vehicle. This 1 dof problem also served to motivate an active structural mode control of the lower elastic modes. Figure C9 gives a conceptual implementation of the control law.

A more detailed diagram of the controller is in the following section illustrating a more complex flight/structural mode control problem.

The analysis of the system response of this 1 dof controller illustrate a problem that has been seen in other work[23,27], an excitation of elastic mode at the pilot station. The system time response to a half of a doublet is shown in Figure C10. While the 1 dof controller, K1, provides some improvement in 1st elastic mode damping, it is still insufficient to eliminate the oscillations at the pilot station, which are unacceptable from the flying qualities requirements[60].

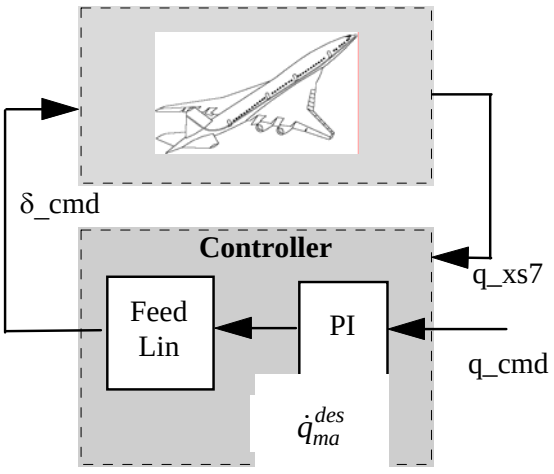

Figure C9: Conceptual dynamic inversion control law implementation.

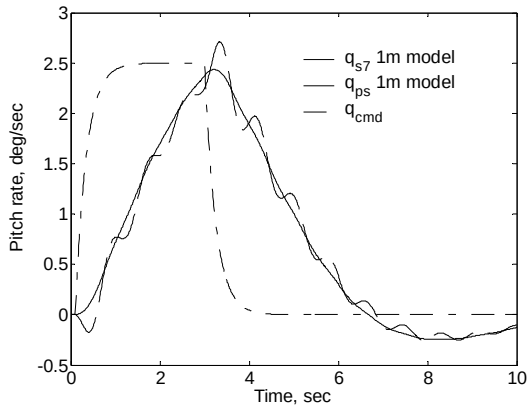

FigureC10: Pitch rate time response of a 1 mode system with the K1 controller to a half of a doublet pitch rate command (dashed - at pilot station; solid - at s7).

The K1 controller is evaluated on the 3 mode system with the very similar results. Figure C11 shows the time response to the commanded pitch rate is similar to that of a 1 mode system. The similarity in the response is explained by the dominance of the first elastic mode as illustrated in Figure C12 comparing 1 and 3 elastic mode systems modal response.

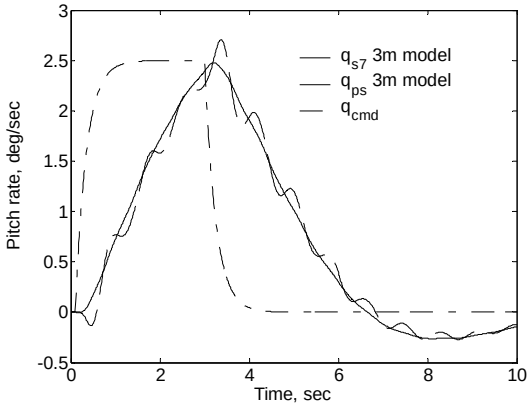

Figure C11: Pitch rate time response of a 3 mode system with the K1 controller to a half of a doublet pitch rate command (dashed - at pilot station; solid - at s7).

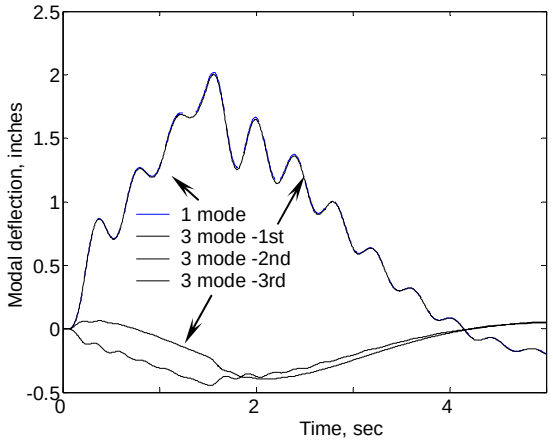

Figure C12: Open loop modal deflection to 2.5 deg elevator command

(solid - 3 mode model; dashed - 1 mode model).

The presence of undesirable oscillation in the pilot station response to elevator deflection producing the commanded pitch rate prompted the consideration of the 2 dof design described in detail in the next section.

C.4.2 Control Design - 2 Degree of Freedom Problem

The 2 dof problem was designed to address the pitch rate oscillations induced by the elevator while performing a command following function. Two aerodynamic surfaces were used to control the pitch rate response at two different positions on the aircraft. The TE surface, due to its location, is not ideal to control the first symmetric elastic mode. However, since a canard-like surface is not available on this vehicle configuration, TE is the only available surface for longitudinal control other than elevator. The problem was formulated such that TE and elevator worked to follow a pitch rate command and to minimize the error between pilot station and mean axis responses, utilizing ps and s7 sensors respectively. The selection of the sensor location s7 ensured minimum phase response; hence, stable zero dynamics. The transmission zeros for the 2x2 problem were also minimum phase resulting in stable zero dynamics.

The controller is illustrated in Figure C13. The controller can be thought of as divided into two parts, (1) a standard linear compensator and (2) a feedback linearization. The linear compensator, in this case, is a PI controller with three selectable gains, similar

in structure to the one used on HARV[2]. These gains can be interpreted as follows: b is the desired bandwidth of the loop response, Fi is the weight on the integral of the error, and Fc is the weight on the commanded inputs.

One important adjustment to a 2x2 dynamic inversion problem formulation, which so far appears to be generic for this type of two surface vehicle configuration, had to be made. A significant difference exists in pitch rate effectiveness for the aircraft between TE and elevon. This is fine if the surface positions are directly commanded — the TE contributes very little pitch rate. However, if pitch rate command is used by the dynamic inversion controller to calculate the surface deflections for both TE and elevon, there will be a very large discrepancy between magnitude deflection with emphasis on the least effective surface. The q_cmd will produce a much larger TE deflection than the elevon because $(CB)^{-1}$ is taken as "control effectiveness." To work around this problem, a weighting is introduced similar to the one described in (3) with the final form given below in (C2). The difference feeding into $(WCB)^{-1}$ can be thought of as the error between the desired and the actual rate of change of pitch rate.

$$\begin{bmatrix} TE \\ \delta elev \end{bmatrix} = (WCB)^{-1} \begin{bmatrix} \dot{q}^e\_s7 \\ \dot{q}^e\_ps \end{bmatrix} \Rightarrow \begin{bmatrix} TE \\ \delta elev \end{bmatrix} = \begin{bmatrix} 0 & b \\ c & d \end{bmatrix} \begin{bmatrix} \dot{q}^e\_s7 \\ \dot{q}^e\_ps \end{bmatrix} \qquad (C2)$$

This means qe_s7 (error between q_cmd and q_s7) produces no TE deflection. Since TE has essentially no influence on q_s7, this adjustment has negligible physical impact. The elevator influence at q_ps is almost equal and opposite to that of TE, and in this formulation, TE is relegated to counter the elevator induced elastic excitation at the pilot station.

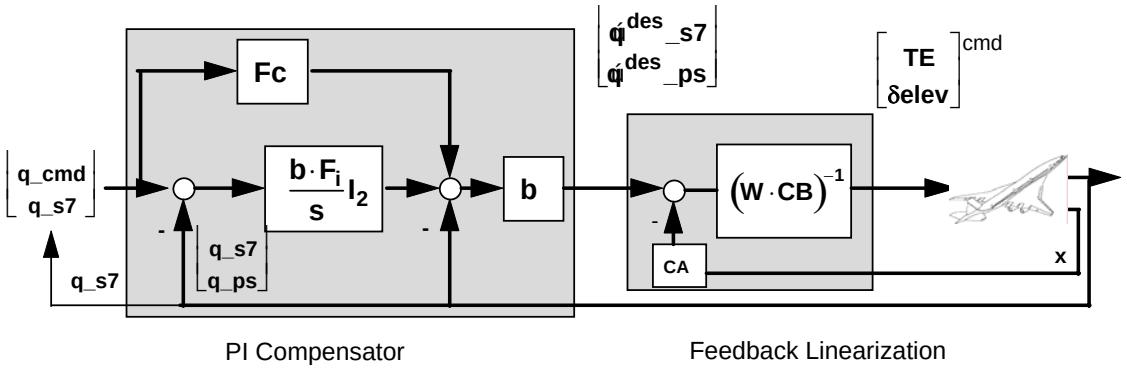

Figure C13: Control law block diagram for a 2 dof dynamic inversion compensator.

The analysis of the resulting controller, K2, applied to a 1 mode system indicate that TE is in fact successful in minimizing the difference between the pilot station response from that of the mean axis of the aircraft (see Fig. C14) without requiring excessive control surface deflections (see Fig. C15). Furthermore, the speed of the response is consistent with that of other comparably large aircraft, e.g. B-747, without producing large overshoot or rapid oscillations.

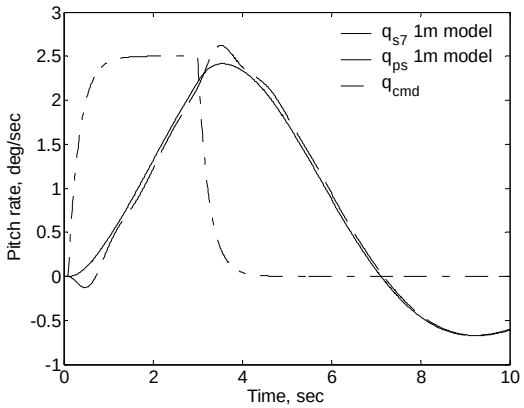

Figure C14: Pitch rate time response of a 1 mode system with the K2 controller to a half of a doublet pitch rate command (dashed - at pilot station; solid - at s7).

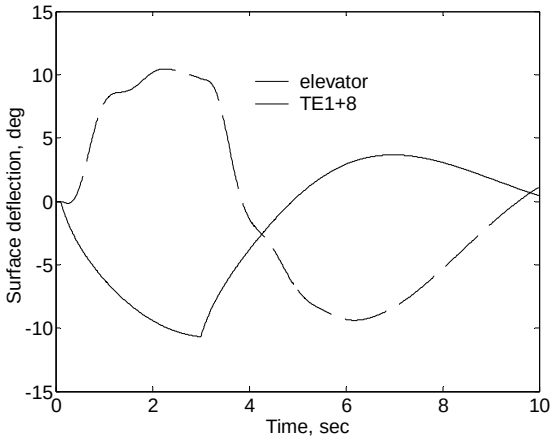

Figure C15: Elevator (solid) and trailing edge 1+8 (dashed) commanded response to q_cmd with the K2 controller.

The stability analysis also indicate relatively good design even though the controller was neither optimized for performance nor designed with special consideration for robustness. The traditional one loop at a time margins are shown in Figures C16 and C17. The gain and phase margin at the pilot station are 10.09 dB and 74.58 deg, respectively. Similarly, for the sensor location s7, the margins are infinite and 80 deg.

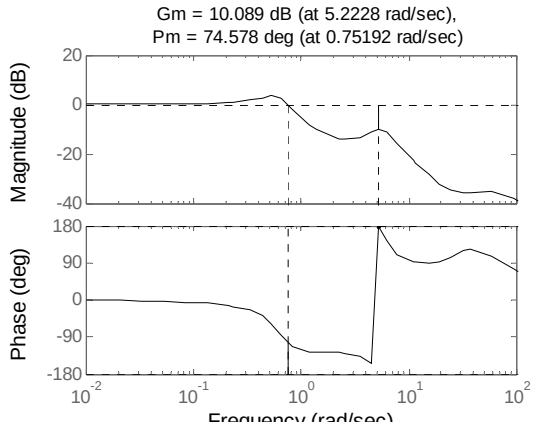

Figure C16: Gain (10.86dB) and phase (68.23 deg) margins for q_ps/q_cmd.

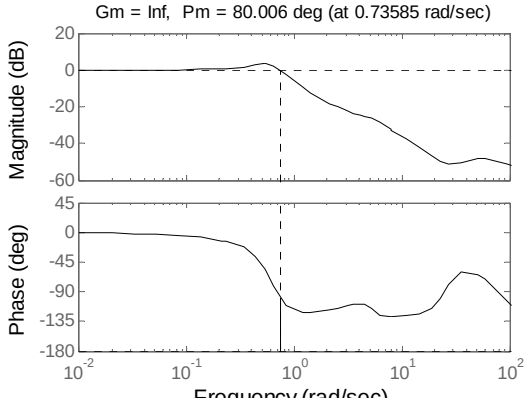

Figure C17: Gain (inf) and phase (72.73 deg) margins for q_s7/q_cmd.

The initial test for robustness focused on uncertainty in the frequency and damping of the first elastic mode. A robust stability μ problem was formulated for parametric uncertainty in frequency, $(\omega+\delta\omega)$, and damping, $(\zeta+\delta\zeta)$. The μ analysis was performed

twice: once treating the uncertainty as complex, and the second time as primarily real, $(\delta_R+\alpha^2\delta_C)$ where α is small[61]. Modeling parametric uncertainty with complex scalars is beneficial from computational point of view and such approximation works reasonably well in some applications without introducing excessive conservatism into the problem. However, it is indisputably evident from the results in Figure C18 that this is not the case here. The difference in the level of tolerable uncertainty is between real and complex formulation is almost two times. From the form of the generalized force equation, (3), one can observe that modeling frequency as a complex scalar immediately introduces the imaginary part as a perturbation on the damping. For relatively high frequency and low damping case, the frequency perturbation would render damping negative, hence making the system unstable and falling the μ robust stability test.

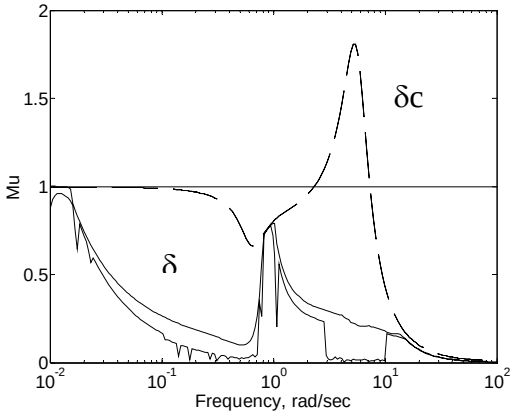

Figure C18: Robust stability for ζ and ω variation in 1st elastic mode (ζ_o = 0.0463; ω_o = 7.712 rad/sec) (uncertainty: $[\delta\zeta\ \delta\omega]$=[-50% -26%]; solid - $(\delta_R+\alpha^2\delta_C)$; dashed - δ_C).

The destabilizing perturbation for the 1st elastic mode uncertainty is $[\delta\zeta\ \delta\omega]$ = [-80% -26%]. From varying the level of uncertainty, it became apparent that the uncertainty in modal frequency has larger effect on stability than does the modal damping. Generally, modal frequency uncertainty in the first few elastic modes is expected to be on the order of 10%, so the μ test shows some promise in controller being robust to frequency and damping uncertainty at the expected levels.

Furthermore, comparing the results between complex and real model of parametric uncertainty indicates a difference of where the system instability to the destabilizing perturbation would occur. The instability for complex model would first occur around a first mode frequency, due to negative damping as described above. For a real uncertainty model, on the other hand, instability occurs at very low frequency. To understand the mechanism of this instability and to confirm the results of the μ test on a mostly real uncertainty model, a real perturbation, derived from the μ test, is incorporated into the nominal open loop model and then the K2 controller is wrapped around the system. The results are presented in Figures C19- C21.

The time responses of the nominal and perturbed closed loop systems are shown in Figure C19. The perturbed closed loop system has a real pole at 0.021, which results in a relatively long time to double. Note that the perturbed system response, while unstable (see Fig. C21), is rather benign. Applying a dynamic inversion controller to a perturbed system is essentially equivalent to an imperfect cancellation of undesirable dynamics. The dynamics of the perturbed system are very different from the model used in controller design primarily from a 26% decrease in natural frequency of the first elastic mode. Yet, despite this mismatch the resulting instability is rather benign. While this type of result cannot be generalized so far, it does offer some promise that imperfect knowledge of the system to be controller would not cause severe instability.

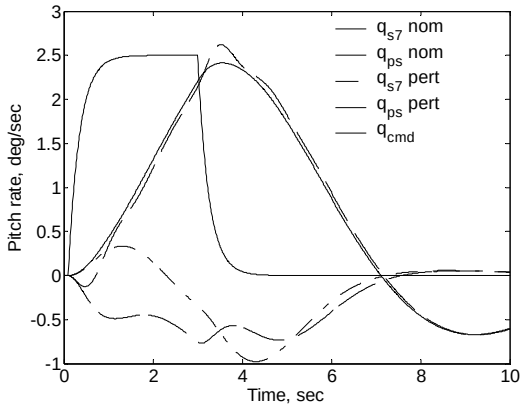

Figure C19: Pitch rate time response of a 1 mode nominal and perturbed systems with the K2 controller to a half of a doublet pitch rate command, [δζ δω]=[-80% -26%].

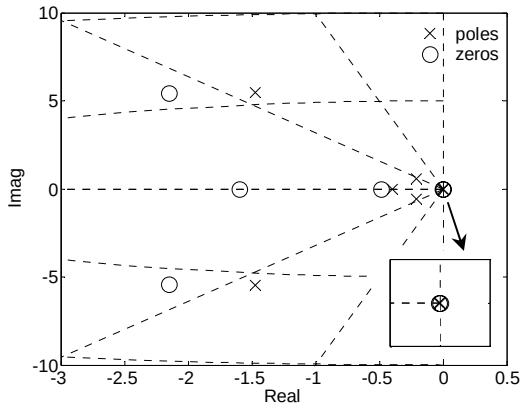

Figure C20: Nominal 1 mode system with K2 controller pole-zero map.

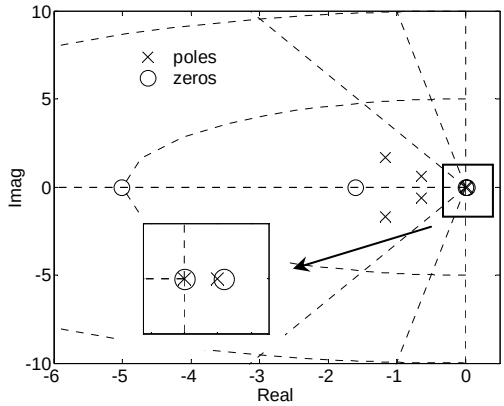

Figure C21: Perturbed 1 mode system with K2 controller pole-zero map

$[\delta\zeta\ \delta\omega]=[-80\%\ -26\%]$.

The difference between nominal and perturbed closed loop systems is illustrated in Figures C20 and C21. The enlarged view around the origin indicates that the nominal closed loop has a double integrator, from the K2 controller, and two zeros essentially at the origin (see Fig. C20). The perturbed system, as is evident from Figure C21, has an unstable pole and a NMP zero in the neighborhood of the origin as well as another NMP zero an order of magnitude away. The precise reason for this particular pole-zero arrangement will be explored analytically in the context of robustness studies.

The application of the K2 controller to a 3 mode system raises a number of issues. This is a potential illustration of interference with adjacent modes of the control action.

While the time response of a 3 mode system with the K2 controller is very similar to a 1 mode system response, *i.e.*, pilot station response almost matches that of the mean axis as the controller is designed to do, the effect on the adjacent modes is less than desirable (see Figs. C22 and C23). The reasons for the move of the 2nd elastic mode from LHP to almost neutral stability on the imaginary axis as well as some movement of the 3rd elastic mode towards the imaginary axis are unclear. One possibility is the move of the 1st mode so far into the LHP to increase its damping by more than 1000%, which as a byproduct also decreases its frequency, causes a corresponding decrease in the damping of the 2nd mode and some decrease in the 3rd. Another, and much less welcome possibility, is that using wing based devices causes the decrease in damping of the 2nd and 3rd modes since they are primarily wing based modes. If this in fact is the case, this would imply that wing mounted surfaces are not available for control that would in turn mandate some rethinking of the configuration.

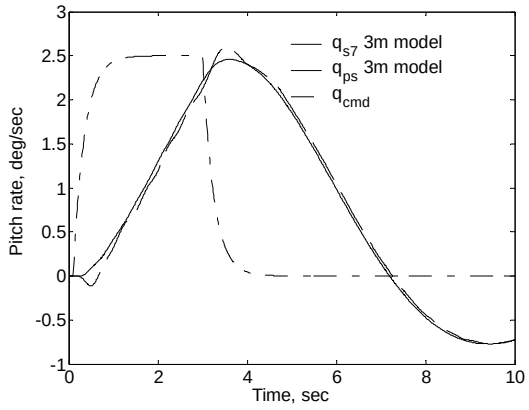

Figure C22: Pitch rate time response of a 3 mode system with K2 controller to a half of a doublet pitch rate command (solid - s7; dashed – ps).

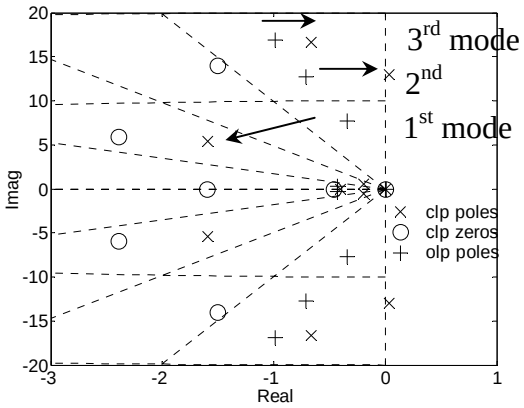

Figure C23: Pole zero map of a 3 mode system and effect of the K2 controller on its elastic modes.

Appendix D – General Derivation of *div*(G) for MIMO system

D.1 General Nonlinear System

Closed loop internal dynamics as $t \to \infty$

$$\begin{pmatrix} \dot{u} \\ \dot{w} \end{pmatrix} = \begin{pmatrix} -g\sin\theta_{cmd} + T/\mathrm{m} \\ g\cos\theta_{cmd} \end{pmatrix} + \frac{\rho S V^2}{2\mathrm{m}} \left\{ \begin{pmatrix} \bar{C}_x(\cdot) \\ \bar{C}_z(\cdot) \end{pmatrix} + \begin{pmatrix} \bar{C}_x^{re}(\cdot) \\ \bar{C}_x^{re}(\cdot) \end{pmatrix} V + \begin{pmatrix} \bar{C}_x^{e}(\cdot) \\ \bar{C}_x^{e}(\cdot) \end{pmatrix} \eta_{cmd} \right\}$$

or

$$\begin{pmatrix} \dot{u} \\ \dot{w} \end{pmatrix} = \begin{pmatrix} -g\sin\theta_{cmd} + \dfrac{T}{\mathrm{m}} \\ g\cos\theta_{cmd} \end{pmatrix} + \frac{1}{\mathrm{m}} \begin{pmatrix} \bar{F}_x(u,w) + \bar{F}_x^{re}(u,w) + \bar{F}_x^{e}(u,w,\eta) \\ \bar{F}_z(u,w) + \bar{F}_z^{re}(u,w) + \bar{F}_z^{e}(u,w,\eta) \end{pmatrix}$$

Define G

$$G \triangleq \begin{pmatrix} -g\sin\theta_{cmd} + \dfrac{T}{\mathrm{m}} \\ g\cos\theta_{cmd} \end{pmatrix} + \frac{1}{\mathrm{m}} \begin{pmatrix} \bar{F}_x(u,w) + \bar{F}_x^{re}(u,w) + \bar{F}_x^{e}(u,w,\eta) \\ \bar{F}_z(u,w) + \bar{F}_z^{re}(u,w) + \bar{F}_z^{e}(u,w,\eta) \end{pmatrix}$$

Then *div*(G) is given by

$$div(G) = \frac{\partial\left(-g\sin\theta_{cmd} + \dfrac{T}{\mathrm{m}} + \dfrac{1}{\mathrm{m}}\left(\bar{F}_x(u,w) + \bar{F}_x^{re}(u,w) + \bar{F}_x^{e}(u,w,\eta) \right) \right)}{\partial u} + \frac{\partial\left(g\cos\theta_{cmd} + \dfrac{1}{\mathrm{m}}\left(\bar{F}_z(u,w) + \bar{F}_z^{re}(u,w) + \bar{F}_z^{e}(u,w,\eta) \right) \right)}{\partial w}$$

To enable simplified calculation taking *div*(G) by parts results in

$$\begin{aligned} div(G) = {} & \frac{\partial\left(-g\sin\theta_{cmd} + \dfrac{T}{\mathrm{m}} \right)}{\partial u} + \frac{\partial\left(g\cos\theta_{cmd} \right)}{\partial w} \\ & + \frac{1}{\mathrm{m}} \frac{\partial\left(\left(\bar{F}_x(u,w) + \bar{F}_x^{re}(u,w) + \bar{F}_x^{e}(u,w,\eta) \right) \right)}{\partial u} \\ & + \frac{1}{\mathrm{m}} \frac{\partial\left(\left(\bar{F}_z(u,w) + \bar{F}_z^{re}(u,w) + \bar{F}_z^{e}(u,w,\eta) \right) \right)}{\partial w} \end{aligned}$$

So eliminating the nondependent parts results in

$$div(G) = \frac{div(\bar{F})}{\mathrm{m}}$$

$$\text{where } \bar{\mathrm{F}} = \begin{pmatrix} \bar{F}_x(u,w) + \bar{F}_x^{re}(u,w) + \bar{F}_x^{e}(u,w,\eta) \\ \bar{F}_z(u,w) + \bar{F}_z^{re}(u,w) + \bar{F}_z^{e}(u,w,\eta) \end{pmatrix}$$

The interest is to obtain *divG* in terms of lift and drag forces, hence requiring coordinate transformation once again. From definitions of α and *V*

$$\frac{d\alpha}{du} = \frac{-\sin\alpha}{V} \quad \frac{d\alpha}{dw} = \frac{\cos\alpha}{V}$$

In addition recall the coefficient conversion equations:

$$\begin{aligned} \bar{C}_x &= \sin\alpha\bar{C}_L - \cos\alpha\bar{C}_D & \bar{C}_z &= -\cos\alpha\bar{C}_L - \sin\alpha\bar{C}_D \\ \bar{C}_x^{re} &= \sin\alpha\bar{C}_L^{re} - \cos\alpha\bar{C}_D^{re} & \bar{C}_z^{re} &= -\cos\alpha\bar{C}_L^{re} - \sin\alpha\bar{C}_D^{re} \\ \bar{C}_x^{e} &= \sin\alpha\bar{C}_L^{e} - \cos\alpha\bar{C}_D^{e} & \bar{C}_z^{e} &= -\cos\alpha\bar{C}_L^{e} - \sin\alpha\bar{C}_D^{e} \end{aligned}$$

The equilibrium force divergence is evaluated below.

$$div(\bar{F}) = \frac{\partial\left(\bar{F}_x(u,w) + \bar{F}_x^{re}(u,w) + \bar{F}_x^{e}(u,w,\eta)\right)}{\partial u} + \frac{\partial\left(\bar{F}_x(u,w) + \bar{F}_x^{re}(u,w) + \bar{F}_x^{e}(u,w,\eta)\right)}{\partial w}$$

u-direction:

$$\frac{\partial\left(\bar{F}_x(u,w) + \bar{F}_x^{re}(u,w) + \bar{F}_x^{e}(u,w,\eta)\right)}{\partial u} =$$

$$\frac{\partial\left(\frac{1}{2}\rho V^2 S\bar{C}_x(\alpha)\right)}{\partial u} + \frac{\partial\left(\frac{1}{2}\rho V^2 S\bar{C}_x^{re}(\alpha)V\right)}{\partial u} + \frac{\partial\left(\frac{1}{2}\rho V^2 S\bar{C}_x^{e}(\alpha)\eta\right)}{\partial u}$$

calculating individual parts

$$\frac{\partial\left(\frac{1}{2}\rho V^2 S\bar{C}_x(\alpha)\right)}{\partial u}=\frac{\partial\left(\frac{1}{2}\rho\left(u^2+w^2\right)S\bar{C}_x(\alpha)\right)}{\partial u}=u\rho S\bar{C}_x(\alpha)+\frac{\rho V^2 S}{2}\frac{\partial\bar{C}_x(\alpha)}{\partial u}$$

$$=V\cos\alpha\rho S\bar{C}_x(\alpha)+\frac{\rho V^2 S}{2}\frac{d\left(\sin\alpha\bar{C}_L-\cos\alpha\bar{C}_D\right)}{d\alpha}\frac{-\sin\alpha}{V}$$

$$=\rho SV\cos\alpha\left(\sin\alpha\bar{C}_L-\cos\alpha\bar{C}_D\right)$$

$$+\frac{\rho V^2 S}{2}\frac{-\sin\alpha}{V}\left(\cos\alpha\bar{C}_L+\sin\alpha\frac{d\bar{C}_L}{d\alpha}+\sin\alpha\bar{C}_D-\cos\alpha\frac{d\bar{C}_D}{d\alpha}\right)$$

$$=\frac{\rho VS}{2}\begin{pmatrix}2\cos\alpha\sin\alpha\bar{C}_L-2\cos^2\alpha\bar{C}_D-\sin\alpha\cos\alpha\bar{C}_L\\-\sin^2\alpha\frac{d\bar{C}_L}{d\alpha}-\sin^2\alpha\bar{C}_D+\sin\alpha\cos\alpha\frac{d\bar{C}_D}{d\alpha}\end{pmatrix}$$

$$=\frac{\rho VS}{2}\left(\cos\alpha\sin\alpha\bar{C}_L-2\cos^2\alpha\bar{C}_D-\sin^2\alpha\bar{C}_D-\sin^2\alpha\frac{d\bar{C}_L}{d\alpha}+\sin\alpha\cos\alpha\frac{d\bar{C}_D}{d\alpha}\right)$$

$$\frac{\partial\left(\frac{1}{2}\rho V^3 S\bar{C}_x^{re}(\alpha)\right)}{\partial u}=\frac{\rho S}{2}\frac{\partial\left(\left(u^2+w^2\right)^{\frac{3}{2}}\bar{C}_x^{re}(\alpha)\right)}{\partial u}=$$

$$\frac{\rho S}{2}\left(\frac{3}{2}\left(u^2+w^2\right)^{\frac{1}{2}}2u\bar{C}_x^{re}(\alpha)+V^3\frac{\partial\bar{C}_x^{re}(\alpha)}{\partial u}\right)$$

$$=\frac{\rho S}{2}\left(3V^2\cos\alpha\left(\sin\alpha\bar{C}_L^{re}-\cos\alpha\bar{C}_D^{re}\right)-V^3\frac{\sin\alpha}{V}\frac{d\left(\sin\alpha\bar{C}_L^{re}-\cos\alpha\bar{C}_D^{re}\right)}{d\alpha}\right)$$

$$=\frac{\rho SV^2}{2}\begin{pmatrix}3\left(\cos\alpha\sin\alpha\bar{C}_L^{re}-\cos^2\alpha\bar{C}_D^{re}\right)\\-\sin\alpha\left(\cos\alpha\bar{C}_L^{re}+\sin\alpha\frac{d\bar{C}_L^{re}}{d\alpha}+\sin\alpha\bar{C}_D^{re}-\cos\alpha\frac{d\bar{C}_D^{re}}{d\alpha}\right)\end{pmatrix}$$

$$=\frac{\rho SV^2}{2}\begin{pmatrix}3\cos\alpha\sin\alpha\bar{C}_L^{re}-3\cos^2\alpha\bar{C}_D^{re}-\sin\alpha\cos\alpha\bar{C}_L^{re}\\-\sin^2\alpha\frac{d\bar{C}_L^{re}}{d\alpha}-\sin^2\alpha\bar{C}_D^{re}+\sin\alpha\cos\alpha\frac{d\bar{C}_D^{re}}{d\alpha}\end{pmatrix}$$

$$=\frac{\rho SV^2}{2}\left(2\cos\alpha\sin\alpha\bar{C}_L^{re}-3\cos^2\alpha\bar{C}_D^{re}-\sin^2\alpha\frac{d\bar{C}_L^{re}}{d\alpha}-\sin^2\alpha\bar{C}_D^{re}+\sin\alpha\cos\alpha\frac{d\bar{C}_D^{re}}{d\alpha}\right)$$

$$\frac{\partial\left(\frac{1}{2}\rho V^2 S\bar{C}_x^e(\alpha)\eta\right)}{\partial u} = u\rho S\bar{C}_x^e(\alpha)\eta + \frac{\rho V^2 S}{2}\frac{\partial\bar{C}_x^e(\alpha)\eta}{\partial u}$$

$$= V\cos\alpha\rho S\left(\sin\alpha\bar{C}_L^e - \cos\alpha\bar{C}_D^e\right)\eta + \frac{\rho V^2 S}{2}\eta\frac{d\left(\sin\alpha\bar{C}_L^e - \cos\alpha\bar{C}_D^e\right)}{d\alpha}\frac{-\sin\alpha}{V}$$

$$= \frac{\rho VS}{2}\left(\begin{array}{l} 2\cos\alpha\sin\alpha\bar{C}_L^e - 2\cos^2\alpha\bar{C}_D^e \\ -\sin\alpha\left(\cos\alpha\bar{C}_L^e + \sin\alpha\frac{d\bar{C}_L^e}{d\alpha} + \sin\alpha\bar{C}_D^e - \cos\alpha\frac{d\bar{C}_D^e}{d\alpha}\right)\end{array}\right)\eta$$

$$= \frac{\rho VS}{2}\left(\cos\alpha\sin\alpha\bar{C}_L^e - 2\cos^2\alpha\bar{C}_D^e - \sin^2\alpha\frac{d\bar{C}_L^e}{d\alpha} - \sin^2\alpha\bar{C}_D^e + \sin\alpha\cos\alpha\frac{d\bar{C}_D^e}{d\alpha}\right)\eta$$

combining terms in the u-direction

$$\frac{\partial\left(\frac{1}{2}\rho V^2 S\bar{C}_x(\alpha)\right)}{\partial u} + \frac{\partial\left(\frac{1}{2}\rho V^2 S\bar{C}_x^{re}(\alpha)V\right)}{\partial u} + \frac{\partial\left(\frac{1}{2}\rho V^2 S\bar{C}_x^e(\alpha)\eta\right)}{\partial u} =$$

$$\frac{\rho VS}{2}\left(\cos\alpha\sin\alpha\bar{C}_L - 2\cos^2\alpha\bar{C}_D - \sin^2\alpha\bar{C}_D - \sin^2\alpha\frac{d\bar{C}_L}{d\alpha} + \sin\alpha\cos\alpha\frac{d\bar{C}_D}{d\alpha}\right)$$

$$+\frac{\rho SV^2}{2}\left(2\cos\alpha\sin\alpha\bar{C}_L^{re} - 3\cos^2\alpha\bar{C}_D^{re} - \sin^2\alpha\frac{d\bar{C}_L^{re}}{d\alpha} - \sin^2\alpha\bar{C}_D^{re} + \sin\alpha\cos\alpha\frac{d\bar{C}_D^{re}}{d\alpha}\right)$$

$$+\frac{\rho VS}{2}\left(\cos\alpha\sin\alpha\bar{C}_L^e - 2\cos^2\alpha\bar{C}_D^e - \sin^2\alpha\frac{d\bar{C}_L^e}{d\alpha} - \sin^2\alpha\bar{C}_D^e + \sin\alpha\cos\alpha\frac{d\bar{C}_D^e}{d\alpha}\right)\eta$$

w-direction:

$$\frac{\partial\left(\bar{F}_z(u,w) + \bar{F}_z^{re}(u,w) + \bar{F}_z^e(u,w,\eta)\right)}{\partial w} =$$

$$\frac{\partial\left(\frac{1}{2}\rho V^2 S\bar{C}_z(\alpha)\right)}{\partial w} + \frac{\partial\left(\frac{1}{2}\rho V^2 S\bar{C}_z^{re}(\alpha)V\right)}{\partial w} + \frac{\partial\left(\frac{1}{2}\rho V^2 S\bar{C}_z^e(\alpha)\eta\right)}{\partial w}$$

calculating individual parts

$$\frac{\partial\left(\frac{1}{2}\rho V^2 S\bar{C}_z(\alpha)\right)}{\partial w}=\frac{\partial\left(\frac{1}{2}\rho\left(u^2+w^2\right)S\bar{C}_z(\alpha)\right)}{\partial u}=w\rho S\bar{C}_z(\alpha)+\frac{\rho V^2 S}{2}\frac{\partial\bar{C}_z(\alpha)}{\partial w}$$

$$=V\sin\alpha\rho S\left(-\cos\alpha\bar{C}_L-\sin\alpha\bar{C}_D\right)+\frac{\rho V^2 S}{2}\frac{d\left(-\cos\alpha\bar{C}_L-\sin\alpha\bar{C}_D\right)}{d\alpha}\frac{\cos\alpha}{V}$$

$$=\frac{\rho SV}{2}\left(-2\sin\alpha\cos\alpha\bar{C}_L-2\sin^2\alpha\bar{C}_D\right)$$

$$+\frac{\rho SV}{2}\cos\alpha\left(\sin\alpha\bar{C}_L-\cos\alpha\frac{d\bar{C}_L(\alpha)}{d\alpha}-\cos\alpha\bar{C}_D-\sin\alpha\frac{d\bar{C}_D(\alpha)}{d\alpha}\right)$$

$$=\frac{\rho SV}{2}\begin{pmatrix}-2\sin\alpha\cos\alpha\bar{C}_L-2\sin^2\alpha\bar{C}_D+\cos\alpha\sin\alpha\bar{C}_L\\-\cos^2\alpha\frac{d\bar{C}_L(\alpha)}{d\alpha}-\cos^2\alpha\bar{C}_D-\cos\alpha\sin\alpha\frac{d\bar{C}_D(\alpha)}{d\alpha}\end{pmatrix}$$

$$=\frac{\rho SV}{2}\begin{pmatrix}-\sin\alpha\cos\alpha\bar{C}_L-2\sin^2\alpha\bar{C}_D-\cos^2\alpha\frac{d\bar{C}_L(\alpha)}{d\alpha}-\cos^2\alpha\bar{C}_D\\-\cos\alpha\sin\alpha\frac{d\bar{C}_D(\alpha)}{d\alpha}\end{pmatrix}$$

$$\frac{\partial\left(\frac{1}{2}\rho V^2 S\bar{C}_z^{re}(\alpha)V\right)}{\partial w}=\frac{\rho S}{2}\frac{\partial\left(\left(u^2+w^2\right)^{\frac{3}{2}}\bar{C}_z^{re}(\alpha)\right)}{\partial w}$$

$$=\frac{\rho S}{2}\left(\frac{3}{2}\left(u^2+w^2\right)^{\frac{1}{2}}2w\bar{C}_z^{re}(\alpha)+V^3\frac{\partial\bar{C}_z^{re}(\alpha)}{\partial w}\right)$$

$$=\frac{\rho S}{2}\left(3V^2\sin\alpha\left(-\cos\alpha\bar{C}_L^{re}-\sin\alpha\bar{C}_D^{re}\right)+V^3\frac{\cos\alpha}{V}\frac{d\left(-\cos\alpha\bar{C}_L^{re}-\sin\alpha\bar{C}_D^{re}\right)}{d\alpha}\right)$$

$$=\frac{\rho SV^2}{2}\begin{pmatrix}-3\sin\alpha\cos\alpha\bar{C}_L^{re}-3\sin^2\alpha\bar{C}_D^{re}\\+\cos\alpha\left(\sin\alpha\bar{C}_L^{re}-\cos\alpha\frac{d\bar{C}_L^{re}(\alpha)}{d\alpha}-\cos\alpha\bar{C}_D^{re}-\sin\alpha\frac{d\bar{C}_D^{re}(\alpha)}{d\alpha}\right)\end{pmatrix}$$

$$=\frac{\rho SV^2}{2}\begin{pmatrix}-2\sin\alpha\cos\alpha\bar{C}_L^{re}-3\sin^2\alpha\bar{C}_D^{re}-\cos^2\alpha\frac{d\bar{C}_L^{re}(\alpha)}{d\alpha}-\cos^2\alpha\bar{C}_D^{re}\\-\cos\alpha\sin\alpha\frac{d\bar{C}_D^{re}(\alpha)}{d\alpha}\end{pmatrix}$$

$$\frac{\partial\left(\frac{1}{2}\rho V^2 S\bar{C}_z^e(\alpha)\eta\right)}{\partial w} = w\rho S\bar{C}_z^e(\alpha)\eta + \frac{\rho V^2 S}{2}\frac{\partial\bar{C}_z^e(\alpha)\eta}{\partial w}$$

$$= V\sin\alpha\rho S\left(-\cos\alpha\bar{C}_L^e - \sin\alpha\bar{C}_D^e\right)\eta + \frac{\rho V^2 S}{2}\eta\frac{d\left(-\cos\alpha\bar{C}_L^e - \sin\alpha\bar{C}_D^e\right)}{d\alpha}\frac{\cos\alpha}{V}$$

$$= \left(w\rho S\bar{C}_z^e(\alpha) + \frac{\rho SV}{2}\cos\alpha\frac{d\bar{C}_z^e(\alpha)}{d\alpha}\right)\eta$$

$$= \left(-2\cos\alpha\bar{C}_L^e - 2\sin^2\alpha\bar{C}_D^e + \cos\alpha\begin{pmatrix}\sin\alpha\bar{C}_L^e - \cos\alpha\frac{d\bar{C}_L^e(\alpha)}{d\alpha}\\ -\cos\alpha\bar{C}_D^e - \sin\alpha\frac{d\bar{C}_D^e(\alpha)}{d\alpha}\end{pmatrix}\right)\frac{\rho SV}{2}\eta$$

$$= \left(-\cos\alpha\bar{C}_L^e - 2\sin^2\alpha\bar{C}_D^e - \cos^2\alpha\frac{d\bar{C}_L^e(\alpha)}{d\alpha} - \cos^2\alpha\bar{C}_D^e - \cos\alpha\sin\alpha\frac{d\bar{C}_D^e(\alpha)}{d\alpha}\right)\frac{\rho SV}{2}\eta$$

combining terms in the w-direction

$$\frac{\partial\left(\frac{\bar{F}_z + \bar{F}_z^{re} + \bar{F}_z^e}{\mathrm{m}}\right)}{\partial w} = \frac{\partial\left(\frac{\rho V^2 S}{2\mathrm{m}}\left(\bar{C}_z(\alpha) + \bar{C}_z^{re}(\alpha)V + \bar{C}_z^e(\alpha)\eta\right)\right)}{\partial w} =$$

$$\frac{\rho SV}{2}\left(-\sin\alpha\cos\alpha\bar{C}_L - 2\sin^2\alpha\bar{C}_D - \cos^2\alpha\frac{d\bar{C}_L(\alpha)}{d\alpha} - \cos^2\alpha\bar{C}_D - \cos\alpha\sin\alpha\frac{d\bar{C}_D(\alpha)}{d\alpha}\right)$$

$$+\frac{\rho SV^2}{2}\begin{pmatrix}-2\sin\alpha\cos\alpha\bar{C}_L^{re} - 3\sin^2\alpha\bar{C}_D^{re} - \cos^2\alpha\frac{d\bar{C}_L^{re}(\alpha)}{d\alpha}\\ -\cos^2\alpha\bar{C}_D^{re} - \cos\alpha\sin\alpha\frac{d\bar{C}_D^{re}(\alpha)}{d\alpha}\end{pmatrix}$$

$$+\frac{\rho SV}{2}\eta\left(-\cos\alpha\bar{C}_L^e - 2\sin^2\alpha\bar{C}_D^e - \cos^2\alpha\frac{d\bar{C}_L^e(\alpha)}{d\alpha} - \cos^2\alpha\bar{C}_D^e - \cos\alpha\sin\alpha\frac{d\bar{C}_D^e(\alpha)}{d\alpha}\right)$$

Hence combining results for the *div*(F) gives

$$\frac{\partial\left(\frac{\rho V^2 S}{2\mathrm{m}}\left(\bar{C}_x(\alpha)+\bar{C}_x^{re}(\alpha)V+\bar{C}_x^{e}(\alpha)\eta\right)\right)}{\partial u}+\frac{\partial\left(\frac{\rho V^2 S}{2\mathrm{m}}\left(\bar{C}_z(\alpha)+\bar{C}_z^{re}(\alpha)V+\bar{C}_z^{e}(\alpha)\eta\right)\right)}{\partial w}=$$

$$\frac{\rho VS}{2}\left(\cos\alpha\sin\alpha\bar{C}_L-2\cos^2\alpha\bar{C}_D-\sin^2\alpha\bar{C}_D-\sin^2\alpha\frac{d\bar{C}_L(\alpha)}{d\alpha}+\sin\alpha\cos\alpha\frac{d\bar{C}_D(\alpha)}{d\alpha}\right)$$

$$+\frac{\rho SV^2}{2}\left(2\cos\alpha\sin\alpha\bar{C}_L^{re}-3\cos^2\alpha\bar{C}_D^{re}-\sin^2\alpha\frac{d\bar{C}_L^{re}(\alpha)}{d\alpha}-\sin^2\alpha\bar{C}_D^{re}+\sin\alpha\cos\alpha\frac{d\bar{C}_D^{re}}{d\alpha}\right)$$

$$+\frac{\rho VS}{2}\left(\cos\alpha\sin\alpha\bar{C}_L^{e}-2\cos^2\alpha\bar{C}_D^{e}-\sin^2\alpha\frac{d\bar{C}_L^{e}(\alpha)}{d\alpha}-\sin^2\alpha\bar{C}_D^{e}+\sin\alpha\cos\alpha\frac{d\bar{C}_D^{e}(\alpha)}{d\alpha}\right)\eta$$

$$+\frac{\rho SV}{2}\begin{pmatrix}-\sin\alpha\cos\alpha\bar{C}_L-2\sin^2\alpha\bar{C}_D-\cos^2\alpha\frac{d\bar{C}_L(\alpha)}{d\alpha}-\cos^2\alpha\bar{C}_D\\-\cos\alpha\sin\alpha\frac{d\bar{C}_D(\alpha)}{d\alpha}\end{pmatrix}$$

$$+\frac{\rho SV^2}{2}\begin{pmatrix}-2\sin\alpha\cos\alpha\bar{C}_L^{re}-3\sin^2\alpha\bar{C}_D^{re}-\cos^2\alpha\frac{d\bar{C}_L^{re}(\alpha)}{d\alpha}\\-\cos^2\alpha\bar{C}_D^{re}-\cos\alpha\sin\alpha\frac{d\bar{C}_D^{re}(\alpha)}{d\alpha}\end{pmatrix}$$

$$+\frac{\rho SV}{2}\eta\begin{pmatrix}-\cos\alpha\sin\alpha\bar{C}_L^{e}-2\sin^2\alpha\bar{C}_D^{e}-\cos^2\alpha\frac{d\bar{C}_L^{e}(\alpha)}{d\alpha}-\cos^2\alpha\bar{C}_D^{e}\\-\cos\alpha\sin\alpha\frac{d\bar{C}_D^{e}(\alpha)}{d\alpha}\end{pmatrix}$$

The aerodynamic equilibrium force divergence is

$$div(\bar{F})=\frac{\rho VS}{2}\left(-3\bar{C}_D-\frac{d\bar{C}_L(\alpha)}{d\alpha}\right)+\frac{\rho SV^2}{2}\left(-4\bar{C}_D^{re}-\frac{d\bar{C}_L^{re}(\alpha)}{d\alpha}\right)+\frac{\rho VS}{2}\eta\left(-3\bar{C}_D^{e}-\frac{d\bar{C}_L^{e}(\alpha)}{d\alpha}\right)$$

The final result for *divG*

$$div(G)=\frac{\rho SV}{2\mathrm{m}}\left(-3\bar{C}_D(\alpha)-\frac{d\bar{C}_L(\alpha)}{d\alpha}\right)+\frac{\rho SV^2}{2\mathrm{m}}\left(-4\bar{C}_D^{re}(\alpha)-\frac{d\bar{C}_L^{re}(\alpha)}{d\alpha}\right)$$
$$+\frac{\rho SV}{2\mathrm{m}}\left(-3\bar{C}_D^{e}(\alpha)-\frac{d\bar{C}_L^{e}(\alpha)}{d\alpha}\right)\eta_{cmd}$$

$$div(G) < 0$$

or

$$\left\{\left(-3\bar{C}_D(\alpha) - \frac{d\bar{C}_L(\alpha)}{d\alpha}\right) + V\left(-4\bar{C}_D^{re}(\alpha) - \frac{d\bar{C}_L^{re}(\alpha)}{d\alpha}\right) + \left(-3\bar{C}_D^{e}(\alpha) - \frac{d\bar{C}_L^{e}(\alpha)}{d\alpha}\right)\eta_{cmd}\right\} < 0$$

D.2 Application of Stability Criterion

In applying the stability results to the HSCT aircraft, for which high fidelity model exists, the structure of the aircraft model must be taken into consideration. The dynamic aeroelastic data is derived in a linear fashion and is then combined with nonlinear rigid body aerodynamic model[62]. The implications of this nonlinear/linear conglomeration on system shown in (6) is the removal of functional dependence of all η and $\dot{\eta}$ terms on *V*. They all become linear functions of α. Define $E_{(\cdot)}$ as a linear representation for the aerodynamic coefficients $C_{(\cdot)}$, then the following replacements are made in system (25):

$$Z_\eta = \frac{1}{2}\rho SV^2 C_{z,\eta}(\alpha, \mathrm{M}, GW^*) \qquad Z_{\dot{\eta}} = \frac{1}{2}\rho SV^2 C_{z,\dot{\eta}}(\alpha, \mathrm{M}, GW^*)$$

$$M_\eta = \frac{1}{2}\rho SV^2 \bar{c} C_{M,\eta}(\alpha, \mathrm{M}, GW^*) \qquad M_{\dot{\eta}} = \frac{1}{2}\rho SV^2 \bar{c} C_{M,\dot{\eta}}(\alpha, \mathrm{M}, GW^*)$$

$$E_\eta = \frac{1}{2}\rho SV^2 \bar{q} C_{\eta\eta}(\mathrm{M}, GW^*) \qquad E_{\dot{\eta}} = \frac{1}{2}\rho SV^2 \bar{q} C_{\eta\dot{\eta}}(\mathrm{M}, GW^*)$$

$$E_u u + E_w w + E_q q = \frac{1}{2}\rho SV^2 \left(C_{\eta u}(\mathrm{M}, GW^*)u + C_{\eta w}(\mathrm{M}, GW^*)w + C_{\eta q}(\mathrm{M}, GW^*)q\right)$$

$$E_{\delta 1} = \frac{1}{2}\rho SV^2 C_{\eta\delta 1}(\mathrm{M}, GW^*)$$

resulting in

$$\begin{pmatrix}\dot{u}\\ \dot{w}\end{pmatrix}=\begin{pmatrix}-qw-g\sin\theta+\dfrac{T}{\mathrm{m}}\\ qu+g\cos\theta\end{pmatrix}+\frac{1}{2\mathrm{m}}\rho SV^2\begin{pmatrix}C_x(\alpha)-\dfrac{C_{x,\delta1}(\alpha)E_{\delta2}}{C_{M,\delta1}(\alpha)E_{\delta2}-C_{M,\delta2}(\alpha)E_{\delta1}}C_M(\alpha)\\ C_z(\alpha)-\dfrac{C_{z,\delta1}(\alpha)E_{\delta2}-C_{z,\delta2}(\alpha)E_{\delta1}}{C_{M,\delta1}(\alpha)E_{\delta2}-C_{M,\delta2}(\alpha)E_{\delta1}}C_M(\alpha)\end{pmatrix}$$

$$+\frac{\eta}{\mathrm{m}}\begin{pmatrix}-\dfrac{C_{x,\delta1}(\alpha)E_{\delta2}}{C_{M,\delta1}(\alpha)E_{\delta2}-C_{M,\delta2}(\alpha)E_{\delta1}}\dfrac{M_\eta}{\bar{c}}+\dfrac{\rho SV^2}{2}\dfrac{C_{x,\delta1}(\alpha)C_{M,\delta2}(\alpha)}{C_{M,\delta1}(\alpha)E_{\delta2}-C_{M,\delta2}(\alpha)E_{\delta1}}E_\eta\\ Z_\eta-\dfrac{C_{z,\delta1}(\alpha)E_{\delta2}-C_{z,\delta2}(\alpha)E_{\delta1}}{C_{M,\delta1}(\alpha)E_{\delta2}-C_{M,\delta2}(\alpha)E_{\delta1}}\dfrac{M_\eta}{\bar{c}}-\dfrac{\rho SV^2}{2}\dfrac{-C_{z,\delta1}(\alpha)C_{M,\delta2}(\alpha)+C_{z,\delta2}(\alpha)C_{M,\delta1}(\alpha)}{C_{M,\delta1}(\alpha)E_{\delta2}-C_{M,\delta2}(\alpha)E_{\delta1}}E_\eta\end{pmatrix}$$

$$+\frac{\dot{\eta}}{\mathrm{m}}\begin{pmatrix}-\dfrac{C_{x,\delta1}(\alpha)E_{\delta2}}{C_{M,\delta1}(\alpha)E_{\delta2}-C_{M,\delta2}(\alpha)E_{\delta1}}\dfrac{M_{\dot{\eta}}}{\bar{c}}+\dfrac{\rho SV^2}{2}\dfrac{C_{x,\delta1}(\alpha)C_{M,\delta2}(\alpha)}{C_{M,\delta1}(\alpha)E_{\delta2}-C_{M,\delta2}(\alpha)E_{\delta1}}E_{\dot{\eta}}\\ Z_{\dot{\eta}}-\dfrac{C_{z,\delta1}(\alpha)E_{\delta2}-C_{z,\delta2}(\alpha)E_{\delta1}}{C_{M,\delta1}(\alpha)E_{\delta2}-C_{M,\delta2}(\alpha)E_{\delta1}}\dfrac{M_{\dot{\eta}}}{\bar{c}}-\dfrac{\rho SV^2}{2}\dfrac{-C_{z,\delta1}(\alpha)C_{M,\delta2}(\alpha)+C_{z,\delta2}(\alpha)C_{M,\delta1}(\alpha)}{C_{M,\delta1}(\alpha)E_{\delta2}-C_{M,\delta2}(\alpha)E_{\delta1}}E_{\dot{\eta}}\end{pmatrix}$$

$$-\frac{1}{2\mathrm{m}}\rho SV^2\begin{pmatrix}\dfrac{-C_{x,\delta1}(\alpha)C_{M,\delta2}(\alpha)}{C_{M,\delta1}(\alpha)E_{\delta2}-C_{M,\delta2}(\alpha)E_{\delta1}}\left(E_u u+E_w w+E_q q\right)\\ \dfrac{-C_{z,\delta1}(\alpha)C_{M,\delta2}(\alpha)+C_{z,\delta2}(\alpha)C_{M,\delta1}(\alpha)}{C_{M,\delta1}(\alpha)E_{\delta2}-C_{M,\delta2}(\alpha)E_{\delta1}}\left(E_u u+E_w w+E_q q\right)\end{pmatrix}$$

$$+\frac{1}{\mathrm{m}}\begin{pmatrix}\dfrac{I_y}{\bar{c}}\dfrac{C_{x,\delta1}(\alpha)E_{\delta2}}{C_{M,\delta1}(\alpha)E_{\delta2}-C_{M,\delta2}(\alpha)E_{\delta1}}\\ \dfrac{I_y}{\bar{c}}\dfrac{C_{z,\delta1}(\alpha)E_{\delta2}-C_{z,\delta2}(\alpha)E_{\delta1}}{C_{M,\delta1}(\alpha)E_{\delta2}-C_{M,\delta2}(\alpha)E_{\delta1}}\end{pmatrix}\dot{q}^{des}$$

$$+\frac{1}{\mathrm{m}}\begin{pmatrix}\dfrac{m_\eta}{2}\rho SV^2\dfrac{-C_{x,\delta1}(\alpha)C_{M,\delta2}(\alpha)}{C_{M,\delta1}(\alpha)E_{\delta2}-C_{M,\delta2}(\alpha)E_{\delta1}}\\ \dfrac{m_\eta}{2}\rho SV^2\dfrac{-C_{z,\delta1}(\alpha)C_{M,\delta2}(\alpha)+C_{z,\delta2}(\alpha)C_{M,\delta1}(\alpha)}{C_{M,\delta1}(\alpha)E_{\delta2}-C_{M,\delta2}(\alpha)E_{\delta1}}\end{pmatrix}\ddot{\eta}^{des}$$

The limiting equations reduce to

$$\begin{pmatrix}\dot{u}\\ \dot{w}\end{pmatrix}=\begin{pmatrix}-g\sin\theta+\dfrac{T}{\mathrm{m}}\\ g\cos\theta\end{pmatrix}+\frac{1}{2\mathrm{m}}\rho SV^2\begin{pmatrix}C_x(\alpha)-\dfrac{C_{x,\delta1}(\alpha)E_{\delta2}}{C_{M,\delta1}(\alpha)E_{\delta2}-C_{M,\delta2}(\alpha)E_{\delta1}}C_M(\alpha)\\ C_z(\alpha)-\dfrac{C_{z,\delta1}(\alpha)E_{\delta2}-C_{z,\delta2}(\alpha)E_{\delta1}}{C_{M,\delta1}(\alpha)E_{\delta2}-C_{M,\delta2}(\alpha)E_{\delta1}}C_M(\alpha)\end{pmatrix}$$

$$+\frac{1}{\mathrm{m}}\begin{pmatrix}\dfrac{-C_{x,\delta1}(\alpha)E_{\delta2}}{\bar{c}\left(C_{M,\delta1}(\alpha)E_{\delta2}-C_{M,\delta2}(\alpha)E_{\delta1}\right)}M_\eta & -\dfrac{\rho SV^2}{2}\dfrac{-C_{x,\delta1}(\alpha)C_{M,\delta2}(\alpha)}{C_{M,\delta1}(\alpha)E_{\delta2}-C_{M,\delta2}(\alpha)E_{\delta1}}E_\eta\\ Z_\eta-\dfrac{C_{z,\delta1}(\alpha)E_{\delta2}-C_{z,\delta2}(\alpha)E_{\delta1}}{\bar{c}\left(C_{M,\delta1}(\alpha)E_{\delta2}-C_{M,\delta2}(\alpha)E_{\delta1}\right)}M_\eta & -\dfrac{\rho SV^2}{2}\dfrac{-C_{z,\delta1}(\alpha)C_{M,\delta2}(\alpha)+C_{z,\delta2}(\alpha)C_{M,\delta1}(\alpha)}{C_{M,\delta1}(\alpha)E_{\delta2}-C_{M,\delta2}(\alpha)E_{\delta1}}E_\eta\end{pmatrix}\eta_{cmd}$$

$$+\frac{1}{2\mathrm{m}}\rho SV^2\begin{pmatrix}\dfrac{C_{x,\delta1}(\alpha)C_{M,\delta2}(\alpha)}{C_{M,\delta1}(\alpha)E_{\delta2}-C_{M,\delta2}(\alpha)E_{\delta1}}\left(E_u u+E_w w\right)\\ \dfrac{C_{z,\delta1}(\alpha)C_{M,\delta2}(\alpha)-C_{z,\delta2}(\alpha)C_{M,\delta1}(\alpha)}{C_{M,\delta1}(\alpha)E_{\delta2}-C_{M,\delta2}(\alpha)E_{\delta1}}\left(E_u u+E_w w\right)\end{pmatrix}$$

and in terms of the modified equilibrium aerodynamic force coefficients introduced in Chapter 6

$$\begin{pmatrix}\dot{u}\\ \dot{w}\end{pmatrix}=\begin{pmatrix}-g\sin\theta_{cmd}+\dfrac{T}{\mathrm{m}}\\ g\cos\theta_{cmd}\end{pmatrix}+\frac{\rho SV^2}{2\mathrm{m}}\begin{pmatrix}\bar{E}_x(\alpha)\\ \bar{E}_z(\alpha)\end{pmatrix}+\frac{\rho SV^2}{2\mathrm{m}}\begin{pmatrix}\bar{E}_x^{re}(\alpha)\\ \bar{E}_z^{re}(\alpha)\end{pmatrix}V+\frac{1}{\mathrm{m}}\begin{pmatrix}\bar{E}_x^{e}(\alpha)\\ \bar{E}_z^{e}(\alpha)\end{pmatrix}\eta_{cmd}$$

where

$$\begin{pmatrix}\bar{E}_x\\ \bar{E}_z\end{pmatrix}(\alpha)=\begin{pmatrix}C_x(\alpha)-\dfrac{C_{x,\delta1}(\alpha)E_{\delta2}}{C_{M,\delta1}(\alpha)E_{\delta2}-C_{M,\delta2}(\alpha)E_{\delta1}}C_M(\alpha)\\ C_z(\alpha)-\dfrac{C_{z,\delta1}(\alpha)E_{\delta2}-C_{z,\delta2}(\alpha)E_{\delta1}}{C_{M,\delta1}(\alpha)E_{\delta2}-C_{M,\delta2}(\alpha)E_{\delta1}}C_M(\alpha)\end{pmatrix}$$

$$\begin{pmatrix}\bar{E}_x^{re}\\ \bar{E}_z^{re}\end{pmatrix}(\alpha)=\begin{pmatrix}\dfrac{C_{x,\delta1}(\alpha)C_{M,\delta2}(\alpha)}{C_{M,\delta1}(\alpha)E_{\delta2}-C_{M,\delta2}(\alpha)E_{\delta1}}\left(E_u\cos\alpha+E_w\sin\alpha\right)\\ \dfrac{C_{z,\delta1}(\alpha)C_{M,\delta2}(\alpha)-C_{z,\delta2}(\alpha)C_{M,\delta1}(\alpha)}{C_{M,\delta1}(\alpha)E_{\delta2}-C_{M,\delta2}(\alpha)E_{\delta1}}\left(E_u\cos\alpha+E_w\sin\alpha\right)\end{pmatrix}$$

$$\begin{pmatrix}\bar{E}_x^{e}\\ \bar{E}_z^{e}\end{pmatrix}(\alpha)=\begin{pmatrix}\dfrac{C_{x,\delta1}(\alpha)}{C_{M,\delta1}(\alpha)E_{\delta2}-C_{M,\delta2}(\alpha)E_{\delta1}}\left(-\dfrac{E_{\delta2}M_\eta}{\bar{c}}+\dfrac{\rho SV^2}{2}C_{M,\delta2}(\alpha)E_\eta\right)\\ Z_\eta-\dfrac{C_{z,\delta1}(\alpha)E_{\delta2}-C_{z,\delta2}(\alpha)E_{\delta1}}{C_{M,\delta1}(\alpha)E_{\delta2}-C_{M,\delta2}(\alpha)E_{\delta1}}\dfrac{M_\eta}{\bar{c}}\\ \qquad+\dfrac{C_{z,\delta1}(\alpha)C_{M,\delta2}(\alpha)-C_{z,\delta2}(\alpha)C_{M,\delta1}(\alpha)}{C_{M,\delta1}(\alpha)E_{\delta2}-C_{M,\delta2}(\alpha)E_{\delta1}}\dfrac{\rho SV^2}{2}E_\eta\end{pmatrix}$$

In terms of the closed loop control effectiveness variables introduced in Chapter 6, the equations are given by

$$\begin{pmatrix}\dot{u}\\ \dot{w}\end{pmatrix}=\begin{pmatrix}-g\sin\theta_{cmd}+\dfrac{T}{\mathrm{m}}\\ g\cos\theta_{cmd}\end{pmatrix}+\frac{\rho SV^2}{2\mathrm{m}}\begin{pmatrix}\bar{E}_x(\alpha)\\ \bar{E}_z(\alpha)\end{pmatrix}+\frac{\rho SV^2}{2\mathrm{m}}\begin{pmatrix}\bar{E}_x^{re}(\alpha)\\ \bar{E}_z^{re}(\alpha)\end{pmatrix}V+\frac{1}{\mathrm{m}}\begin{pmatrix}\bar{E}_x^{e}(\alpha)\\ \bar{E}_z^{e}(\alpha)\end{pmatrix}\eta_{cmd}$$

Define G

$$G\triangleq\begin{pmatrix}-g\sin\theta_{cmd}+\dfrac{T}{\mathrm{m}}\\ g\cos\theta_{cmd}\end{pmatrix}+\frac{\rho SV^2}{2\mathrm{m}}\begin{pmatrix}\bar{E}_x(\alpha)\\ \bar{E}_z(\alpha)\end{pmatrix}+\frac{\rho SV^2}{2\mathrm{m}}\begin{pmatrix}\bar{E}_x^{re}(\alpha)\\ \bar{E}_z^{re}(\alpha)\end{pmatrix}V+\frac{1}{\mathrm{m}}\begin{pmatrix}\bar{E}_x^{e}(\alpha)\\ \bar{E}_z^{e}(\alpha)\end{pmatrix}\eta_{cmd}$$

Then *div*(G) is given by

$$div(G)=\frac{\partial\left(-g\sin\theta_{cmd}+\dfrac{T}{\mathrm{m}}+\dfrac{1}{2\mathrm{m}}\rho SV^2\left(\bar{E}_x(\alpha)+\bar{E}_x^{re}(\alpha)V\right)+\dfrac{1}{\mathrm{m}}\bar{E}_x^{e}(\alpha)\eta_{cmd}\right)}{\partial u}$$
$$+\frac{\partial\left(g\cos\theta_{cmd}+\dfrac{1}{2\mathrm{m}}\rho SV^2\left(\bar{E}_z(\alpha)+\bar{E}_z^{re}(\alpha)V\right)+\dfrac{1}{\mathrm{m}}\bar{E}_z^{e}(\alpha)\eta_{cmd}\right)}{\partial w}$$

The interest is to obtain *divG* in terms of lift and drag forces, hence requiring coordinate transformation once again. From definitions of α and *V*

$$\frac{d\alpha}{du} = \frac{-\sin\alpha}{V} \quad \frac{d\alpha}{dw} = \frac{\cos\alpha}{V}$$

and *divG* becomes

$$div(G) = \frac{\partial\left(-g\sin\theta_{cmd} + \frac{T}{\mathrm{m}} + \frac{1}{2\mathrm{m}}\rho SV^2\left(\bar{E}_x(\alpha) + \bar{E}_x^{re}(\alpha)V\right) + \frac{1}{\mathrm{m}}\bar{E}_x^{e}(\alpha)\eta_{cmd}\right)}{\partial\alpha}\frac{d\alpha}{du}$$
$$+\frac{\partial\left(g\cos\theta_{cmd} + \frac{1}{2\mathrm{m}}\rho SV^2\left(\bar{E}_z(\alpha) + \bar{E}_z^{re}(\alpha)V\right) + \frac{1}{\mathrm{m}}\bar{E}_z^{e}(\alpha)\eta_{cmd}\right)}{\partial\alpha}\frac{d\alpha}{dw}$$

In addition recall the coefficient conversion equations:

$$\begin{aligned}
\bar{E}_x &= \sin\alpha\bar{E}_L - \cos\alpha\bar{E}_D & \bar{E}_z &= -\cos\alpha\bar{E}_L - \sin\alpha\bar{E}_D \\
\bar{E}_x^{re} &= \sin\alpha\bar{E}_L^{re} - \cos\alpha\bar{E}_D^{re} & \bar{E}_z^{re} &= -\cos\alpha\bar{E}_L^{re} - \sin\alpha\bar{E}_D^{re} \\
\bar{E}_x^{e} &= \sin\alpha\bar{E}_L^{e} - \cos\alpha\bar{E}_D^{e} & \bar{E}_z^{e} &= -\cos\alpha\bar{E}_L^{e} - \sin\alpha\bar{E}_D^{e}
\end{aligned}$$

Now, evaluating each individual component.

u-direction:

$$\frac{\partial\left(-g\sin\theta_{cmd} + \frac{T}{\mathrm{m}} + \frac{1}{2\mathrm{m}}\rho SV^2\left(\bar{E}_x(\alpha) + \bar{E}_x^{re}(\alpha)V\right) + \frac{1}{\mathrm{m}}\bar{E}_x^{e}(\alpha)\eta_{cmd}\right)}{\partial\alpha}\frac{d\alpha}{du} =$$
$$\frac{-\sin\alpha}{V}\frac{1}{\mathrm{m}}\frac{\partial\left(\frac{1}{2}\rho SV^2\left(\sin\alpha\bar{E}_L(\alpha) - \cos\alpha\bar{E}_D(\alpha) + \left(\sin\alpha\bar{E}_L^{re}(\alpha) - \cos\alpha\bar{E}_D^{re}(\alpha)\right)V\right)\right)}{\partial\alpha} +$$
$$\frac{-\sin\alpha}{V}\frac{1}{\mathrm{m}}\eta_{cmd}\frac{\partial\left(\sin\alpha\bar{E}_L^{e}(\alpha) - \cos\alpha\bar{E}_D^{e}(\alpha)\right)}{\partial\alpha}$$

$$\frac{-\sin\alpha}{V}\frac{1}{2\mathrm{m}}\rho SV^2\frac{\partial\left(\sin\alpha\bar{E}_L(\alpha)-\cos\alpha\bar{E}_D(\alpha)+\left(\sin\alpha\bar{E}_L^{re}(\alpha)-\cos\alpha\bar{E}_D^{re}(\alpha)\right)V\right)}{\partial\alpha}$$

$$=\frac{-\sin\alpha}{V}\frac{1}{2\mathrm{m}}\rho SV^2\left(\cos\alpha\bar{E}_L(\alpha)+\sin\alpha\frac{d\bar{E}_L(\alpha)}{d\alpha}+\sin\alpha\bar{E}_D(\alpha)-\cos\alpha\frac{d\bar{E}_D(\alpha)}{d\alpha}\right)$$

$$\frac{-\sin\alpha}{V}\frac{1}{2\mathrm{m}}\rho SV^2V\left(\cos\alpha\bar{E}_L^{re}(\alpha)+\sin\alpha\frac{d\bar{E}_L^{re}(\alpha)}{d\alpha}+\sin\alpha\bar{E}_D^{re}(\alpha)-\cos\alpha\frac{d\bar{E}_D^{re}(\alpha)}{d\alpha}\right)$$

$$=\frac{1}{2\mathrm{m}}\rho SV\left(-\sin\alpha\cos\alpha\bar{E}_L(\alpha)-\sin^2\alpha\frac{d\bar{E}_L(\alpha)}{d\alpha}-\sin^2\alpha\bar{E}_D(\alpha)+\sin\alpha\cos\alpha\frac{d\bar{E}_D(\alpha)}{d\alpha}\right)$$

$$+\frac{1}{2\mathrm{m}}\rho SV^2\left(-\sin\alpha\cos\alpha\bar{E}_L^{re}(\alpha)-\sin^2\alpha\frac{d\bar{E}_L^{re}(\alpha)}{d\alpha}-\sin^2\alpha\bar{E}_D^{re}(\alpha)+\sin\alpha\cos\alpha\frac{d\bar{E}_D^{re}(\alpha)}{d\alpha}\right)$$

$$\frac{-\sin\alpha}{V}\frac{\eta_{cmd}}{\mathrm{m}}\frac{\partial\left(\sin\alpha\bar{E}_L^e(\alpha)-\cos\alpha\bar{E}_D^e(\alpha)\right)}{\partial\alpha}$$

$$=\frac{-\sin\alpha}{V}\frac{\eta_{cmd}}{\mathrm{m}}\left(\cos\alpha\bar{E}_L^e(\alpha)+\sin\alpha\frac{d\bar{E}_L^e(\alpha)}{d\alpha}+\sin\alpha\bar{E}_D^e(\alpha)-\cos\alpha\frac{d\bar{E}_D^e(\alpha)}{d\alpha}\right)$$

$$=\frac{\eta_{cmd}}{V\mathrm{m}}\left(-\sin\alpha\cos\alpha\bar{E}_L^e(\alpha)-\sin^2\alpha\frac{d\bar{E}_L^e(\alpha)}{d\alpha}-\sin^2\alpha\bar{E}_D^e(\alpha)+\sin\alpha\cos\alpha\frac{d\bar{E}_D^e(\alpha)}{d\alpha}\right)$$

combining terms in the u-direction

$$\frac{\partial\left(-g\sin\theta_{cmd}+\frac{T}{\mathrm{m}}+\frac{1}{2\mathrm{m}}\rho SV^2\left(\bar{E}_x(\alpha)+\bar{E}_x^{re}(\alpha)V\right)+\frac{1}{\mathrm{m}}\bar{E}_x^e(\alpha)\eta_{cmd}\right)}{\partial\alpha}\frac{d\alpha}{du}=$$

$$\frac{1}{2\mathrm{m}}\rho SV\left(-\sin\alpha\cos\alpha\bar{E}_L(\alpha)-\sin^2\alpha\frac{d\bar{E}_L(\alpha)}{d\alpha}-\sin^2\alpha\bar{E}_D(\alpha)+\sin\alpha\cos\alpha\frac{d\bar{E}_D(\alpha)}{d\alpha}\right)$$

$$+\frac{1}{2\mathrm{m}}\rho SV^2\left(-\sin\alpha\cos\alpha\bar{E}_L^{re}(\alpha)-\sin^2\alpha\frac{d\bar{E}_L^{re}(\alpha)}{d\alpha}-\sin^2\alpha\bar{E}_D^{re}(\alpha)+\sin\alpha\cos\alpha\frac{d\bar{E}_D^{re}(\alpha)}{d\alpha}\right)$$

$$+\frac{\eta_{cmd}}{V\mathrm{m}}\left(-\sin\alpha\cos\alpha\bar{E}_L^e(\alpha)-\sin^2\alpha\frac{d\bar{E}_L^e(\alpha)}{d\alpha}-\sin^2\alpha\bar{E}_D^e(\alpha)+\sin\alpha\cos\alpha\frac{d\bar{E}_D^e(\alpha)}{d\alpha}\right)$$

w-direction:

$$\frac{\partial\left(g\cos\theta_{cmd}+\frac{1}{2\mathrm{m}}\rho SV^2\left(\bar{E}_z(\alpha)+\bar{E}_z^{re}(\alpha)V\right)+\frac{1}{\mathrm{m}}\bar{E}_z^{e}(\alpha)\eta_{cmd}\right)}{\partial\alpha}\frac{d\alpha}{dw}$$

$$=\frac{\cos\alpha}{V}\frac{1}{2\mathrm{m}}\rho SV^2\frac{\partial\left(-\cos\alpha\bar{E}_L(\alpha)-\sin\alpha\bar{E}_D(\alpha)+\left(-\cos\alpha\bar{E}_L^{re}(\alpha)-\sin\alpha\bar{E}_D^{re}(\alpha)\right)V\right)}{\partial\alpha}$$

$$+\frac{\cos\alpha}{V}\frac{\eta_{cmd}}{\mathrm{m}}\frac{\partial\left(-\cos\alpha\bar{E}_L^{e}(\alpha)-\sin\alpha\bar{E}_D^{e}(\alpha)\right)}{\partial\alpha}$$

calculating by parts

$$\frac{\cos\alpha}{V}\frac{1}{2\mathrm{m}}\rho SV^2\frac{\partial\left(-\cos\alpha\bar{E}_L(\alpha)-\sin\alpha\bar{E}_D(\alpha)+\left(-\cos\alpha\bar{E}_L^{re}(\alpha)-\sin\alpha\bar{E}_D^{re}(\alpha)\right)V\right)}{\partial\alpha}$$

$$=\frac{\cos\alpha}{V}\frac{1}{2\mathrm{m}}\rho SV^2\left(\sin\alpha\bar{E}_L(\alpha)-\cos\alpha\frac{d\bar{E}_L(\alpha)}{d\alpha}-\cos\alpha\bar{E}_D(\alpha)-\sin\alpha\frac{d\bar{E}_D(\alpha)}{d\alpha}\right)$$

$$+\frac{\cos\alpha}{V}\frac{1}{2\mathrm{m}}\rho SV^2V\left(\sin\alpha\bar{E}_L^{re}(\alpha)-\cos\alpha\frac{d\bar{E}_L^{re}(\alpha)}{d\alpha}-\cos\alpha\bar{E}_D^{re}(\alpha)-\sin\alpha\frac{d\bar{E}_D^{re}(\alpha)}{d\alpha}\right)$$

$$=\frac{1}{2\mathrm{m}}\rho SV\left(\cos\alpha\sin\alpha\bar{E}_L(\alpha)-\cos^2\alpha\frac{d\bar{E}_L(\alpha)}{d\alpha}-\cos^2\alpha\bar{E}_D(\alpha)-\cos\alpha\sin\alpha\frac{d\bar{E}_D(\alpha)}{d\alpha}\right)$$

$$+\frac{1}{2\mathrm{m}}\rho SV^2\left(\cos\alpha\sin\alpha\bar{E}_L^{re}(\alpha)-\cos^2\alpha\frac{d\bar{E}_L^{re}(\alpha)}{d\alpha}-\cos^2\alpha\bar{E}_D^{re}(\alpha)-\cos\alpha\sin\alpha\frac{d\bar{E}_D^{re}(\alpha)}{d\alpha}\right)$$

$$\frac{\cos\alpha}{V}\frac{\eta_{cmd}}{\mathrm{m}}\frac{\partial\left(-\cos\alpha\bar{E}_L^{e}(\alpha)-\sin\alpha\bar{E}_D^{e}(\alpha)\right)}{\partial\alpha}$$

$$=\frac{\cos\alpha}{V}\frac{\eta_{cmd}}{\mathrm{m}}\left(\sin\alpha\bar{E}_L^{e}(\alpha)-\cos\alpha\frac{d\bar{E}_L^{e}(\alpha)}{d\alpha}-\cos\alpha\bar{E}_D^{e}(\alpha)-\sin\alpha\frac{d\bar{E}_D^{e}(\alpha)}{d\alpha}\right)$$

$$=\frac{\eta_{cmd}}{V\mathrm{m}}\left(\cos\alpha\sin\alpha\bar{E}_L^{e}(\alpha)-\cos^2\alpha\frac{d\bar{E}_L^{e}(\alpha)}{d\alpha}-\cos^2\alpha\bar{E}_D^{e}(\alpha)-\cos\alpha\sin\alpha\frac{d\bar{E}_D^{e}(\alpha)}{d\alpha}\right)$$

combining terms in the w-direction

$$\frac{\partial\left(g\cos\theta_{cmd}+\frac{1}{2\mathrm{m}}\rho SV^2\left(\bar{E}_z(\alpha)+\bar{E}_z^{re}(\alpha)V\right)+\frac{1}{\mathrm{m}}\bar{E}_z^{e}(\alpha)\eta_{cmd}\right)}{\partial\alpha}\frac{d\alpha}{dw}$$

$$=\frac{1}{2\mathrm{m}}\rho SV\left(\cos\alpha\sin\alpha\bar{E}_L(\alpha)-\cos^2\alpha\frac{d\bar{E}_L(\alpha)}{d\alpha}-\cos^2\alpha\bar{E}_D(\alpha)-\cos\alpha\sin\alpha\frac{d\bar{E}_D(\alpha)}{d\alpha}\right)$$

$$+\frac{1}{2\mathrm{m}}\rho SV^2\left(\cos\alpha\sin\alpha\bar{E}_L^{re}(\alpha)-\cos^2\alpha\frac{d\bar{E}_L^{re}(\alpha)}{d\alpha}-\cos^2\alpha\bar{E}_D^{re}(\alpha)-\cos\alpha\sin\alpha\frac{d\bar{E}_D^{re}(\alpha)}{d\alpha}\right)$$

$$+\frac{\eta_{cmd}}{V\mathrm{m}}\left(\cos\alpha\sin\alpha\bar{E}_L^{e}(\alpha)-\cos^2\alpha\frac{d\bar{E}_L^{e}(\alpha)}{d\alpha}-\cos^2\alpha\bar{E}_D^{e}(\alpha)-\cos\alpha\sin\alpha\frac{d\bar{E}_D^{e}(\alpha)}{d\alpha}\right)$$

combining *u* and *w* directions:

$$\frac{\partial\left(\frac{1}{2\mathrm{m}}\rho SV^2\left(\bar{E}_x(\alpha)+\bar{E}_x^{re}(\alpha)V\right)+\frac{\eta_{cmd}}{\mathrm{m}}\bar{E}_x^{e}(\alpha)\right)}{\partial\alpha}\frac{d\alpha}{du}$$

$$+\frac{\partial\left(\frac{1}{2\mathrm{m}}\rho SV^2\left(\bar{E}_z(\alpha)+\bar{E}_z^{re}(\alpha)V\right)+\frac{\eta_{cmd}}{\mathrm{m}}\bar{E}_z^{e}(\alpha)\right)}{\partial\alpha}\frac{d\alpha}{dw}=$$

$$\frac{1}{2\mathrm{m}}\rho SV\begin{pmatrix}-\sin\alpha\cos\alpha\bar{E}_L(\alpha)-\sin^2\alpha\frac{d\bar{E}_L(\alpha)}{d\alpha}-\sin^2\alpha\bar{E}_D(\alpha)+\sin\alpha\cos\alpha\frac{d\bar{E}_D(\alpha)}{d\alpha}\\+\cos\alpha\sin\alpha\bar{E}_L(\alpha)-\cos^2\alpha\frac{d\bar{E}_L(\alpha)}{d\alpha}-\cos^2\alpha\bar{E}_D(\alpha)-\cos\alpha\sin\alpha\frac{d\bar{E}_D(\alpha)}{d\alpha}\end{pmatrix}$$

$$+\frac{\rho SV^2}{2\mathrm{m}}\begin{pmatrix}-\sin\alpha\cos\alpha\bar{E}_L^{re}(\alpha)-\sin^2\alpha\frac{d\bar{E}_L^{re}(\alpha)}{d\alpha}-\sin^2\alpha\bar{E}_D^{re}(\alpha)+\sin\alpha\cos\alpha\frac{d\bar{E}_D^{re}(\alpha)}{d\alpha}\\+\cos\alpha\sin\alpha\bar{E}_L^{re}(\alpha)-\cos^2\alpha\frac{d\bar{E}_L^{re}(\alpha)}{d\alpha}-\cos^2\alpha\bar{E}_D^{re}(\alpha)-\cos\alpha\sin\alpha\frac{d\bar{E}_D^{re}(\alpha)}{d\alpha}\end{pmatrix}$$

$$+\frac{\eta_{cmd}}{V\mathrm{m}}\begin{pmatrix}-\sin\alpha\cos\alpha\bar{E}_L^{e}(\alpha)-\sin^2\alpha\frac{d\bar{E}_L^{e}(\alpha)}{d\alpha}-\sin^2\alpha\bar{E}_D^{e}(\alpha)+\sin\alpha\cos\alpha\frac{d\bar{E}_D^{e}(\alpha)}{d\alpha}\\+\cos\alpha\sin\alpha\bar{E}_L^{e}(\alpha)-\cos^2\alpha\frac{d\bar{E}_L^{e}(\alpha)}{d\alpha}-\cos^2\alpha\bar{E}_D^{e}(\alpha)-\cos\alpha\sin\alpha\frac{d\bar{E}_D^{e}(\alpha)}{d\alpha}\end{pmatrix}$$

The final result for *divG*

$$div(G)=$$

$$\frac{\rho SV}{2\mathrm{m}}\left(-\bar{E}_D(\alpha)-\frac{d\bar{E}_L(\alpha)}{d\alpha}\right)+\frac{\rho SV^2}{2\mathrm{m}}\left(-\bar{E}_D^{re}(\alpha)-\frac{d\bar{E}_L^{re}(\alpha)}{d\alpha}\right)+\frac{\eta_{cmd}}{\mathrm{m}}\frac{1}{V}\left(-\bar{E}_D^{e}(\alpha)-\frac{d\bar{E}_L^{e}(\alpha)}{d\alpha}\right)$$

$$div(G) < 0$$

or

$$-\frac{\rho SV}{2\mathrm{m}}\left(\bar{E}_D(\alpha)+\frac{d\bar{E}_L(\alpha)}{d\alpha}\right)-\frac{\rho SV^2}{2\mathrm{m}}\left(\bar{E}_D^{re}(\alpha)+\frac{d\bar{E}_L^{re}(\alpha)}{d\alpha}\right)-\frac{\eta_{cmd}}{\mathrm{m}}\frac{1}{V}\left(\bar{E}_D^{e}(\alpha)+\frac{d\bar{E}_L^{e}(\alpha)}{d\alpha}\right)<0$$

where

$$\bar{E}_D(\alpha) = -\cos\alpha\bar{E}_x(\alpha)-\sin\alpha\bar{E}_z(\alpha) \qquad \bar{E}_L(\alpha) = \sin\alpha\bar{E}_x(\alpha)-\cos\alpha\bar{E}_z(\alpha)$$

$$\bar{E}_D^{re}(\alpha) = -\cos\alpha\bar{E}_x^{re}(\alpha)-\sin\alpha\bar{E}_z^{re}(\alpha) \qquad \bar{E}_L^{re}(\alpha) = \sin\alpha\bar{E}_x^{re}(\alpha)-\cos\alpha\bar{E}_z^{re}(\alpha)$$

$$\bar{E}_D^{e}(\alpha) = -\cos\alpha\bar{E}_x^{e}(\alpha)-\sin\alpha\bar{E}_z^{e}(\alpha) \qquad \bar{E}_L^{e}(\alpha) = \sin\alpha\bar{E}_x^{e}(\alpha)-\cos\alpha\bar{E}_z^{e}(\alpha)$$

$$\bar{E}_{D,\delta_2}(\alpha) = -\cos\alpha\bar{E}_{x,\delta_2}(\alpha)-\sin\alpha\bar{E}_{z,\delta_2}(\alpha) \qquad \bar{E}_{L,\delta_2}(\alpha) = \sin\alpha\bar{E}_{x,\delta_2}(\alpha)-\cos\alpha\bar{E}_{z,\delta_2}(\alpha)$$

and

$$\begin{pmatrix}\bar{E}_x\\ \bar{E}_z\end{pmatrix}(\alpha)=\begin{pmatrix} C_x(\alpha)-\dfrac{C_{x,\delta1}(\alpha)E_{\delta2}}{C_{M,\delta1}(\alpha)E_{\delta2}-C_{M,\delta2}(\alpha)E_{\delta1}}C_M(\alpha)\\ C_z(\alpha)-\dfrac{C_{z,\delta1}(\alpha)E_{\delta2}-C_{z,\delta2}(\alpha)E_{\delta1}}{C_{M,\delta1}(\alpha)E_{\delta2}-C_{M,\delta2}(\alpha)E_{\delta1}}C_M(\alpha)\end{pmatrix}$$

$$\begin{pmatrix}\bar{E}_x^{re}\\ \bar{E}_z^{re}\end{pmatrix}(\alpha)=\begin{pmatrix} \dfrac{C_{x,\delta1}(\alpha)C_{M,\delta2}(\alpha)}{C_{M,\delta1}(\alpha)E_{\delta2}-C_{M,\delta2}(\alpha)E_{\delta1}}\left(E_u\cos\alpha+E_w\sin\alpha\right)\\ \dfrac{C_{z,\delta1}(\alpha)C_{M,\delta2}(\alpha)-C_{z,\delta2}(\alpha)C_{M,\delta1}(\alpha)}{C_{M,\delta1}(\alpha)E_{\delta2}-C_{M,\delta2}(\alpha)E_{\delta1}}\left(E_u\cos\alpha+E_w\sin\alpha\right)\end{pmatrix}$$

$$\begin{pmatrix}\bar{E}_x^{e}\\ \bar{E}_z^{e}\end{pmatrix}(\alpha)=\begin{pmatrix} \dfrac{C_{x,\delta1}(\alpha)}{C_{M,\delta1}(\alpha)E_{\delta2}-C_{M,\delta2}(\alpha)E_{\delta1}}\left(-\dfrac{E_{\delta2}M_\eta}{\bar{c}}+\dfrac{\rho SV^2}{2}C_{M,\delta2}(\alpha)E_\eta\right)\\ Z_\eta-\dfrac{C_{z,\delta1}(\alpha)E_{\delta2}-C_{z,\delta2}(\alpha)E_{\delta1}}{C_{M,\delta1}(\alpha)E_{\delta2}-C_{M,\delta2}(\alpha)E_{\delta1}}\dfrac{M_\eta}{\bar{c}}\\ \qquad\qquad+\dfrac{C_{z,\delta1}(\alpha)C_{M,\delta2}(\alpha)-C_{z,\delta2}(\alpha)C_{M,\delta1}(\alpha)}{C_{M,\delta1}(\alpha)E_{\delta2}-C_{M,\delta2}(\alpha)E_{\delta1}}\dfrac{\rho SV^2}{2}E_\eta\end{pmatrix}$$

Appendix E – Longitudinal plus Flexible Mode Model Stability Analysis

Additional discussion of analytical stability analysis for the longitudinal plus one flexible mode dynamics with a modified dynamic inversion using first order filter in the flexible dynamics loop is considered in this Appendix. The linear version of the nonlinear equations of motion exploiting the linear nature of the flexible dynamics model (see (4.18)) is given as

$$\begin{bmatrix} \dot{u} \\ \dot{w} \\ \dot{q} \\ \dot{\theta} \\ \ddot{\eta} \\ \dot{\eta} \\ \dot{x}_f \end{bmatrix} = \begin{bmatrix} \bar{X}_u & \bar{X}_w & \bar{X}_q & \bar{X}_\theta & \bar{X}_{\dot{\eta}} & \bar{X}_\eta & \bar{X}_{\delta 2} \\ \bar{Z}_u & \bar{Z}_w & \bar{Z}_q & \bar{Z}_\theta & \bar{Z}_{\dot{\eta}} & \bar{Z}_\eta & \bar{Z}_{\delta 2} \\ 0 & -\phi' E_w & -\phi' E_q & 0 & -\phi' E_{\dot{\eta}} & -\phi' E_\eta & -\phi' \bar{E}_{\delta 2} \\ 0 & 0 & 1 & 0 & 0 & 0 & 0 \\ 0 & E_w & E_q & 0 & E_{\dot{\eta}} & E_\eta & \bar{E}_{\delta 2} \\ 0 & 0 & 0 & 0 & 1 & 0 & 0 \\ 0 & -\frac{\Delta\phi'}{b} E_w & -\frac{\Delta\phi'}{b} E_q & 0 & -\frac{\Delta\phi'}{b} E_{\dot{\eta}} & -\frac{\Delta\phi'}{b} E_\eta & -\frac{1}{b} \end{bmatrix} \begin{bmatrix} u \\ w \\ q \\ \theta \\ \dot{\eta} \\ \eta \\ x_f \end{bmatrix}$$

$$+ \begin{bmatrix} \bar{X}_{\delta 1} & \bar{Z}_{\delta 1} & 1 & 0 & 0 & 0 & 0 \\ 0 & 0 & 0 & 0 & 0 & 0 & \frac{1}{b} \end{bmatrix}^T \begin{bmatrix} \dot{y}_1^{des} \\ \dot{y}_2^{des} \end{bmatrix}$$

$$\begin{bmatrix} \dot{y}_1 \\ \dot{y}_2 \end{bmatrix} = \begin{bmatrix} 0 & 0 & 0 & 0 & 0 & 0 & 0 \\ 0 & \Delta\phi' E_w & \Delta\phi' E_q & 0 & \Delta\phi' E_{\dot{\eta}} & \Delta\phi' E_\eta & 1 \end{bmatrix} \begin{bmatrix} u \\ w \\ q \\ \theta \\ \dot{\eta} \\ \eta \\ x_f \end{bmatrix} + \begin{bmatrix} 1 & 0 \\ 0 & 0 \end{bmatrix} \begin{bmatrix} \dot{y}_1^{des} \\ \dot{y}_2^{des} \end{bmatrix}$$

For different structure of $\dot{y}^{des}$ the variation of closed loop poles are given below.

Consider cases 1 ($W = I$) and 2 ($W = \begin{bmatrix} 1 & 0 \\ 0 & b/(s+b) \end{bmatrix}$) and different combination of P and PI controller structure in the feedback loops.

E.1 Controller Structure and Closed Loop Dynamics

The inversion loop $\dot{y}^{des}$ to y eigenvalues are

$$\text{case 1:}\begin{matrix} -0.6294 & -0.0185 \\ 0 & 0 \\ 0 & 0 \end{matrix} \qquad \text{case 2:}\begin{matrix} -0.5791 & -0.0204 \\ -5.5704 \pm i8.7464 & 0 \\ 0 & 0 \end{matrix}$$

Note that in case 1 because of the separation between controlled variables and internal dynamics, it can be stated with certainty that the two nonzero eigenvalues are associated with internal dynamics of (u, w). In case 2, the flexible mode dynamics are modified in the inversion loop, the pitch rate dynamics appear as integrators, and the real negative eigenvalues, similar in value to those found in case 1, should belong to (u, w).

The closed loop eigenvalues and the associated linear controller structure are:

$$\begin{pmatrix} \dot{y}_1^{des} \\ \dot{y}_2^{des} \end{pmatrix} = \begin{pmatrix} k1\left(q_{cmd} - \left(q + \phi'\dot{\eta}\right)\right) \\ k3\left(-\Delta\phi'\dot{\eta}\right) \end{pmatrix}$$

$$\text{case 1:}\begin{matrix} -0.6294 & -0.0185 \\ -6.004 & -1.1997 \\ 0 & 0 \end{matrix} \qquad \text{case 2:}\begin{matrix} -0.5979 & -0.0197 \\ -5.5614 \pm i11.6796 & -1.1997 \\ 0 & 0 \end{matrix}$$

$$\begin{pmatrix} \dot{y}_1^{des} \\ \dot{y}_2^{des} \end{pmatrix} = \begin{pmatrix} k1\left(q_{cmd} - \left(q + \phi'\dot{\eta}\right)\right) + k2\left(\theta_{cmd} - \theta\right) \\ k3\left(-\Delta\phi'\dot{\eta}\right) \end{pmatrix}$$

$$\text{case 1:}\begin{matrix} -0.6294 & -0.0185 \\ -6.0004 & 0 \\ -0.5999 \pm i0.8001 & \end{matrix} \qquad \text{case 2:}\begin{matrix} -0.6057 & -0.0195 \\ -5.5618 \pm i11.6801 & -0.5956 \pm i0.7958 \\ 0 & \end{matrix}$$

$$\begin{pmatrix} \dot{y}_1^{des} \\ \dot{y}_2^{des} \end{pmatrix} = \begin{pmatrix} k1\left(q_{cmd} - \left(q + \phi'\dot{\eta}\right)\right) \\ k3\left(-\Delta\phi'\dot{\eta}\right) + k4\left(-\Delta\phi'\eta\right) \end{pmatrix}$$

$$\text{case 1:}\begin{matrix} -0.6294 & -0.0185 \\ 0 & -0.1997 \\ -3.0002 \pm i9.5390 & \end{matrix} \qquad \text{case 2:}\begin{matrix} -0.6330 & -0.0185 \\ -7.1617 & 0 \\ -1.9636 \pm i11.6193 & \end{matrix}$$

$$\begin{pmatrix} \dot{y}_1^{des} \\ \dot{y}_2^{des} \end{pmatrix} = \begin{pmatrix} k1\left(q_{cmd} - \left(q + \phi'\dot{\eta}\right)\right) + k2\left(\theta_{cmd} - \theta\right) \\ k3\left(-\Delta\phi'\dot{\eta}\right) + k4\left(-\Delta\phi'\eta\right) \end{pmatrix}$$

$$\text{case } 1: \begin{matrix} -0.6294 & -0.0185 \\ -0.5998 \pm i0.8001 & -3.002 \pm i9.5390 \end{matrix}$$

$$\text{case } 2: \begin{matrix} -0.6321 & -0.0185 \\ -1.9643 \pm i11.6192 & -0.5996 \pm i0.8012 \end{matrix} \qquad -7.1615$$

The presence of PI structure in both loops eliminates eigenvalues on the jω-axis and thus allows for existence of a unique P, symmetric positive definite, solution of the Lyapunov equation $AP + PA^T = -Q$. This ensures that $\mathrm{V}(x) = x^T Px$ is a Lyapunov function with $\dot{\mathrm{V}}(x) < 0$ resulting in $x = 0$ being globally asymptotically stable. The LaSalle theorem relaxes the demand on $\dot{\mathrm{V}}(x)$ to be strictly positive definite and allows for positive semi-definiteness to guarantee stability in the Lyapunov sense, or uniform asymptotic stability if $\dot{\mathrm{V}}(x)$ does not vanish identically. But using the specific characteristics of a linear case, requiring positive definiteness of $\dot{\mathrm{V}}(x)$ guarantees global asymptotic stability and using PI controller structure allows for this stronger specification of stability. Furthermore, the PI structure in the flexible dynamics loop insures that there is no residual $\dot{\eta}$ in steady state due to an error build up.

E.2 Analytical Stability Analysis

In light of this analysis, the PI/PI structure is used in a linear system to derive a symbolic Lyapunov function with a full knowledge that it exists for a numeric representation of the system. The linear system with PI controller structure is shown below

$$\begin{bmatrix} \dot{u} \\ \dot{w} \\ \dot{q} \\ \dot{\theta} \\ \ddot{\eta} \\ \dot{\eta} \\ \dot{x}_f \end{bmatrix} = \begin{bmatrix} \bar{X}_{\delta 1} & 0 \\ \bar{Z}_{\delta 1} & 0 \\ 1 & 0 \\ 0 & 0 \\ 0 & 0 \\ 0 & 0 \\ 0 & \frac{1}{b} \end{bmatrix} \begin{pmatrix} k1 q_{cmd} + k2\theta_{cmd} \\ 0 \end{pmatrix} +$$

$$\begin{bmatrix} \bar{X}_u & \bar{X}_w & \bar{X}_q - \bar{X}_{\delta 1} k1 & \bar{X}_\theta - \bar{X}_{\delta 1} k2 & \bar{X}_{\dot{\eta}} - \bar{X}_{\delta 1} k1\phi' & \bar{X}_\eta & \bar{X}_{\delta 2} \\ \bar{Z}_u & \bar{Z}_w & \bar{Z}_q - \bar{Z}_{\delta 1} k1 & \bar{Z}_\theta - \bar{Z}_{\delta 1} k2 & \bar{Z}_{\dot{\eta}} - \bar{Z}_{\delta 1} k1\phi' & \bar{Z}_\eta & \bar{Z}_{\delta 2} \\ 0 & -\phi' E_w & -\phi' E_q - k1 & -k2 & -\phi'\left(E_{\dot{\eta}} + k1\right) & -\phi' E_\eta & -\phi' \bar{E}_{\delta 2} \\ 0 & 0 & 1 & 0 & 0 & 0 & 0 \\ 0 & E_w & E_q & 0 & E_{\dot{\eta}} & E_\eta & \bar{E}_{\delta 2} \\ 0 & 0 & 0 & 0 & 1 & 0 & 0 \\ 0 & -\frac{\Delta\phi'}{b} E_w & -\frac{\Delta\phi'}{b} E_q & 0 & -\frac{\Delta\phi'}{b}\left(E_{\dot{\eta}} + k3\right) & -\frac{\Delta\phi'}{b}\left(E_\eta + k4\right) & -\frac{1}{b} \end{bmatrix} \begin{bmatrix} u \\ w \\ q \\ \theta \\ \dot{\eta} \\ \eta \\ x_f \end{bmatrix}$$

(E.1)

In the specific case finding a suitable Lyapunov function is achieved by simply solving the standard Lyapunov equation. Alas, such approach does not work for symbolic analysis. One potential approach to find the appropriate P for the quadratic Lyapunov function is to write out the elements of P in terms of the elements of the closed loop system matrix **A** and then apply the Sylvester's theorem. By requiring that all the principal minors of **P** to be strictly positive places restrictions on the relations between the elements of the A matrix. These relationships are potentially very restrictive and have no physical basis.

Another approach is to assume $P = I$ and use the physics of the problem to find conditions under which a candidate function $\mathrm{V}(x) = \frac{1}{2}\left(V^2 + q^2 + \theta^2 + \dot{\eta}^2 + \eta^2 + x_f^2\right)$ will be Lyapunov. This is the currently preferred approach. Clearly $\mathrm{V}(0) = 0$ and $\mathrm{V}(x) > 0,\ \forall x \neq 0$. The question now rests with positive definiteness of $\dot{\mathrm{V}}(x)$.

$$\begin{aligned} \dot{\mathrm{V}}(x) &= V\dot{V} + q\dot{q} + \theta\dot{\theta} + \dot{\eta}\ddot{\eta} + \eta\dot{\eta} + x_f \dot{x}_f \\ &= u\dot{u} + w\dot{w} + q\dot{q} + \theta\dot{\theta} + \dot{\eta}\ddot{\eta} + \eta\dot{\eta} + x_f \dot{x}_f \end{aligned}$$

$$
\begin{aligned}
&\dot{\mathrm{V}}(x) = \\
&u\begin{pmatrix} \bar{X}_u u + \bar{X}_w w + \left(\bar{X}_q - \bar{X}_{\delta 1} k1\right) q + \left(\bar{X}_\theta - \bar{X}_{\delta 1} k2\right)\theta + \left(\bar{X}_{\dot{\eta}} - \bar{X}_{\delta 1} k1\phi'\right)\dot{\eta} + \bar{X}_\eta \eta + \bar{X}_{\delta 2} x_f \\ + \bar{X}_{\delta 1}\left(k1 q_{cmd} + k2\theta_{cmd}\right) \end{pmatrix} \\
&+w\begin{pmatrix} \bar{Z}_u u + \bar{Z}_w w + \left(\bar{Z}_q - \bar{Z}_{\delta 1} k1\right) q + \left(\bar{Z}_\theta - \bar{Z}_{\delta 1} k2\right)\theta + \left(\bar{Z}_{\dot{\eta}} - \bar{Z}_{\delta 1} k1\phi'\right)\dot{\eta} + \bar{Z}_\eta \eta + \bar{Z}_{\delta 2} x_f \\ + \bar{Z}_{\delta 1}\left(k1 q_{cmd} + k2\theta_{cmd}\right) \end{pmatrix} \\
&+q\begin{pmatrix} -\phi' E_w w - \left(\phi' E_q + k1\right) q - k2\theta - \phi'\left(E_{\dot{\eta}} + k1\right)\dot{\eta} - \phi' E_\eta \eta - \phi' / \Delta\phi' x_f \\ + \left(k1 q_{cmd} + k2\theta_{cmd}\right) \end{pmatrix} \\
&+\theta q + \eta\dot{\eta} \\
&+\dot{\eta}\left(E_w w + E_q q + E_{\dot{\eta}}\dot{\eta} + E_\eta \eta + 1/\Delta\phi' x_f\right) \\
&+x_f\begin{pmatrix} -\frac{\Delta\phi'}{b} E_w w - \frac{\Delta\phi'}{b} E_q q - \frac{\Delta\phi'}{b}\left(E_{\dot{\eta}} + k3\right)\dot{\eta} - \frac{\Delta\phi'}{b}\left(E_\eta + k4\right)\eta - \frac{1}{b} x_f \\ + \frac{1}{b}\left(k3\Delta\phi'\dot{\eta}_{cmd} + k4\Delta\phi'\eta_{cmd}\right) \end{pmatrix}
\end{aligned}
$$

(E.2)

Looking at the system in wind-axes coordinates brings an advantage of looking at vehicle velocity in terms magnitude, always greater than or equal to zero, and angle. Converting (E.1) into polar coordinates results in

$$
\begin{aligned}
&\dot{\mathrm{V}}(x) = \\
&V\cos\alpha\begin{pmatrix} \bar{X}_u V\cos\alpha + \bar{X}_w V\sin\alpha + \left(\bar{X}_q - \bar{X}_{\delta 1} k1\right) q + \left(\bar{X}_\theta - \bar{X}_{\delta 1} k2\right)\theta + \left(\bar{X}_{\dot{\eta}} - \bar{X}_{\delta 1} k1\phi'\right)\dot{\eta} \\ + \bar{X}_\eta \eta + \bar{X}_{\delta 2} x_f + \bar{X}_{\delta 1}\left(k1 q_{cmd} + k2\theta_{cmd}\right) \end{pmatrix} \\
&+V\sin\alpha\begin{pmatrix} \bar{Z}_u V\cos\alpha + \bar{Z}_w V\sin\alpha + \left(\bar{Z}_q - \bar{Z}_{\delta 1} k1\right) q + \left(\bar{Z}_\theta - \bar{Z}_{\delta 1} k2\right)\theta + \left(\bar{Z}_{\dot{\eta}} - \bar{Z}_{\delta 1} k1\phi'\right)\dot{\eta} \\ + \bar{Z}_\eta \eta + \bar{Z}_{\delta 2} x_f + \bar{Z}_{\delta 1}\left(k1 q_{cmd} + k2\theta_{cmd}\right) \end{pmatrix} \\
&+q\begin{pmatrix} -\phi' E_w V\sin\alpha - \left(\phi' E_q + k1\right) q - k2\theta - \phi'\left(E_{\dot{\eta}} + k1\right)\dot{\eta} - \phi' E_\eta \eta - \phi' / \Delta\phi' x_f \\ + \left(k1 q_{cmd} + k2\theta_{cmd}\right) \end{pmatrix} \\
&+\theta q + \eta\dot{\eta} + \dot{\eta}\left(E_w V\sin\alpha + E_q q + E_{\dot{\eta}}\dot{\eta} + E_\eta \eta + 1/\Delta\phi' x_f\right) \\
&+x_f\begin{pmatrix} -\frac{\Delta\phi'}{b} E_w V\sin\alpha - \frac{\Delta\phi'}{b} E_q q - \frac{\Delta\phi'}{b}\left(E_{\dot{\eta}} + k3\right)\dot{\eta} - \frac{\Delta\phi'}{b}\left(E_\eta + k4\right)\eta - \frac{1}{b} x_f \\ + \frac{1}{b}\left(k3\Delta\phi'\dot{\eta}_{cmd} + k4\Delta\phi'\eta_{cmd}\right) \end{pmatrix}
\end{aligned}
$$

and collecting terms

$$\dot{\mathrm{V}}(x) = V^2\left(\bar{X}_u\cos^2\alpha + \left(\bar{X}_w + \bar{Z}_u\right)\sin\alpha\cos\alpha + \bar{Z}_w\sin^2\alpha\right) + E_{\dot{\eta}}\dot{\eta}^2 - \left(\phi' E_q + k1\right)q^2 - \frac{x^2{}_f}{b}$$

$$+V\left(\begin{array}{l}\cos\alpha\left(\begin{array}{l}\left(\bar{X}_q - \bar{X}_{\delta 1}k1\right)q + \left(\bar{X}_\theta - \bar{X}_{\delta 1}k2\right)\theta + \left(\bar{X}_{\dot{\eta}} - \bar{X}_{\delta 1}k1\phi'\right)\dot{\eta} + \bar{X}_\eta\eta + \bar{X}_{\delta 2}x_f \\ + \bar{X}_{\delta 1}\left(k1q_{cmd} + k2\theta_{cmd}\right)\end{array}\right) \\ +\sin\alpha\left(\begin{array}{l}\left(\bar{Z}_q - \bar{Z}_{\delta 1}k1 - \phi' E_w\right)q + \left(\bar{Z}_\theta - \bar{Z}_{\delta 1}k2\right)\theta + \left(\bar{Z}_{\dot{\eta}} - \bar{Z}_{\delta 1}k1\phi' + E_w\right)\dot{\eta} + \bar{Z}_\eta\eta \\ + \bar{Z}_{\delta 2}x_f + \bar{Z}_{\delta 1}\left(k1q_{cmd} + k2\theta_{cmd}\right) - x_f\dfrac{\Delta\phi'}{b}E_w\end{array}\right)\end{array}\right)$$

$$+\left(E_q - \phi'\left(E_{\dot{\eta}} + k1\right)\right)\dot{\eta}q + \left(E_\eta + 1\right)\eta\dot{\eta} + \left(\frac{1}{\Delta\phi'} - \frac{\Delta\phi'}{b}\left(E_{\dot{\eta}} + k3\right)\right)\dot{\eta}x_f$$

$$-\phi' E_\eta\eta q - \left(\frac{\phi'}{\Delta\phi'} + \frac{\Delta\phi'}{b}E_q\right)x_f q + \left(1 - k2\right)\theta q - \frac{\Delta\phi'}{b}\left(E_\eta + k4\right)\eta x_f$$

$$+\frac{\Delta\phi'}{b}\left(k3\dot{\eta}_{cmd} + k4\eta_{cmd}\right)x_f + \left(k1q_{cmd} + k2\theta_{cmd}\right)q$$

(E.3)

with $\dot{\eta}_{cmd} = \eta_{cmd} = 0$. Under what conditions will (E.3) be negative definite. From a physical perspective the V^2 term would dominate provided that there are no unbounded flex dynamics. The pitch rate is a controlled variable and because the standard dynamic inversion is recovered for this loop it is a stable bounded response by design. The same assertion cannot immediately be made about the $\dot{\eta}$ dynamics since there are filter dynamics involved. The following condition should work for $\dot{\mathrm{V}}(x) < 0$

$$\begin{gathered}\left|\bar{X}_u\cos^2\alpha + \bar{Z}_w\sin^2\alpha\right| > \left|\left(\bar{X}_w + \bar{Z}_u\right)\sin\alpha\cos\alpha\right| \\ \left(\bar{X}_u\cos^2\alpha + \bar{Z}_w\sin^2\alpha\right) < 0 \\ \text{and} \\ V > \left|\dot{\eta}\right|\end{gathered} \qquad \text{(E.4)}$$

The first should guarantee that V^2 coefficient is negative and the second stipulates that flexible dynamics are bounded. These conditions are not based on any physical insight, might be overly conservative, and do not lend themselves to a generalized statement about closed loop stability akin to a result in Chapter 6.

If the flexible dynamics were not present the stability analysis would reduce to a single loop pitch dynamic case as shown below. Consider nonlinear system described by (4.11). If the flexible dynamics were not present the system would reduce to

$$\begin{bmatrix}\dot{u}\\ \dot{w}\\ \dot{q}\\ \dot{\theta}\end{bmatrix}=\begin{pmatrix}-qw-g\sin\theta+\dfrac{T}{\mathrm{m}}\\ qu+g\cos\theta\\ 0\\ q\end{pmatrix}+\frac{1}{2}\rho SV^2\left\{\begin{pmatrix}\dfrac{C_x(\alpha)}{\mathrm{m}}\\ \dfrac{C_z(\alpha)}{\mathrm{m}}\\ \dfrac{\bar{c}C_M(\alpha)}{I_y}\\ 0\end{pmatrix}+\begin{pmatrix}\dfrac{C_{x,\delta 1}(\alpha)}{\mathrm{m}} & 0\\ \dfrac{C_{z,\delta 1}(\alpha)}{\mathrm{m}} & \dfrac{C_{z,\delta 2}(\alpha)}{\mathrm{m}}\\ \dfrac{\bar{c}C_{M,\delta 1}(\alpha)}{I_y} & \dfrac{\bar{c}C_{M,\delta 2}(\alpha)}{I_y}\\ 0 & 0\end{pmatrix}\begin{pmatrix}\delta_1\\ \delta_2\end{pmatrix}\right\}$$

$$y=q$$

(E.5)

with the filter equations given by

$$W=\begin{bmatrix}1 & 0\\ 0 & \dfrac{1}{bs+1}\end{bmatrix}\Rightarrow\begin{aligned}\dot{x}_f&=A_f x_f+\begin{bmatrix}0 & b_f\end{bmatrix}\begin{bmatrix}\bar{u}_1\\ \bar{u}_2\end{bmatrix}\\ y_f&=\begin{bmatrix}0\\ 1\end{bmatrix}x_f+\begin{bmatrix}1 & 0\\ 0 & 0\end{bmatrix}\begin{bmatrix}\bar{u}_1\\ \bar{u}_2\end{bmatrix}\end{aligned}$$

Schematically the controller would change from the one in Figure 7.1 to the one in Figure E1 below.

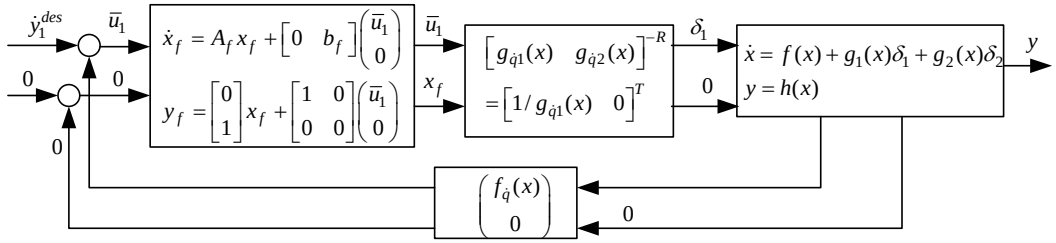

Figure E1: Transition of modified dynamic inversion controller when flexible dynamics are not present.

With removal of flexible dynamics the filter state becomes an internal state and input-output is a single loop pitch rate feedback dynamics. The closed loop system becomes

$$\begin{pmatrix} \dot{u} \\ \dot{w} \\ \dot{q} \\ \dot{\theta} \\ \dot{x}_f \end{pmatrix} = \begin{pmatrix} f_{\dot{u}}(x) \\ f_{\dot{w}}(x) \\ f_{\dot{q}}(x) \\ f_{\dot{\theta}}(x) \\ A_f x_f \end{pmatrix} + \begin{pmatrix} g_{\dot{u}1}(x) & 0 \\ g_{\dot{w}1}(x) & g_{\dot{w}2}(x) \\ g_{\dot{q}1}(x) & g_{\dot{q}2}(x) \\ 0 & 0 \\ 0 & b_f \end{pmatrix} \begin{pmatrix} 1/g_{\dot{q}1}(x) \\ 0 \end{pmatrix} \left[\dot{y}_1^{des} - f_{\dot{q}}(x) \right] \tag{E.6}$$

$$y_{sensed} = q$$

$$\Downarrow$$

$$\begin{pmatrix} \dot{u} \\ \dot{w} \\ \cdots \\ \dot{x}_f \\ \cdots \\ \dot{q} \\ \dot{\theta} \end{pmatrix} = \begin{pmatrix} f_{\dot{u}}(x) - f_{\dot{q}}(x) g_{\dot{u}1}(x)/g_{\dot{q}1}(x) \\ f_{\dot{w}}(x) - f_{\dot{q}}(x) g_{\dot{w}1}(x)/g_{\dot{q}1}(x) \\ \cdots \\ A_f x_f \\ \cdots \\ 0 \\ q \end{pmatrix} + \begin{pmatrix} g_{\dot{u}1}(x)/g_{\dot{q}1}(x) \\ g_{\dot{w}1}(x)/g_{\dot{q}1}(x) \\ \cdots \\ 0 \\ \cdots \\ 1 \\ 0 \end{pmatrix} \dot{y}_1^{des}$$

In terms of actual aerodynamic coefficients, these equations can be rewritten as

$$\begin{bmatrix} \dot{u} \\ \dot{w} \\ \dot{q} \\ \dot{\theta} \\ \dot{x}_f \end{bmatrix} = \begin{pmatrix} -qw - g\sin\theta + \dfrac{T}{\mathrm{m}} \\ qu + g\cos\theta \\ 0 \\ q \\ -\dfrac{1}{b} \end{pmatrix} + \frac{1}{2}\rho S V^2 \begin{pmatrix} \dfrac{C_x(\alpha)}{\mathrm{m}} \\ \dfrac{C_z(\alpha)}{\mathrm{m}} \\ \dfrac{\bar{c}C_M(\alpha)}{I_y} \\ 0 \\ 0 \end{pmatrix} +$$

$$\frac{\rho S V^2}{2} \begin{pmatrix} \dfrac{C_{x,\delta 1}(\alpha)}{\mathrm{m}} & 0 \\ \dfrac{C_{z,\delta 1}(\alpha)}{\mathrm{m}} & \dfrac{C_{z,\delta 2}(\alpha)}{\mathrm{m}} \\ \dfrac{\bar{c}C_{M,\delta 1}(\alpha)}{I_y} & \dfrac{\bar{c}C_{M,\delta 2}(\alpha)}{I_y} \\ 0 & 0 \\ 0 & \dfrac{1}{b} \end{pmatrix} \begin{pmatrix} \dfrac{2}{\rho S V^2} \dfrac{I_y}{\bar{c}C_M(\alpha)} \\ 0 \end{pmatrix} \left[\dot{y}_1^{des} - \frac{\rho S V^2}{2} \frac{\bar{c}C_M(\alpha)}{I_y} \right]$$

$$y = q$$

$$\Downarrow$$

$$\begin{bmatrix} \dot{u} \\ \dot{w} \\ \dot{x}_f \\ \dot{q} \\ \dot{\theta} \end{bmatrix} = \begin{pmatrix} -qw - g\sin\theta + \dfrac{T}{\mathrm{m}} \\ qu + g\cos\theta \\ -\dfrac{1}{b_f}x_f \\ 0 \\ q \end{pmatrix} + \frac{\rho S V^2}{2\mathrm{m}} \begin{pmatrix} C_x(\alpha) - C_{x,\delta 1}(\alpha)\dfrac{C_M(\alpha)}{C_{M,\delta 1}(\alpha)} \\ C_z(\alpha) - C_{z,\delta 1}(\alpha)\dfrac{C_M(\alpha)}{C_{M,\delta 1}(\alpha)} \\ 0 \\ 0 \\ 0 \end{pmatrix} + \begin{pmatrix} \dfrac{C_{x,\delta 1}(\alpha)}{\mathrm{m}}\dfrac{I_y}{\bar{c}C_{M,\delta 1}(\alpha)} \\ \dfrac{C_{z,\delta 1}(\alpha)}{\mathrm{m}}\dfrac{I_y}{\bar{c}C_{M,\delta 1}(\alpha)} \\ 0 \\ 1 \\ 0 \end{pmatrix} \dot{y}_1^{des} \tag{E.7}$$

Note that the closed loop system divides nicely into two subsystems. One is the controlled variables (q, θ) which do not depend on the internal dynamics of (u, w, x_f), and the other is the internal dynamics. The controlled variables are stable by design, and hence the closed loop stability depends exclusively on the stability of the internal dynamics. The internal dynamics subsystem has a natural separation between filter dynamics and velocity dynamics with filter dynamics stable by construction. Therefore the closed loop system stability depends on the stability of the (u, w) dynamics. The stability of these dynamics has been shown in Reference 14.

Appendix E – Longitudinal plus Flexible Mode Stability Analysis